Supported by 日本財団 THE NIPPON FOUNDATION

第 44 期　　研究者番号：G4401　　　　　　　　作成日　：2023 年 3 月 13 日

氏　名	李 君鵬	LI JUNPENG	性別	M	生年月日　1983/01/15
所属機関（役職）	吉林省人民医院急診外科（主治医師）				
研究先（指導教官）	東北大学大学院医学系研究科消化器外科学分野（亀井 尚）				
研究テーマ	胃癌、食道胃接合部癌における癌微小免疫環境の解析と至適治療の確立 Cancer microenvironmental research in gastric and esophago-gastric junction carcinoma				
専攻種別	□論文博士			☑課程博士	

研究者評価（指導教官記入欄）

成績状況	⑱　良　可　不可 学業成績係数=	取得単位数
		0／30

学生本人が行った 研究の概要	"Glucocorticoid の Barrett 食道癌発生予防および治療への応用"を研究テーマとし、周辺の知識整理と研究計画を作成しました。新型コロナウイルスで入国が夏になったこともあり、実際の実験は、食道癌細胞株の培養技術など基礎的な実験手技の修練にとどまりましたが来年度にむけての基礎的な研究力を付けることができました。現在は実際のテーマに関する実験を開始したところになります。
総合評価	【良かった点】 研究テーマについて意欲的に学習し情報収集を行いました。これによって実現可能な実験計画が立案できました。また、英語が苦手でありましたが我々のグループでのミーティングで自身の研究について英語で発表するなど積極的に取り組みました。 【改善すべき点】 基礎実験の経験が少ないため、手技の習得をもう少し頑張ってもらいます。 また実験以外では、大学院での単位取得も積極的におこなってもらいます。 【今後の展望】 引き続き実験を進めてもらい、いくつかの結果を出すように進めます。また、自身の研究テーマについての Review article などにもチャレンジしてもらえればと考えています。
学位取得見込	奨学金支援終了後 2 年以内に博士学位取得の見込みあり

評価者（指導教官名）　亀井　尚

第44期　　　　研究者番号：　G4401　　　　　作成日：2023年3月 7 日

氏名	李 君鵬	LI JUNPENG	性別	M	生年月日　1983/01/15
所属機関(役職)	吉林省人民医院急診外科（主治医師）				
研究先(指導教官)	東北大学大学院医学系研究科消化器外科学分野（亀井 尚　教授）				
研究テーマ	胃癌、食道胃接合部癌における癌微小免疫環境の解析と至適治療の確立 Cancer microenvironmental research in gastric and esophago-gastric junction carcinoma				
専攻種別	論文博士		□	課程博士	☑

1．研究概要（1）

1）目的（Goal）
① Barrett食道癌におけるGlucocorticois receptor (GR)の発見が腫瘍の浸潤増殖や予後に与える影響を明らかにすること
②ステロイド(Glucocorticoids；GCs)投与がBattett食道癌に与える影響を明らかとし、発症予防や治療に対する有効性を検討すること

2）戦略（Approach）
背景
Barrett食道癌は胃酸と胆汁酸の暴露による慢性炎症により発生する。前癌病変であるBarrett食道の有病率は10~12%と高いが、その癌化率は年間0.12%と低い(N Engl J Med 2011)。しかし、癌化すると5年生存率は15-20%と予後不良な疾患である(N Engl J Med 2009)。Barrett食道癌は稀な疾患であるものの、近年欧米において著しい増加傾向にあり、日本においても肥満人口の増加や欧米や欧米型の高脂肪食の普及により罹患する患者が増加している。Barrett食道患者に対して、胸焼けを中心とした酸逆流症状緩和のためにProton pump inhibitor (PPI)などの制酸剤の投与が広く行われているが、これらの薬剤による発癌抑制効果は明らかになっていない。また、Barrett食道癌に対する手術以外の治療法も確立しておらず、胃癌に準じた治療が行われているのが現状である(GERD診療ガイドライン2015、食道癌治療ガイドライン2017)。
Glucocorticoids(GCs)は細胞内でGC receptor(GR)と結合し標的遺伝子の転写活性を調節することで、その作用を発揮する。気管支喘息、炎症性腸疾患、その他の自己免疫性疾患において、ステロイド薬が慢性炎症や過剰な免疫応答を抑制することは周知の通りである。
癌治療の分野においても、GRの発見が検討されている。乳癌、大腸癌、卵巣癌、食道扁平上皮癌などではGRの発見が予後不良因子であることや化学療法抵抗性と関係していることが報告されている。一方で我々は、以前Barrett食道癌におけるGRの発現を免疫組織化学的に検討し、上記の報告とは異なりBarrett食道癌ではGR発現が予後良好因子であることを初めて明らかにした(Gokon et al. Pathol Int. 2020)。

研究の科学的合理性の根拠
この機序については、Barrett食道は炎症性発癌の要素が強いため、GCsが抗炎症作用を通じて
Barrett食道癌の予後に良い影響を与えているものと仮定した。しかし、GCsの抗炎症作用が実際に
Barrett食道癌において機能しているかについては十分に検討していない。また、胃酸と胆汁酸の暴露に関係する臨床病理学的因子との対比も行っていない。例えば、逆流を助長する食道裂孔ヘルニアの有無、術前内視鏡における逆流性食道炎の有無、PPI内服の有無などである。さらには、外因性のGCsがBarrett食道癌患者の予後を改善させるか否かについて、Barrett食道癌の発生自体を抑制するか否かについても明らかになっていない。免疫組織化学的検討と細胞増殖試験等によりBarrett食道癌の腫瘍組織および周囲組織におけるGR発現が予後良好となる機序や予後良好な患者群の特徴を明らかにし、細胞実験と動物実験においてGCsのBarrett食道、Barrett食道癌に与える影響を明らかにすることができれば、GCsを術前後の集学的治療に付加できる可能性や、GCs投与が有効な患者群を選別できる可能性がある。加えて、GCsによってBarrett食道からの発癌を抑制できる可能性がある。多くの先行研究はGCsの癌患者に対する悪影響について検討しているが、本研究はこれまでの基礎研究からGCsがBarrett食道癌患者に良い影響を及ぼすという点でこれまでにない学術的独創性がある。安価で汎用されているステロイド薬がBarrett食道癌の予後を改善する可能性と発癌を予防する可能性を示すことができれば、今後のBarrett食道癌治療に大きく寄与する点で独創性があり、社会に大きく寄与するものと考える。

1．研究概要（2）

3）材料と方法（Materials and methods）
培養細胞実験

　機能評価のための培養細胞実験を行う。食道腺癌細胞株（OE33）において、リアルタイムPCRによりGRとSGK1の発現動態を検討する。また、interleukin(IL)-6,IL-8、vascular endothelial growth factor (VEGF)などの炎症性サイトカイン遺伝子の発現も検討する。これに10nM、100nMのデキサメタゾンを添加し、上記因子の変化と細胞増殖能と遊走能を検討する。これにより、外因性のステロイドがGR-SGK1経路を活性化し、炎症性サイトカインの自己産生を抑制することで、癌細胞の増殖と転移の抑制に寄与するか明らかにしたい。

逆流モデルラット逆流モデルラットにおいてBarrett食道、Barrett食道癌が発生することが報告されている（Cancer Sci.2007）。これを用いてGCs投与とBarrett食道癌の発生及び増殖との関連を検討する。約100匹のラットに対し、ジェチルエーテルを用いた吸入麻酔下に手術を行う。腹部に正中切開をおき、食道胃接合部を離断し7-0吸収糸を用いて食道と上部空腸に側端吻合をおく。食道への逆流を減少させるために食道胃接合部吊り上げ縫合を追加する。デキサメタゾンを放出するペレットを皮下に埋め込む群とプラセボ群に分類し（各50匹ずつ）、生存例は30週後に屠殺する（先行研究において20週目まではBarrett食道癌が生じず、30週目には27%の症例で発癌することが示されたため）。食道を摘出しHematoxylin Eosin(HE)染色を行い組織学的に評価し、GRとSGK1の免疫染色を施行する。Barrett食道もしくはBarrett食道癌の有無を検索し、確認できた場合はGRとSGK1の発現と腫瘍径、深達度を検討する。これによりGCs投与がBarrett食道発生およびBarrett食道癌の増殖に与える影響を明らかにする。

4）実験結果（Results）
まだ具体的には出ていません。

5）考察（Discussion）
未確定

6）参考文献（References）
Kenro, et al. Gastroenterol Endosc. 2017 ; 59 :70-80
Eusebi LH, et al. Gut 2021;70:456-463
Frederik, et al. N Engl J Med 365 ; 1375-1383:2011
Desai TK, et al. Gut 61 ; 970—976 : 2012
Sikkema M, et al. Clin Gastroenterol Hepatol 8 ; 235—244
Kathleen, et al. Mechanisms of Ageing and Development 125 (2004) 697-706
Pamela N, et al. Clin Cancer Res.2022 Aug 2;28(15):3214-3224
Jacob T,et al. Clin Exp Metastasis. 2004;21(6):477-83
Navneet K, et al. Int J Mol Sci. 2018 May 31;19(6):1625
Gokon, et al. Pathol Int 70(6): 355-363

2．執筆論文　Publication of thesis　※記載した論文を添付してください。Attach all of the papers listed below.

論文名 1 Title						
掲載誌名 Published journal						
	年　　　　月		巻（号）	頁　～　　頁	言語 Language	
第1著者名 First author		第2著者名 Second author		第3著者名 Third author		
その他著者名 Other authors						
論文名 2 Title						
掲載誌名 Published journal						
	年　　　　月		巻（号）	頁　～　　頁	言語 Language	
第1著者名 First author		第2著者名 Second author		第3著者名 Third author		
その他著者名 Other authors						
論文名 3 Title						
掲載誌名 Published journal						
	年　　　　月		巻（号）	頁　～　　頁	言語 Language	
第1著者名 First author		第2著者名 Second author		第3著者名 Third author		
その他著者名 Other authors						
論文名 4 Title						
掲載誌名 Published journal						
	年　　　　月		巻（号）	頁　～　　頁	言語 Language	
第1著者名 First author		第2著者名 Second author		第3著者名 Third author		
その他著者名 Other authors						
論文名 5 Title						
掲載誌名 Published journal						
	年　　　　月		巻（号）	頁　～　　頁	言語 Language	
第1著者名 First author		第2著者名 Second author		第3著者名 Third author		
その他著者名 Other authors						

3. 学会発表　Conference presentation　※筆頭演者として総会・国際学会を含む主な学会で発表したものを記載してくだ

※Describe your presentation as the principal presenter in major academic meetings including general meetings or international me

学会名 Conference	
演　題 Topic	
開催日 date	年　　　　月　　　　日 ｜ 開催地 venue
形式　method	□　口頭発表　Oral　□　ポスター発表　Poster｜言語　Language ｜□　日本語　□　英語　　□　中国語
共同演者名 Co-presenter	
学会名 Conference	
演　題 Topic	
開催日 date	年　　　　月　　　　日 ｜ 開催地 venue
形式　method	□　口頭発表　Oral　□　ポスター発表　Poster｜言語　Language ｜□　日本語　□　英語　　□　中国語
共同演者名 Co-presenter	
学会名 Conference	
演　題 Topic	
開催日 date	年　　　　月　　　　日 ｜ 開催地 venue
形式　method	□　口頭発表　Oral　□　ポスター発表　Poster｜言語　Language ｜□　日本語　□　英語　　□　中国語
共同演者名 Co-presenter	
学会名 Conference	
演　題 Topic	
開催日 date	年　　　　月　　　　日 ｜ 開催地 venue
形式　method	□　口頭発表　Oral　□　ポスター発表　Poster｜言語　Language ｜□　日本語　□　英語　　□　中国語
共同演者名 Co-presenter	

4. 受賞（研究業績）Award（Research achievement）

名　称 Award name					
	国名 Country		受賞年 Year of	年　　　　月	
名　称 Award name					
	国名 Country		受賞年 Year of	年　　　　月	

5．本研究テーマに関わる他の研究助成金受給 Other research grants concerned with your resarch theme

受給実績 Receipt record	☐ 有　　■ 無				
助成機関名称 Funding agency					
助成金名称 Grant name					
受給期間 Supported period	年	月 〜	年	月	
受給額 Amount received	円				
受給実績 Receipt record	☐ 有　　■ 無				
助成機関名称 Funding agency					
助成金名称 Grant name					
受給期間 Supported period	年	月 〜	年	月	
受給額 Amount received	円				

6．他の奨学金受給 Another awarded scholarship

受給実績 Receipt record	■ 有　　☐ 無				
助成機関名称 Funding agency	東北大学				
奨学金名称 Scholarship name	挑戦的研究支援プロジェクト				
受給期間 Supported period	2022 年 10 月 〜	2026 年 3 月			
受給額 Amount received	18万 円				

7．研究活動に関する報道発表 Press release concerned with your research activities

※記載した記事を添付してください。 Attach a copy of the article described below

報道発表 Press release	☐ 有　　■ 無	発表年月日 Date of release	
発表機関 Released medium			
発表形式 Release method	・新聞　・雑誌　・Web site　・記者発表　・その他（　　　　　　　　　　　　　）		
発表タイトル Released title			

8．本研究テーマに関する特許出願予定 Patent application concerned with your research theme

出願予定 Scheduled	☐ 有　　■ 無	出願国 Application	
出願内容（概要） Application contents			

9．その他 Others

指導責任者（記名）　　　　亀井　尚

日中笹川医学奨学金制度(学位取得コース)中間評価書
課程博士：指導教官用

第 44 期　　研究者番号：G4402　　　　　　　　　　　　作成日　：2023 年 3 月 1 日

氏　名	黄璐嬌	HUANG LUJIAO	性別	F	生年月日　1988/09/10
所属機関（役職）	四川省医学科学院・四川省人民医院臨床栄養科（主管技師）				
研究先（指導教官）	筑波大学大学院人間総合科学研究科生命システム医学専攻 国際発達ケア：エンパワメント科学研究室（安梅 勅江　教授）				
研究テーマ	高齢栄養リスクの指数と高齢入院者の入院時間、入院費用との関係 Associations of Geriatric Nutritional Risk Index with length of hospital stay and hospital cost in elderly inpatients				
専攻種別	□論文博士		☑課程博士		

研究者評価（指導教官記入欄）

成績状況	㊴ 良　可　不可 学業成績係数=	取得単位数
		取得単位数／取得すべき単位総数 23/30
学生本人が行った研究の概要	良好な栄養状況は、高齢者の健康レベル及び疾病予後を向上させるための必須条件である。本研究は病院診療のビッグデータに基づき、GNRIにより高齢入院者の栄養リスクを評価し、栄養リスクと短期入院成果（入院期間、入院費用）との関連を明確にする。本研究の結果により、入院中の健康リスク管理やヘルスプロモーション支援方法を検討できる。	
総合評価	【良かった点】 1. 本領域の研究方向性について示唆を得る。 2. チームワークを強化している。 3. 研究の基礎方法と技術を習得している。 【改善すべき点】 1. タイムマネジメントをさらに効率化する。 2. 統計学の知識や技術をさらに習得する。 【今後の展望】 今後とも研究に真摯に取り組み、卒業後は日中の架け橋としての研究者として活躍してほしいと願っている。	
学位取得見込	博士学位取得見込	

評価者（指導教官名） Juki Anne

第44期	研究者番号： G4402	作成日：2023年3月　1　日		
氏名	黄 璐娇　　HUANG LUJIAO	性別	F	生年月日　1988/09/10

所属機関(役職)	四川省医学科学院・四川省人民医院臨床栄養科（主管技師）			
研究先（指導教官）	筑波大学大学院人間総合科学研究科生命システム医学専攻 国際発達ケア：エンパワメント科学研究室（安梅 勅江　教授）			
研究テーマ	高齢栄養リスクの指数と高齢入院者の入院時間、入院費用との関係 Associations of Geriatric Nutritional Risk Index with length of hospital stay and hospital cost in elderly inpatients			
専攻種別	論文博士	□	課程博士	☑

1．研究概要（1）

1）目的（Goal）
Applying GNRI (Geriatric Nutritional Risk Index) to assess the nutritional risk of elderly hospitalized patients in China, and evaluating its validity and applicability. Clarifying the relationships between GNRI and length of hospital stay, hospital costs, and in-hospital mortality in elderly inpatients, and providing a scientific basis for timely and appropriate nutritional interventions in elderly patients, so as to improve the clinical outcomes and quality of life among elderly patients.

2）戦略（Approach）
Good nutritional status is an essential condition for improving the health and disease prognosis of elderly patients. Malnutrition not only causes a decline in immune function in elderly patients, which seriously affects body function, disease prognosis, and social function, but also makes those with nutritional risk more prone to hospital infection, which is one of the main factors affecting the clinical outcome of elderly patients.

However, malnutrition can be identified and diagnosed early through nutritional screening and nutritional assessment tools. With the higher number of elderly hospitalized patients, lower nutritional risk screening rates (18.96%), and greater prevalence of malnutrition (32.6%)in China, there is an urgent need to improve the rates of nutritional risk screening and assessment. Currently, the gold standard for nutritional screening and assessment of elderly patients is unclear, and most studies recommend the use of nutritional screening and assessment tools developed specifically for elderly patients. Determining which tool is the best for screening and assessing the nutritional status of this population remains conflicting.

A good nutritional screening tool should be reliable, valid, and easy to use. GNRI is a modified version of the Nutritional Risk Index (NRI), which is an objective nutritional screening and assessment tool for older patients based on height (knee height), weight, and serum albumin levels. The validity and reliability of the GNRI have been well studied in most other countries. Compared with other nutritional risk screening tools, the indicators required to calculate GNRI are simple and easy to obtain, and well operationalized. It is very easy to use in clinical practice, allowing for early nutritional interventions for patients.

Studies have shown that the GNRI score correlates with severity scores for nutrition-related complications (bedsores and infections) and can quantitatively determine the risk of morbidity and mortality of nutrition-related complications in elderly patients at admission. GNRI is also a valid predictor of postoperative complications and long-term prognosis in diseases such as malignancy, it also identifies potential patients in need of nutritional support and provides a reliable assessment in most health care settings, especially in elderly patients with dementia, aphasia or disuse. The advantages of GNRI make it more suitable for nutritional risk screening and assessment of elderly patients, which has a good reference value for their prognosis and, in turn, is an important reference to assist clinical decision-making and management.

At present, there are few studies on the application of GNRI to elderly inpatients in China. Further evidence is needed to support the effectiveness of GNRI, and its applicable value needs to be further evaluated and explored. This study intends to apply GNRI to assess the nutritional risk of elderly inpatients based on the big data of hospital diagnosis and treatment, and to explore the impact of nutritional risk assessed by GNRI on short-term hospitalization outcomes (length of stay, hospitalization cost) of the elderly inpatients, and to verify the applicability of GNRI in elderly inpatients in China.

１．研究概要（2）

3）材料と方法（Materials and methods）

3-1 Research population

This study is a retrospective cohort study. The population of the study is elderly inpatients aged 65 and above in a hospital in Southwest China. Based on the big data of hospital diagnosis and treatment, this study plans to build a data set of elderly inpatients through big data extraction, and collect retrospective information for patients who meet the inclusion and exclusion criteria. According to the sample size calculation formula, 40,000 elderly inpatients will be included in the research.

Inclusion criteria: ①Hospitalized patients; ②Age≥65 years old. Exclusion criteria: ①The length of hospital stay is less than 2 days; ②The patient's height, weight, and albumin values are missing.

3-2 Research methods

① Data collection

General information: age, gender, ethnicity, marital status, admission diagnosis (ICD-10 code), operation status, admission date, discharge date, hospitalization expenses, etc.

Anthropometric indicators: height (cm), weight (kg), and calculate body mass index BMI (Body Mass Index), BMI=weight (kg)/[height (m)]2.

Laboratory indicators: serum albumin (Alb, g/L).

② Application of GNRI to assess nutritional risk and grading range

Using the data of serum albumin (g/L), height (cm), and weight (kg) of the patient at admission, the GNRI will be calculated according to the formula, GNRI=1.489*serum albumin+41.7*(actual weight/ideal weight), when the actual weight is greater than the ideal weight, the ratio of actual weight/ideal weight will be set to 1. Among them, the ideal weight is calculated according to the Lorentz formula, ideal weight(male)=height-100-[(height-150)/4], ideal weight(female)=height-100-[(height-150)/2.5]. The grading range for the degree of nutritional risk assessed by GNRI is: GNRI>98 means no nutritional risk; 92≤GNRI≤98 means low nutritional risk; 82≤GNRI<92 means moderate nutritional risk; GNRI<82 means high nutritional risk.

③ End of observation

The death and discharge of the inpatients are used as the observation endpoint, and length of hospital stay(days), hospital expenses (CNY), and weight change are used as the outcome indicators.

Calculation of length of hospital stay: Length of hospital stay (days)=Discharge Date-Admission Date

Calculation of hospital expenses: Hospital expenses (CNY)=Total expenses during hospitalization (CNY)

Calculation of weight loss: Weight loss (kg)=Weight at discharge (kg)-Weight at admission (kg)

④ Statistical analysis

In the statistical description, the mean (standard deviation) is used for continuous variables; the number (percentage%) is used for categorical variables; the t-test or χ2 test is used for inter-group comparison according to the variable attributes. In the correlation analysis, the marginal structural model based on inverse probability weighting is proposed to estimate the length of hospital stay (days), hospital expenses (CNY), and weight loss (kg) of elderly inpatients with different GNRIs.

4）実験結果（Results）

Expected results

①Distribution of geriatric nutritional risk assessed by GNRI among elderly hospitalized patients in China

②The relationship between GNRI and length of hospital stay, hospital costs, and weight loss of elderly patients.

5）考察（Discussion）

Not available

6）参考文献（References）

1. Olivier Bouillanne, Gilles Morineau, Claire Dupont, et al. Geriatric Nutritional Risk Index: a new index for evaluating at-risk elderly medical patients. Am J Clin Nutr 2005;82:777-83.

2. Emanuele Cereda, Catherine Klersy, Carlo Pedrolli, et al. The Geriatric Nutritional Risk Index predicts hospital length of stay and in-hospital weight loss in elderly patients. Clin Nutr. 2015;34(1):74-8.

3. Zhao Y, Xia X, Xie D, et al. Geriatric Nutritional Risk Index can predict postoperative delirium and hospital length of stay in elderly patients undergoing non-cardiac surgery. Geriatr Gerontol Int. 2020;20(8):759-764.

4. Emanuele Cereda , Carlo Pedrolli . The geriatric nutritional risk index. Curr Opin Clin Nutr Metab Care. 2009;12(1):1-7.

5. Abd-El-Gawad WM, et al. The validity of Geriatric Nutrition Risk Index: Simple tool for prediction of nutritional-related complication of hospitalized elderly patients. Comparison with Mini Nutritional Assessment. Clin Nutr. 2014;33(6): 1108-16.

2．執筆論文　Publication of thesis　※記載した論文を添付してください。Attach all of the papers listed below.

論文名 1 Title							
掲載誌名 Published journal							
	年	月	巻（号）	頁　～	頁	言語 Language	
第1著者名 First author			第2著者名 Second author		第3著者名 Third author		
その他著者名 Other authors							
論文名 2 Title							
掲載誌名 Published journal							
	年	月	巻（号）	頁　～	頁	言語 Language	
第1著者名 First author			第2著者名 Second author		第3著者名 Third author		
その他著者名 Other authors							
論文名 3 Title							
掲載誌名 Published journal							
	年	月	巻（号）	頁　～	頁	言語 Language	
第1著者名 First author			第2著者名 Second author		第3著者名 Third author		
その他著者名 Other authors							
論文名 4 Title							
掲載誌名 Published journal							
	年	月	巻（号）	頁　～	頁	言語 Language	
第1著者名 First author			第2著者名 Second author		第3著者名 Third author		
その他著者名 Other authors							
論文名 5 Title							
掲載誌名 Published journal							
	年	月	巻（号）	頁　～	頁	言語 Language	
第1著者名 First author			第2著者名 Second author		第3著者名 Third author		
その他著者名 Other authors							

3．学会発表　Conference presentation　※筆頭演者として総会・国際学会を含む主な学会で発表したものを記載してく

※Describe your presentation as the principal presenter in major academic meetings including general meetings or interna

学会名 Conference	
演　題 Topic	
開催日 date　　　　年　　　　月　　　　日	開催地 venue
形式　method　□　口頭発表　Oral　□　ポスター発表 Poster	言語　Language　□　日本語　□　英語　□　中国語
共同演者名 Co-presenter	
学会名 Conference	
演　題 Topic	
開催日 date　　　　年　　　　月　　　　日	開催地 venue
形式　method　□　口頭発表　Oral　□　ポスター発表 Poster	言語　Language　□　日本語　□　英語　□　中国語
共同演者名 Co-presenter	
学会名 Conference	
演　題 Topic	
開催日 date　　　　年　　　　月　　　　日	開催地 venue
形式　method　□　口頭発表　Oral　□　ポスター発表 Poster	言語　Language　□　日本語　□　英語　□　中国語
共同演者名 Co-presenter	
学会名 Conference	
演　題 Topic	
開催日 date　　　　年　　　　月　　　　日	開催地 venue
形式　method　□　口頭発表　Oral　□　ポスター発表 Poster	言語　Language　□　日本語　□　英語　□　中国語
共同演者名 Co-presenter	

4．受賞（研究業績）Award (Research achievement)

名　称 Award name				
	国名 Country name		受賞年 Year of	年　　　　月
名　称 Award name				
	国名 Country name		受賞年 Year of	年　　　　月

５．本研究テーマに関わる他の研究助成金受給 Other research grants concerned with your resarch

受給実績 Receipt record	☐ 有　■ 無			
助成機関名称 Funding agency				
助成金名称 Grant name				
受給期間 Supported	年　　　月 ～		年　　　月	
受給額 Amount received	円			
受給実績 Receipt record	☐ 有　■ 無			
助成機関名称 Funding agency				
助成金名称 Grant name				
受給期間 Supported	年　　　月 ～		年　　　月	
受給額 Amount received	円			

６．他の奨学金受給 Another awarded scholarship

受給実績 Receipt record	☐ 有　■ 無			
助成機関名称 Funding agency				
奨学金名称 Scholarship				
受給期間 Supported	年　　　月 ～		年　　　月	
受給額 Amount received	円			

７．研究活動に関する報道発表 Press release concerned with your research activities

※記載した記事を添付してください。 Attach a copy of the article described below

報道発表 Press release	☐ 有　■ 無	発表年月日 Date of release	
発表機関 Released medium			
発表形式 Release method	・新聞　・雑誌　・Web site　・記者発表　・その他（　　　　　　　　　　　　　　　）		
発表タイトル Released title			

８．本研究テーマに関する特許出願予定 Patent application concerned with your research theme

出願予定 Scheduled	☐ 有　■ 無	出願国 Application	
出願内容（概要） Application contents			

９．その他 Others

None

指導責任者（記名）　　_Juki Anne_

日中笹川医学奨学金制度（学位取得コース）中間評価書
課程博士：指導教官用

第44期　　研究者番号：G4403　　　　　　　　　　作成日　：2023年3月1日

氏　名	楊　勇	YANG YONG	性別	M	生年月日　1986/07/22
所属機関（役職）	\multicolumn{5}{l}{懐化市第一人民医院神経外科（主治医師）}
研究先（指導教官）	\multicolumn{5}{l}{千葉大学社会精神保健教育研究センター 病態解析研究部門（橋本 謙二　副センター長・教授）}
研究テーマ	\multicolumn{5}{l}{脳疾患の病因解明と新規治療法の開発 Study of brain disorders and development of new therapeutic drugs}
専攻種別	\multicolumn{2}{c}{□論文博士}	\multicolumn{3}{c}{☑課程博士}

研究者評価（指導教官記入欄）

成績状況	㊲良　可　不可 学業成績係数=	取得単位数 33／30
学生本人が行った 研究の概要	\multicolumn{2}{l}{楊氏は、α7ニコチン受容体遺伝子欠損マウスのうつ様行動に横隔膜迷走神経が重要であることを示し、筆頭著者として国際誌に発表した。また本論文を学位論文として、2023年1月12日の学位論文審査会で合格した。この論文以外にもコロニー刺激性因子阻害薬の投与が、脳内ミクログリアを減少させるだけでなく、腸内細菌や細菌が生成する代謝物に影響を与えることを見出し、筆頭著者として国際誌に発表した。これらの論文以外に、共著者として7本の論文を国際誌に発表した。また肝臓疾患モデルとうつ様行動に関する論文等を3本執筆中であり、帰国までに多くの原著論文を筆頭著者として発表できると思います。}
総合評価	\multicolumn{2}{l}{【良かった点】 平日だけでなく、休日も実験に集中し、多くの論文を発表したことは特筆すべき点である。また研究室内の他の大学院生（中国からの留学生）や研究者とも共同研究を積極的に行い、多くの共著論文を発表した点は良かった。 【改善すべき点】 改善する点は特にない。 【今後の展望】 楊氏は、優秀な研究者であるので、中国に帰国した後も、医療業務や研究などに従事し、日本と中国の今後の国際共同研究に貢献していく人材になって頂きたい。}
学位取得見込	\multicolumn{2}{l}{2023年1月12日に学位審査発表会があり、無事合格したので、2023年3月に千葉大学より医学博士の学位を授与される見込みである。}

評価者（指導教官名）　　橋本謙二

Supported by
THE NIPPON FOUNDATION
日本財団

第44期　　　研究者番号：　G4403　　　　作成日：2023年2月22日

氏名	杨 勇	YANG YONG	性別	M	生年月日　1986/07/22
所属機関(役職)	懐化市第一人民医院神経外科(主治医師)				
研究先(指導教官)	千葉大学社会精神保健教育研究センター病態解析研究部門(橋本 謙二　副センター長・教授)				
研究テーマ	脳疾患の病因解明と新規治療法の開発 Study of brain disorders and development of new therapeutic drugs				
専攻種別	論文博士		□	課程博士	☑

1．研究概要(1)

1）目的（Goal）According to the World Health Organization, about 300 million people worldwide suffer from depression and more than 800,000 die by suicide each year.In addition, about 30% of patients with depression were patients with treatment-resistant depression that did not respond to existing antidepressants.Ketamine, a drug used in anesthetics, is one of the most concerned drugs in the field of psychiatry because of its rapid antidepressant effect and its effect on reducing the suicidal tendency in patients with drug-resistant depression.(R,S)-ketamine is a racemic mixture of equal amounts of (R)-ketamine (or arketamine) and (S)-ketamine (or esketamine).In our previous study, arketamine has been found to have more potent antidepressant-like actions than esketamine in rodents. This is the first time in the world that an action other than NMDA receptors has been reported to be related to the antidepressant effects of ketamine. Arketamine is currently being tested in phase Ⅱ clinical trials in patients with depression in the United States and Europe. However, the mechanism underlying the antidepressant effect of arketamine remains unclear.Further research on the anti-depression mechanism of ketamine will greatly benefit patients with depression around the world.

2）戦略（Approach）On the one hand, we comprehensively investigated non-coding microRNAs associated with the antidepressant effects of arketamine using the chronic social defeat stress(CSDS) model of depression. Non-coding microRNAs with differential expression are currently being studied. On the other hand, we established a depression-like mouse model of systemic inflammation caused by peripheral organ lesions such as hepatobiliary system and evaluated the protective effect of arketamine.In addition, we also studied the effect of subdiaphragmatic vagotomy(SDV) in a variety of depression-like mice model.

3）材料と方法（Materials and methods）(1). Animals: Male adult C57BL/6NCr mice were purchased from the Japan SLC. (Hamamatsu, Shizuoka, Japan). (2). Reagents: Arketamine hydrochloride was prepared as our previously method. The dose (10mg/Kg as hydrochloride salt) of arketamine was dissolved in the saline, also as our described previously. (3).CSDS: The C57BL/6 mice were exposed to a different CD1 aggressor mouse for 10 min each day for a total of 10 days. The resident CD1 mouse and the invader mouse were kept in one half of the cage after the social defeat session concluded, separated by a perforated Plexiglas divider to allow visual, olfactory, and auditory interaction for the remaining 24h. (4). Small RNA sequencing and data processing: Total RNA is extracted from blood and brain tissue respectively, and then PCR amplification is carried out, and then library is built. The raw sequencing data are called raw tags. The raw tags were processed using the following steps: remove low quality tags; remove tags with 5 primer contaminants; remove tags without 3 primer; remove tags without insertion; remove tags with poly A; remove tags shorter than 18 nt. After filtering, the clean tags were mapped to the reference genome and other sRNA database including miRbase, siRNA, piRNA and snoRNA with Bowtie2. Particularly, cmsearch was performed for Rfam mapping.The software miRDeep2 was used to predict novel miRNA by exploring the secondary structure, and Piano was used to predict piRNAs. RNAhybrid,miRanda and TargetScan were used to predict target genes of miRNAs. The small RNA expression level is calculated by counting absolute numbers of molecules using unique molecular identifiers. Differential expression analysis was performed using the DEGseq, Q value≤ 0.001 and the absolute value of Log2Ratio ≥ 1 as the default threshold to judge the significance of expression difference. To annotate gene functions, all target genes were aligned against the Kyoto Encyclopedia of Genes (KEGG) and Gene Ontology (GO) database. GO enrichment analysis and KEGG enrichment analysis of target genes were performed using phyper, a function of R. The P-value was corrected using the Bonferroni method, and a corrected P-value ≤ 0.05 was taken as a threshold. GO terms or KEGG terms fulfilling this condition were defined as significantly enriched terms.

1．研究概要（2）

(5). 70% Hepatic Ischemia-Reperfusion Injury (HIRI): 70% HIRI or sham surgery was performed under continuous inhalation anesthesia with 4-5% isoflurane by using an inhalation small animal anesthesia apparatus (KN-1071 NARCOBIT-E; Natsume Seisakusho, Tokyo, Japan), as previously method with a slight modification. Briefly, each mouse was placed in the supine position, after the mice were fully anesthetized, the abdominal operation area was prepared with skin. Then the skin is disinfected with iodophor disinfectant. A median incision of approximately 1.5cm in length was made along the midline of the abdomen, starting 0.5cm below the xiphoid process. The incision was gently opened with Mini incision spreader to expose the underlying liver tissue. The liver tissue was carefully pushed upward using a small cotton ball moistened with physiological saline solution and with the aid of an animal surgical microscope (Leica, Heidelberg, Germany), the fascia between the caudate lobe and the left lobe of the liver was sharply cut and a wet cotton ball was inserted between the right lobe and middle lobe of the liver to fully expose the hilar area. A mini arterial clip was placed to block blood supply to the left and middle lobes of the liver, preserving blood flow to the right and caudate lobes. At this time, we would observe that the left lobe and middle lobe of the liver changed from normal bright red to earthen yellow immediately, while the posterior lobe and caudate lobe remained bright red, and it was considered that the model of partial liver ischemia was successfully established. After the ischemia modeling was successful, mice were supplemented with about 0.5ml of normal saline in the abdominal cavity, and the abdomen was fully closed. After the mice were covered with wet gauze, the mice were placed in a warm chamber at 32℃ for 1 hour for partial liver ischemia. After the ischemia process was completed, the mice were removed from the warm chamber, the mini arterial clip and the wet cotton ball were carefully removed after re-opening the abdomen. It was observed that the ischemic liver lobe immediately changed back from earthen yellow to bright red, which was considered as a successful model of postischemia-reperfusion. After that, no bleeding was detected, and no additional injury of liver and other organs was checked, the liver tissue was returned to its original normal position gently. Then 5-0 surgical silk sutures were used to suture the abdominal incision muscle and skin layers layer by layer, ensuring aseptic operation throughout the operation. During the sham operation, the abdominal wall incision of the same size was made in the same way at the same site. After the hilar region was also fully exposed but not place a mini arterial clip to block blood supply to the live. The other remaining steps were performed according to the same protocol as the surgery group. (6)Behavioral tests. (7).RT-PCR. (8). Western blot. (9).ELISA. (10). 16s rRNA sequencing. (11).Bilateral subdiaphragmatic vagotomy.

4）実験結果（Results）(1).Differentially expressed non-coding RNA has been found in both blood and brain tissue of CSDS model mice, and the sample size is now being expanded for RT-PCR validation.(2).The presence of depression-like phenotype was detected by behavioral tests in mice with peripheral organ lesions, and there were also changes in plasma inflammatory cytokines and synaptic proteins in brain tissue. Arketamine blocked these series of changes.(3).SDV have also been shown to block these series of changes such as depression-like phenotypes et al.

5）考察（Discussion）Clinical epidemiological studies have found that depression co-exists with many other systemic diseases. Therefore, further studies to determine whether depression has a common pathogenesis with other diseases, or whether organic lesions of other organs have inducing effects on the pathogenesis of depression, will be conducive to in-depth understanding of the pathogenesis of depression.The research on the epigenetic effects of Arketamine in the anti-depression effect, which has attracted the most attention at present, will be conducive to further in-depth and comprehensive understanding of the mechanism of action of Arketamine, and will benefit the majority of patients with depression.

6）参考文献（References）(1). Hashimoto K. Rapid-acting antidepressant ketamine, its metabolites and other candidates: A historical overview and future perspective. Psychiatry Clin Neurosci. 2019;73(10):613-627. doi:10.1111/pcn.12902.(2). Hashimoto K. Molecular mechanisms of the rapid-acting and long-lasting antidepressant actions of (R)-ketamine. Biochem Pharmacol. 2020;177:113935. doi:10.1016/j.bcp.2020.113935.(3). Wei Y, Chang L, Hashimoto K. A historical review of antidepressant effects of ketamine and its enantiomers. Pharmacol Biochem Behav. 2020;190:172870. doi:10.1016/j.pbb.2020.172870.(4). Wei Y, Chang L, Hashimoto K. Molecular mechanisms underlying the antidepressant actions of arketamine: beyond the NMDA receptor. Mol Psychiatry. 2022;27(1):559-573. doi:10.1038/s41380-021-01121-1.(5). Wang X, Yang J, Hashimoto K. (R)-ketamine as prophylactic and therapeutic drug for neurological disorders: Beyond depression. Neurosci Biobehav Rev. 2022;139:104762. doi:10.1016/j.neubiorev.2022.104762.(6). Zhang K, Hashimoto K. An update on ketamine and its two enantiomers as rapid-acting antidepressants. Expert Rev Neurother. 2019;19(1):83-92. doi:10.1080/14737175.2019.1554434.(7). Zhang JC, Yao W, Hashimoto K. Arketamine, a new rapid-acting antidepressant: A historical review and future directions. Neuropharmacology. 2022;218:109219. doi:10.1016/j.neuropharm.2022.109219.(8). Yang C, Yang J, Luo A, Hashimoto K. Molecular and cellular mechanisms underlying the antidepressant effects of ketamine enantiomers and its metabolites. Transl Psychiatry. 2019;9(1):280. Published 2019 Nov 7. doi:10.1038/s41398-019-0624-1.

2．執筆論文　Publication of thesis　※記載した論文を添付してください。Attach all of the papers listed below.

論文名 1 Title	(R)-ketamine ameliorates demyelination and facilitates remyelination in cuprizone-treated mice: A role of gut-microbiota-brain axis				
掲載誌名 Published journal	Neurobiology of Disease				
	2022 年　4 月	165　巻（号）	105635 頁 ～　　頁	言語 Language	English
第1著者名 First author	Xingming Wang	第2著者名 Second author	Lijia Chang	第3著者名 Third author	Xiayun Wan
その他著者名 Other authors	Yunfei Tan, Youge Qu, Jiajing Shan, Yong Yang, Li Ma and Kenji Hashimoto				
論文名 2 Title	Gut-microbiota-brain axis in the vulnerability to psychosis in adulthood after repeated cannabis exposure during adolescence				
掲載誌名 Published journal	European Archives of Psychiatry and Clinical Neuroscience				
	2022 年　6 月	272　巻（号）	1297 頁 ～　1309 頁	言語 Language	English
第1著者名 First author	Xiayun Wan	第2著者名 Second author	Akifumi Eguchi	第3著者名 Third author	Youge Qu
その他著者名 Other authors	Yong Yang, Lijia Chang, Jiajing Shan, Chisato Mori and Kenji Hashimoto				
論文名 3 Title	Effects of (R)-ketamine on reduced bone mineral density in ovariectomized mice: A role of gut microbiota				
掲載誌名 Published journal	Neuropharmacology				
	2022 年　8 月	213　巻（号）	109139 頁 ～　　頁	言語 Language	English
第1著者名 First author	Xiayun Wan	第2著者名 Second author	Akifumi Eguchi	第3著者名 Third author	Yuko Fujita
その他著者名 Other authors	Li Ma, Xingming Wang, Yong Yang, Youge Qu, Lijia Chang, Jiancheng Zhang, Chisato Mori and Kenji Hashimoto				
論文名 4 Title	Long-lasting beneficial effects of maternal intake of sulforaphane glucosinolate on gut microbiota in adult offspring				
掲載誌名 Published journal	The Journal of Nutritional Biochemistry				
	2022 年　11 月	109　巻（号）	109098 頁 ～　　頁	言語 Language	English
第1著者名 First author	Yan Wei	第2著者名 Second author	Lijia Chang	第3著者名 Third author	Guoqi Liu
その他著者名 Other authors	Xingming Wang, Yong Yang and Kenji Hashimoto				
論文名 5 Title	Key role of the gut-microbiota-brain axis via the subdiaphragmatic vagus nerve in demyelination of the cuprizone-treated mouse brain				
掲載誌名 Published journal	Neurobiology of Disease				
	2023 年　1 月	176　巻（号）	105951 頁 ～　　頁	言語 Language	English
第1著者名 First author	Xingming Wang	第2著者名 Second author	Akifumi Eguchi	第3著者名 Third author	Yong Yang
その他著者名 Other authors	Lijia Chang, Xiayun Wan, Jiajing Shan, Youge Qu, Li Ma, Chisato Mori, Jianjun Yang and Kenji Hashimoto				

2．執筆論文　Publication of thesis　※記載した論文を添付してください。Attach all of the papers listed below.

論文名 6 Title	A role of gut-microbiota-brain axis via subdiaphragmatic vagus nerve in depression-like phenotypes in *Chrna7* knock-out mice					
掲載誌名 Published journal	Progress in Neuro-Psychopharmacology and Biological Psychiatry					
	2023 年　1 月	120　巻（号）	110652 頁 ～　　頁	言語 Language	English	
第1著者名 First author	Yong Yang	第2著者名 Second author	Akifumi Eguchi	第3著者名 Third author	Xiayun Wan	
その他著者名 Other authors	Lijia Chang, Xingming Wang, Youge Qu, Chisato Mori and Kenji Hashimoto					
論文名 7 Title	Repeated use of 3,4-methylenedioxymethamphetamine is associated with the resilience in mice after chronic social defeat stress: A role of gut-microbiota-brain axis					
掲載誌名 Published journal	Psychiatry Research					
	2023 年　2 月	320　巻（号）	115020 頁 ～　　頁	言語 Language	English	
第1著者名 First author	Youge Qu	第2著者名 Second author	Akifumi Eguchi	第3著者名 Third author	Xiayun Wan	
その他著者名 Other authors	Li Ma, Lijia Chang, Jiajing Shan, Yong Yang, Chisato Mori and Kenji Hashimoto					
論文名 8 Title	Impact of broad-spectrum antibiotics on the gut-microbiota-spleen-brain axis					
掲載誌名 Published journal	Brain, Behavior, & Immunity - Health					
	2023 年　2 月	27　巻（号）	100573 頁 ～　　頁	言語 Language	English	
第1著者名 First author	Xiayun Wan	第2著者名 Second author	Akifumi Eguchi	第3著者名 Third author	Akemi Sakamoto	
その他著者名 Other authors	Yuko Fujita, Yong Yang, Youge Qu, Masahiko Hatano, Chisato Mori and Kenji Hashimoto					
論文名 9 Title						
掲載誌名 Published journal						
	年　　月	巻（号）	頁 ～　　頁	言語 Language		
第1著者名 First author		第2著者名 Second author		第3著者名 Third author		
その他著者名 Other authors						
論文名 10 Title						
掲載誌名 Published journal						
	年　　月	巻（号）	頁 ～　　頁	言語 Language		
第1著者名 First author		第2著者名 Second author		第3著者名 Third author		
その他著者名 Other authors						

3．学会発表 Conference presentation ※筆頭演者として総会・国際学会を含む主な学会で発表したものを記載してください

※Describe your presentation as the principal presenter in major academic meetings including general meetings or international meetin

学会名 Conference	The 9th International Human Microbiome Consortium (IHMC) Congress 2022						
演 題 Topic	A role of subdiaphragmatic vagus nerve in depressive-like phenotypes in *Chrna7* knock-out mice						
開催日 date	2022　年　11　月　8　日	開催地 venue	Kobe				
形式 method	□　口頭発表 Oral　☑ ポスター発表 Poster	言語 Language	□　日本語　☑　英語　□　中国語				
共同演者名 Co-presenter							
学会名 Conference							
演 題 Topic							
開催日 date	年　　月　　日	開催地 venue					
形式 method	□　口頭発表 Oral　□ ポスター発表 Poster	言語 Language	□　日本語　□　英語　□　中国語				
共同演者名 Co-presenter							
学会名 Conference							
演 題 Topic							
開催日 date	年　　月　　日	開催地 venue					
形式 method	□　口頭発表 Oral　□ ポスター発表 Poster	言語 Language	□　日本語　□　英語　□　中国語				
共同演者名 Co-presenter							
学会名 Conference							
演 題 Topic							
開催日 date	年　　月　　日	開催地 venue					
形式 method	□　口頭発表 Oral　□ ポスター発表 Poster	言語 Language	□　日本語　□　英語　□　中国語				
共同演者名 Co-presenter							

4．受賞（研究業績） Award（Research achievement）

名 称 Award name					
	国名 Country		受賞年 Year of award	年	月
名 称 Award name					
	国名 Country		受賞年 Year of award	年	月

5. 本研究テーマに関わる他の研究助成金受給 Other research grants concerned with your research theme

受給実績 Receipt record	■ 有　　□ 無							
助成機関名称 Funding agency	Academic Research & Innovation Man-agement Organization of Chiba University							
助成金名称 Grant name	全方位イノベーション創発博士人材養成プロジェクト							
受給期間 Supported period	2021　年　10　月　〜　2023　年　3　月							
受給額 Amount received	1,220,000 円							
受給実績 Receipt record	□ 有　　□ 無							
助成機関名称 Funding agency								
助成金名称 Grant name								
受給期間 Supported period	年　　　月　〜　　　年　　　月							
受給額 Amount received	円							

6. 他の奨学金受給 Another awarded scholarship

受給実績 Receipt record	□ 有　　■ 無
助成機関名称 Funding agency	
奨学金名称 Scholarship name	
受給期間 Supported period	年　　　月　〜　　　年　　　月
受給額 Amount received	円

7. 研究活動に関する報道発表 Press release concerned with your research activities

※記載した記事を添付してください。Attach a copy of the article described below

報道発表 Press release	□ 有　　■ 無	発表年月日 Date of release	
発表機関 Released medium			
発表形式 Release method	・新聞　・雑誌　・Web site　・記者発表　・その他（　　　　　　　　　　　　）		
発表タイトル Released title			

8. 本研究テーマに関する特許出願予定 Patent application concerned with your research theme

出願予定 Scheduled	□ 有　　■ 無	出願国 Application	
出願内容（概要） Application contents			

9. その他 Others

I have been completed the defense of the doctoral program, and will obtain the doctoral certificate in March 2023. From April, I will continue my scientific research in the Division of Clinical Neuroscience, Chiba University Center for Forensic Mental Health as a assistant professor.

指導責任者（記名）　　橋本謙二
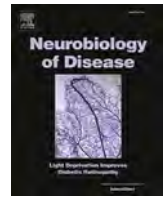
(R)-ketamine ameliorates demyelination and facilitates remyelination in cuprizone-treated mice: A role of gut–microbiota–brain axis

Xingming Wang, Lijia Chang, Xiayun Wan, Yunfei Tan, Youge Qu, Jiajing Shan, Yong Yang, Li Ma, Kenji Hashimoto[*]

Division of Clinical Neuroscience, Chiba University Center for Forensic Mental Health, Chiba 260-8670, Japan

ARTICLE INFO

ABSTRACT

Multiple sclerosis (MS) is the most common demyelinating disease that attacks the central nervous system. We recently reported that the new antidepressant (R)-ketamine could ameliorate the disease progression in experimental autoimmune encephalomyelitis model of MS. Cuprizone (CPZ) has been used to produce demyelination which resembles demyelination in MS patients. This study was undertaken to investigate whether (R)-ketamine could affect demyelination in CPZ-treated mice and remyelination after CPZ withdrawal. Repeated treatment with (R)-ketamine (10 mg/kg/day, twice weekly, for 6 weeks) significantly ameliorated demyelination and activated microglia in the brain compared with saline-treated mice. Furthermore, pretreatment with ANA-12 (TrkB antagonist) significantly blocked the beneficial effects of (R)-ketamine on the demyelination and activated microglia in the brain of CPZ-treated mice. The 16S rRNA analysis showed that (R)-ketamine significantly improved abnormal composition of gut–microbiota and decreased levels of lactic acid of CPZ-treated mice. In addition, there were significant correlations between demyelination (or microglial activation) in the brain and the relative abundance of several microbiome, suggesting a link between gut microbiota and brain. Interestingly, (R)-ketamine could facilitate remyelination in the brain after CPZ withdrawal. In conclusion, the study suggests that (R)-ketamine could ameliorate demyelination in the brain of CPZ-treated mice through TrkB activation, and that gut–microbiota–microglia crosstalk may play a role in the demyelination of CPZ-treated mice. Therefore, it is likely that (R)-ketamine could be a new therapeutic drug for MS.

1. Introduction

Multiple sclerosis (MS) is the most common inflammatory demyelinating disease on the central nervous system (CNS). Symptoms of MS patients cause a major economic burden on the patients, their families and caregivers, employers, and the healthcare system (Dahham et al., 2021; Nicholas et al., 2021). Therefore, the development of new drugs to attenuate demyelination and to facilitate remyelination in MS patients is an unmet medical need.

Increasing preclinical findings demonstrated that the new antidepressant (R)-ketamine, (R)-enantiomer of (R,S)-ketamine, has potent anti-inflammatory effects in several animal models (Fujita and Hashimoto, 2020; Fujita et al., 2020; Fujita et al., 2021; Qu et al., 2021; Xiong et al., 2019; Yang et al., 2015; Yang et al., 2018; Yao et al., 2021; Zhang et al., 2014; Zhang et al., 2018; Zhang et al., 2020; Zhang et al., 2021a; Zhang et al., 2021b; Zhang et al., 2021c). Interestingly, side effects of (R)-ketamine in animals and humans were lower than those of (R,S)-ketamine and (S)-ketamine (Bonaventura et al., 2021; Chang et al., 2019; Hashimoto et al., 2017; Leal et al., 2021; Tan and Hashimoto, 2020; Tian et al., 2018; Yang et al., 2015; Yang et al., 2016b). Collectively, (R)-ketamine could be a novel anti-inflammatory drug without ketamine-like side effects (Hashimoto, 2019; Hashimoto, 2020; Yang et al., 2019; Wei et al., 2020; Wei et al., 2021a; Zhang and Hashimoto, 2019).

It is well recognized that MS patients have high rates of depression (Jones et al., 2021; Skokou et al., 2012). Given high incidence of depression in MS patients, we recently reported that (R)-ketamine could ameliorate the disease progression in experimental autoimmune

---

encephalomyelitis model of MS (Wang et al., 2021a). Cuprizone (CPZ), a selective and sensitive copper-chelating agent, has been used to produce the toxic demyelination that resembles demyelination in MS patients (Procaccini et al., 2015; Torkildsen et al., 2008; Zhan et al., 2020). Interestingly, spontaneous remyelination can be observed as early as 4 days after CPZ withdrawal, indicating that CPZ model could be excellent to discover potential therapeutic drugs which can prevent demyelination and stimulate remyelination (Franklin and Ffrench-Constant, 2017; Torkildsen et al., 2008).

The present study was undertaken to investigate whether (*R*)-ketamine could affect demyelination and remyelination in CPZ-treated mice. Furthermore, we examined the role of TrkB in the effects of (*R*)-ketamine in CPZ -treated mice since brain-derived neurotrophic factor (BDNF) and its receptor TrkB plays a role in the beneficial effects of (*R*)-ketamine in other animal models such as depression, Parkinson's disease, osteoporosis, and ulcer colitis (Fujita et al., 2020; Fujita et al., 2021; Tan et al., 2020; Tan et al., 2022; Yang et al., 2015). Accumulating evidence shows the role of gut microbiota in pathogenesis of MS (Cantarel et al., 2015; Cekanaviciute et al., 2017; Farshbafnadi et al., 2021; Ghezzi et al., 2021; Maghzi and Weiner, 2020; Parodi and Kerlero de Rosbo, 2021; The iMSMS Consortium, 2020). Finally, we examined the role of gut microbiota in the effects of (*R*)-ketamine in CPZ model since gut–microbiota–brain axis may play a role in the antidepressant-like effects of (*R*)-ketamine in rodents (Qu et al., 2017; Yang et al., 2017).

2. Materials and methods

2.1. Animals

Adult male C57BL/6J mice (8–10 weeks old, body weight 19–22 g, Japan SLC, Inc., Hamamatsu, Japan) were acclimated housed under controlled temperatures and 12 h light/dark cycles (lights on between 07:00 and 19:00 h) with food (CE-2; CLEA Japan, Inc., Tokyo, Japan) and water ad libitum. The experimental protocol was approved by the Chiba University Institutional Animal Care and Use Committee (Permission number: 1–466). This study was carried out in strict accordance with the recommendations in the Guide for the Care and Use of Laboratory Animals of the National Institutes of Health, USA. Animals were deeply anesthetized with isoflurane before being killed by cervical dislocation. All efforts were made to minimize suffering.

2.2. Cuprizone (CPZ) model

CPZ model was induced by feeding mice with 0.2% *w*/w cuprizone (bis-cyclohexanone oxaldihydrazone; catalog number: B0476, Tokyo Chemical Industry Co., Ltd. Tokyo, Japan,) in powder chow. Mice received 0.2% CPZ food pellets for demyelination (6 weeks) and remyelination (6 weeks followed by 2 weeks normal chow) paradigms. Chow was replaced three times a week. Age-matched untreated controls were fed powder chow without CPZ.

2.3. Reagents

(*R*)-ketamine hydrochloride was prepared as described previously (Zhang et al., 2014). The dose (10 mg/kg as hydrochloride salt, I.P.) of (*R*)-ketamine was dissolved in the saline, as described previously (Qu et al., 2021; Yang et al., 2015; Yang et al., 2018; Zhang et al., 2021c). ANA-12, N2-(2-{[(2-oxoazepan-3-yl) amino] carbonyl} phenyl) benzo [*b*]thiophene-2-carboxamide (0.5 mg/kg, I.P., Sigma–Aldrich Co., Ltd., Tokyo, Japan), was dissolved in 17% dimethylsulfoxide (DMSO) in saline (Fujita et al., 2020; Ren et al., 2015; Tan et al., 2020; Tan et al., 2022; Zhang et al., 2015).

2.4. Collection of fecal samples from mice

Fresh mouse fecal samples were collected at around 9:00 a.m. and

then placed into sterilized screw-cap microtubes. Then the microtube containing mouse fecal samples was immediately placed into liquid nitrogen and stored under −80 °C until use.

2.5. 16S rRNA analysis of feces

Extraction of DNA from fecal samples and 16S rRNA analysis were done at MyMetagenome Co, Ltd. (Tokyo, Japan), as previously described (Kim et al., 2013; Pu et al., 2021; Shinno-Hashimoto et al., 2021; Wang et al., 2020; Wang et al., 2021b). Briefly, the common primer 27Fmod (5′-AGRGTTTGATYMTGGCTCAG-3′) and 338R (5′-TGCTGCCTCCCGTAGGAGT-3′) were used to amplify the V1–V2 region of the bacterial 16S rRNA gene by polymerase chain reaction (PCR).

α-diversity was analyzed by Shannon, the observed OTUs. β-diversity was measured by the principal component analysis (PCA) and principal coordinates analysis (PCoA) and statistical significance was done by analysis of similarities (ANOSIM). Linear discriminant analysis (LDA) effect size (LEfSe) (Segata et al., 2011) was based on the bacterial abundance to explore significant differential biomarkers between groups with different taxonomic levels (http://huttenhower.sph. harvard.edu/galaxy/). Only taxa with LDA scores >4.0 and *p* value <0.05 were considered significantly enriched. The results with taxonomic bar charts and cladograms were visualized.

2.6. Determination of short-chain fatty acids (SCFAs)

The levels of short chain fatty acids (SCFAs) (i.e., succinic acid, lactic acid, acetic acid, malic acid, butyric acid) in stool samples were determined at TechnoSuruga Laboratory, Co., Ltd. (Shizuoka, Japan), as reported previously (Pu et al., 2021; Shinno-Hashimoto et al., 2021; Wang et al., 2020; Wei et al., 2021b; Zhang et al., 2019). The results of SCFAs were recorded as milligrams per gram of excrement.

2.7. Histopathology and immunofluorescence

The mice were anesthetized with 5% isoflurane and sodium pentobarbital (50 mg/kg), and perfused transcardially with isotonic saline and ice-cold 4% paraformaldehyde in 0.1 mM phosphate buffer (30 ml per mouse, pH 7.4). Then the brain was collected, post-fixed overnight at 4 °C, and cut into 30 μm slice by vibratome (VT1000S, Leica Microsystems AG, Wetzlar, Germany). The slices were selected from bregma 1.10 to −0.58 in mice brain for immunofluorescence. The immunofluorescence is performed as reported previously (Wang et al., 2021a). Briefly, the slices were washed with 0.1 mM phosphate buffer three times for 15 mins and blocked with 3% BSA with 0.3% TritonX-100 for 2 h. Incubation with primary antibody [mouse, anti-MBP (myelin basic protein), Catalog number: sc-271,524, Santa Cruz Biotechnology, Inc., CA, USA, 1:100; rabbit, anti-Iba1, Catalog number: 019–19,741, Fuji-Film Wako Pure Chemical Corporation, Tokyo, Japan, 1:250] was conducted overnight at 4 °C, then the slices were incubated by secondary antibody (Alexa Fluor 546 goat anti-mouse IgG$_1$, 1:1000; Alexa Fluor 488 donkey anti-rabbit IgG, 1:1000) for 2 h at room temperature. Then the slices were washed by 0.1 mM phosphate buffer with 0.1% tween-20 for three times for 15 mins, and were coverslipped with mounting medium with DAPI (4′,6′-diamino-2-phenylindole, Catalog number: H-1200, Vector laboratories, Inc., USA) and analyzed by Keyence BZ-900 microscope (Tokyo, Japan) and Image J software.

2.8. Statistical analysis

Data represent the mean ± standard error of the mean (S.E.M.). The demyelination area in MBP immunofluorescence, Iba1-positive area and SCFA levels were analyzed by one-way analysis of variance (ANOVA), followed by Fisher's least significant difference (LSD) test. The Kruskal-Wallis test with Dunn's post-hoc test was utilized to analyze the α-diversity data of the gut microbiota and the relative bacterial abundance

at different level. For β-diversity of the gut microbiota, principal component analysis (PCA) of OUT level, Principal Coordinates Analysis (PCoA) and the unweighted UniFrac phylogenetic distance were performed using analysis of similarities (ANOSIM) by R package vegan (2.5.4) (Xia and Sun, 2017; Wei et al., 2021b). Correlation between demyelination and Iba1 expression was analyzed using Pearson correlation analysis. Correlations among SCFA levels, demyelination area, Iba1 positive area or the relative abundance of bacteria were analyzed using Spearman rank test. Integrative network of associations between the relative abundance of microbiota and SCFAs, Iba1-positive area, or demyelination area were tested with Spearman's analysis and visualized by Cytoscape (Version 3.8.1). The level of significance was set as $P <$ 0.05 for all analyses.

3. Results

3.1. Effects of (R)-ketamine on the demyelination and microglia activation of CPZ-treated mice

(R)-ketamine or saline was injected to mice twice per week for 6 weeks (Fig. 1A). To examine the role of TrkB signaling, vehicle or TrkB antagonist ANA-12 was injected to mice 30 mins before (R)-ketamine (or saline) administration (Fig. 1A). The demyelination area in the brain was examined using MBP immunofluorescence. The feeding of CPZ for 6 weeks caused complete demyelination in the corpus callosum of mice (Fig. 1B, C, E). Treatment of (R)-ketamine significantly ameliorated the demyelination area in the corpus callosum of CPZ-treated mice. Furthermore, effects of (R)-ketamine were significantly blocked by ANA-12 (Fig. 1B, C, E). Moreover, ANA-12 alone did not affect the demyelination area in the corpus callosum of CPZ-treated mice (Fig. 1B, C, E). Collectively, (R)-ketamine could ameliorate the demyelination in the brain of CPZ-treated mice through TrkB activation.

It is reported that microglial activation plays a key role in MS development (Deng and Sriram, 2005; Kalafatakis and Karagogeos, 2021; Mayrhofer et al., 2021). In this study, we performed immunofluorescence of the microglial marker Iba1 in the corpus callosum of CPZ-treated mice. In the control + saline group, Iba1-positive cells were broadly and evenly distributed in the corpus callosum of mice, indicating that these cells were small and ramified, a morphology typical of resting microglia (Fig. 1B, D, F). In the corpus callosum of CPZ + saline group, there was a robust increase in the area of Iba1-positive staining compared with control +saline group. Treatment of (R)-ketamine significantly attenuated the Iba1-positive area in the corpus callosum of CPZ-treated mice. Furthermore, ANA-12 significantly blocked the effects of (R)-ketamine on Iba1-positive staining in the corpus callosum of CPZ-treated mice (Fig. 1B, D, F). Furthermore, ANA-12 alone did not affect the demyelination area in the CPZ-treated mice (Fig. 1B, D, F). There was a significant positive correlation [$r = 0.6995$, $P < 0.001$] between demyelination area and Iba1-positive area (Fig. 1G), suggesting a link between demyelination and microglial activation. Collectively, (R)-ketamine could ameliorate the microglia activation in the brain of CPZ-treated mice through TrkB activation.

3.2. Composition of gut microbiota

The composition of the gut microbiota among control + saline group, CPZ + saline group, CPZ + (R)-ketamine group was analyzed using α- and β-diversity. For α-diversity, there were no differences in the Shannon and observed_OTUs among the three groups (Fig. 2A and B). Regarding β-diversity, PCA and PCoA were applied to analyze the bacterial community composition of gut microbiota among the three groups. PCA revealed significant separation in the community composition evaluated by ANOSIM ($R = 0.6231$, $P = 0.001$) (Fig. 2C) based on the OTU level. The ordination of unweighted UniFrac distance by PCoA revealed separation of among three groups using the ANOSIM ($R = 0.7128$, $P = 0.001$) (Fig. 2D). Importantly, boxplot of Unweighted

Unifrac distance by Wilcox rank tests showed that the β-diversity among the three groups were significant difference ($R = 0.7128$, $P = 0.001$) (Fig. 2E). Collectively, (R)-ketamine could ameliorate abnormal β-diversity of gut microbiota in the CPZ-treated mice.

3.3. Altered composition in the gut microbiota at different levels

At the phylum level, the relative abundance of *Proteobacteria* in the CPZ + (R)-ketamine group was significantly lower than that of the CPZ + saline group (Fig. 3A and B). At genus level, there were significant differences in the relative abundance of *Eisenbergiella, Barnesiella, Prevotella, Butyrivibrio, Faecalibaculum, Dorea, Parabacteroides, Turicibacter, Mailhella, Parvibacter,* and *Mordavella* among the three groups (Fig. 3C, D, Table S1). Furthermore, at species level, the relative abundances of *Eisenbergiella massiliensis, Barnesiella viscericola, Lactobacillus murinus, Lactobacillus intestinalis, [Clostridium] bolteae, Butyrivibrio proteoclasticus, Faecalibaculum rodentium, Prevotella loescheii, Bacteroides sartorii,* and *Eubacterium ramulus* were significant different among the three groups (Fig. 3E, F, Table S2).

3.4. LEfSe analysis

The gut microbiota changes of the abundant taxa among Control + saline group, CPZ + saline group, CPZ + (R)-ketamine group were analyzed using the LEfSe algorithm, which permits the identification of microbial markers that are more important in one group than in another group. The color differences illustrated differences in the abundant taxa among the groups (Kwak et al., 2020). LEfSe analysis showed that (R)-ketamine produced significant different effects on gut microbiota (Fig. 4A). The species level phylotype including *Lactobacillus_murinus, Clostridium bolteae, E. ramulus,* and *Clostridium aminophilum* were identified as potential gut microbial markers for control + saline group (Fig. 4B). Two species level phylotypes including the *Eisenbergiella_massiliensis, B. proteoclasticus* were identified as potential gut microbial markers for CPZ + saline group (Fig. 4B). Four species level phylotypes including *Lactobacillus_intestinalis, Barnesiella_viscericola, Faecalibaculum_rodentium,* and *Prevotella_loescheii* were identified as potential gut microbial markers for CPZ + (R)-ketamine group in mice (Fig. 4B and Table S3).

3.5. Levels of SCFAs in the fecal samples and correlations among bacterial relative abundance, SCFAs, demyelination area, or Iba1-positive area

The concentration of lactic acid was significantly lower in the CPZ + saline group than that in control + saline group and CPZ + (R)-ketamine group (Fig. 5A). In contrast, there were no significant differences in the other SCFAs (succinic acid, acetic acid, malic acid, and butyric acid) among the three groups (Fig. 5A).

The heat map shown the correlations between lactic acid, demyelination, Iba1-positive area and the relative bacterial abundance that differ significantly at species level (Fig. 5B). Furthermore, the correlations (Spearman analysis $r > 0.5$, $P < 0.05$) among lactic acid, demyelination area, Iba1-positive area, the bacterial relative abundance that differ significantly with any other group were also shown in correlation network (Fig. 5C).

The concentration of lactic acid was significantly and negatively correlated with the relative abundance of *Eisenbergiella massiliensis* (Fig. 5B and C).

There were significant positive correlations between demyelination area (or Iba1-positive area) and the relative abundance of *Eisenbergiella massiliensis* or *B. proteoclasticus*. Furthermore, there were significant negative correlations between demyelination area and the relative abundance of L. *murinus, [Clostridium] bolteae*, or *E. ramulus* (Fig. 5B).

The Iba1-positive area was positively correlated with the relative abundance of *Eisenbergiella massiliensis, B. proteoclasticus. Faecalibaculum rodentium,* or *B. sartorii*. The Iba1-positive area was negatively correlated
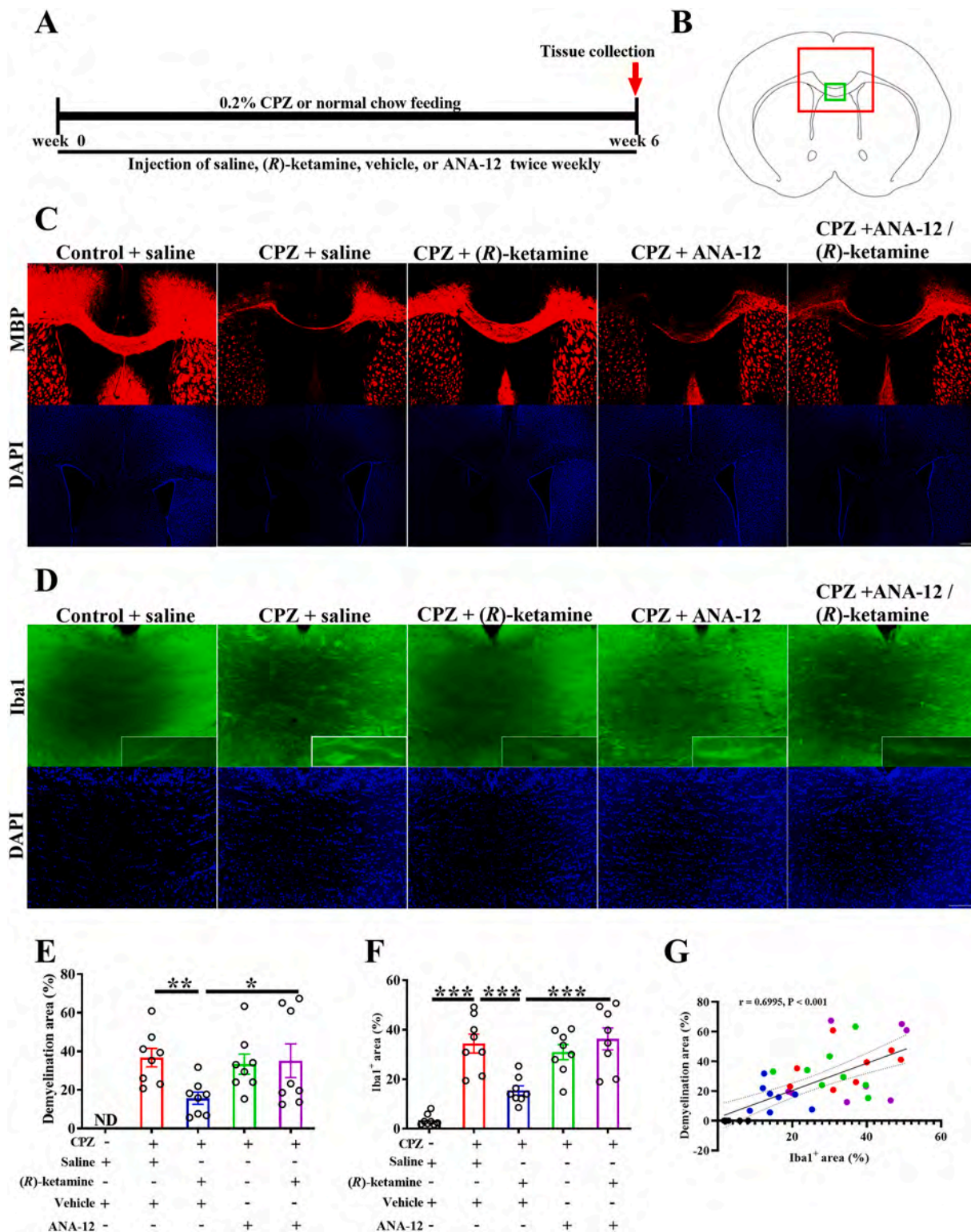
Fig. 1. Effects of (*R*)-ketamine on the demyelination of CPZ-treated mice.

A: The protocol of the experiment. B: The MBP (myelin basic protein) staining images were taken of the area outlined by the red line box. The Iba1 staining images were taken of the area outlined by the green line box. C: The representative photos of MBP and DAPI (4′,6′-diamino-2-phenylindole) in the corpus callosum of brain from Control + saline, CPZ + saline, CPZ + (*R*)-ketamine, CPZ + ANA-12, and CPZ + ANA-12/(*R*)-ketamine groups. D: The representative photos of Iba1 and DAPI in the corpus callosum of brain from Control + saline, CPZ + saline, CPZ + (*R*)-ketamine, CPZ + ANA-12, and CPZ + ANA-12/(*R*)-ketamine groups. E: Quantitative data of demyelination area in the corpus callosum (one-way ANOVA: $F_{4,35} = 9.402$, $P < 0.001$). The percentage of demyelination area was determined by the calculation [(corpus callosum area -MBP-positive area)/corpus callosum area × 100%]. *$P < 0.05$, **$P < 0.01$. F: Quantitative data of Iba1-positive area in the corpus callosum (one-way ANOVA: $F_{4,35} = 20.938$, $P < 0.001$). The percentage of Iba1-positive area was determined by the calculation [(Iba1-positive area/corpus callosum area) × 100%]. G: A positive correlation ($r = 0.6995$, $P < 0.001$) between the demyelination area and Iba1-positive area from three groups. *$P < 0.05$, **$P < 0.01$, ***$P < 0.001$. $N = 8$/group. Scale bar for MBP immunostaining was 300 μm. Scale bar for Iba1 immunostaining was 100 μm. ND ; no detectable. (For interpretation of the references to color in this figure legend, the reader is referred to the web version of this article.)
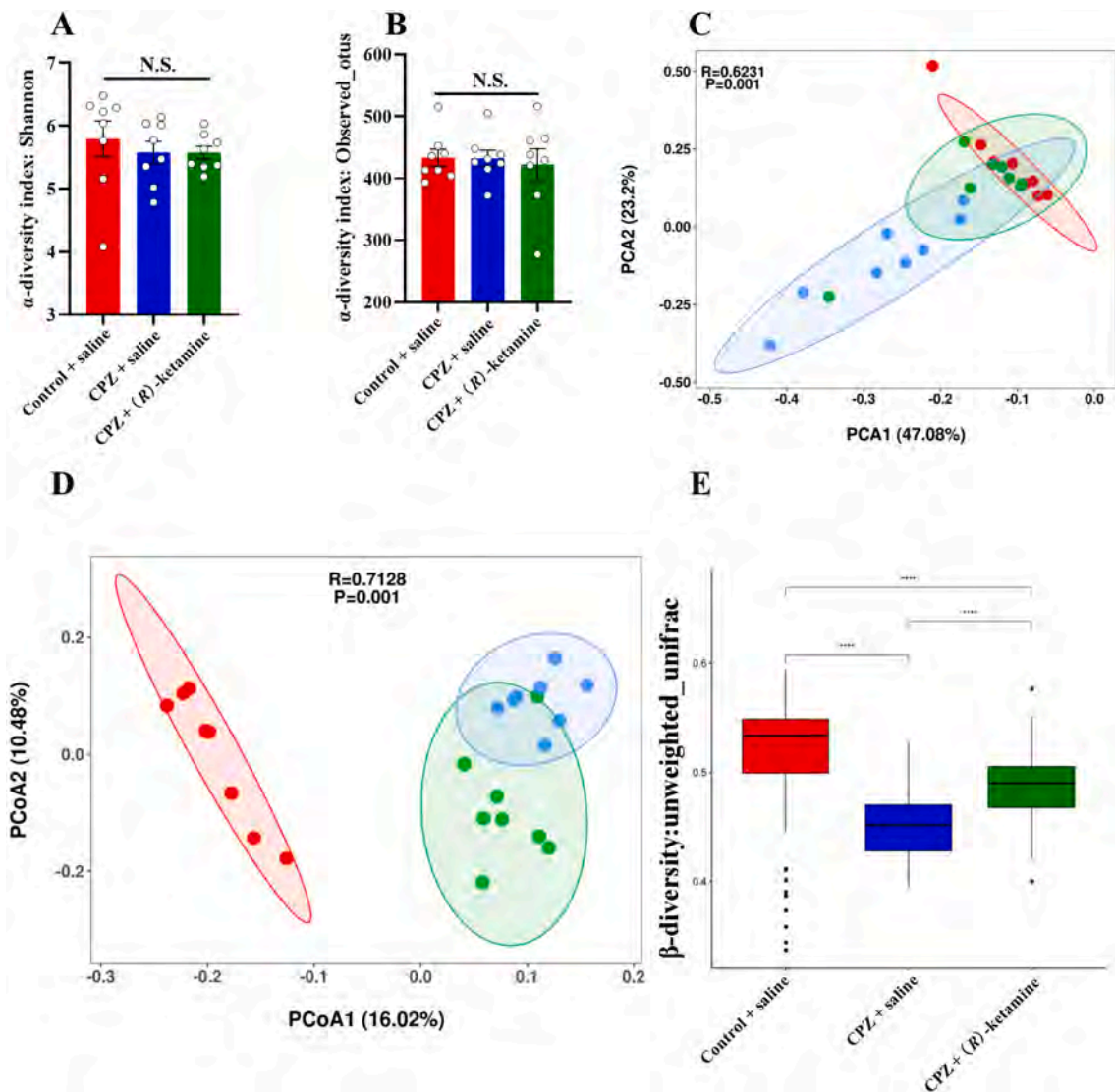
Fig. 2. Alpha-diversity and beta-diversity of gut microbiota.
A: Alpha-diversity index of shannon (Kruskal-Wallis test, H = 2.795, *P* = 0.2472). B: Alpha-diversity index of observed_otus (Kruskal-Wallis test, H = 0.1389, *P* = 0.9329). C: Principal component analysis (PCA) of beta-diversity based on the OTU level, where each point represents a single sample colored by group circle, indicated by the second principal component of 23.2% on the Y- axis and the first principal component of 47.08% on the X-axis (ANOSIM, R = 0.6231, *P* = 0.001). D: Principal Coordinates Analysis (PCoA) plot based upon unweighted UniFrac distance (ANOSIM, R = 0.7128, *P* = 0.001). Each dot represents a single sample indicated by a principal component of 16.02% on the X-axis and another principal component of 10.48% on the Y- axis, contributing to discrepancy among the three groups. E: Boxplot of beta-diversity based on Unweighted Unifrac distance (ANOSIM, R = 0.7128, *P* = 0.001). Wilcox rank tests were performed for analysis of significance of difference between groups. N = 8/group. ***P* < 0.001. N.S.: no significant.

with L. *murinus, [Clostridium] bolteae*, or *E. ramulus* (Fig. 5B).

There were also significant positive or negative correlations among the relative abundance of *B. sartorii, Eisenbergiella massiliensis, B. proteoclasticus, L. murinus, Faecalibaculum rodentium, P. loescheii, B. viscericola, E. ramulus, [Clostridium] bolteae* (Fig. 5C).

3.6. Effects of (R)-ketamine on remyelination and microglia activation in the CPZ-treated mice

During the last 2 weeks, CPZ food pellet was withdrawn. All mice were fed with normal chow (Fig. 6A). (*R*)-ketamine or saline was injected i.p. to mice twice per week for the last 2 weeks (Fig. 6A). After CPZ withdrawal, spontaneous remyelination was shown in CPZ-treated mice (Franklin and Ffrench-Constant, 2017; Torkildsen et al., 2008). Treatment with (*R*)-ketamine (10 mg/kg/day, twice weekly for 2 weeks) significantly reduced the demyelination area in the corpus callosum of CPZ-treated mice, suggesting that (*R*)-ketamine can facilitate the

remyelination in CPZ-treated mice (Fig. 6B, C, E). Furthermore, (*R*)-ketamine ameliorated the microglial activation in the corpus callosum following CPZ withdrawal (Fig. 6B, D, F). Collectively, (*R*)-ketamine could stimulate the remyelination in the brain after CPZ withdrawal through anti-inflammation.

4. Discussion

The main findings of this study are as follows: First, (*R*)-ketamine ameliorated demyelination and microglial activation in the corpus callosum of CPZ-treated mice through TrkB activation compared to saline-treated mice. There was a positive correlation between demyelination and microglial activation in the corpus callosum. Second, (*R*)-ketamine partially normalized abnormal beta-diversity of gut microbiota of CPZ-treated mice. The LEfSe algorithm identified the species *Lactobacillus_intestinalis, Barnesiella_viscericola, Faecalibaculum_rodentium*, and *Prevotella_loescheii* as specific microbial biomarkers for CPZ + (*R*)-ketamine
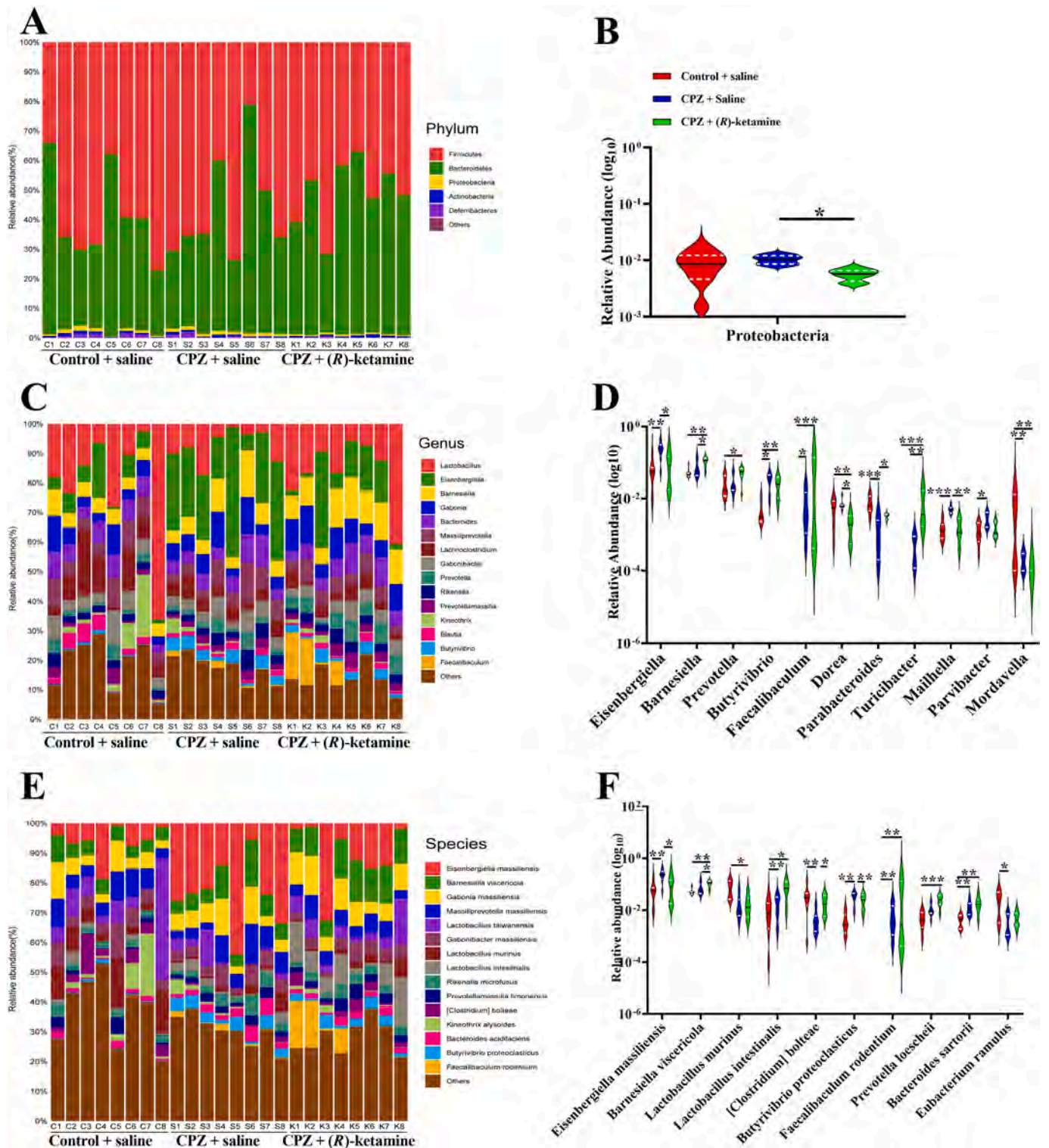
Fig. 3. Altered composition in the gut microbiota at different levels.

A, B: Phylum. Relative abundance distribution and the significantly changed bacteria among Control + saline, CPZ + saline, CPZ + (R)-ketamine group (Kruskal-Wallis test, H = 9.215, P = 0.01). C, D: Genus. Relative abundance distribution and the significantly changed bacteria among the three groups. The statistical results were in the Table S1. E, F: Species. Relative abundance distribution and the significantly changed bacteria among the three groups. N = 8/group. The statistical results were in the Table S2. *P < 0.05; **P < 0.01 ***P < 0.001.

group. Third, (R)-ketamine improved the decreased levels of lactic acid in the feces from CPZ-treated mice. Interestingly, there was a positive correlation between the relative abundance of the species *Eisenbergiella massiliensis* and lactic acid in the feces. Fourth, there were positive (or negative) correlations between the relative abundance of the species

bacteria and demyelination (or microglial activation) in the brain. Finally, (R)-ketamine significantly facilitated remyelination in the corpus callosum after CPZ withdrawal. Collectively, (R)-ketamine could attenuate demyelination of CPZ-treated mice through TrkB activation, and (R)-ketamine could facilitate remyelination in the brain after CPZ
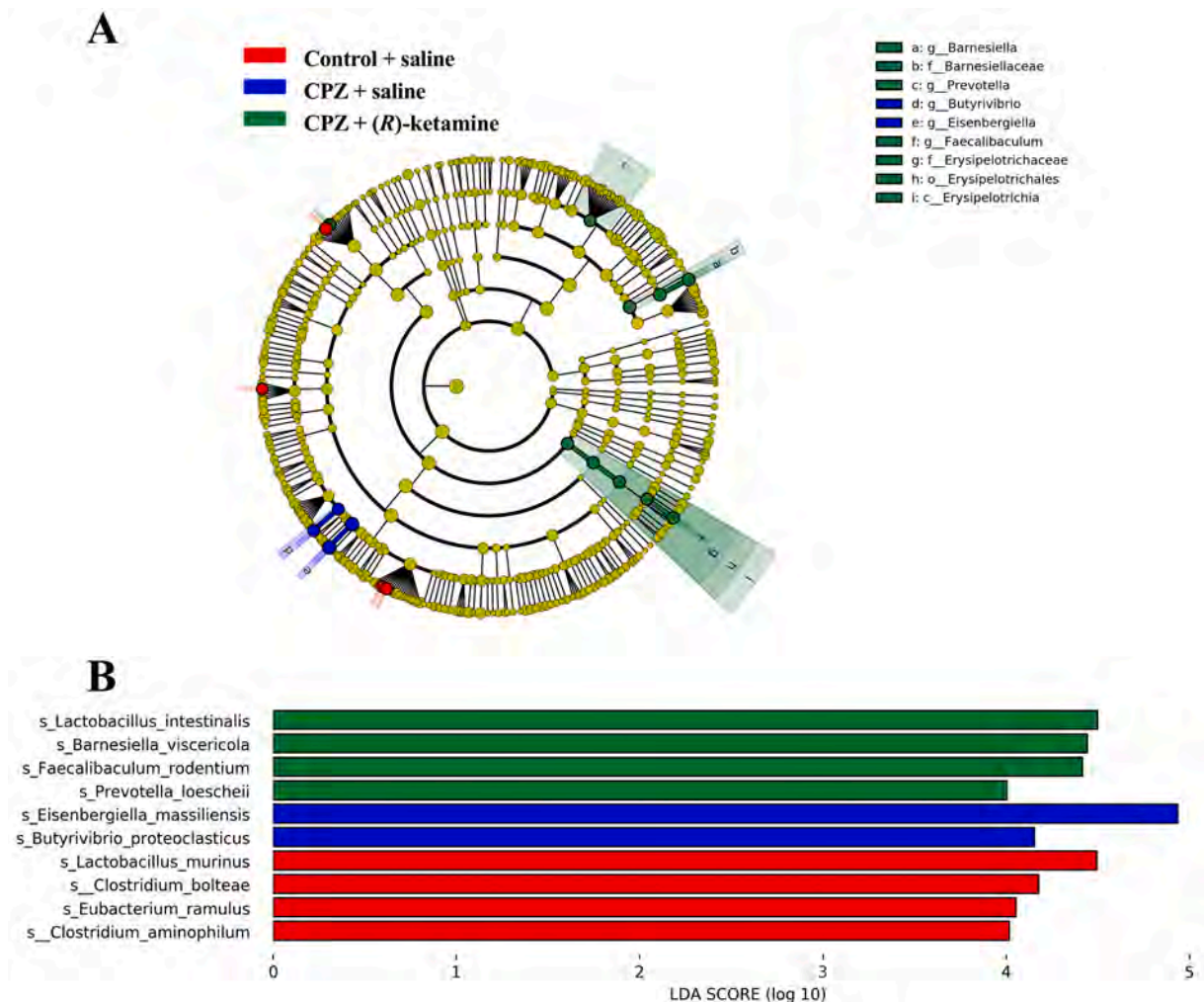
Fig. 4. The LEfSe algorithm of gut microbiota.
A: Cladogram (LDA score > 4.0, P < 0.05) showed the taxonomic distribution difference among Control + saline, CPZ + saline, CPZ + (*R*)-ketamine group, indicating with different color region. Each successive circle represents a differentially abundant taxonomic clades at phylum, class, order, family, genus and species level from the inner to outer rings. B: Histograms of the different abundant taxa based on the cutoff value of LDA score ($\log_{10}$) > 4.0 and P < 0.05 among. N = 8/group. p, phylum; c, class; o, order; f, family; g, genus; s, species.

withdrawal. Therefore, it is likely that (*R*)-ketamine would be a potential therapeutic drug for MS.

Multiple lines of evidence suggest a key role of microglia in the pathology of MS (Chu et al., 2018; Deng and Sriram, 2005; Gao and Tsirka, 2011; Guerrero and Sicotte, 2020; Rawji and Yong, 2013; Voet et al., 2019). It is reported that microglial activation in the brain plays a role in the pathological changes of CPZ-treated mice and MS patients (Clarner et al., 2012). Depletion of microglia in the brain by BLZ945 [colony-stimulating factor-1 receptor (CSF1R) inhibitor] attenuated demyelination in the cortex and external capsule of CPZ-treated mice (Wies Mancini et al., 2019), suggesting a role of microglia in the demyelination. In contrast, BLZ945 failed to protect myelin or foster remyelination in myelin-rich areas such as corpus callosum (Wies Mancini et al., 2019), indicating regional differences. Recently, we reported that depletion of microglia in the brain by another CSF1R inhibitor PLX5622 caused abnormalities in gut microbiota in rodents (Yang et al., 2021), suggesting that repeated treatment of CSF1R inhibitor may affect behavioral and biological functions in animals. Therefore, it is possible that depletion of microglia in the brain by CSF1R inhibitor and subsequent abnormalities in the composition of gut microbiota may affect brain functions.

In this study, we found a positive correlation between demyelination

and microglial activation in the brain of CPZ-treated mice, supporting a link between demyelination and microglial activation. Thus, the current data suggest that attenuation of demyelination in the corpus callosum by (*R*)-ketamine might come along with reductions of microglial activation in the same area. We reported that (*R*)-ketamine could produce beneficial effects in several animal models of inflammation through TrkB activation (Fujita and Hashimoto, 2020; Fujita et al., 2021; Tan et al., 2020; Tan et al., 2022). Furthermore, (*R*)-ketamine significantly attenuated the increases in microglial activation in the brain after a single administration of lipopolysaccharide or cecum ligation and puncture (Zhang et al., 2021a; Zhang et al., 2021b). Collectively, it is likely that (*R*)-ketamine can produce potent anti-inflammatory actions in a variety of models of inflammation (Wei et al., 2021a). Given the role of microglial activation in the brain of MS patients, it is possible that (*R*)-ketamine could ameliorate the demyelination of CPZ-treated mice through its potent anti-inflammatory actions.

Increasing evidence suggests that abnormalities in gut microbiota play a role in the pathogenesis of MS (Cantarel et al., 2015; Cekanaviciute et al., 2017; Farshbafnadi et al., 2021; Ghezzi et al., 2021; Maghzi and Weiner, 2020; Parodi and Kerlero de Rosbo, 2021; The iMSMS Consortium, 2020). In this study, we found that (*R*)-ketamine could attenuate the increased relative abundance of *Eisenbergiella massiliensis*
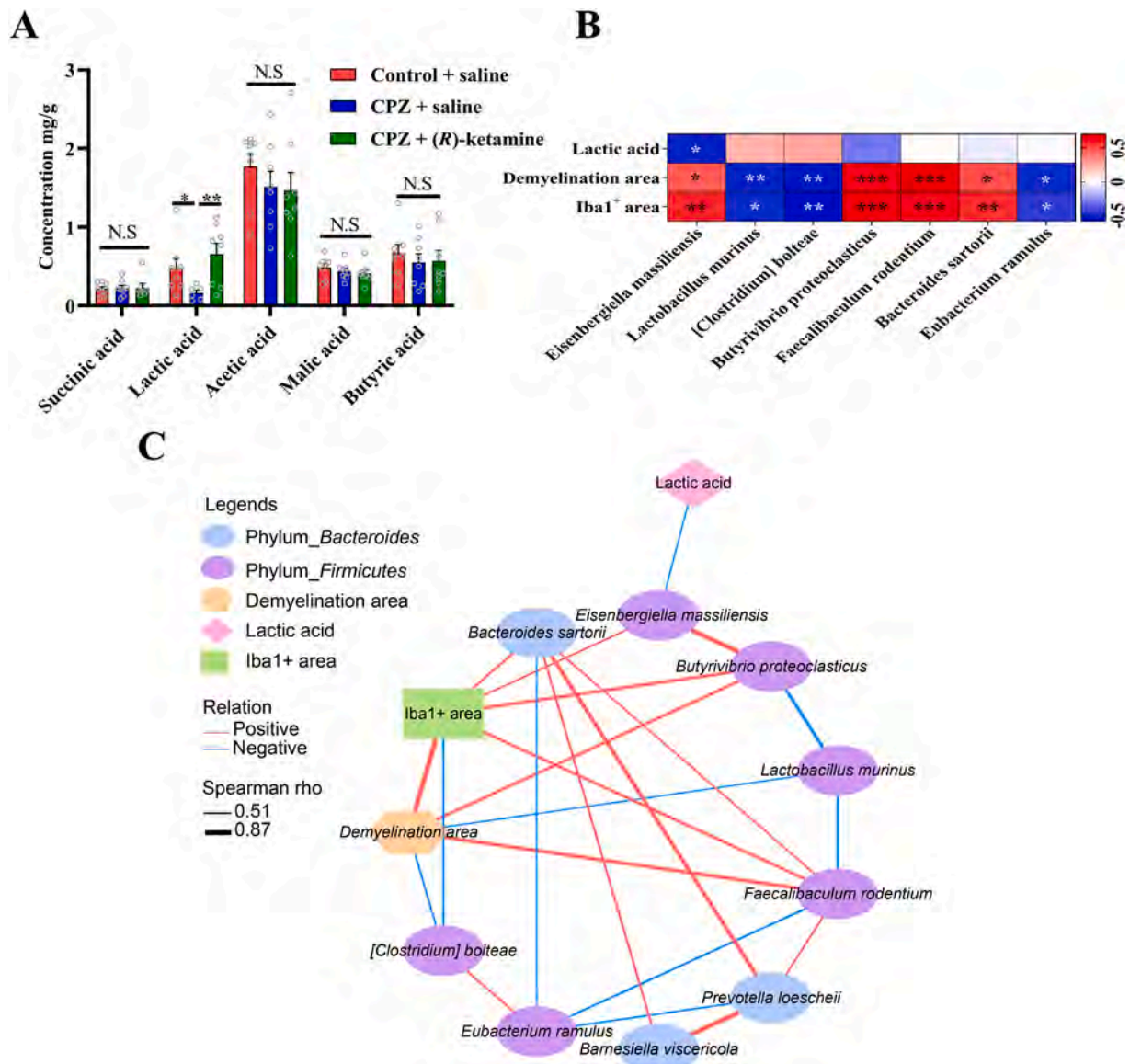
Fig. 5. Levels of SCFAs in the fecal samples and correlations between bacterial relative abundance and SCFAs, demyelination area, and Iba1-positive area. A: Levels of SCFAs in fecal samples from Control + saline, CPZ + saline, CPZ + (R)-ketamine groups. (one-way ANOVA, succinic acid: $F_{2,20} = 0.035$, $P = 0.966$; lactic acid: $F_{2,19} = 4.173$, $P = 0.031$; acetic acid: $F_{2,21} = 0.687$, $P = 0.514$; malic acid: $F_{2,21} = 0.702$, $P = 0.507$; butyric acid: $F_{2,21} = 0.291$, $P = 0.751$). B: The heat map displayed the correlation coefficient between bacterial abundance at species level and lactic acid, demyelination area, or Iba1-positive area. *$P < 0.05$; **$P < 0.01$ ***$P < 0.001$. C: The integrative network shown the correlations (Spearman analysis $r > 0.5$, $P < 0.05$) among lactic acid, demyelination area, Iba1-positive area, the bacterial relative abundance that differ significantly at species level. N = 8/group. The succinic acid level of one mouse in CPZ + (R)-Ketamine group and the lactic acid levels of two mice in CPZ + saline group were no detectable.

in the CPZ-treated mice. Furthermore, we also found positive correlations between the relative abundance of *Eisenbergiella massiliensis* and demyelination (or microglial marker) in the brain. A recent study showed that the relative abundance of *Eisenbergiella massiliensis* was increased in the stools of mice with ketogenic diet, compared with normal diet (Ferrere et al., 2021). Although the precise functions of *Eisenbergiella massiliensis* remain unclear, it is possible that *Eisenbergiella massiliensis* or its produced metabolite(s) may play a role in the demyelination through neuroinflammation. Nonetheless, it is noteworthy that (R)-ketamine could attenuate the increased relative abundance of *Eisenbergiella massiliensis* in the CPZ-treated mice. Previously, we reported that (R)-ketamine could ameliorate abnormal composition of gut microbiota in mice with depression-like phenotypes (Qu et al., 2017; Yang et al., 2017). Collectively, it is possible that gut microbiota may play a role in the beneficial actions of (R)-ketamine (Hashimoto, 2019;

Hashimoto, 2020; Wei et al., 2021a) although further study is needed.

Increasing evidence suggests that gut microbiota might regulate microglial functions in the brain (Abdel-Haq et al., 2019; Cryan et al., 2019; Lynch et al., 2021; Ma et al., 2019; Wang et al., 2018; Yang et al., 2021). A recent study shows that antibiotic-induced gut dysbiosis leads to microglial activation in the hippocampus, resulting in impairment of cholinergic gamma oscillation (Çalışkan et al., 2021). Furthermore, a recent study showed that microglia play a critical role in driving gut microbiome-mediated alterations of cerebral amyloid-β deposition (Dodiya et al., 2022). In this study, we found correlations between microglial marker in the brain and the relative abundance of several bacteria. For example, we found a positive correlation between relative abundance of several microbiome (*Eisenbergiella massiliensis*, *B. proteoclasticus*. *Faecalibaculum rodentium*, *B. sartorii*) and microglial activation, suggesting that these microbes may play a role in the

(caption on next page)

Fig. 6. Effects of (*R*)-ketamine on remyelination and microglia activation in the CPZ-treated mice.
A: The protocol of the experiment. B: The MBP (myelin basic protein) staining images were taken of the area outlined by the red line box. The Iba1 staining images were taken of the area outlined by the green line box. C: The representative photos of MBP and DAPI in the corpus callosum of brain. Scale bar: 300 μm. D: The representative photos of Iba1 and DAPI in the corpus callosum of brain. Scale bar: 100 μm. E: Quantitative data of demyelination area in the corpus callosum (one-way ANOVA: $F_{2,29} = 21.233$, $P < 0.001$). The percentage of demyelination area was determined by the calculation [(corpus callosum area -MBP-positive area)/ corpus callosum area × 100%]. F: Quantitative data of Iba1-positive area in the corpus callosum (one-way ANOVA: $F_{2,29} = 57.598$, $P < 0.001$). The percentage of Iba1-positive was determined by the calculation [Iba1-positive area/corpus callosum area) × 100%]. $N = 10$ or 11/group. **$P < 0.01$. ***$P < 0.001$. ND ; no detectable. (For interpretation of the references to color in this figure legend, the reader is referred to the web version of this article.)

neuroinflammation. Recently, we reported that ingestion of *Faecalibaculum rodentium* to *Ephx2* knock-out mice showed depression-like behaviors through systemic inflammation (Wang et al., 2021b), consistent with the current data. We also found a negative correlation between the relative abundance of L. *murinus* and microglial activation. Since L. *murinus* have anti-inflammatory action (Pan et al., 2018), this microbiome may play a role in the anti-inflammatory effects in CPZ-treated mice. Taken together, it is likely that microbiome-microglia crosstalk may play a role in the demyelination in the brain of CPZ-treated mice through gut–microbiota–brain axis.

The current study suggests that (*R*)-ketamine could prevent demyelination in the CNS of MS patients, resulting in attenuation of clinical symptoms in MS patients. In addition, (*R*)-ketamine may facilitate the recovery of clinical symptoms in MS patients by acceleration of remyelination. A phase 1 study demonstrated safety profile of (*R*)-ketamine in healthy subjects, and a phase 2 study in depressed patients is underway (Wei et al., 2021a). Therefore, it is of great interest to perform a randomized double-blind placebo-controlled study whether (*R*)-ketamine can improve clinical symptoms in MS patients. Considering a risk of depression in the progression of clinical symptoms in MS (Skokou et al., 2012), it is also important to treat depression in MS patients using the novel antidepressant (*R*)-ketamine (Hashimoto, 2019; Hashimoto, 2020; Wei et al., 2021a).

This study has some limitations. First, we examined the demyelination and remyelination in the corpus callosum since 0.2% CPZ diet is known to induce demyelination in the corpus callosum, with spontaneous remyelination following CPZ withdrawal. In contrast, CPZ was reported to induce demyelination in other brain regions including cerebral cortex and external capsule (Wies Mancini et al., 2019). Therefore, further study on the effects of (*R*)-ketamine in other brain regions is needed. Second, (*R*)-ketamine is reported to stimulate phosphorylation of TrkB, resulting in its pharmacological effects (Tan et al., 2020; Yang et al., 2015; Yang et al., 2016a). In this study, we did not examine phosphorylation of TrkB although further study is needed.

In summary, this study show that (*R*)-ketamine could ameliorate demyelination of CPZ-treated mice through TrkB activation, and that it could facilitate remyelination after CPZ withdrawal. Therefore, it is likely that (*R*)-ketamine would be a new therapeutic drug for MS patients. Finally, it is possible that gut–microbiome–microglia crosstalk might play a role in the beneficial effects of (*R*)-ketamine in the CPZ-treated model of MS.

Supplementary data to this article can be found online at https://doi.org/10.1016/j.nbd.2022.105635.

Data and code availability

The 16s rRNA sequencing data have been deposited to the NCBI Sequence Read Archive and are available at the accession number PRJNA768302.

CRediT authorship contribution statement

Xingming Wang: Investigation, Data curation, Formal analysis, Writing – original draft, Writing – review & editing. **Lijia Chang**: Investigation, Writing – review & editing. **Xiayun Wan**: Investigation, Writing – review & editing. **Yunfei Tan**: Investigation, Writing – review & editing. **Youge Qu**: Investigation, Writing – review & editing. **Jiajing**

Shan: Investigation, Writing – review & editing. **Yong Yang**: Investigation, Writing – review & editing. **Li Ma**: Investigation, Writing – review & editing. **Kenji Hashimoto**: Conceptualization, Funding acquisition, Writing – original draft, Writing – review & editing.

Declaration of competing interest

Dr. Hashimoto is the inventor of filed patent applications on "The use of *R*-Ketamine in the treatment of psychiatric diseases", "(*S*)-norketamine and salt thereof as pharmaceutical", "*R*-Ketamine and derivative thereof as prophylactic or therapeutic agent for neurodegeneration disease or recognition function disorder", "Preventive or therapeutic agent and pharmaceutical composition for inflammatory diseases or bone diseases", "*R*-Ketamine and its derivatives as a preventive or therapeutic agent for a neurodevelopmental disorder", and "Preventive or therapeutic agent and pharmaceutical composition for inflammatory diseases" by the Chiba University. Dr. Hashimoto also declares that he has received research support and consultant from Dainippon Sumitomo, Otsuka, Taisho, Murakami Farm, and Perception Neuroscience. The other authors have no conflict of interest.

References

Abdel-Haq, R., Schlachetzki, J., Glass, C.K., Mazmanian, S.K., 2019. Microbiome-microglia connections via the gut-brain axis. J. Exp. Med. 216 (1), 41–59.

Bonaventura, J., Lam, S., Carlton, M., Boehm, A.M., Gomez, L.J., Solís, O., Sánchez-Soto, M., Morris, J.P., Fredriksson, I., Thomas, J.C., Sibley, R.D., Shaham, Y., Zarate Jr., A.C., Michaelides, M., 2021. Pharmacological and behavioral divergence of ketamine enantiomers: implications for abuse liability. Mol. Psychiatry 26 (11), 6704–6722.

Çalışkan, G., French, T., Enrile Lacalle, S., Del Angel, M., Steffen, J., Heimesaat, M.M., Rita Dunay, I., Stork, O., 2021. Antibiotic-induced gut dysbiosis leads to activation of microglia and impairment of cholinergic gamma oscillations in the hippocampus. Brain Behav. Immun. 99, 203–217.

Cantarel, B.L., Waubant, E., Chehoud, C., Kuczynski, J., DeSantis, T.Z., Warrington, J., Venkatesan, A., Fraser, C.M., Mowry, E.M., 2015. Gut microbiota in multiple sclerosis: possible influence of immunomodulators. J. Investig. Med. 63 (5), 729–734.

Cekanaviciute, E., Yoo, B.B., Runia, T.F., Debelius, J.W., Singh, S., Nelson, C.A., Kanner, R., Bencosme, Y., Lee, Y.K., Hauser, S.L., Crabtree-Hartman, E., Sand, I.K., Gacias, M., Zhu, Y., Casaccia, P., Cree, B.A.C., Knight, R., Mazmanian, S.K., Baranzini, S.E., 2017. Gut bacteria from multiple sclerosis patients modulate human T cells and exacerbate symptoms in mouse models. Proc. Natl. Acad. Sci. U. S. A. 114 (40), 10713–10718.

Chang, L., Zhang, K., Pu, Y., Qu, Y., Wang, S., Xiong, Z., Ren, Q., Dong, C., Fujita, Y., Hashimoto, K., 2019. Comparison of antidepressant and side effects in mice after intranasal administration of (*R,S*)-ketamine, (*R*)-ketamine, and (*S*)-ketamine. Pharmacol. Biochem. Behav. 181, 53–59.

Chu, F., Shi, M., Zheng, C., Shen, D., Zhu, J., Zheng, X., Cui, L., 2018. The roles of macrophages and microglia in multiple sclerosis and experimental autoimmune encephalomyelitis. J. Neuroimmunol. 318, 1–7.

Clarner, T., Diederichs, F., Berger, K., Denecke, B., Gan, L., van der Valk, P., Beyer, C., Amor, S., Kipp, M., 2012. Myelin debris regulates inflammatory responses in an experimental demyelination animal model and multiple sclerosis lesions. Glia 60 (10), 1468–1480.

Cryan, J.F., O'Riordan, K.J., Cowan, C.S.M., Sandhu, K.V., Bastiaanssen, T.F.S., Boehme, M., Codagnone, M.G., Cussotto, S., Fulling, C., Golubeva, A.V., Guzzetta, K. E., Jaggar, M., Long-Smith, C.M., Lyte, J.M., Martin, J.A., Molinero-Perez, A., Moloney, G., Morelli, E., Morillas, E., O'Connor, R., Cruz-Pereira, J.S., Peterson, V.L., Rea, K., Ritz, N.L., Sherwin, E., Spichak, S., Teichman, E.M., van de Wouw, M., Ventura-Silva, A.P., Wallace-Fitzsimons, S.E., Hyland, N., Clarke, G., Dinan, T.G., 2019. The microbiota-gut-brain axis. Physiol. Rev. 99 (4), 1877–2013.

Dahham, J., Rizk, R., Kremer, I., Evers, S., Hiligsmann, M., 2021. Economic burden of multiple sclerosis in low- and middle-income countries: a systematic review. PharmacoEconomics 39, 789–807.

Deng, X., Sriram, S., 2005. Role of microglia in multiple sclerosis. Curr. Neurol. Neurosci. Rep. 5, 239–244.

Dodiya, H.B., Lutz, H.L., Weigle, I.Q., Patel, P., Michalkiewicz, J., Roman-Santiago, C.J., Zhang, C.M., Liang, Y., Srinath, A., Zhang, X., Xia, J., Olszewski, M., Zhang, X., Schipma, M.J., Chang, E.B., Tanzi, R.E., Gilbert, J.A., Sisodia, S.S., 2022. Gut microbiota-driven brain Aβ amyloidosis in mice requires microglia. J. Exp. Med. 219 (1), e20200895.

Farshbafnadi, M., Agah, E., Rezaei, N., 2021. The second brain: the connection between gut microbiota composition and multiple sclerosis. J. Neuroimmunol. 360, 577700.

Ferrere, G., Tidjani Alou, M., Liu, P., Goubet, A.G., Fidelle, M., Kepp, O., Durand, S., Iebba, V., Fluckiger, A., Daillère, R., Thelemaque, C., Grajeda-Iglesias, C., Alves Costa Silva, C., Aprahamian, F., Lefevre, D., Zhao, L., Ryffel, B., Colomba, E., Arnedos, M., Drubay, D., Rauber, C., Raoult, D., Asnicar, F., Spector, T., Segata, N., Derosa, L., Kroemer, G., Zitvogel, L., 2021. Ketogenic diet and ketone bodies enhances the anticancer effects of CD-1 blockade. JCI Insight 6 (2), e145207.

Franklin, R.J.M., Ffrench-Constant, C., 2017. Regenerating CNS myelin–from mechanisms to experimental medicines. Nat. Rev. Neurosci. 18 (12), 753–769.

Fujita, Y., Hashimoto, K., 2020. Decreased bone mineral density in ovariectomized mice is ameliorated after subsequent repeated intermittent administration of (*R*)-ketamine, but not (*S*)-ketamine. Neuropsychopharmacol. Rep. 40 (4), 401–406.

Fujita, A., Fujita, Y., Pu, Y., Chang, L., Hashimoto, K., 2020. MPTP-induced dopaminergic neurotoxicity in mouse brain is attenuated after subsequent intranasal administration of (*R*)-ketamine: a role of TrkB signaling. Psychopharmacology 237 (1), 83–92.

Fujita, Y., Hashimoto, Y., Hashimoto, H., Chang, L., Hashimoto, K., 2021. Dextran sulfate sodium-induced inflammation and colitis in mice are ameliorated by (*R*)-ketamine, but not (*S*)-ketamine: a role of TrkB signaling. Eur. J. Pharmacol. 897, 173954.

Gao, Z., Tsirka, E.S., 2011. Animal models of MS reveal multiple roles of microglia in disease pathogenesis. Neurol. Res. Int. 2011, 383087.

Ghezzi, L., Cantoni, C., Pinget, G.V., Zhou, Y., Piccio, L., 2021. Targeting the gut to treat multiple sclerosis. J. Clin. Invest. 131 (13), e143774.

Guerrero, L.B., Sicotte, L.N., 2020. Microglia in multiple sclerosis: friend or foe? Front. Immunol. 11, 374.

Hashimoto, K., 2019. Rapid-acting antidepressant ketamine, its metabolites and other candidates: a historical overview and future perspective. Psychiatry Clin. Neurosci. 73 (10), 613–627.

Hashimoto, K., 2020. Molecular mechanisms of the rapid-acting and long-lasting antidepressant actions of (*R*)-ketamine. Biochem. Pharmacol. 177, 113935.

Hashimoto, K., Kakiuchi, T., Ohba, H., Nishiyama, S., Tsukada, H., 2017. Reduction of dopamine D$_{2/3}$ receptor binding in the striatum after a single administration of esketamine, but not *R*-ketamine: a PET study in conscious monkeys. Eur. Arch. Psychiatry Clin. Neurosci. 267 (2), 173–176.

Jones, C.D., Motl, R., Sandroff, B.M., 2021. Depression in multiple sclerosis: is one approach for its management enough? Mult. Scler. Relat. Disord. 51, 102904.

Kalafatakis, I., Karagogeos, D., 2021. Oligodendrocytes and microglia: key players in myelin development, damage and repair. Biomolecules 11 (7), 1058.

Kim, S.W., Suda, W., Kim, S., Oshima, K., Fukuda, S., Ohno, H., Morita, H., Hattori, M., 2013. Robustness of gut microbiota of healthy adults in response to probiotic intervention revealed by high-throughput pyrosequencing. DNA Res. 20 (3), 241–253.

Kwak, M.S., Cha, J.M., Shin, H.P., Jeon, J.W., Yoon, J.Y., 2020. Development of a novel metagenomic biomarker for prediction of upper gastrointestinal tract involvement in patients with Crohn's disease. Front. Microbiol. 11, 1162.

Leal, G.C., Bandeira, I.D., Correia-Melo, F.S., Telles, M., Mello, P.R., Vieira, F., Lima, S.C., Jesus-Nunes, P.A., Guerreiro-Costa, N.F.L., Marback, F.R., Caliman-Fontes, T.A., Marques, L.S.B., Bezerra, L.O.M., Dias-Neto, L.A., Silva, S.S., Sampaio, S.A., Sanacora, G., Turecki, G., Loo, C., Lacerda, L.T.A., Quarantini, C.L., 2021. Intravenous arketamine for treatment-resistant depression: open-label pilot study. Eur. Arch. Psychiatry Clin. Neurosci. 271 (3), 577–582.

Lynch, C.M.K., Clarke, G., Cryan, J.F., 2021. Powering up microbiome-microglia interactions. Cell Metab. 33 (11), 2097–2099.

Ma, Q., Xing, C., Long, W., Wang, H.Y., Liu, Q., Wang, R.F., 2019. Impact of microbiota on central nervous system and neurological diseases: the gut-brain axis. J. Neuroinflammation 16 (1), 53.

Maghzi, A.H., Weiner, H.L., 2020. A one-two punch in the gut may trigger multiple sclerosis. Immunity 53 (4), 707–709.

Mayrhofer, F., Dariychuk, Z., Zhen, A., Daugherty, D.J., Bannerman, P., Hanson, A.M., Pleasure, D., Soulika, A., Deng, W., Chechneva, O.V., 2021. Reduction in CD11c^{+} microglia correlates with clinical progression in chronic experimental autoimmune demyelination. Neurobiol. Dis. 161, 105556.

Nicholas, J., Zhou, H., Deshpande, C., 2021. Annual cost burden by level of relapse severity in patients with multiple sclerosis. Adv. Ther. 38 (1), 758–771.

Pan, F., Zhang, L., Li, M., Hu, Y., Zeng, B., Yuan, H., Zhao, L., Zhang, C., 2018. Predominant gut Lactobacillus murinus strain mediates anti-inflammaging effects in calorie-restricted mice. Microbiome 6 (1), 54.

Parodi, B., Kerlero de Rosbo, N., 2021. The gut-brain axis in multiple sclerosis. Is it dysfunction a pathological trigger or a consequence of the disease? Front. Immunol. 12, 718220.

Procaccini, C., De Rosa, V., Pucino, V., Formisano, L., Matarese, G., 2015. Animal models of multiple sclerosis. Eur. J. Pharmacol. 759, 182–191.

Pu, Y., Tan, Y., Qu, Y., Chang, L., Wang, S., Wei, Y., Wang, X., Hashimoto, K., 2021. A role of the subdiaphragmatic vagus nerve in depression-like phenotypes in mice after fecal microbiota transplantation from *Chrna7* knock-out mice with depression-like phenotypes. Brain Behav. Immun. 94, 318–326.

Qu, Y., Yang, C., Ren, Q., Ma, M., Dong, C., Hashimoto, K., 2017. Comparison of (*R*)-ketamine and lanicemine on depression-like phenotype and abnormal composition of gut microbiota in a social defeat stress model. Sci. Rep. 7 (1), 15725.

Qu, Y., Shan, J., Wang, S., Chang, L., Pu, Y., Wang, X., Tan, Y., Yamamoto, M., Hashimoto, K., 2021. Rapid-acting and long-lasting antidepressant-like action of (*R*)-ketamine in *Nrf2* knock-out mice: a role of TrkB signaling. Eur. Arch. Psychiatry Clin. Neurosci. 271 (3), 439–446.

Rawji, K.S., Yong, V.W., 2013. The benefits and detriments of macrophages/microglia in models of multiple sclerosis. Clin. Dev. Immunol. 2013, 948976.

Ren, Q., Ma, M., Yang, C., Zhang, J.C., Yao, W., Hashimoto, K., 2015. BDNF-TrkB signaling in the nucleus accumbens shell of mice has key role in methamphetamine withdrawal symptoms. Transl. Psychiatry 5 (10), e666.

Segata, N., Izard, J., Waldron, L., Gevers, D., Miropolsky, L., Garrett, W.S., Huttenhower, C., 2011. Metagenomic biomarker discovery and explanation. Genome Biol. 12, R60.

Shinno-Hashimoto, H., Hashimoto, Y., Wei, Y., Chang, L., Fujita, Y., Ishima, T., Matsue, H., Hashimoto, K., 2021. Abnormal composition of microbiota in the gut and skin of imiquimod-treated mice. Sci. Rep. 11 (1), 11265.

Skokou, M., Soubasi, E., Gourzis, P., 2012. Depression in multiple sclerosis: a review of assessment and treatment approaches in adult and pediatric populations. ISRN Neurol. 2012, 427102.

Tan, Y., Hashimoto, K., 2020. Risk of psychosis after repeated intermittent administration of (*S*)-ketamine, but not (*R*)-ketamine, in mice. J. Affect. Disord. 269, 198–200.

Tan, Y., Fujita, Y., Qu, Y., Chang, L., Pu, Y., Wang, S., Wang, X., Hashimoto, K., 2020. Phencyclidine-induced cognitive deficits in mice are ameliorated by subsequent repeated intermittent administration of (*R*)-ketamine, but not (*S*)-ketamine: role of BDNF-TrkB signaling. Pharmacol. Biochem. Behav. 188, 172839.

Tan, Y., Fujita, Y., Pu, Y., Chang, L., Qu, Y., Wang, X., Hashimoto, K., 2022. Repeated intermittent administration of (R)-ketamine during juvenile and adolescent stages prevents schizophrenia-relevant phenotypes in adult offspring after maternal immune activation: a role of TrkB signaling. Eur. Arch. Psychiatry Clin. Neurosci. https://doi.org/10.1007/s00406-021-01365-6, 2022 Jan 3.

The iMSMS Consortium, 2020. Household paired design reduces variance and increases power in multi-city gut microbiome study in multiple sclerosis. Mult. Scler. https://doi.org/10.1177/1352458520924594, 2020 Jun 26; 1352458520924594.

Tian, Z., Dong, C., Fujita, A., Fujita, Y., Hashimoto, K., 2018. Expression of heat shock protein HSP-70 in the retrosplenial cortex of rat brain after administration of (*R*,*S*)-ketamine and (*S*)-ketamine, but not (*R*)-ketamine. Pharmacol. Biochem. Behav. 172, 17–21.

Torkildsen, O., Brunborg, L.A., Myhr, K.M., Bø, L., 2008. The cuprizone model for demyelination. Acta Neurol. Scand. 188, 72–76.

Voet, S., Prinz, M., Loo, V.G., 2019. Microglia in central nervous system inflammation and multiple sclerosis pathology. Trends Mol. Med. 25 (2), 112–123.

Wang, Y., Wang, Z., Wang, Y., Li, F., Jia, J., Song, X., Qin, S., Wang, R., Jin, F., Kitazato, K., Wang, Y., 2018. The gut-microglia connection: implications for central nervous system diseases. Front. Immunol. 9, 2325.

Wang, S., Ishima, T., Zhang, J., Qu, Y., Chang, L., Pu, Y., Fujita, Y., Tan, Y., Wang, X., Hashimoto, K., 2020. Ingestion of *Lactobacillus intestinalis* and *Lactobacillus reuteri* causes depression- and anhedonia-like phenotypes in antibiotic-treated mice via the vagus nerve. J. Neuroinflammation 17 (1), 241.

Wang, X., Chang, L., Tan, Y., Qu, Y., Shan, J., Hashimoto, K., 2021a. (R)-ketamine ameliorates the progression of experimental autoimmune encephalomyelitis in mice. Brain Res. Bull. 177, 316–323.

Wang, S., Ishima, T., Qu, Y., Shan, J., Wei, Y., Chang, L., Qu, Y., Zhang, J., Pu, Y., Fujita, Y., Tan, Y., Wang, X., Ma, L., Wan, X., Hammock, B.D., Hashimoto, K., 2021b. Ingestion of *Faecalibacterium rodentium* causes depression-like phenotypes in resilient *Ephx2* knock-out mice: a role of brain–gut–microbiota axis via the subdiaphragmatic vagus nerve. J. Affect. Disord. 292, 565–573.

Wei, Y., Chang, L., Hashimoto, K., 2020. A historical review of antidepressant effects of ketamine and its enantiomers. Pharmacol. Biochem. Behav. 190, 172870.

Wei, Y., Chang, L., Hashimoto, K., 2021a. Molecular mechanisms underlying the antidepressant actions of arketamine: beyond the NMDA receptor. Mol. Psychiatry. https://doi.org/10.1038/s41380-021-01121-1. Advance online publication.

Wei, Y., Chang, L., Ishima, T., Wan, X., Ma, L., Wuyun, G., Pu, Y., Hashimoto, K., 2021b. Abnormalities of the composition of the gut microbiota and short-chain fatty acids in mice after splenectomy. Brain Behav. Immun. Health 11, 100198.

Wies Mancini, V.S.B., Pasquini, J.M., Correale, J.D., Pasquini, L.A., 2019. Microglial modulation through colony-stimulating factor-1 receptor inhibition attenuates demyelination. Glia 67 (2), 291–308.

Xia, Y., Sun, J., 2017. Hypothesis testing and statistical analysis of microbiome. Genes Dis. 4, 138–148.

Xiong, Z., Fujita, Y., Zhang, K., Pu, Y., Chang, L., Ma, M., Chen, J., Hashimoto, K., 2019. Beneficial effects of (*R*)-ketamine, but not its metabolite (2*R*,6*R*)-

hydroxynorketamine, in the depression-like phenotype, inflammatory bone markers, and bone mineral density in a chronic social defeat stress model. Behav. Brain Res. 368, 111904.

Yang, C., Shirayama, Y., Zhang, J.C., Ren, Q., Yao, W., Ma, M., Dong, C., Hashimoto, K., 2015. *R*-ketamine: a rapid-onset and sustained antidepressant without psychotomimetic side effects. Transl. Psychiatry 5 (9), e632.

Yang, B., Zhang, J.C., Han, M., Yao, W., Yang, C., Ren, Q., Ma, M., Chen, Q.X., Hashimoto, K., 2016a. Comparison of R-ketamine and rapastinel antidepressant effects in the social defeat stress model of depression. Psychopharmacology 233 (19–20), 3647–3657.

Yang, C., Han, M., Zhang, J.C., Ren, Q., Hashimoto, K., 2016b. Loss of parvalbumin-immunoreactivity in mouse brain regions after repeated intermittent administration of esketamine, but not *R*-ketamine. Psychiatry Res. 239, 281–283.

Yang, C., Qu, Y., Fujita, Y., Ren, Q., Ma, M., Dong, C., Hashimoto, K., 2017. Possible role of the gut microbiota-brain axis in the antidepressant effects of (*R*)-ketamine in a social defeat stress model. Transl. Psychiatry 7 (12), 1294.

Yang, C., Ren, Q., Qu, Y., Zhang, J.C., Ma, M., Dong, C., Hashimoto, K., 2018. Mechanistic target of rapamycin-independent antidepressant effects of (*R*)- ketamine in a social defeat stress model. Biol. Psychiatry 83 (1), 18–28.

Yang, C., Yang, J., Luo, A., Hashimoto, K., 2019. Molecular and cellular mechanisms underlying the antidepressant effects of ketamine enantiomers and its metabolites. Transl. Psychiatry 9 (1), 280.

Yang, Y., Ishima, T., Wan, X., Wei, Y., Chang, L., Zhang, J., Qu, Y., Hashimoto, K., 2021. Microglial depletion and abnormalities in gut microbiota composition and short-chain fatty acids in mice after repeated administration of colony stimulating factor 1 receptor inhibitor PLX5622. Eur. Arch. Psychiatry Clin. Neurosci. https://doi.org/10.1007/s00406-021-01325-0, 2021 Sep 4.

Yao, W., Cao, Q., Luo, S., He, L., Yang, C., Chen, J., Qi, Q., Hashimoto, K., Zhang, J.C., 2021. Microglial ERK-NRBP1-CREB-BDNF signaling in sustained antidepressant actions of (*R*)-ketamine. Mol. Psychiatry. https://doi.org/10.1038/s41380-021-01377-7, 2021 Nov 24.

Zhan, J., Mann, T., Joost, S., Behrangi, N., Frank, M., Kipp, M., 2020. The cuprizone model: dos and do nots. Cells 9 (4), 843.

Zhang, K., Hashimoto, K., 2019. An update on ketamine and its two enantiomers as rapid-acting antidepressants. Expert. Rev. Neurother. 19 (1), 83–92.

Zhang, J.C., Li, S.X., Hashimoto, K., 2014. *R* (−)-ketamine shows greater potency and longer lasting antidepressant effects than *S* (+)-ketamine. Pharmacol. Biochem. Behav. 116, 137–141.

Zhang, J.C., Yao, W., Dong, C., Yang, C., Ren, Q., Ma, M., Han, M., Hashimoto, K., 2015. Comparison of ketamine, 7,8-dihydroxyflavone, and ANA-12 antidepressant effects in the social defeat stress model of depression. Psychopharmacology 232 (23), 4325–4335.

Zhang, K., Ma, M., Dong, C., Hashimoto, K., 2018. Role of inflammatory bone markers in the antidepressant actions of (*R*)-ketamine in a chronic social defeat stress model. Int. J. Neuropsychopharmacol. 21 (11), 1025–1030.

Zhang, K., Fujita, Y., Chang, L., Qu, Y., Pu, Y., Wang, S., Shirayama, Y., Hashimoto, K., 2019. Abnormal composition of gut microbiota is associated with resilience versus susceptibility to inescapable electric stress. Transl. Psychiatry 9 (1), 231.

Zhang, K., Yang, C., Chang, L., Sakamoto, A., Suzuki, T., Fujita, Y., Qu, Y., Wang, S., Pu, Y., Tan, Y., Wang, X., Ishima, T., Shirayama, Y., Hatano, M., Tanaka, K.F., Hashimoto, K., 2020. Essential role of microglial transforming growth factor-β1 in antidepressant actions of (*R*)-ketamine and the novel antidepressant TGF-β1. Transl. Psychiatry 10 (1), 32.

Zhang, J., Ma, L., Hashimoto, Y., Wan, X., Shan, J., Qu, Y., Hashimoto, K., 2021a. (R)-ketamine ameliorates lethal inflammatory responses and multi-organ injury in mice induced by cecum ligation and puncture. Life Sci. 284, 119882.

Zhang, J., Ma, L., Wan, X., Shan, J., Hashimoto, K., 2021b. (R)-ketamine attenuates LPS-induced endotoxin-derived delirium through inhibition of neuroinflammation. Psychopharmacology 238 (10), 2743–2753.

Zhang, K., Sakamoto, A., Chang, L., Qu, Y., Wang, S., Pu, Y., Tan, Y., Wang, X., Fujita, Y., Ishima, T., Hatano, M., Hashimoto, K., 2021c. Splenic NKG2D confers resilience versus susceptibility in mice after chronic social defeat stress: beneficial effects of (*R*)-ketamine. Eur. Arch. Psychiatry Clin. Neurosci. 271 (3), 447–456.

ORIGINAL PAPER

Gut–microbiota–brain axis in the vulnerability to psychosis in adulthood after repeated cannabis exposure during adolescence

Xiayun Wan[1] · Akifumi Eguchi[2] · Youge Qu[1] · Yong Yang[1] · Lijia Chang[1] · Jiajing Shan[1] · Chisato Mori[2,3] · Kenji Hashimoto[1]

Abstract

Increasing epidemiological evidence shows that the use of cannabis during adolescence could increase the risk for psychosis in adulthood. However, the precise mechanisms underlying long-lasting cannabis-induced risk for psychosis remain unclear. Accumulating evidence suggests the role of gut microbiota in the pathogenesis of psychiatric disorders. Here, we examined whether gut microbiota plays a role in the risk for psychosis of adult after exposure of cannabinoid (CB) receptor agonist WIN55,212–2 during adolescence. Repeated administration of WIN55,212–2 (2 mg/kg/day) during adolescence (P35–P45) significantly increased the expression of Iba1 (ionized calcium-binding adapter molecule 1) in the medial prefrontal cortex (mPFC) and nucleus accumbens (NAc) of adult mice after administration of lipopolysaccharide (LPS: 0.5 mg/kg). In contrast, there were no changes in blood levels of pro-inflammatory cytokines between the two groups. Although alpha-diversity and beta-diversity of gut microbiota were no differences between the two groups, there were several microbes altered between the two groups. Interestingly, there were significant correlations between the relative abundance of microbiota and Iba1 expression in the mPFC and NAc. Furthermore, there were also significant correlations between the relative abundance of microbiota and several metabolites in the blood. These findings suggest that gut microbiota may play a role in the microglial activation in the mPFC and NAc of adult mice after repeated WIN55,212–2 exposure during adolescence. Therefore, it is likely that gut–microbiota–microglia crosstalk might play a role in increased risk for psychosis in adults with cannabis use during adolescence.

Keywords Adolescence · Cannabis · Gut microbiota · Inflammation · Microglia

Introduction

Cannabis, the most widely used addictive drug in the world, has pronounced effects on the developing adolescent brain, with 42% of United State (U.S.) adolescents reporting marijuana use before age 18 [1]. Adolescent cannabis consumption contributes to the risk of multiple harmful outcomes, including the effects of short-term use (i.e., reduced short-term memory and motor coordination disorders, reduced judgment sensitivity, paranoia, and psychosis) and the effects of long-term or heavy use (i.e., addiction, altered neurodevelopment, cognitive impairment, and increased risk of chronic psychosis) [2]. Epidemiological evidence shows that the use of cannabis during adolescence is a risk factor for the onset of psychiatric disorders such as schizophrenia in adulthood [3–7]. A meta-analysis showed an association of cannabis use in adolescence and risk of depression, anxiety, and suicidality in young adulthood [8]. A linear mixed-effects model analysis using magnetic resonance images from 799 participants showed that cannabis use during adolescence was associated with accelerated age-related cortical thinning from 14 to 19 years of age in predominantly prefrontal regions [9]. Collectively, it is well recognized that adolescence is particularly vulnerable to the adverse effects of abused drugs including cannabis [10–13]. Although the

✉ Kenji Hashimoto
   hashimoto@faculty.chiba-u.jp

1   Division of Clinical Neuroscience, Chiba University Center for Forensic Mental Health, 1-8-1 Inohana, Chiba 260-8670, Japan

2   Department of Sustainable Health Science, Chiba University Center for Preventive Medical Sciences, Chiba 263-8522, Japan

3   Department of Bioenvironmental Medicine, Graduate School of Medicine, Chiba University, Chiba 260-8670, Japan

🍐 Springer

use of cannabis during adolescence could disrupt normal brain development, the precise mechanisms underlying the long-lasting consequences of adolescent exposure to cannabis remain unclear.

The cannabinoid system involves two types of cannabinoid receptors (CB1 and CB2 receptors), and it acts as crucial neuromodulator in the central nervous system (CNS) [14, 15]. Furthermore, synthetic cannabinoids have been related with psychosis and psychosis-like conditions [16], and exogenous cannabinoid agonists, administered during adolescence to rodents or non-human primates, produce schizophrenia-like behaviors in adulthood [17–19]. The synthetic cannabinoid WIN55,212–2 is a potent CB receptor agonist with Ki of 62.3 nM (human recombinant CB1) and 3.3 nM (human recombinant CB2) [20]. Cass et al. [17] reported that exposure to WIN55,212–2 during early and mild adolescence (P35–P45) impaired the maturation of γ-aminobutyric acid (GABA) function in the prefrontal cortex (PFC) of rat brain, resulting in the long-lasting cognitive deficits resulting from early cannabis exposure. Subsequently, we reported that the repeated exposure of WIN55,212–2 during adolescence (P35–P45) could increase methamphetamine-induced hyperlocomotion in adulthood (P70–P74) through activation of brain-derived neurotrophic factor (BDNF) and its receptor TrkB signaling in the nucleus accumbens (NAc) [21]. Collectively, it is likely that cannabis exposure during adolescence might increase the risk for psychosis in adulthood.

Accumulating evidence suggests that gut–microbiota–brain axis plays an important role in the pathophysiology of a number of psychiatric disorders such as schizophrenia [22–26]. Interestingly, gut–microbiota–brain axis as a regulator of the reward process has been demonstrated [27]. However, there are no articles reporting the role of gut microbiota in the risk for psychosis in adulthood after exposure to cannabis during adolescence.

The present study was performed to investigate whether gut–microbiota–brain axis plays a role in the risk for psychosis in adulthood after repeated exposure of WIN55,212–2 during adolescence. First, we examined whether repeated exposure of WIN55,212–2 during adolescence (P35–P45) can affect the composition of gut microbiota in adulthood (P70). Next, we examined the effects of lipopolysaccharide (LPS)-induced inflammation on blood levels of pro-inflammatory cytokines [i.e., interleukin-6 (IL-6), tumor necrosis factor-α (TNF-α)] and microglial activation in the brain regions [i.e., medial prefrontal cortex (mPFC), hippocampus, NAc] of adult mice after repeated exposure of WIN55,212–2 during adolescence. Furthermore, we performed metabolomics analysis of blood samples since gut microbiota play a role in the production of a number of metabolites including short-chain fatty acids (SCFAs). Finally, we examined the correlations between the relative abundance of microbes and metabolites, blood levels of cytokines, or microglial activation in the brain regions.

Methods

Animals

Male C57BL/6 mice (age: 5 weeks old, body weight 17–20 g; Japan SLC, Inc., Hamamatsu, Japan) were kept at monitored temperature with a 12-h light/dark cycle (lights turn on between 7:00 and 19:00) at a fixed room temperature of 23 °C and relative humidity of $55 \pm 5\%$, food and water available as needed. The experimental protocol used in our research was supported by the Institutional Animal Care and Use Committee of Chiba University (permission number 3–356).

Drugs

(R)-$(+)$-WIN55,212–2 mesylate salt (Selleck Chemicals, Tokyo, Japan) was dissolved in physiological saline containing 1% dimethylsulfoxide (DMSO). The dose of WIN55,212–2 (2 mg/kg) was selected as reported previously [17, 21]. Lipopolysaccharide (LPS) was purchased from Sigma-Aldrich Corporation (Tokyo, Japan).

Exposure of WIN55,212–2 during adolescence and collection of samples

Mice were randomized assigned to the two groups. WIN55,212–2 (2 mg/kg/day) or vehicle (10 ml/kg/day) was administered intraperitoneally to adolescent mice from postnatal day 35 to postnatal day 45 (P35–P45) (Fig. 1A), as reported previously [17, 21].

Fresh fecal samples were collected at approximately 10 a.m. to prevent the influence of circadian rhythm effect on the microbiota in adulthood (P70). All fecal samples were quickly frozen in liquid nitrogen and stored at −80 °C until the assay of gut microbiota.

Subsequently, all mice were given intraperitoneal injections of LPS (0.5 mg/kg), as reported previously (Fig. 1A) [28–31]. Twenty-four hours after LPS injection, mice were deeply anesthetized with inhaled isoflurane (5%). Blood samples were obtained by cardiac puncture and collected into tubes containing ethylenediaminetetraacetic acid (EDTA), and plasma was acquired by centrifugation at 3000 g for 5 min at 4 °C and stored at −80 °C. Subsequently, the bilateral medial prefrontal cortex (mPFC), nucleus accumbens (NAc), and hippocampus were rapidly isolated on ice and stored at −80 °C prior to analysis (Fig. 1A).
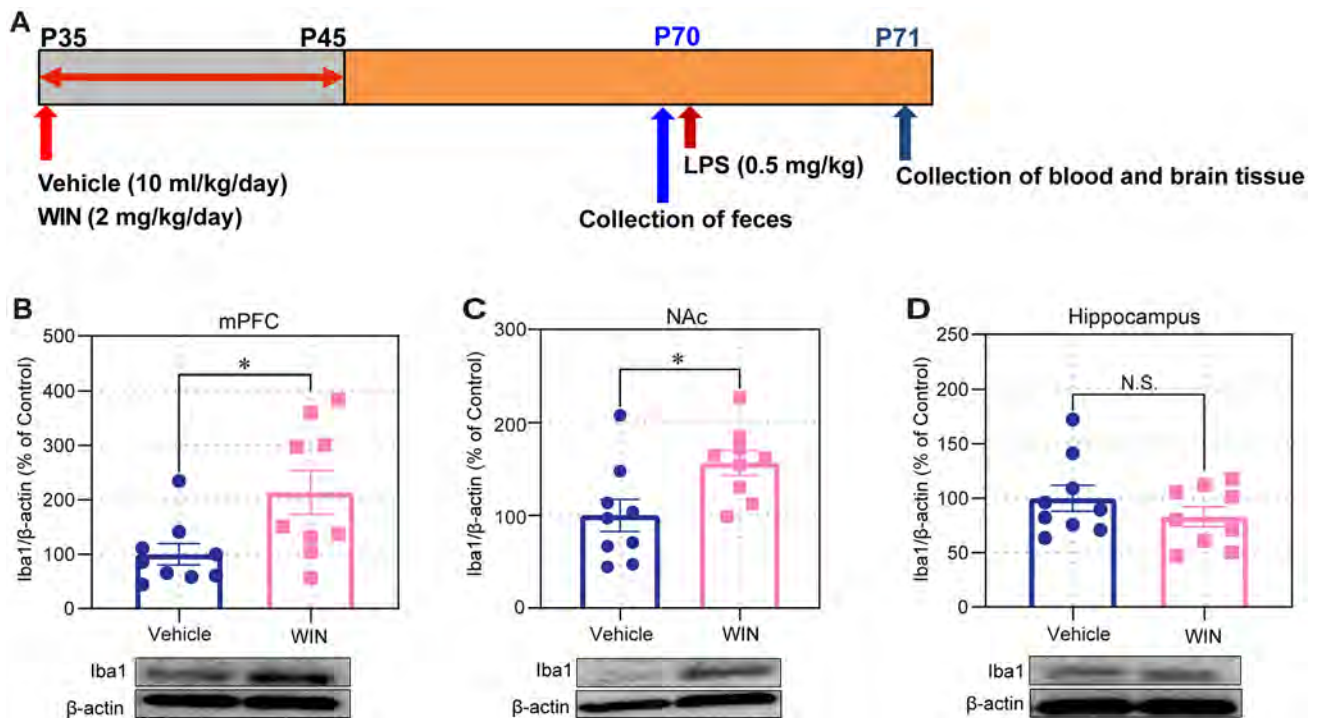
Fig. 1 Experimental schedule and the expression of microglial marker in the brain. **A** Experimental schedule. Vehicle (10 ml/kg/day) or WIN55,212–2 (2 mg/kg/day) was administered i.p. into mice from P35 to P45. On P70, fresh fecal samples were collected before LPS (0.5 mg/kg) administration. **B**, **C**, **D** Western blot analysis of ionized calcium-binding adapter molecule 1 (Iba1) and β-actin in the medial prefrontal cortex (mPFC), nucleus accumbens (NAc) and hippocampus. The values represent the mean ± S.E.M. Unpaired Student's t-test ($n = 9$). *$P < 0.05$, *N.S.* not significant

Measurement of plasma levels of pro-inflammatory cytokines

Plasma levels of IL-6 (Cat Number: 88- 7064, Invitrogen, Camarillo, CA, USA) and TNF-α (Cat Number: 88–7324, Invitrogen, Camarillo, CA, USA) were measured using commercial ELISA kits, according to the manufacturer's instructions.

Western blot analysis of Iba1 in the brain regions

Western blot analysis was performed as previously reported [32–37]. The obtained tissues were milled in frozen Laemmli lysis buffer, centrifuged with $3000 \times g$ (RCF) for 10 min at 4 °C, and the supernatant was gathered. The protein concentration of each sample was determined with the DC protein assay kit (Bio-Rad, Hercules, CA) and balanced with sample buffer (125 mM Tris/HCl (pH 6.8), 20% glycerol, 0.1% bromophenol blue, 10% β-mercaptoethanol, 4% sodium dodecyl sulfate) for 10 min, 95 °C. 10% sodium dodecyl sulfate–polyacrylamide gel electrophoresis (SDS-PAGE) gels (Mini-PROTEAN® TGX™ precast gels; Bio-Rad) was utilized to separate target proteins (corresponding to molecular weight), followed by electrotransferred to

polyvinylidene difluoride (PVDF) membrane with Trans Blot Mini Cell (Bio-Rad). The membrane was subjected to 5% non-fat milk powder and 0.1% Tween 20 in TBS solution for 60 min, and the corresponding primary antibodies were proceeded to incubation. Iba1 (1:1000, Cat No. 016–20,001, 1 µg/mL, FUJIFILM, Tokyo, Japan) or β-actin (1:10,000; Cat no.: A5441 Sigma-Aldrich Co., Ltd, St Louis, MO, USA) was incubated at 4 °C, overnight, followed by incubated with indicated secondary antibody (1:5000) for 1 h. Bands were excited with an enhanced chemiluminescence (ECL) kit and the ChemiDoc™ Touch Imaging System (170–01,401; Bio-Rad Laboratories, Hercules, CA) was utilized to quantify the bands.

16S rRNA gene amplicon sequencing and data processing

DNA extraction from fecal samples and 16S rRNA data analysis were performed at MyMetagenome Co, Ltd. (Tokyo, Japan) as reported previously [37–42]. Briefly, the common primer 27Fmod (5′-AGRGTTTGATYMTGG CTCAG-3′) and 338R (5′-TGCTGCCTCCCGTAGGAG T-3′) were used to amplify the V1-V2 region of the bacterial 16S rRNA gene by polymerase chain reaction (PCR).

Amplicons were sequenced using the MiSeq System (Illumina). The 16 s rRNA sequencing data have been deposited to the NCBI Sequence Read Archive and are available at the accession number PRJNA773659.

Alpha diversity was assessed according to Observed_OTU, Chao1, ACE, and Shannon index, estimated from the gene profile of each sample, while beta diversity was estimated by calculating the weighted Unifrac distance between samples. Differences in bacterial taxa between the two groups at the genus level were calculated via linear discriminant analysis (LDA) effect size (LEfSe) using LEfSe software (LDA score > 3.0, $P < 0.05$) [43].

To determine the genomic potential of these two groups, we computationally predicted the metagenome using PICRUSt 2 [44]. Welch's t-test identified pathways with significant abundance differences between the two groups. To correct for multiple testing, the Storey FDR (false discovery rate) method was used simultaneously. We also applied STAMP [45] software (v2.1.3) for statistical analysis and visualization of significant difference pathways.

Measurement of short-chain fatty acids (SCFAs)

Quantification of short-chain fatty acids (acetic acid, propionic acid, butyric acid, succinic acid, and lactic acid) in the fecal samples was determined by gas chromatography at TechnoSuruga Laboratories Ltd. (Shizuoka, Japan), as reported previously [37, 38, 42, 46, 47].

Metabolomics analysis of plasma samples and data preprocessing

Metabolomics analysis was performed using an ExionLC AD UPLC system (SCIEX, Tokyo, Japan) interfaced with an X500R LC-QToFMS system (SCIEX, Tokyo, Japan) with electrospray ionization (ESI) operating in positive and negative ionization mode. First, 100 μL of methanol containing internal standards (100 μM N, N-diethyl-2-phenylacetamide and d-camphor-10-sulfonic acid) was added into the plasma samples (100 μL), and then samples were centrifuged at $14,000 \times$ rpm for 5 min. After centrifugation, the supernatant was transferred to an Amicon® Ultra-0.5 3 kDa filter column (Merck Millipore, Tokyo, Japan) and centrifuged at $14,000 \times$ rpm for 1 h. The filtrate was transferred to glass vials for subsequent analysis.

The metabolome data were analyzed by Mass Spectrometry—Data Independent AnaLysis (MS-DIAL) software version 4.60 [48] and R statistical environment Ver 4.0.5. Metabolites were detected at least 50% from the analyzed samples and the coefficient of variation (CV) values of 30% of metabolites in pooled QC samples, and annotation level 2 proposed by Schymanski et al. [49] were used for data analysis. Since we used plasma samples to measure

pro-inflammatory cytokines, the remaining sample size was insufficient. Therefore, we performed metabolomics analysis for seven samples from each group.

Statistical analysis

The data were expressed as the mean ± the standard error of the mean (SEM). Statistical analyses were performed using unpaired Student's t-test or Wilcoxon rank sum tests. For beta-diversity analysis, statistically significant differences between the groups were made with analysis of similarities (ANOSIM). Spearman rank correlation test was used to evaluate the correlations between bacterial taxa, SCFAs, and Iba1 levels in the different brain regions. P values below 0.05 or less were considered statistically significant.

For multivariate analysis of the metabolome data, orthogonal partial least squares discriminant analysis (OPLS-DA) was performed in Simca-P V.14.0 (Umetrics AB). Metabolites with variable importance in the projection (VIP) of > 1, P value < 0.05 (Wilcoxon rank-sum test) were regarded as differentially abundant.

Results

Effects of adolescent WIN55,212–2 exposure on the expression of microglial marker in the brain regions of adult mice after LPS administration

Western blot analysis of microglial marker Iba1 in the mPFC, NAc, and hippocampus of adult mice after LPS administration was performed. Expression of Iba1 in the mPFC and NAc of WIN55,212–2-treated group was significantly higher than that of control group whereas the expression of Iba1 in the hippocampus was not different between the two groups (Fig. 1B–D). In contrast, there were no changes in plasma levels of pro-inflammatory cytokines (IL-6 and TNF-α) between the two groups (Fig. S1). These data suggest that repeated WIN55,212–2 exposure during adolescence could enhance LPS-induced microglial activation in the mPFC and NAc of adult mice.

Composition of gut microbiota

There were no significant changes in α-diversity, including Observed_OTUs, Chao1, ACE, and Shannon between the two groups (Fig. S2A–D). For β-diversity, PCoA based on the weighted UniFrac distance matrix was performed to assess changes in community composition. Although the community of WIN55,212–2 group was deviated from the vehicle group in terms of overall microbiome structure, there were no statistical differences (Fig. S2E).

The relative abundance of the phylum *Firmicutes* was 63.4% in the vehicle group and 56.6% in the WIN55,212–2 group, respectively. *Bacteroidetes* is the second most abundant phylum, with a relative abundance of 35.1% in the vehicle group and 42.0% in the WIN55,212–2 group (Fig. S3A). At the genus level, *Lactobacillus* was predominant, with a relative abundance of 24.0% in the vehicle group and 30.5% in the WIN55,212–2 group, followed by *Eisenbergiella*, which represented 23.1% in the vehicle group and 11.6% in the WIN55,212–2 group, respectively (Fig. S3B). At the species level, the two groups had distinctly different microbiome compositions. The two most abundant bacteria in the vehicle group were *Eisenbergiella massiliensis* (23.1%) and *Lactobacillus murinus* (10.1%); however, the two highest bacteria in the WIN55,212–2 group were *Lactobacillus taiwanensis* (14.5%) and *Eisenbergiella massiliensis* (11.6%) (Fig. S3C).

LEfSe was conducted to identify microbial biomarkers at different classification levels between the two groups. We identified 5 microbial biomarkers such as the genus *Absiella*, *Gabonia*, *Prevotella*, *Fusicatenibacter*, and *Rikenella* were more abundant in the WIN55,212–2 group in comparison with the vehicle group (Fig. 2A and B). In contrast, 2 microbial biomarkers such as the genus *Cuneatibacter* and *Eisenbergiella* showed higher abundance in the vehicle group compared to the WIN55,212–2 group (Fig. 2A and B).

Taxonomic signatures of the gut microbiota

The association of bacteria with WIN55,212–2 treatment was assessed by comparing the relative abundance of different microbiota levels between the two groups. At the phylum level, the relative abundance of the phylum *Verrucomicrobia* in the WIN55,212–2 group was 0%, which was significantly lower than that in the vehicle group, with a relative abundance of 0.02% (Fig. 3A).

The genus *Acetoanaerobium*, *Dehalobacter*, *Desnuesiella*, *Jeotgalibacillus*, *Lysobacter*, *Mobilitalea*, *Prevotella*, *Rikenella*, and *Thermosyntropha* had significantly higher relative abundance in the WIN55,212–2 group than the vehicle group (Fig. 3B). In contrast, the relative

abundance of 8 genera, including *Adlercreutzia*, *Akkermansia*, *Dorea*, *Eisenbergiella*, *Gellertiella*, *Hungatella*, *Photobacterium*, and *Phyllobacterium* in the WIN55,212–2 group was significantly lower than the vehicle group (Fig. 3B).

At the species level, 14 taxa including *Prevotella baroniae*, *Clostridium bolteae*, *Rikenella microfusus*, *Prevotella dentasini*, *Butyricicoccus faecihominis*, *Desnuesiella massiliensis*, *Blautia hydrogenotrophica*, *Mobilitalea sibirica*, *Acetoanaerobium sticklandii*, *Jeotgalibacillus malaysiensis*, *Thermosyntropha tengcongensis*, *Paraprevotella xylaniphila*, *Lysobacter oligotrophicus*, and *Dehalobacter restrictus*, were higher abundances in the WIN55,212–2 group than the vehicle group (Fig. 3C). In contrast, 9 taxa including *Eisenbergiella massiliensis*, *Dorea formicigenerans*, *Hungatella hathewayi*, *Adlercreutzia muris*, *Blautia hominis*, *Gellertiella hungarica*, *Photobacterium damselae*, *Phyllobacterium loti*, and *Akkermansia muciniphila* were lower abundances in the WIN55,212–2 group than the vehicle group (Fig. 3C).

The concentration of fecal SCFAs and its association with the relative abundance of taxa

There were no significant differences in the concentrations of SCFAs (i.e., acetic acid, lactic acid, *N*-butyric acid, propionic acid, and succinic acid) between the two groups (Fig. S4A). Next, we performed a correlation analysis between the relative abundance of bacterial species and the concentration of fecal SCFAs. We found significant associations between the relative abundance of several bacteria and the concentration of fecal SCFAs levels (absolute r value > 0.6, $P < 0.05$) (Fig. S4B).

Metabolomic analysis of plasma samples

Given the interaction between the gut microbiome and host metabolism, we conducted a non-targeted metabolomics analysis of plasma samples from the two groups. After quality control and removal of low-abundance peaks, a subset of 153 metabolites was annotated. The OPLS-DA showed that the metabolic composition of WIN55,212–2

Fig. 2 LEfSe analysis of gut microbiota. **A** Evolutionary branching diagram obtained from LEfSe analysis. **B** The histogram shows the overrepresented taxa with LDA score of 3.0 or higher. Wilcoxon rank-sum test ($n = 9$). *LDA* linear discriminant analysis, *LEfSe* linear discriminant analysis effect size, *N.S* not significant. *WIN* WIN55,212–2
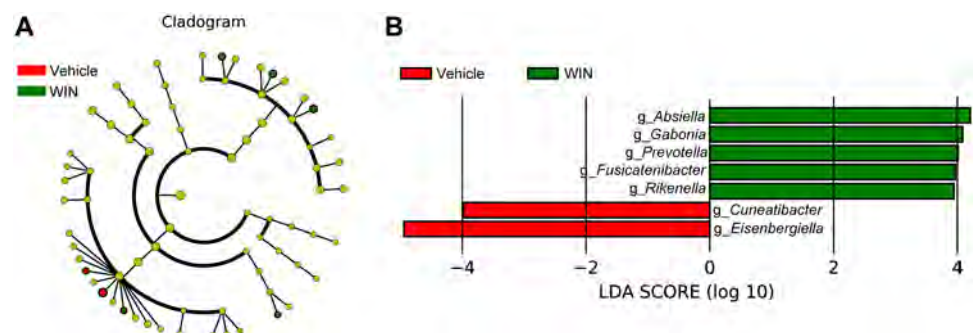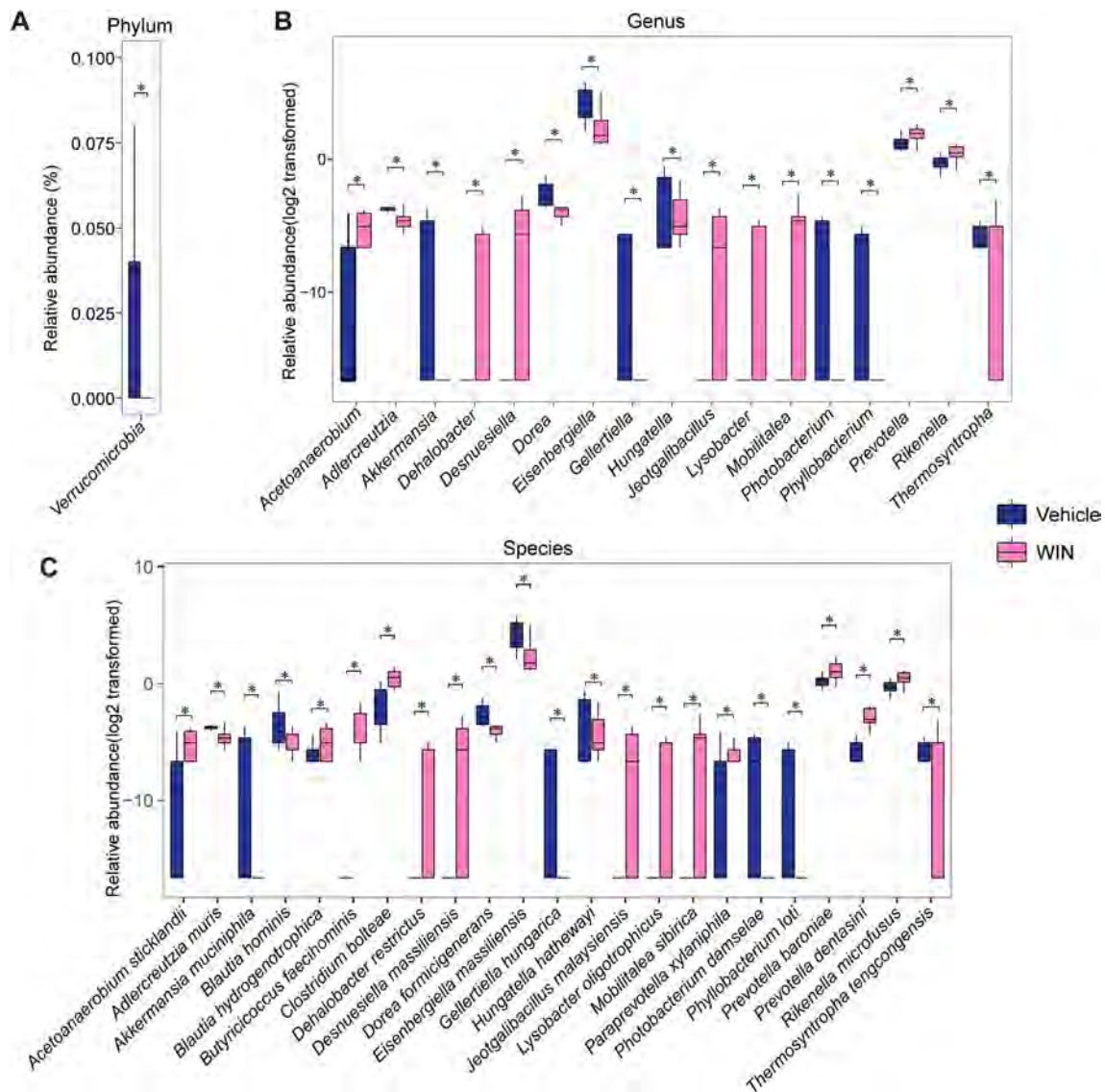
Fig. 3 Effects of adolescent WIN 55,212–2 exposure on the taxonomic abundance of intestinal bacteria in the adult mice. **A** There was significant difference in the relative abundance of the phylum *Verrucomicrobia* between the two groups. **B** There were significant different in the relative abundance of 17 bacteria at the genus level between the two groups. **C** There were significant different in the relative abundance of 23 bacteria at the species level between the two groups. The relative abundance data of microbiomes were transformed with log2. The box plot represents the 25th–75th quartiles, the line inside the box represents the median, and the vertical lines outside represent the maximum and minimum values. Wilcoxon rank-sum test ($n=9$) *$P_{FDR} < 0.05$

group was significantly deviated from that of the vehicle group (Fig. S5). After thresholding the metabolites (VIP value > 1.0, Wilcoxon rank P value < 0.05), we identified 7 metabolites altered between the two groups (Fig. 4A). The seven metabolites increased in the WIN55,212–2 group were allylamine, glutamate-glutamine (Glu-Gln), glycerophosphocholine, L-glutamine, L-threoninamide, propynoic acid, and trifluoroacetic acid (Fig. 4B).

Associations between the gut microbiota and plasma metabolites

Spearman correlation analysis was adopted to investigate the correlation between the species and the seven metabolites (Fig. 4C). There were significant correlations between the relative abundance of several bacteria and the metabolites in the two groups (Fig. 4C). Glu-Gln, a diamino acid composed of glutamate and glutamine, was elevated in

the WIN55,212–2 group and negatively correlated with the WIN55,212–2-depleted species *Akkermansia muciniphila* ($R = -0.55$, $P = 0.042$) (Fig. 4C and D), but positively correlated with the WIN55,212–2-enriched species *Prevotella dentasini* ($R = 0.55$, $P = 0.043$) (Fig. 4C and D). Increased abundance of *Clostridium bolteae* (observed in the WIN55,212–2 group) was positively correlated with glycerophosphocholine ($R = 0.59$, $P = 0.026$) and L-glutamine ($R = 0.59$, $P = 0.027$) (Fig. 4C and D). *Akkermansia muciniphila*, the species decreased in WIN55,212–2 group, was negatively correlated with glycerophosphocholine ($R = -0.61$, $P = 0.021$) (Fig. 4C and D).

Associations of microbiome taxa and metabolites with Iba1 expression in the brain regions

To further understand whether WIN55,212–2-related taxa and metabolites contribute to Iba1 expression in the mPFC and NAc, we tested their correlations using Spearman correlation. The fecal microbes and metabolites differentially abundant in the two groups exhibited more associations with Iba1 expression in the mPFC (Fig. 5A). Several bacteria including *Eisenbergiella massiliensis*, *Dorea formicigenerans*, *Phyllobacterium loti*, and *Gellertiella hungarica* were negatively correlated with Iba1 expression in the mPFC (Fig. 5A). In contrast, several bacteria including *Prevotella baroniae*, *Rikenella microfusus*, *Lysobacter oligotrophicus*, and *Dehalobacter restrictus* were positively correlated with Iba1 expression in the mPFC (Fig. 5A). Interestingly, *Phyllobacterium loti* and *Gellertiella hungarica*, were also negatively correlated with the Iba1 expression in the NAc (Fig. 5A). Furthermore, trifluoroacetic acid enriched in WIN55,212–2 group had suggestive correlation with the Iba1 expression in the NAc (Fig. 5A). The data suggest that several bacteria might regulate microglial activation in the mPFC and NAc of adult mice through gut–microbiota–brain axis.

Predicting functional changes in the gut microbiota

To understand the gut microbial functions associated with adolescent WIN55,212–2 exposure, we used PICRUSt2 to infer the putative metagenome from 16S rRNA gene profiles and annotated using the MetaCyc metabolic pathway database. We found 16 pathways differed ($P < 0.05$) between the two groups. Microbial catabolic and biosynthesis pathways such as pyruvate fermentation to propanoate I, superpathway of UDP-*N*-acetylglucosamine-derived O-antigen building blocks biosynthesis, thiazole biosynthesis I (facultative anaerobic bacteria) were present at higher levels in the WIN55,212–2 group than the vehicle group. In contrast, the adenine and adenosine salvage III pathway was more abundant in the vehicle group than the WIN55,212–2 group.

The remaining 12 pathways were obviously enriched in the WIN55,212–2 group, but the effect size (difference of mean between groups) was minimal (Fig. 5B).

Discussion

The major findings of the present study are as follows: First, LPS significantly increased the expression of Iba1 in the mPFC and NAc of adult mice after repeated WIN55,212–2 exposure during adolescence compared to vehicle exposure during adolescence. In contrast, LPS-induced increases in the plasma IL-6 and TNF-α were not different between the two groups. Second, several bacteria at genus and species levels were significantly different between the two groups. Third, levels of SCFAs in the feces samples were similar in the two groups. However, there were correlations between the relative abundance of microbiome and levels of SCFAs. Fourth, metabolomics analysis of plasma samples showed higher levels of several metabolites in the WIN55,212–2-treated group than vehicle-treated group. Fifth, there were positive (or negative) correlations between the relative abundance of microbiome and metabolites. Interestingly, the relative abundance of microbiome was significantly associated with Iba1 expression in the mPFC and NAc. Finally, several pathways were different between the two groups. Taken together, repeated exposure of WIN55,212–2 during adolescence could produce long-lasting alterations in gut microbiota and LPS-induced microglial activation in the mPFC and NAc of adult mice.

Repeated administration of WIN55,212–2 during early (P35–P40) and mid- (P40–P45) adolescence was reported to produce an enduring state of frequency-dependent prefrontal disinhibition in adulthood [17], suggesting that early and mid-adolescence (P35–P45) is a critical period. Here, we found that repeated administration of WIN55,212–2 during adolescence (P35–P45) caused a marked increase of Iba1 expression in the mPFC and NAc of adult mice after LPS administration. We previously reported that repeated administration of WIN55,212–2 during adolescence (P35–P45) caused a marked increase of methamphetamine-induced hyperlocomotion in adulthood [21]. Collectively, it is likely that repeated stimulation of CB receptor during adolescence could produce long-lasting vulnerability to neuroinflammation in the specific brain regions such as mPFC and NAc of adult brain.

In this study, we found higher abundance of the dominant enrichment bacterium *Clostridium bolteae* in the WIN55,212–2 group than the vehicle group. *Clostridium bolteae* has been associated with a number of inflammatory diseases such as autism spectrum disorder, multiple sclerosis, neuromyelitis optica spectrum disorder, insulin resistance, and dyslipidemia [50–52]. Interestingly, *Clostridium*
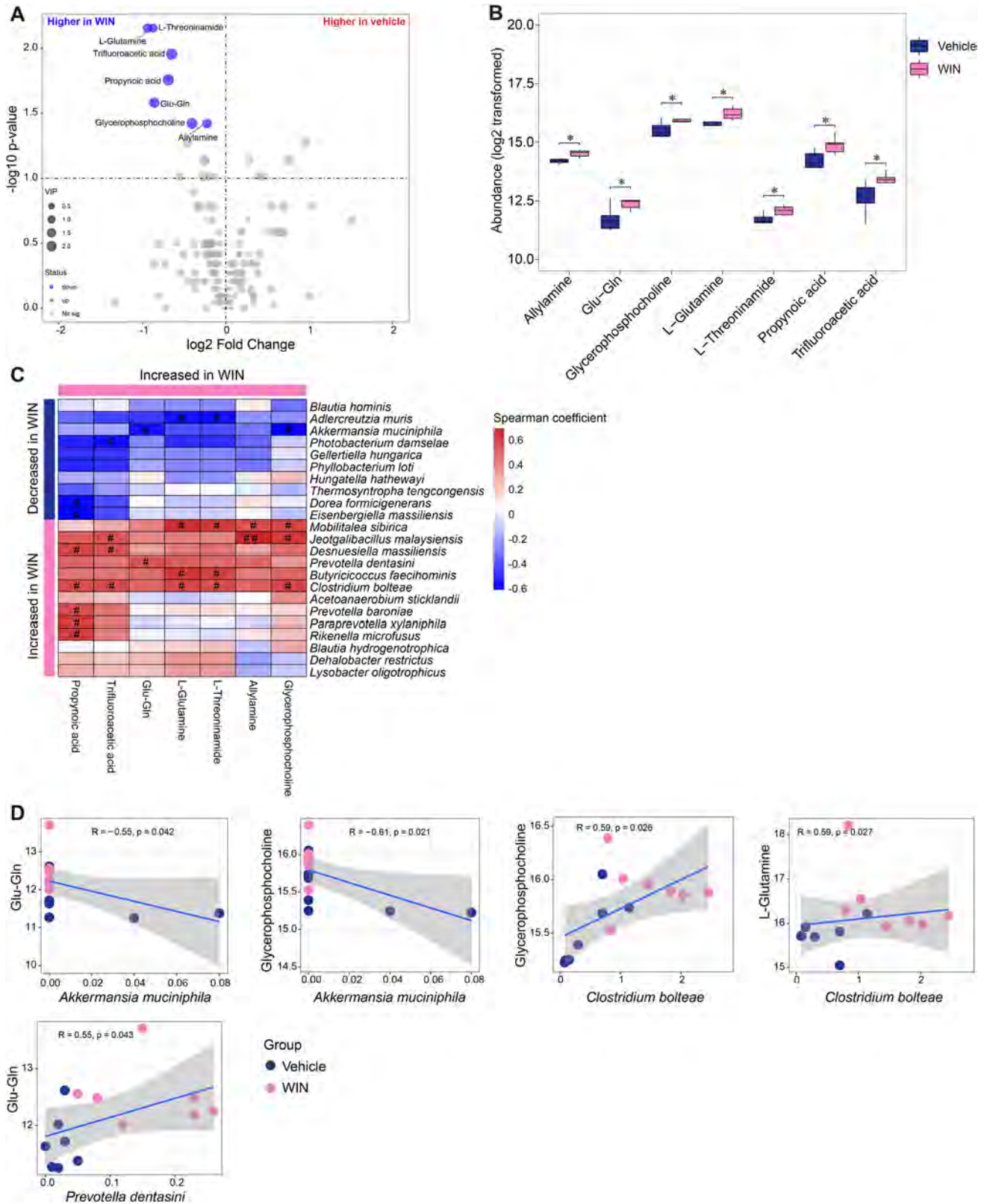
bolteae was also associated with the induction of Th17 cells [52, 53], suggesting a role of inflammatory actions of *Clostridium bolteae*. Collectively, it seems that higher abundance of *Clostridium bolteae* in the WIN55,212–2 group might contribute to neuroinflammation through activation of Th17 signaling although further study is needed.

◄**Fig. 4** Effects of adolescent WIN 55,212–2 exposure on plasma metabolites in the adult mice. **A** Volcano plot shows the differential metabolites between the two groups. The X-axis indicates the log2-transformed plasma metabolite abundance of fold change, and the y-axis indicates the −log10-transformed P value using the Wilcoxon rank-sum test. Horizontal lines indicate $P < 0.05$. Metabolites with increased or decreased metabolites are marked in red and blue, respectively. The size of the dot represents the size of the VIP value. Metabolites with $P < 0.05$ and VIP > 1.0 are marked in text. **B** Changes in metabolic characteristics associated with WIN 55,212–2 group (the relative abundance data of metabolites were transformed with log2, Wilcoxon Rank sum test). **C** Spearman correlation between WIN55,212–2-associated bacteria and WIN55,212–2-associated plasma metabolites. **D** Representative taxon—metabolite correlation diagram. *$P_{FDR} < 0.05$, #$P < 0.05$, ##$P < 0.01$. *VIP* variable importance in projection

Furthermore, we found lower abundance of *Eisenbergiella massiliensis* in the WIN55,212–2 group than the vehicle group. Although detailed functions of *Eisenbergiella massiliensis* is currently unclear, a recent study showed increased abundance of this bacteria in the stools of ketogenic diet fed mice [54]. In addition, there was significantly difference in the abundance of *Eisenbergiella massiliensis* between depressed patients and healthy controls [55]. In this study, we found a negative correlation between the relative abundance of *Eisenbergiella massiliensis* and the expression of Iba1 in the mPFC. Collectively, it is possible that *Eisenbergiella massiliensis* may have anti-inflammatory effects in the host.

Erny et al. [56] reported that germ-free mice showed global defects in microglia with altered cell proportions and an immature phenotype, leading to impaired innate immune response. Furthermore, SCFAs, microbiota-derived products, regulated homeostasis of microglia. The study suggests that gut microbiota in the host are crucial for microglia maturation and activation during health and diseases such as psychiatric and neurological disorders [56]. In this study, we also found a negative correlation between the relative abundance of *Dorea formicigenerans* and the expression of Iba1 in the mPFC. In addition, *Phyllobacterium loti* and *Gellertiella hungarica* were negatively correlated with Iba1 expression in the mPFC and NAc. Given the role of gut–microbiota–microglia crosstalk in the body [56–58], it seems that these bacteria might contribute to neuroinflammation by microglial activation in the brain through gut–microbiota–brain axis.

In this study, we found 7 metabolites increased in the WIN55,212–2 group compared to the vehicle group. Although detailed functions of these metabolites are unknown, it seems that increased levels of these metabolites may contribute to risk for psychosis in adult after adolescent WIN55,212–2 exposure. Interestingly, several bacteria were positively (or negatively) correlated with WIN55,212–2-enriched plasma metabolites, such as glycerophosphocholine,

L-glutamine, L-threoninamide, trifluoroacetic acid, and propynoic acid. For example, there was a positive correlation between the relative abundance of *Clostridium bolteae* and glycerophosphocholine. A recent study showed that glycerophosphocholine may be a novel and specific marker for visceral fat-related peripheral inflammation [59]. Given the inflammatory role of glycerophosphocholine, it is possible that increased levels of this metabolite may play a role in the risk for psychosis after adolescent exposure of WIN55,212–2.

Through the combined analysis of multi-omics data, we found a series of host–microbiome interactions with potential mechanistic implications. Microorganisms in the intestine, including *Prevotella baroniae*, *Rikenella microfususus*, *Lysobacter oligotrophicus*, *Dehalobacter restrictus*, *Acetoanaerobium sticklandii,* and *Paraprevotella xylaniphila* were uniquely elevated in WIN55,212–2-treated mice and positively correlated with Iba1 expression in the mPFC. *Prevotella baroniae* was found to be elevated in the saliva of patients with Crohn's disease and periodontitis [60, 61]. In contrast, *Eisenbergiella massiliensis* and *Dorea formicigenerans* were reduced in WIN55,212–2-treated mice, and were negatively associated with Iba1 levels in the mPFC. In addition, *Phyllobacterium loti*, *Gellertiella hungarica,* and *Photobacterium damselae* decreased in the WIN55,212–2 group were negatively associated with Iba1 levels in the mPFC and NAc. It is reported that *Photobacterium damselae* was a pathogenic bacterium that may cause fatal infections such as necrotizing fasciitis [62, 63]. Taking together, these findings suggest that these microbes may contribute to microglial activation in the mPFc and NAc of adult brain through gut–microbiota–brain axis.

The functional prediction of PICRUSt2 indicated that the pyruvate fermentation to propanoate I pathway was significantly enriched in the WIN55,212–2 group. Propionate has been demonstrated to facilitate Treg differentiation, suppress Th17 differentiation [64], alter hepatic (mitochondrial) metabolism [65], induce apoptosis in neutrophils [66], and affect hematopoiesis and airway inflammation [67]. Furthermore, elevated propionate levels have been associated with modulation of CD4^{+} T cell effector functions through changes in cellular metabolism [68]. Although levels of propionate in the feces samples were not different between the two groups, increased propionate production from pyruvate in the WIN55,212–2 group may lead to long-lasting inflammation of adult mouse brain.

In conclusion, the present study shows that abnormalities in gut microbiota composition and metabolites in adulthood after repeated exposure to WIN55,212–2 during adolescence might play a role in the long-lasting microglial activation in the mPFC and NAc of adult brain. It is likely that gut–microbiota–microglia crosstalk might play
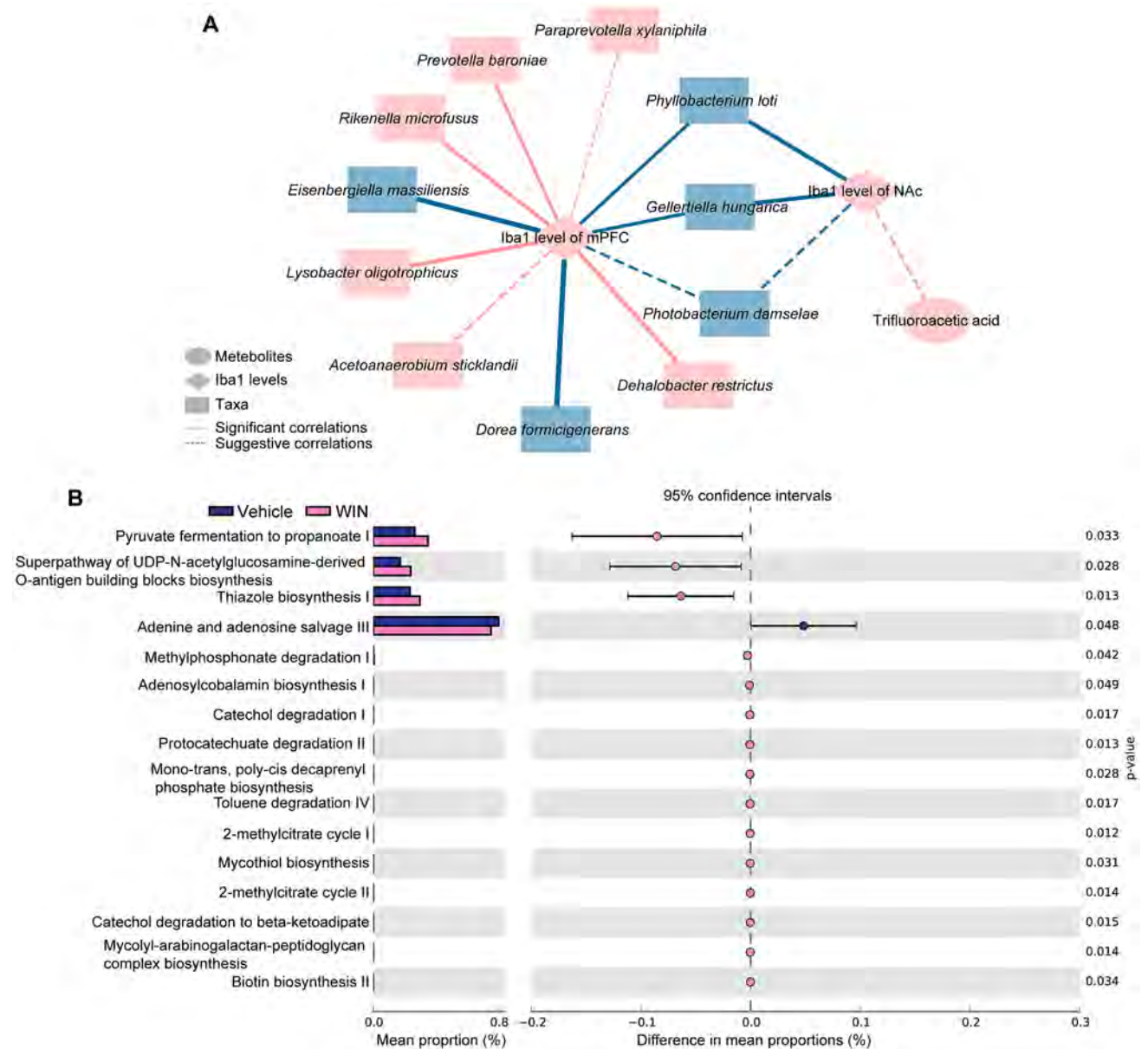
Fig. 5 An integrated association network representing host–microbe interactions, gut microbiome, metabolic profiles and Iba1 levels in the brain regions. **A** Network revealing the association between differentially abundant taxa or metabolites in the WIN 55,212–2 group and vehicle group and Iba1 expression in the mPFC and NAc, Spearman correlation analysis (absolute correlation coefficient > 0.4), nodes represent enriched (red) or depleted (blue) features in the WIN 55,212–2 group compared to vehicle group. The red line connecting the nodes indicates positive correlation and the blue line indicates negative correlation. Solid lines represent significant correlations ($P_{FDR} < 0.05$), and dashed lines indicate suggestive correlations ($P < 0.05$). **B** PICRUSt2 predicted differential pathways between the WIN 55,212–2 group and vehicle group

a role in increased risk for psychosis in adult with cannabis use during adolescence. Finally, brain–gut–microbiota axis could be a potential prophylactic and therapeutic target for psychosis in young adult after repeated use of cannabis during adolescence.

Declarations

Conflict of interest Dr. K. Hashimoto is the inventor of filed patent applications on "The use of *R*-Ketamine in the treatment of psychiatric diseases", "(*S*)-norketamine and salt thereof as pharmaceutical", "*R*-Ketamine and derivative thereof as prophylactic or therapeutic agent for neurodegeneration disease or recognition function disorder", "Preventive or therapeutic agent and pharmaceutical composition for inflammatory diseases or bone diseases", and "*R*-Ketamine and its derivatives as a preventive or therapeutic agent for a neurodevelopmental disorder" by the Chiba University. Dr. K. Hashimoto has also received speakers' honoraria, consultant fee, or research support from Abbott, Meiji Seika Pharma, Daiichi-Sankyo, Dainippon-Sumitomo, Taisho, Otsuka, Seikagaku Corporation, Murakami Farm and Perception Neuroscience. Other authors declare no conflict of interest.

References

1. Johnston LD, O'Malley PM, Bachman JG, Schulenberg JE (2010) Monitoring the future: National Survey Results on Drug Use, 1975–2009. Volume I: Secondary School Students. National Institute on Drug Abuse. NIH Publication No. 10–7584

2. Volkow ND, Baler RD, Compton WM, Weiss SR (2014) Adverse health effects of marijuana use. N Engl J Med 370:2219–2227. https://doi.org/10.1056/NEJMra1402309

3. Linszen DH, Dingemans PM, Lenior ME (1994) Cannabis abuse and the course of recent-onset schizophrenic disorders. Arch Gen Psychiatry 51:273–279. https://doi.org/10.1001/archpsyc.1994.03950040017002

4. Arseneault L, Cannon M, Poulton R, Murray R, Caspi A, Moffitt TE (2002) Cannabis use in adolescence and risk for adult psychosis: longitudinal prospective study. BMJ 325:1212–1213. https://doi.org/10.1136/bmj.325.7374.1212

5. Veen ND, Selten JP, van der Tweel I, Feller WG, Hoek HW, Kahn RS (2004) Cannabis use and age at onset of schizophrenia. Am J Psychiatry 161:501–506. https://doi.org/10.1176/appi.ajp.161.3.501

6. Henquet C, Krabbendam L, Spauwen J, Kaplan C, Lieb R, Wittchen HU, van Os J (2005) Prospective cohort study of cannabis use, predisposition for psychosis, and psychotic symptoms in young people. BMJ 330:11. https://doi.org/10.1136/bmj.38267.664086.63

7. Moore TH, Zammit S, Lingford-Hughes A, Barnes TR, Jones PB, Burke M, Lewis G (2007) Cannabis use and risk of psychotic or affective mental health outcomes: a systematic review. Lancet 370:319–328. https://doi.org/10.1016/S0140-6736(07)61162-3

8. Gobbi G, Atkin T, Zytynski T, Wang S, Askari S, Boruff J, Ware M, Marmorstein N, Cipriani A, Dendukuri N, Mayo N (2019) Association of cannabis use in adolescence and risk of depression, anxiety, and suicidality in young adulthood: a systematic review and meta-analysis. JAMA Psychiat 76:426–434. https://doi.org/10.1001/jamapsychiatry.2018.4500

9. Albaugh MD, Ottino-Gonzalez J, Sidwell A, Lepage C, Juliano A, Owens MM, Chaarani B, Spechler P, Fontaine N, Rioux P, Lewis L, Jeon S, Evans A, D'Souza D, Radhakrishnan R, Banaschewski T, Bokde ALW, Quinlan EB, Conrod P, Desrivières S, Flor H, Grigis A, Gowland P, Heinz A, Ittermann B, Martinot JL, Paillère Martinot ML, Nees F, Papadopoulos Orfanos D, Paus T, Poustka L, Millenet S, Fröhner JH, Smolka MN, Walter H, Whelan R, Schumann G, Potter A, Garavan H, IMAGEN Consortium (2021) Association of cannabis use during adolescence with neurodevelopment. JAMA Psychiatry 78:1–11. https://doi.org/10.1001/jamapsychiatry.2021.1258

10. Lubman DI, Cheetham A, Yücel M (2015) Cannabis and adolescent brain development. Pharmacol Ther 148:1–16. https://doi.org/10.1016/j.pharmthera.2014.11.009

11. Blest-Hopley G, Giampietro V, Bhattacharyya S (2020) A systematic review of human neuroimaging evidence of memory-related functional alterations associated with cannabis use complemented with preclinical and human evidence of memory performance alterations. Brain Sci 10:102. https://doi.org/10.3390/brainsci10020102

12. Stark T, Di Martino S, Drago F, Wotjak CT, Micale V (2021) Phytocannabinoids and schizophrenia: Focus on adolescence as a critical window of enhanced vulnerability and opportunity for treatment. Pharmacol Res 174:105938. https://doi.org/10.1016/j.phrs.2021.105938

13. Stringfield SJ, Torregrossa MM (2021) Disentangling the lasting effects of adolescent cannabinoid exposure. Prog Neuropsychopharmacol Biol Psychiatry 104:110067. https://doi.org/10.1016/j.pnpbp.2020.110067

14. Colizzi M, McGuire P, Pertwee RG, Bhattacharyya S (2016) Effect of cannabis on glutamate signaling in the brain: A systematic review of human and animal evidence. Neurosci Biobehav Rev 64:359–381. https://doi.org/10.1016/j.neubiorev.2016.03.010

15. Curran HV, Freeman TP, Mokrysz C, Lewis DA, Morgan CJ, Parsons LH (2016) Keep off the grass? Cannabis, cognition and addiction. Nat Rev Neurosci 17:293–306. https://doi.org/10.1038/nrn.2016.28

16. van Amsterdam J, Brunt T, van den Brink W (2015) The adverse health effects of synthetic cannabinoids with emphasis on psychosis-like effects. J Psychopharmacol 29:254–263. https://doi.org/10.1177/0269881114565142

17. Cass DK, Flores-Barrera E, Thomases DR, Vital WF, Caballero A, Tseng KY (2014) CB1 cannabinoid receptor stimulation during adolescence impairs the maturation of GABA function in the adult rat prefrontal cortex. Mol Psychiatry 19:536–543. https://doi.org/10.1038/mp.2014.14

18. Verrico CD, Gu H, Peterson ML, Sampson AR, Lewis DA (2014) Repeated Δ9-tetrahydrocannabinol exposure in adolescent monkeys: persistent effects selective for spatial working memory. Am J Psychiatry 171:416–425. https://doi.org/10.1176/appi.ajp.2013.13030335

19. Aguilar DD, Giuffrida A, Lodge DJ (2018) Adolescent synthetic cannabinoid exposure produces enduring changes in dopamine neuron activity in a rodent model of schizophrenia susceptibility. Int J Neuropsychopharmacol 21:393–403. https://doi.org/10.1093/ijnp/pyy003

20. Felder CC, Joyce KE, Briley EM, Mansouri J, Mackie K, Blond O, Lai Y, Ma AL, Mitchell RL (1995) Comparison of the pharmacology and signal transduction of the human cannabinoid CB1 and CB2 receptors. Mol Pharmacol 48:443–450

21. Dong C, Tian Z, Zhang K, Chang L, Qu Y, Pu Y, Ren Q, Fujita Y, Ohgi Y, Futamura T, Hashimoto K (2019) Increased BDNF-TrkB signaling in the nucleus accumbens plays a role in the risk for psychosis after cannabis exposure during adolescence. Pharmacol Biochem Behav 177:61–68. https://doi.org/10.1016/j.pbb.2019.01.002

22. Ma X, Asif H, Dai L, He Y, Zheng W, Wang D, Ren H, Tang J, Li C, Jin K, Li Z, Chen X (2020) Alteration of the gut microbiota in first-episode drug-naïve and chronic medicated schizophrenia correlate with regional brain volumes. J Psychiatr Res 123:136–144. https://doi.org/10.1016/j.jpsychires.2020.02.005

23. Zhu F, Ju Y, Wang W, Wang Q, Guo R, Ma Q, Sun Q, Fan Y, Xie Y, Yang Z, Jie Z, Zhao B, Xiao L, Yang L, Zhang T, Feng J, Guo L, He X, Chen Y, Chen C, Gao C, Xu X, Yang H, Wang J, Dang Y, Madsen L, Brix S, Kristiansen K, Jia H, Ma X (2020) Metagenome-wide association of gut microbiome features for schizophrenia. Nat Commun 11:1612. https://doi.org/10.1038/s41467-020-15457-9

24. Minichino A, Brondino N, Solmi M, Del Giovane C, Fusar-Poli P, Burnet P, Cipriani A, Lennox BR (2021) The gut-microbiome as a target for the treatment of schizophrenia: A systematic review and meta-analysis of randomised controlled trials of add-on strategies. Schizophr Res 234:1–13. https://doi.org/10.1016/j.schres.2020.02.012

25. Spichak S, Bastiaanssen TFS, Berding K, Vlckova K, Clarke G, Dinan TG, Cryan JF (2021) Mining microbes for mental health: determining the role of microbial metabolic pathways in human brain health and disease. Neurosci Biobehav Rev 125:698–761. https://doi.org/10.1016/j.neubiorev.2021.02.044

26. Wei Y, Chang L, Hashimoto K (2022) Molecular mechanisms underlying the antidepressant actions of arketamine: beyond the NMDA receptor. Mol Psychiatry 27:559–573. https://doi.org/10.1038/s41380-021-01121-1

27. García-Cabrerizo R, Carbia C, O Riordan KJ, Schellekens H, Cryan JF (2021) Microbiota-gut-brain axis as a regulator of reward processes. J Neurochem 157:1495–1524. https://doi.org/10.1111/jnc.15284

28. Zhang JC, Wu J, Fujita Y, Yao W, Ren Q, Yang C, Li SX, Shirayama Y, Hashimoto K (2014) Antidepressant effects of TrkB ligands on depression-like behavior and dendritic changes in mice after inflammation. Int J Neuropsychopharmacol https://doi.org/10.1093/ijnp/pyu077

29. Ma M, Ren Q, Yang C, Zhang JC, Yao W, Dong C, Ohgi Y, Futamura T, Hashimoto K (2017) Antidepressant effects of combination of brexpiprazole and fluoxetine on depression-like behavior and dendritic changes in mice after inflammation. Psychopharmacology 234:525–533. https://doi.org/10.1007/s00213-016-4483-7

30. Zhang J, Ma L, Chang L, Pu Y, Qu Y, Hashimoto K (2020) A key role of the subdiaphragmatic vagus nerve in the depression-like phenotype and abnormal composition of gut microbiota in mice after lipopolysaccharide administration. Transl Psychiatry 10:186. https://doi.org/10.1007/s00213-016-4483-7

31. Ma L, Zhang J, Fujita Y, Qu Y, Shan J, Wan X, Wang X, Ishima T, Kobayashi K, Wang L, Hashimoto K (2022) Nuclear factor of activated T cells 4 in the prefrontal cortex is required for prophylactic actions of (R)-ketamine. Transl Psychiatry 12:27. https://doi.org/10.1038/s41398-022-01803-6

32. Zhang J, Ma L, Wan X, Shan J, Qu Y, Hashimoto K (2021) (R)-Ketamine attenuates LPS-induced endotoxin-derived delirium through inhibition of neuroinflammation. Psychopharmacology 238:2743–2753. https://doi.org/10.1007/s00213-021-05889-6

33. Pu Y, Yang J, Chang L, Qu Y, Wang S, Zhang K, Xiong Z, Zhang J, Tan Y, Wang X, Fujita Y, Ishima T, Wang D, Hwang SH, Hammock BD, Hashimoto K (2020) Maternal glyphosate exposure causes autism-like behaviors in offspring through increased expression of soluble epoxide hydrolase. Proc Natl Acad Sci USA 117:11753–11759. https://doi.org/10.1073/pnas.1922287117

34. Shan J, Qu Y, Wang S, Wei Y, Chang L, Ma L, Hashimoto K (2021) Regulation of neurotoxicity in the striatum and colon of MPTP-induced Parkinson's disease mice by gut microbiome. Brain Res Bull 177:103–110. https://doi.org/10.1016/j.brainresbull.2021.09.009

35. Zhang J, Ma L, Hashimoto Y, Wan X, Shan J, Qu Y, Hashimoto K (2021) (R)-Ketamine ameliorates lethal inflammatory responses and multi-organ injury in mice induced by cecum ligation and puncture. Life Sci 284:119882. https://doi.org/10.1016/j.lfs.2021.119882

36. Qu Y, Shan J, Wang S, Chang L, Pu Y, Wang X, Tan Y, Yamamoto M, Hashimoto K (2021) Rapid-acting and long-lasting antidepressant-like action of (R)-ketamine in Nrf2 knock-out mice: a role of TrkB signaling. Eur Arch Psychiatry Clin Neurosci 271:439–446. https://doi.org/10.1007/s00406-020-01208-w

37. Yang Y, Ishima T, Wan X, Wei Y, Chang L, Zhang J, Qu Y, Hashimoto K (2022) Microglial depletion and abnormalities in gut microbiota composition and short-chain fatty acids in mice after repeated administration of colony stimulating factor 1 receptor inhibitor PLX5622. Eur Arch Psychiatry Clin Neurosci 272:483–495. https://doi.org/10.1007/s00406-021-01325-0

38. Guo W, Wan X, Ma L, Zhang J, Hashimoto K (2021) Abnormalities in the composition of the gut microbiota in mice after repeated administration of DREADD ligands. Brain Res Bull 173:66–73. https://doi.org/10.1016/j.brainresbull.2021.05.012

39. Wang S, Ishima T, Zhang J, Qu Y, Chang L, Pu Y, Fujita Y, Tan Y, Wang X, Hashimoto K (2020) Ingestion of Lactobacillus intestinalis and Lactobacillus reuteri causes depression- and anhedonia-like phenotypes in antibiotic-treated mice via the vagus nerve. J Neuroinflammation 17:241. https://doi.org/10.1186/s12974-020-01916-z

40. Wang S, Ishima T, Qu Y, Shan J, Chang L, Wei Y, Zhang J, Pu Y, Fujita Y, Tan Y, Wang X, Ma L, Wan X, Hammock BD, Hashimoto K (2021) Ingestion of Faecalibaculum rodentium causes depression-like phenotypes in resilient Ephx2 knock-out mice: A role of brain-gut-microbiota axis via the subdiaphragmatic vagus nerve. J Affect Disord 292:565–573. https://doi.org/10.1016/j.jad.2021.06.006

41. Pu Y, Tan Y, Qu Y, Chang L, Wang S, Wei Y, Wang X, Hashimoto K (2021) A role of the subdiaphragmatic vagus nerve in depression-like phenotypes in mice after fecal microbiota transplantation from Chrna7 knock-out mice with depression-like phenotypes. Brain Behav Immun 94:318–326. https://doi.org/10.1016/j.bbi.2020.12.032

42. Shinno-Hashimoto H, Hashimoto Y, Wei Y, Chang L, Fujita Y, Ishima T, Matsue H, Hashimoto K (2021) Abnormal composition of microbiota in the gut and skin of imiquimod-treated mice. Sci Rep 11:11265. https://doi.org/10.1038/s41598-021-90480-4

43. Segata N, Izard J, Waldron L, Gevers D, Miropolsky L, Garrett WS, Huttenhower C (2011) Metagenomic biomarker discovery and explanation. Genome Biol 12:R60. https://doi.org/10.1186/gb-2011-12-6-r60

44. Douglas GM, Maffei VJ, Zaneveld JR, Yurgel SN, Brown JR, Taylor CM, Huttenhower C, Langille MGI (2020) PICRUSt2 for prediction of metagenome functions. Nat Biotechnol 38:685–688. https://doi.org/10.1038/s41587-020-0548-6

45. Parks DH, Tyson GW, Hugenholtz P, Beiko RG (2014) STAMP: statistical analysis of taxonomic and functional profiles. Bioinformatics 30:3123–3124. https://doi.org/10.1093/bioinformatics/btu494

46. Zhang K, Fujita Y, Chang L, Qu Y, Pu Y, Wang S, Shirayama Y, Hashimoto K (2019) Abnormal composition of gut microbiota is associated with resilience versus susceptibility to inescapable electric stress. Transl Psychiatry 9:231. https://doi.org/10.1038/s41398-019-0571-x

47. Qu Y, Zhang K, Pu Y, Chang L, Wang S, Tan Y, Wang X, Zhang J, Ohnishi T, Yoshikawa T, Hashimoto K (2020) Betaine supplementation is associated with the resilience in mice after chronic social defeat stress: a role of brain-gut-microbiota axis. J Affect Disord 272:66–76. https://doi.org/10.1016/j.jad.2020.03.095

48. Tsugawa H, Cajka T, Kind T, Ma Y, Higgins B, Ikeda K, Kanazawa M, VanderGheynst J, Fiehn O, Arita M (2015) MS-DIAL: data-independent MS/MS deconvolution for comprehensive metabolome analysis. Nat Methods 12:523–526. https://doi.org/10.1038/nmeth.3393

49. Schymanski EL, Jeon J, Gulde R, Fenner K, Ruff M, Singer HP, Hollender J (2014) Identifying small molecules via high resolution mass spectrometry: communicating confidence. Environ Sci Technol 48:2097–2098. https://doi.org/10.1021/es5002105

50. Campisciano G, de Manzini N, Delbue S, Cason C, Cosola D, Basile G, Ferrante P, Comar M, Palmisano S (2020) The obesity-related gut bacterial and viral dysbiosis can impact the risk of colon cancer development. Microorganisms 8:431. https://doi.org/10.3390/microorganisms8030431

51. Pandit L, Cox LM, Malli C, D'Cunha A, Rooney T, Lokhande H, Willocq V, Saxena S, Chitnis T (2020) *Clostridium bolteae* is elevated in neuromyelitis optica spectrum disorder in India and shares sequence similarity with AQP4. Neurol Neuroimmunol Neuroinflamm 8:e907. https://doi.org/10.1212/NXI.0000000000000907

52. Cox LM, Maghzi AH, Liu S, Tankou SK, Dhang FH, Willocq V, Song A, Wasén C, Tauhid S, Chu R, Anderson MC, De Jager PL, Polgar-Turcsanyi M, Healy BC, Glanz BI, Bakshi R, Chitnis T, Weiner HL (2021) Gut microbiome in progressive multiple sclerosis. Ann Neurol 89:1195–1211. https://doi.org/10.1002/ana.26084

53. Pequegnat B, Monteiro MA (2019) Carbohydrate scaffolds for the study of the autism-associated Bacterium, *Clostridium bolteae*. Curr Med Chem 26:6341–6348. https://doi.org/10.2174/0929867326666190225164527

54. Ferrere G, Tidjani Alou M, Liu P, Goubet AG, Fidelle M, Kepp O, Durand S, Iebba V, Fluckiger A, Daillère R, Thelemaque C, Grajeda-Iglesias C, Alves Costa Silva C, Aprahamian F, Lefevre D, Zhao L, Ryffel B, Colomba E, Arnedos M, Drubay D, Rauber C, Raoult D, Asnicar F, Spector T, Segata N, Derosa L, Kroemer G, Zitvogel L (2021) Ketogenic diet and ketone bodies enhance the anticancer effects of PD-1 blockade. JCI Insight 6:e145207. https://doi.org/10.1172/jci.insight.145207

55. Fontana A, Manchia M, Panebianco C, Paribello P, Arzedi C, Cossu E, Garzilli M, Montis MA, Mura A, Pisanu C, Congiu D, Copetti M, Pinna F, Carpiniello B, Squassina A, Pazienza V (2020) Exploring the role of gut microbiota in major depressive disorder and in treatment resistance to antidepressants. Biomedicines 8:311. https://doi.org/10.3390/biomedicines8090311

56. Erny D, Hrabě de Angelis AL, Jaitin D, Wieghofer P, Staszewski O, David E, Keren-Shaul H, Mahlakoiv T, Jakobshagen K, Buch T, Schwierzeck V, Utermöhlen O, Chun E, Garrett WS, McCoy KD, Diefenbach A, Staeheli P, Stecher B, Amit I, Prinz M (2015) Host microbiota constantly control maturation and function of microglia in the CNS. Nat Neurosci 18:965–977. https://doi.org/10.1038/nn.4030

57. Abdel-Haq R, Schlachetzki JCM, Glass CK, Mazmanian SK (2019) Microbiome-microglia connections via the gut-brain axis. J Exp Med 216:41–59. https://doi.org/10.1084/jem.20180794

58. Ma Q, Xing C, Long W, Wang HY, Liu Q, Wang RF (2019) Impact of microbiota on central nervous system and neurological diseases: the gut-brain axis. J Neuroinflammation 16:53. https://doi.org/10.1186/s12974-019-1434-3

59. Syme C, Pelletier S, Shin J, Abrahamowicz M, Leonard G, Perron M, Richer L, Veillette S, Gaudet D, Pike B, Strug LJ, Wang Y, Xu H, Taylor G, Bennett S, Paus T, Pausova Z (2019) Visceral fat-related systemic inflammation and the adolescent brain: a mediating role of circulating glycerophosphocholines. Int J Obes 43:1223–1230. https://doi.org/10.1038/s41366-018-0202-2

60. Rôcas IN, Siqueira JF Jr (2009) Prevalence of new candidate pathogens *Prevotella baroniae*, *Prevotella multisaccharivorax* and as-yet-uncultivated Bacteroidetes clone X083 in primary endodontic infections. J Endod 35:1359–1362. https://doi.org/10.1016/j.joen.2009.05.033

61. Sun B, Liu B, Gao X, Xing K, Xie L, Guo T (2021) Metagenomic analysis of saliva reveals disease-associated microbiotas in patients with periodontitis and Crohn's disease-associated periodontitis. Front Cell Infect Microbiol 11:719411. https://doi.org/10.3389/fcimb.2021.719411

62. Rivas AJ, Lemos ML, Osorio CR (2013) Photobacterium damselae subsp. damselae, a bacterium pathogenic for marine animals and humans. Front Microbiol 4:283 https://doi.org/10.3389/fmicb.2013.00283

63. Sahu KK, Sherif AA, Davaro R (2019) A rare cause of cellulitis: *Photobacterium damselae*. J Microsc Ultrastruct 8:25–26. https://doi.org/10.4103/JMAU.JMAU_63_18

64. Haghikia A, Jörg S, Duscha A, Berg J, Manzel A, Waschbisch A, Hammer A, Lee DH, May C, Wilck N, Balogh A, Ostermann AI, Schebb NH, Akkad DA, Grohme DA, Kleinewietfeld M, Kempa S, Thöne J, Demir S, Müller DN, Gold R, Linker RA (2015) Dietary fatty acids directly impact central nervous system autoimmunity via the small intestine. Immunity 43:817–829. https://doi.org/10.1016/j.immuni.2015.09.007

65. Perry RJ, Borders CB, Cline GW, Zhang XM, Alves TC, Petersen KF, Rothman DL, Kibbey RG, Shulman GI (2016) Propionate increases hepatic pyruvate cycling and anaplerosis and alters mitochondrial metabolism. J Biol Chem 291:12161–12170. https://doi.org/10.1074/jbc.M116.720631

66. Aoyama M, Kotani J, Usami M (2010) Butyrate and propionate induced activated or non-activated neutrophil apaoptosis via HDAC inhibitor activity but without activating GPR-41/GPR-43 pathways. Nutrition 26:653–661. https://doi.org/10.1016/j.nut.2009.07.006

67. Trompette A, Gollwitzer ES, Yadava K, Sichelstiel AK, Sprenger N, Ngom-Bru C, Blanchard C, Junt T, Nicod LP, Harris NL, Marsland BJ (2014) Gut microbiota metabolism of dietary fiber influences allergic airway disease and hematopoiesis. Nat Med 20:159–166. https://doi.org/10.1038/nm.3444

68. Schilf P, Künstner A, Olbrich M, Waschina S, Fuchs B, Galuska CE, Braun A, Neuschütz K, Seutter M, Bieber K, Hellberg L, Sina C, Laskay T, Rupp J, Ludwig RJ, Zillikens D, Busch H, Sadik CD, Hirose M, Ibrahim SM (2021) A mitochondrial polymorphism alters immune cell metabolism and protects mice from skin inflammation. Int J Mol Sci 22:1006. https://doi.org/10.3390/ijms22031006

Effects of (R)-ketamine on reduced bone mineral density in ovariectomized mice: A role of gut microbiota

Xiayun Wan [a], Akifumi Eguchi [b], Yuko Fujita [a], Li Ma [a], Xingming Wang [a], Yong Yang [a], Youge Qu [a], Lijia Chang [a], Jiancheng Zhang [a,1], Chisato Mori [b,c], Kenji Hashimoto [a,*]

[a] Division of Clinical Neuroscience, Chiba University Center for Forensic Mental Health, Chiba, 260-8670, Japan
[b] Department of Sustainable Health Science, Chiba University Center for Preventive Medical Sciences, Chiba, 263-8522, Japan
[c] Department of Bioenvironmental Medicine, Chiba University Graduate School of Medicine, Chiba, 260-8670, Japan

ARTICLE INFO

ABSTRACT

Depression is a high risk for osteoporosis, suggesting an association between depression and low bone mineral density (BMD). We reported that the novel antidepressant (R)-ketamine could ameliorate the reduced BMD in the ovariectomized (OVX) mice which is an animal model of postmenopausal osteoporosis. Given the role of gut microbiota in depression and bone homeostasis, we examined whether gut microbiota plays a role in the beneficial effects of (R)-ketamine in the reduced BMD of OVX mice. OVX or sham was operated for female mice. Subsequently, saline (10 ml/kg/day, twice weekly) or (R)-ketamine (10 mg/kg/day, twice weekly) was administered intraperitoneally into OVX or sham mice for the six weeks. The reduction of cortical BMD and total BMD in the OVX mice was significantly ameliorated after subsequent repeated intermittent administration of (R)-ketamine. Furthermore, there were significant changes in the α- and β-diversity between OVX + saline group and OVX + (R)-ketamine group. There were correlations between several OTUs and cortical (or total) BMD. There were also positive correlations between the genera *Turicibacter* and cortical (or total) BMD. Moreover, there were correlations between several metabolites in blood and cortical (or total) BMD. These data suggest that (R)-ketamine may ameliorate the reduced cortical BMD and total BMD in OVX mice through anti-inflammatory actions via gut microbiota. Therefore, it is likely that (R)-ketamine would be a therapeutic drug for depressed patients with low BMD or patients with osteoporosis.

This article is part of the Special Issue on 'Ketamine and its Metabolites'.

1. Introduction

Osteoporosis, the common bone disease, is characterized by low bone mass and structural deterioration of bone tissue, leading to fragility of the bone. It is well known that people with osteoporosis have depression, suggesting depression as a risk factor for osteoporosis (Cizza et al., 2009; Wu et al., 2009). Furthermore, bone mineral density (BMD) in patients with depression is lower than that of subjects without depression (Schweiger et al., 2016; Yirmiya et al., 2009), suggesting depression as a risk factor for low BMD. Interestingly, the use of antidepressants such as selective serotonin reuptake inhibitors (SSRIs) is associated with osteoporotic fracture in elderly peoples (Kindilien et al., 2018; Rizzoli et al., 2012; Wadhwa et al., 2017) Therefore, it is

important to develop the novel drugs which can produce antidepressant effects for depression in patients with osteoporosis.

The N-methyl-ᴅ-aspartate receptor (NMDAR) antagonist ketamine has rapid-acting and sustained antidepressant actions in severe patients with depression (Bahji et al., 2021; Zhang and Hashimoto, 2019). We demonstrated that (R)-ketamine, (R)-enantiomer of ketamine, would be a novel antidepressant without side effects of ketamine (Hashimoto, 2019, 2020, 2022; Wei et al., 2022; Yang et al., 2015; Zhang et al., 2014). We recently reported that (R)-ketamine significantly ameliorated plasma receptor activator of NF-κB ligand (RANKL) levels and osteoprotegerin (OPG)/RANKL ratio in mice with depression-like phenotypes (Xiong et al., 2019; Zhang et al., 2018). Furthermore, (R)-ketamine significantly attenuated the reduction of cortical BMD and total BMD in mice with depression-like phenotypes (Xiong et al., 2019) and

Abbreviation

ANOSIM	analysis of similarities
BMD	bone mineral density
ESI	electrospray ionization
IFN-γ	interferon gamma
IL-6	interleukin-6
IL-8	interleukin-8
NCG	N-carbamoylglutamic acid
NF-κB	nuclear factor kappa-light-chain-enhancer of activated B cells
NMDAR	*N*-methyl-D-aspartate receptor
OPG	osteoprotegerin
OPLS-DA	orthogonal partial least squares discriminant analysis
OTU	operational taxonomic units
OVX	ovariectomized
RANKL	receptor activator of nuclear factor kappa-B ligand
R-KT	(*R*)-ketamine
SCFA	short-chain fatty acid
SSRI	selective serotonin reuptake inhibitor
SUCNR1	succinate receptor 1
TNF-α	tumor necrosis factor α
VIP	variable importance in projection

ovariectomized (OVX) mice (Fujita and Hashimoto, 2020). These findings suggest that (*R*)-ketamine would be a potential drug for reduced BMD and depression in patients with osteoporosis (Wei et al., 2022). However, the precise mechanisms underlying (*R*)-ketamine's beneficial actions in OVX mouse model remain unclear.

Accumulating evidence suggests that gut microbiota plays a key role in health and diseases such as osteoporosis (Fan et al., 2021; Seely et al., 2021; Zhang et al., 2021). Several studies showed significant differences in the composition of gut microbiota in patients with osteoporosis compared to healthy control group (Xu et al., 2020; Wei et al., 2021). It is suggested that gut microbiota play an important role in bone remodeling and bone health maintenance through the regulation of the immune system (Hernandez et al., 2022; Lu et al., 2021; Tu et al., 2021; Zhong et al., 2021). Previously, we reported that abnormal composition of gut microbiota in mice with depression-like phenotypes was ameliorated after subsequent single administration of (*R*)-ketamine (Qu et al., 2017; Yang et al., 2017), suggesting a possible role of gut-microbiota-brain axis for (*R*)-ketamine's actions (Hashimoto, 2019, 2020; Wei et al., 2022). Given the role of gut microbiota in bone health maintenance, it is of great interest to investigate the role of gut microbiota in the beneficial actions of (*R*)-ketamine in OVX model.

The present study was undertaken to investigate whether gut microbiota play a role in the beneficial effects of (*R*)-ketamine in OVX model. First, we examined the effects of (*R*)-ketamine on reduced BMD of OVX mice. Second, we performed 16S rRNA gene amplicon sequencing of feces samples for gut microbiota analysis. Third, we performed the metabolomic analysis of plasma samples and measurement of short-chain fatty acids (SCFAs) in fecal samples since gut microbiota are known to play a role in the production of a number of metabolites such as SCFAs (Agus et al., 2021; Dalile et al., 2019; Morrison et al., 2016).

2. Material and methods

2.1. Animals

We obtained mice C57BL/6 (female, 8 weeks old, 16–20 g body weight) from Japan SLC Inc. (Hamamatsu, Shizuoka, Japan). All mice were carefully and gently kept in translucent polycarbonate cages (21 ×

30 × 22.5 cm) with 4–5 mice in each cage under automatically controlled 12 h/12 h of illuminating light/dark cycle (lights were on from 7:00 a.m. to 7:00 p.m.), with a constant and stable room temperature settled at 23 ± 1 °C and relative humidity of 55 ± 5%. The experimental procedure used in this study was approved by the Chiba University Institutional Animal Care and Use Committee (Permission number 2–144 and 2–389). Deep anesthesia was induced with an inhaled form of isoflurane, and the animals were rapidly sacrificed by the cervical dislocation method with skilled maneuvers. We did our best to minimize the suffering of animals.

2.2. Materials

(*R*)-ketamine hydrochloride was prepared as previously reported (Zhang et al., 2014). (*R*)-ketamine was dissolved in saline and the dose was (10 mg/kg as hydrochloride, intraperitoneal injection) as previously reported (Fujita and Hashimoto, 2020).

2.3. Surgery, treatment and collection of samples

A total of 27 female mice were randomly and equally divided into three groups. All female mice used in the experiments were under isoflurane-induced anesthesia and underwent ovariectomy or sham surgery on day 0. After the mice were anesthetized, hair on the back below the rib was shaved, betadine was used to sterilize the surgical area, and a 1–2 cm incision was made in the skin and muscle layer under the rib on one side to locate the ovary, ligate the fallopian tube and remove the ovary. The muscle layer and skin were then sutured and disinfected. The same procedure was performed on the opposite side. Mice in the sham-operated group underwent the same procedure, except for ovaries removal and tubal ligation. Subsequently, (*R*)-ketamine (10 mg/kg/day, twice weekly) or saline (10 ml/kg/day, twice weekly) was administered intraperitoneally (i.p.) to mice for 6 weeks (day 1–day 39). On the morning of day 43, fresh fecal samples were collected from all mice for 16S ribosomal RNA sequencing and short-chain fatty acids (SCFAs) assay. On the afternoon of day 43, femur samples were collected and maintained in 4% paraformaldehyde, 4 °C overnight, for subsequent bone mineral density (BMD) measurements. Furthermore, plasma samples were collected and stored at −80 °C for untargeted metabolomics analysis. On the morning of day 44, femurs were washed with phosphate saline buffer, merged with 25%, 50%, 75%, and 100% ethanol, and stored at 4 °C until measurement of BMD as previously reported (Fujita and Hashimoto, 2020).

2.4. Measurement of bone mineral density (BMD)

CT imaging system (LaTheta LCT-200; Hitachi Arouca Medical, Tokyo, Japan) was employed to determine the density of cortical, cancellous, planar, and total bone of the femoral neck. The LaTheta software (version 3.40) was used to measure and quantify the bone mineral density as previously reported (Fujita and Hashimoto, 2020; Xiong et al., 2019; Zhang et al., 2020).

2.5. 16S rRNA sequencing analysis and measurement of SCFAs

Fecal samples from all mice in this experiment were collected fresh and stored at −80 °C immediately after collection. The extraction of DNA from mouse fecal samples and the corresponding 16S rRNA data analysis was conducted at MyMetagenome Co, Ltd. (Tokyo, Japan), as previously reported (Guo et al., 2021). Sequences are available via the National Center for Biotechnology Information Sequence Read Archive (accession number PRJNA768302). We calculated the beta-diversity of microbial communities using the weighted UniFrac distance matrix. Alpha-diversity was calculated ACE, and observed_OTU indices.

Quantification of SCFAs (acetic acid, propionic acid, butyric acid, succinic acid, *N*-valeric acid, and lactic acid) in the fecal samples was

measured at TechnoSuruga Laboratories Ltd. (Shizuoka, Japan), as previously reported (Guo et al., 2021).

The software PICRUSt2 (Douglas et al., 2020) was applied to predict the metagenomic functional compositions. Welch's *t*-test was identified pathways with significant differences of abundance between the OVX + saline and OVX + (*R*)-ketamine groups. To correct for multiple testing, the Storey FDR (false discovery rate) method was used simultaneously. We also applied STAMP (Parks et al., 2014) software (v2.1.3) for statistical analysis and visualization of significant difference pathways.

2.6. Untargeted metabolomics analysis

Analysis was performed on an ExionLC AD UPLC system (SCIEX, Tokyo, Japan) interfaced with an X500R LC-QToFMS system (SCIEX, Tokyo, Japan) with electrospray ionization (ESI) operated in both positive and negative ion modes. After adding the 100 µL methanol containing internal standards (100 µM N,*N*-diethyl-2-phenylacetamide, and d-camphor-10-sulfonic acid), plasma samples (100 µL) were centrifuged

at 14000 × rpm for 5 min. After centrifuge, the supernatant was transferred to Amicon® Ultra-0.5 3 kDa filter columns (Merck Millipore, Tokyo, Japan) and centrifuged at 14000 × rpm for 1 h. Filtrates were transferred to glass vial for analysis.

The metabolome data was analyzed by Mass Spectrometry - Data Independent AnaLysis (MS-DIAL) software version 4.60 (Tsugawa et al., 2015) and R statistical environment Ver 4.0.5. In this study, metabolomes were detected at least 50% from the analyzed samples, and the coefficient of variation (CV) values of 30% of metabolomes, and annotation level 2 proposed by Schymanski et al. (2014) were used for data analysis. Peak heights were nomadized by peak heights of internal standards and locally weighted least-square regression (locally estimated smoothing function, LOESS) and cubic spline with QC samples.

Orthogonal partial least squares discriminant analysis (OPLS-DA) is a multivariate analysis model implemented in SIMCA-P (V.14.0). Significant peaks were determined by combination of variable importance in projection (VIP) value > 0.3 and Wilcox rank test P values < 0.05 (FDR < 0.51).
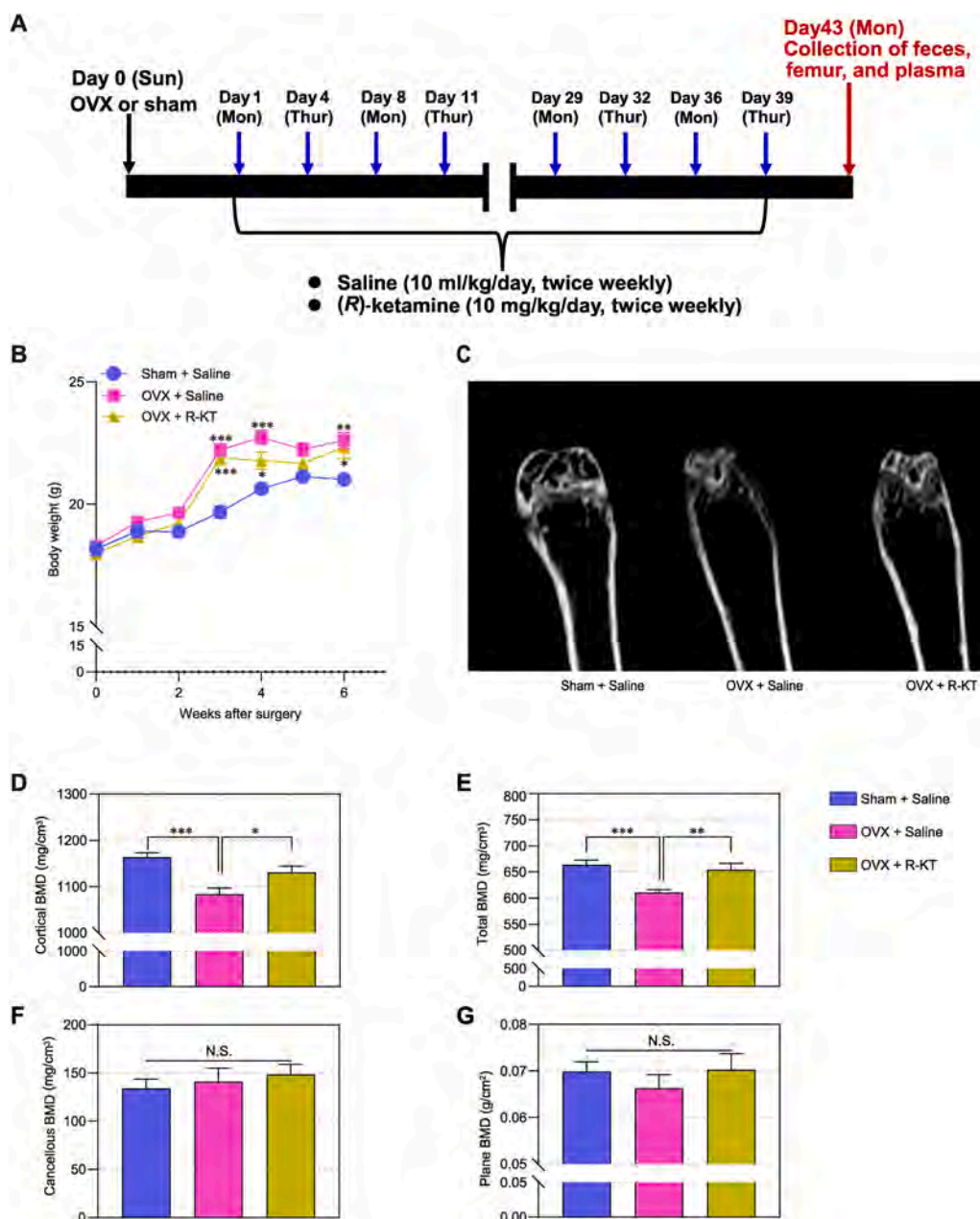
Fig. 1. Experimental design and data of body weight change and BMD. A: Experimental schedule. Surgery for sham or ovariectomy (OVX) was performed on day 0 (Sunday). Subsequently, saline (10 ml/kg/day, twice weekly) or (*R*)-ketamine (10 mg/kg/day, twice weekly) was administered i. p. to mice for 6 weeks (day 1–day 39). In the morning of day 43, fresh fecal samples were collected from the mice. Then plasma samples were collected from all mice in the afternoon of day 43. B: Changes in body weight of three groups of mice. There were significant changes in body weight among the three groups (repeated-measures ANOVA, $F_{(7.14, 85.691)} = 13.919$, $P < 0.0005$). C: The representative image of femur bone mass observed by microcomputed tomography (CT). (*R*)-ketamine ameliorated the femur bone loss by OVX. D: Cortical BMD (one-way ANOVA, $F_{(2, 24)} = 11.07$, $P = 0.0004$). E: Total BMD (one-way ANOVA, $F_{(2, 24)} = 10.22$, $P = 0.0006$). F: Cancellous BMD (one-way ANOVA, $F_{(2, 24)} = 0.41$, $P = 0.67$). G: Plane BMD (one-way ANOVA, $F_{(2, 24)} = 0.58$, $P = 0.57$). The values represent the mean ± S.E.M. (n = 9). *$P < 0.05$, **$P < 0.01$, ***$P < 0.001$. BMD: bone mineral density. N.S.: not significant. OVX: ovariectomized. R-KT: (*R*)-ketamine.

2.7. Statistical analysis

The data are expressed as the mean ± the standard error of the mean (SEM). Significant differences of BMD data among the three groups were analyzed by one-way analysis of variance (ANOVA), followed by Tukey's multiple comparisons test. For body weight data, we used repeated measures ANOVA. For α-diversity, SCFAs, abundances of microbial taxa, metabolite abundances analysis, the differences among the three groups were assessed using the Kruskal-Wallis rank test, followed by pairwise comparisons using the Wilcoxon rank-sum test with FDR correction. For β-diversity analysis, differences between the groups were analyzed using analysis of similarities (ANOSIM). The P-values of less than 0.05 were considered statistically significant.

3. Results

3.1. Effects of (R)-ketamine on reduced BMD of OVX mice

Surgery of OVX or sham was performed on day 0. Subsequently, saline (10 ml/kg/day) or (R)-ketamine (10 mg/kg/day) was administered to mice from day 1 to day 39 (Fig. 1A). Body weight of all mice was increased gradually. At the third, fourth, and sixth weeks after surgery, body weight of OVX + saline group and OVX + (R)-ketamine group was significantly higher than that in the sham + saline group (Fig. 1B). Representative CT images of femurs from each group were shown (Fig. 1C). Compared to the sham + saline group, cortical BMD and total BMD of OVX mice were significantly lower than those of sham + saline group (Fig. 1D and E). (R)-ketamine significantly ameliorated these reductions of OVX mice (Fig. 1D and E). In contrast, there were no changes in cancellous BMD and plane BMD among the three groups (Fig. 1F and G). The data are consistent with our previous report (Fujita and
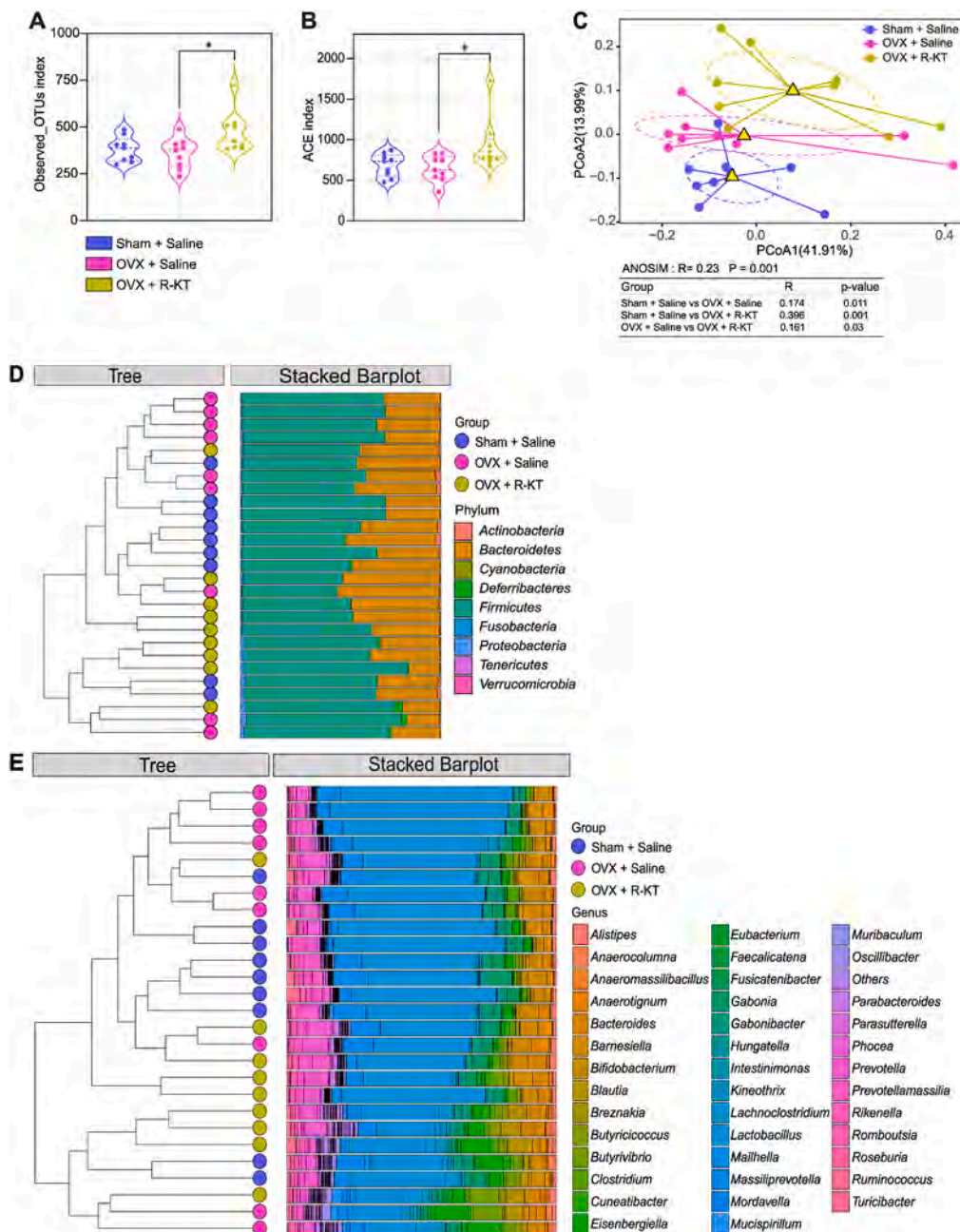
Fig. 2. Alpha-diversity, beta-diversity and composition of gut microbiota. A: Observed_OTUs index (Kruskal-Wallis test, P = 0.035). B: ACE index (Kruskal-Wallis test, P = 0.037). C: Principal coordinate analysis based on weighted Unifrac distances (ANOSIM, R = 0.23, P = 0.001). D: Bacterial Composition at the phylum level. E: Bacterial Composition at the genus level. In violin plots, the horizontal dotted lines indicate median, quartiles. The number of mice in each group was n = 9. *P < 0.05. N.S.: not significant. OVX: ovariectomized. R-KT: (R)-ketamine.

Hashimoto, 2020).

3.2. Composition of gut microbiota

For α-diversity, observed _OTUs and ACE indices in OVX + (R)-ke-tamine were significantly greater than those in OVX + saline group although there were no changes in these indices between sham + saline group and OVX + saline group (Fig. 2A and B). To determine the simi-larity (β-diversity) between microbial communities in each group, a principal component analysis (PCoA) was performed using the weighted UniFrac distance matrix. There were significant differences of β-di-versity among the three groups (Fig. 2C).

Next, we specified the relative proportions of dominant taxa at the phylum level. A total of 9 phyla were ultimately clarified in each group

(Fig. 2D). *Firmicutes* was the most dominant phylum with a relative abundance of 62.7% in the sham + saline group, 66.1% in the OVX + saline group, and 63.1% in the OVX + (R)-ketamine group. *Bacteroidetes* was second dominant phylum with a relative abundance of 35.1% in the sham + saline group, 31.3% in the OVX + saline group, and 34.3% in the OVX + (R)-ketamine group (Fig. 2D).

We investigated the top 40 most abundant microbiome at the genus level (Fig. 2E). The most dominant genus, *Lactobacillus*, was accounted for 41.1% across all samples. Based on the Bray-Curtis difference index, we clustered microbial community components to explore the microbial community profiles in each group. There was significant clustering be-tween the sham + saline group and OVX + (R)-ketamine group. In contrast, there was no obvious clustering between the OVX + saline and sham + saline group or OVX + (R)-ketamine group (Fig. 2D and E).
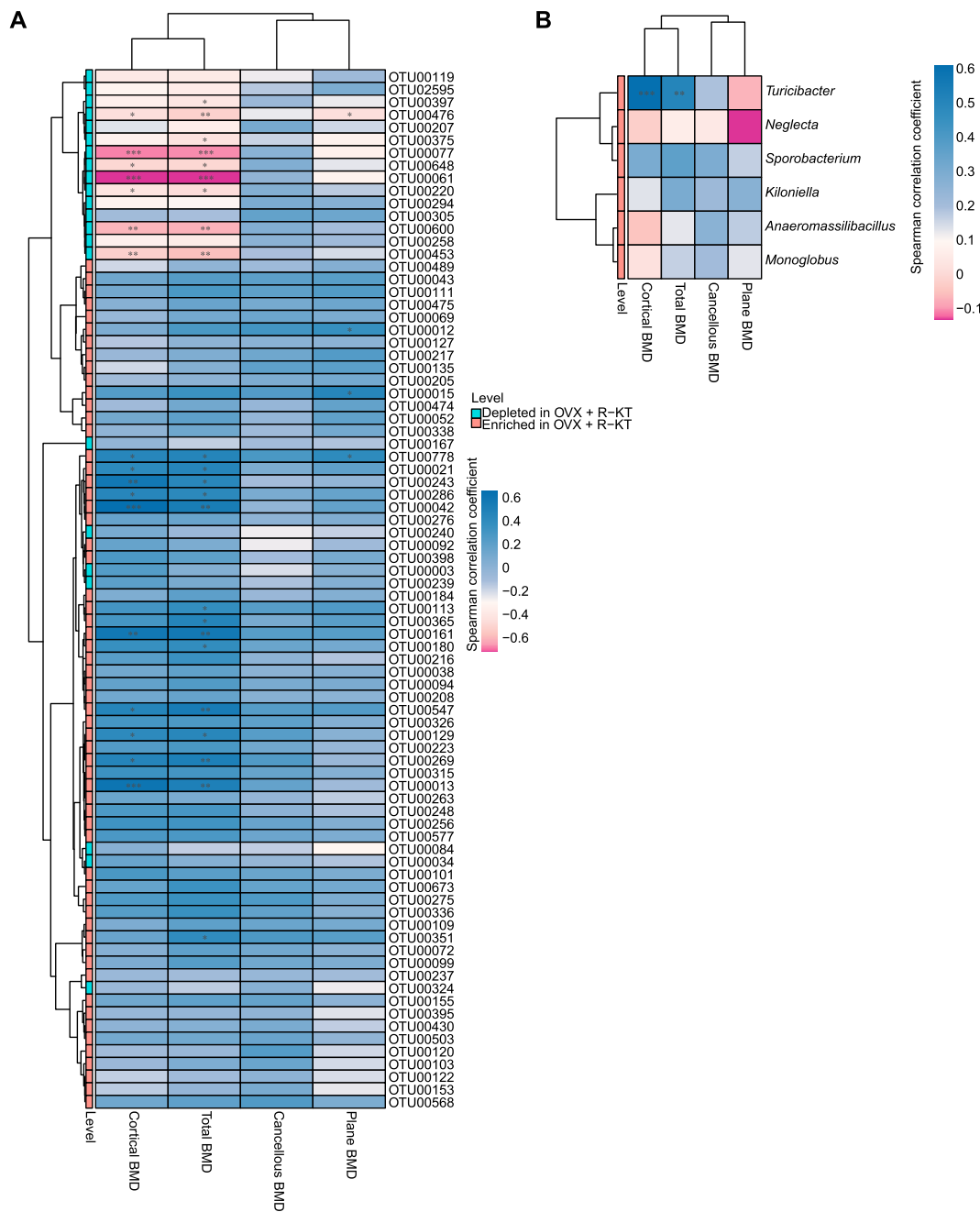
Fig. 3. Spearman correlations between (R)-ketamine-associated gut microbiota and BMD. A: Correlations between representative OTUs with cortical BMD, total BMD, cancellous BMD and plane BMD of the mouse femur. B: Correlations between (R)-ketamine-related genera and cortical BMD, total BMD, cancellous BMD, and plane BMD of the mouse femur. *P_{FDR} < 0.05, **P_{FDR} < 0.01, ***P_{FDR} < 0.001. BMD: bone mineral density. OVX: ovariectomized. R-KT: (R)-ketamine.

3.3. Correlations of gut microbiota with BMD

Considering the role of gut microbiota in bone function, we hypothesized that altered gut microbiota abundances might be associated with beneficial effects of (*R*)-ketamine on reduced BMD in OVX mice. In this study, we pay attention to the gut microbiota that differed markedly in abundance between the OVX + saline and OVX + (*R*)-ketamine groups. The gut microbiota abundance in each group was then investigated at the OTU and genus levels. Our results showed that 82 of 2838 OTUs and 6 of 188 genera reached statistically significant between OVX + saline group and OVX + (*R*)-ketamine group (P < 0.05, Supplementary Table 1). The distribution of the relative abundance of differential OTUs between the OVX + saline group and OVX + (*R*)-ketamine group was shown in Supplementary Fig. 1. We quantified correlations between (*R*)-ketamine-related OTUs (or genera) and BMD using the Spearman correlation method (Fig. 3A and B). We identified that the relative abundance of 9 OTUs, including OTU00061 (*Kineothrix*), OTU00077 (*Blautia*), OTU00220 (*Faecalicatena*), OTU00375 (*Magnetovibrio*), OTU00397 (*G_undefined_Ruminococcaceae*), OTU00453 (*Pseudoflavonifractor*), OTU00476 (*Flavonifractor*), OTU00600 (*Butyricicoccus*), and OTU00648 (*Faecalicatena*) were significantly negatively correlated with cortical BMD and total BMD or plane BMD of the femoral neck. In contrast, the relative abundances of 16 OTUs such as OTU00012 (*Rikenella*), OTU00013 (*Turicibacter*), OTU00015 (*Gabonia*), OTU00021 (*Blautia*), OTU00042 (*Eisenbergiella*), OTU00113 (*Kineothrix*), OTU00129 (*Eubacterium*), OTU00161 (*Lachnoclostridium*), OTU00180 (*Alkaliphilus*), OTU00243 (*Eisenbergiella*), OTU00269 (*Anaeromassilibacillus*), OTU00286 (*Fusicatenibacter*), OTU00351 (*Monoglobus*), OTU00365 (*Erysipelatoclostridium*), OTU00547 (*Lachnoclostridium*), and OTU00778 (*Oscillibacter*) were significantly positively correlated with cortical BMD and total BMD or plane BMD (Fig. 3A). At the genus level, *Turicibacter,* one of the (*R*)-ketamine-related genera, was positively correlated with cortical BMD (coefficient = 0.61, P = 0.0007) and total BMD (coefficient = 0.51, P = 0.007) (Fig. 3B). These data suggest that the genera *Turicibacter* may play a role in the beneficial effects of (*R*)-ketamine in reduced BMD of OVX mice.

3.4. Correlations of gut microbiota with SCFAs

We measured SCFAs in these fecal samples (Supplementary Fig. 2A). There were significant changes in succinic acid among the three groups (Kruskal-Wallis rank test, P = 0.035). Levels of succinic acid in the OVX + (*R*)-ketamine group were significantly lower than those of sham + saline group. In contrast, there were no changes in other SCFAs (lactic acid, acetic acid, propionic acid, N-butyric acid, and N-valeric acid) among the three groups (Supplementary Fig. 2A).

Interestingly, SCFAs were significantly associated with some OTUs. Spearman correlation network (absolute value of correlation coefficient >0.6, P < 0.05) was shown in Supplementary Fig. 2B. Specifically, the concentration of succinic acid in mouse feces was negatively correlated with the abundance of the following 11 OTUs, such as OTU00041 (*Kineothrix*), OTU00056 (*Eisenbergiella*), OTU00072 (*Anaeromassilibacillus*), OTU00103 (*Faecalicatena*), OTU00146 (*Intestinimonas*), OTU00153 (*Neglecta*), OTU00189 (*Frisingicoccus*), OTU00194 (*Lachnoclostridium*), OTU00218 (*Breznakia*), OTU00309 (*Blautia*), and OTU00430 (*Roseburia*) (Supplementary Fig. 2B). In contrast, there was a positive correlation between *OTU00003* (*Lactobacillus*) and succinic acid (Supplementary Fig. 2B). Lactic acid was positively correlated with the abundance of OTU00104 (*Anaerocolumna*), and acetic acid was correlated with the relative abundance of OTU00020 (*Bifidobacterium*), OTU00216 (*Colidextribacter*), OTU00361 (*Anaerotignum*), OTU00365 (*Erysipelatoclostridium*), and OTU00457 (*Eubacterium*). Propionic acid was correlated with the abundance of OTU00457 (*Eubacterium*), OTU00979 (*Bacteroides*), OTU01702 (*Barnesiella*), OTU02595 (*Prevotella*). N-valeric acid was positively correlated with the abundance of OTU00512 (*Roseburia*), but negatively correlated with the abundance of

OTU00260 (*Streptococcus*) (Supplementary Fig. 2B).

3.5. Metabolomic analysis of plasma samples

To examine the interaction between gut microbiota and host metabolism at the plasma metabolic level, we performed untargeted metabolomics analysis of plasma samples. After quality control and removal of low-abundance peaks, a total of 199 positive ion pattern features and 73 negative ion pattern features were identified. The OPLS-DA model was employed to represent the distribution of plasma metabolic components in the OVX + saline group and the OVX + (*R*)-ketamine group. The scatter plots of the scores of the two models are shown (Supplementary Figs. 3A and 3B). After thresholding metabolites (VIP values > 0.3, Wilcoxon rank P values < 0.05, FDR < 0.51), we identified a total of 24 metabolites with significant abundance differences between the OVX + saline group and OVX + (*R*)-ketamine group (Fig. 4A). Includes 15 features that can be classified based on the data Human Metabolome Database and 9 features that cannot be classified (Supplementary Table 2). Specifically, 17 metabolites were downregulated in the OVX + (*R*)-ketamine group versus the OVX + saline group. These metabolites were [(aminocarbonyl)(methyl)amino]acetic acid, 2,4-dichloro-5-ethyl-3-methylphenol, 2,5-dimethylthiazole, 2-aminoethylphosphonate, 2-methyl-1-butanethiol, 2-vinylthiophene, 3-methylthiophene, 9,10-dihydrojasmonic acid, D-alanine, dihydrouracil, DL-arginine, ethyl 3-mercaptobutyrate, ethyl 4-hydroxy-2-methyl-6-quinolinecarboxylate, L-citrulline, *N*-carbamoyl-glutamic acid, *N*-nitroethylenediamine, xi-2-mercapto-3-methyl-1-butanol (Fig. 4A). In contrast, a total of 7 plasma metabolites were upregulated in the OVX + (*R*)-ketamine group compared to the OVX + saline group. These metabolites included 1,2,5-oxadiazole-3,4-dicarboxylic acid, 3-(3-acetyl-2,6-dihydroxy-5-methyl-benzyl)-4-hydroxy-5-methylfuran-2(5H)-one, 4-deoxyerythronic acid, 5-[(4-nitrobenzoyl)amino]isophthalic acid, 5-keto-D-gluconic acid, citric acid, dihydroxyacetone (Fig. 4A). Furthermore, we depicted the abundance distribution of these metabolites across the three groups (Supplementary Fig. 4).

Next, we investigated the correlations between the above identified metabolites and BMD. A total of 9 plasma metabolites were significantly associated with BMD indices in mice (Fig. 4B). Among them, 8 plasma metabolites, such as ethyl 4−hydroxy−2−methyl−6−quinolinecarboxylate, dihydrouracil, 2,4−dichloro−5−ethyl−3−methylphenol, 2−aminoethylphosphonate, 2,5−dimethylthiazole, 3−methylthiophene, 2−vinylthiophene, and *N*−carbamoylglutamic acid, were negatively correlated with the cortical BMD or total BMD (Fig. 4B). These metabolites were classified into organic phosphonic acids, heteroaromatic compounds, pyrimidines and pyrimidine derivatives etc. In contrast, 5−[(4−nitrobenzoyl)amino]isophthalic acid was positively correlated with total BMD (Fig. 4B).

These data suggest that metabolites including SCFAs may play a role in the beneficial effects of (*R*)-ketamine on the reduced BMD of OVX mice.

3.6. Relationships between gut microbiota and plasma metabolites

Finally, we analyzed the Spearman correlation between (*R*)-ketamine-associated microbiome and plasma metabolites (Supplementary Fig. 5). There were Spearman correlations between the taxa and plasma metabolites (Supplementary Fig. 5). A total of 14 (*R*)-ketamine-related OTUs (relative abundance >0.1%) were significantly associated with 24 plasma metabolites (Spearman absolute rho > 0.5, P < 0.05), which were further related to mouse femoral BMD indices (Fig. 5A). More specifically, succinic acid, and 2 OTUs [OTU00003 (*Lactobacillus*), and OTU00094 (*Eubacterium*)], as well as 2 plasma metabolites (1,2,5-oxadiazole-3,4-dicarboxylic acid and ethyl 4−hydroxy−2−methyl−6−quinolinecarboxylate) were significantly associated. Plasma metabolite ethyl 4−hydroxy−2−methyl−6−quinolinecarboxylate was negatively associated with total BMD. In addition, N-laveric acid was
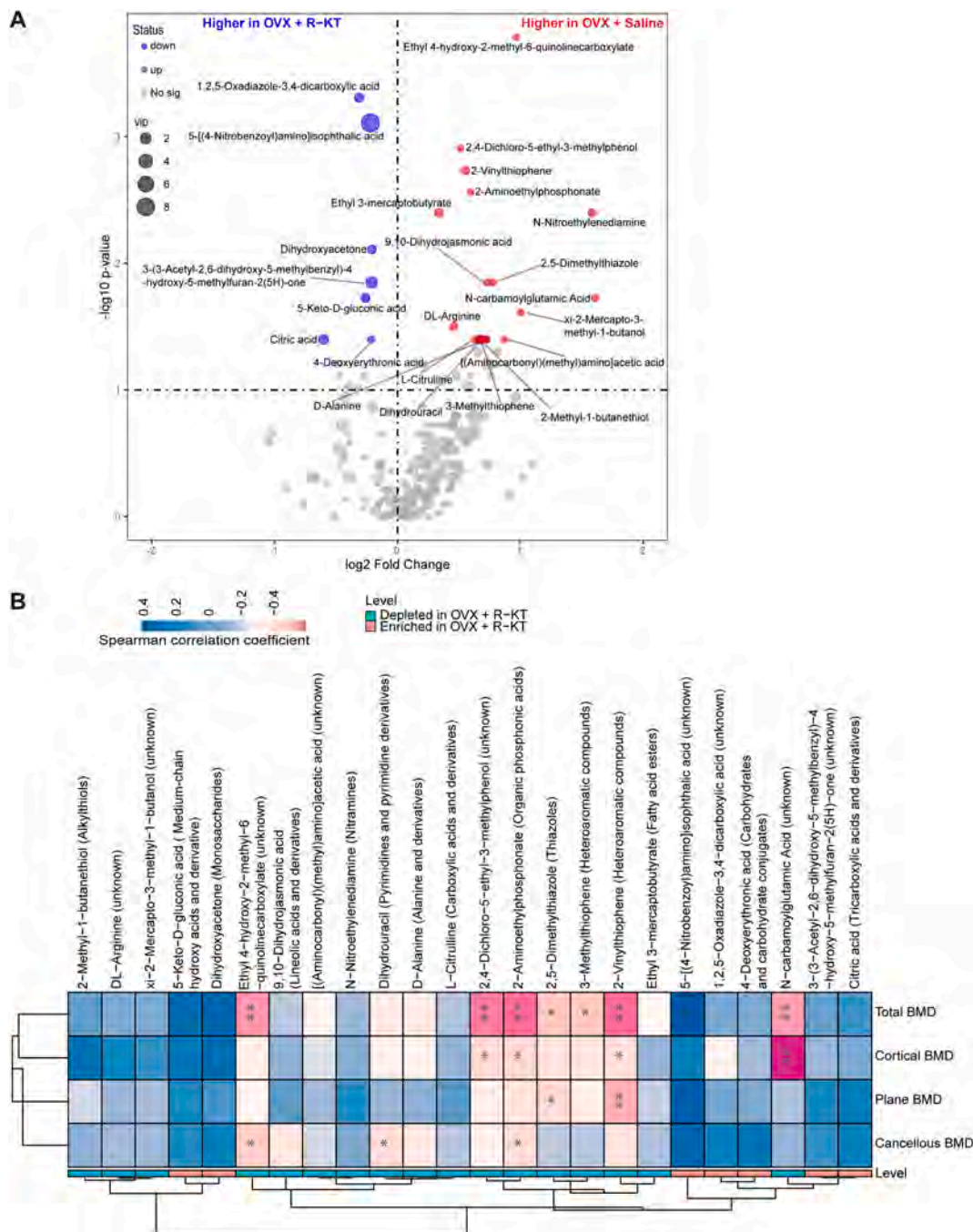
Fig. 4. Plasma metabolomic changes between OVX + saline group and OVX + (*R*)-ketamine group and Spearman correlations between metabolites and femoral BMD. A: Volcano plots show the metabolite changes between OVX + saline group and OVX + (*R*)-ketamine group. X-axis indicates the log2-transformed plasma metabolite abundance of fold change, and the y-axis indicates the -log10-transformed p value using the Wilcoxon rank sum test. Horizontal lines indicate p < 0·05. Increased or decreased metabolites are marked in red and blue, respectively. The size of the dot represents the size of VIP (variable importance in projection) value. Metabolites with P < 005 and VIP > 0·3 are marked in text. B: Correlations between (*R*)-ketamine-associated metabolites with cortical BMD, total BMD, cancellous BMD and plane BMD of the mouse femur. *P < 0.05, **P < 0.01, ***P < 0.001. BMD: bone mineral density. OVX: ovariectomized. R-KT: (*R*)-ketamine.

associated with OTU00042 (*Eisenbergiella*), which was associated with the (*R*)-ketamine-depleted metabolite *N*-carbamoylglutamic acid. *N*-carbamoylglutamic acid was negatively associated with cortical BMD and total BMD. More importantly, (*R*)-ketamine-enriched genera OTU00013 (*Turicibacter*) and OTU00042 (*Eisenbergiella*) were positively associated with both cortical BMD and total BMD, while (*R*)-ketamine-depleted genus OTU00061 (*Kineothrix*) was negatively correlated with cortical BMD and total BMD.

At the plasma metabolite level, five (*R*)-ketamine-depleted

metabolites, N-carbamoylglutamic acid (unknown), ethyl 4-hydroxy-2-methyl-6-quinolinecarboxylate (unknown), 2-vinylthiophene (hetero-aromatic compounds), 2-aminoethylphosphonate (organic phosphonic acids), and 2,4-dichloro-5-ethyl-3-methylphenol (unknown) were directly or indirectly negatively associated with BMD (Fig. 5A). The relative abundances of the identified flora and metabolites that were associated with BMD in the femoral neck of OVX mice across different groups are shown (Fig. 5B and C).
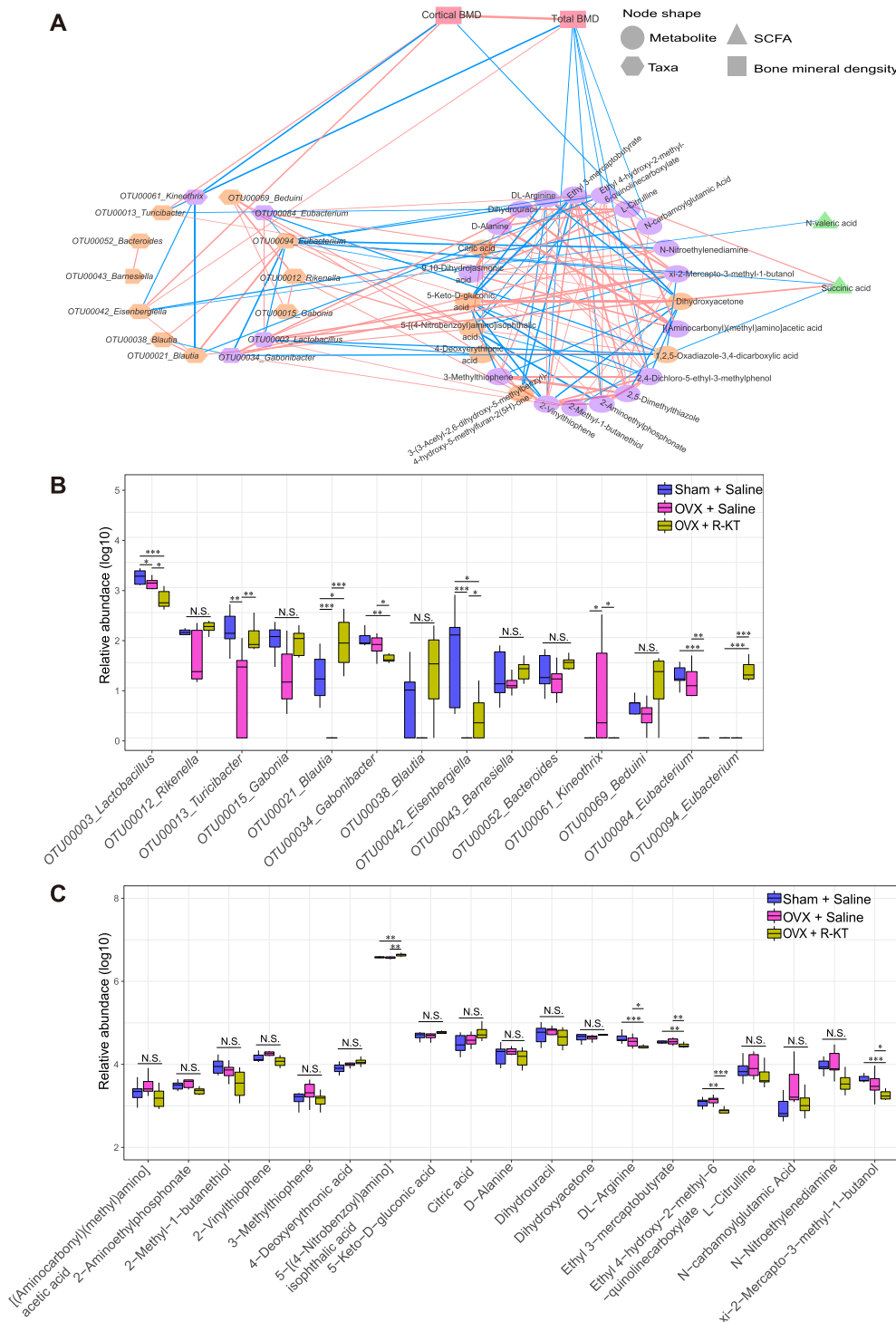
Fig. 5. An integrated association network reflecting host-microbe interactions, relative abundance and metabolic characteristics of key (*R*)-ketamine-related OTUs in different groups. A: Network plots were used to investigate (*R*)-ketamine-associated flora (relative abundance >0.1%), (*R*)-ketamine-associated metabolites (P$_{FDR}$ < 0.05, VIP >0.3, OVX + saline group vs. OVX + R-KT group), and the interrelationship of fecal SCFAs, and their relationship with mouse femoral BMD index. Red connections indicate positive correlations, blue connections indicate negative correlations, and thicker connection lines indicate larger correlation coefficients (Spearman correlation analysis, absolute value of correlation coefficient >0.5, P$_{FDR}$ < 0.05). The red square nodes represent the BMD index, the hexagonal nodes represent the intestinal flora, the circular nodes represent the plasma metabolites, orange indicates (*R*)-ketamine enriched OTUs or metabolites, purple indicates (*R*)-ketamine depleted OTUs or metabolites, the green triangular nodes represent the short chain fatty acids in feces. B: Changes in important OTUs associated with (*R*)-ketamine in the three groups. C: Changes in important (*R*)-ketamine-related metabolic profiles in the three groups. Wilcoxon Rank sum test. *P$_{FDR}$ < 0.05, **P$_{FDR}$ < 0.01, ***P$_{FDR}$ < 0.001. BMD, bone mineral density. R-KT: (*R*)-ketamine. VIP, variable importance in projection. SCFAs, short-chain fatty acids.

3.7. Predicted functional pathway analysis

Prediction of metagenomic function was achieved using the PIC-RUSt2 tool based on the MetaCyc database. In this study, a total of 27 pathways with different abundance between the OVX + saline group and the OVX + (*R*)-ketamine group (P < 0.05, FDR < 0.3, difference between means > 0.02) (Supplementary Fig. 6). In the OVX + (*R*)-ketamine group, a total of five pathways such as glycerol degradation to butanol, L-methionine biosynthesis III, cob(II)yrinate a,c-diamide biosynthesis I (early cobalt insertion), L-lysine fermentation to acetate and butanoate, and superpathway of fucose and rhamnose degradation were enriched (Supplementary Fig. 6). In contrast, a total of 22 pathways were reduced in the OVX + (*R*)-ketamine group. These pathways included hexitol fermentation to lactate, formate, ethanol and acetate, superpathway of N-acetylneuraminate degradation, superpathway of glycolysis and the Entner-Doudoroff pathway, superpathway of pyrimidine nucleobases salvage, pyruvate fermentation to acetate and lactate II, guanosine ribonucleotides *de novo* biosynthesis, phosphatidylglycerol biosynthesis II (non-plastidic), phosphatidylglycerol biosynthesis I (plastidic), UDP-N-acetylmuramoyl-pentapeptid biosynthesis I, peptidoglycan biosynthesis III (mycobacteria), peptidoglycan biosynthesis I, superpathway of phospholipid biosynthesis I (bacteria), S-adenosyl-L-

methionine cycleI, UMP biosynthesis I, UDP-*N*-acetylmuramoyl-penta-peptide biosynthesis II, adenosine ribonucleotides *de novo* biosynthesis, D-galactose degradation I (Leloir pathway), coenzyme A biosynthesis I (prokaryotic), glycolysis III (from glucose), L-lysine biosynthesis VI, L-lysine biosynthesis III, and tRNA charging pathway (Supplementary Fig. 6).

4. Discussion

The major findings of this study are as follows: First, repeated intermittent administration of (*R*)-ketamine could attenuate the reduction of cortical BMD and total BMD of femoral neck from OVX mice, consistent with our previous report (Fujita and Hashimoto, 2020). Second, there were significant changes in α- and β-diversity among the three groups. Furthermore, there were significant changes in the α- and β-diversity between OVX + saline group and OVX + (*R*)-ketamine group. Third, there were correlations between several OTUs and cortical (or total) BMD. At the OTU level, (*R*)-ketamine significantly attenuated the reduced abundance of *Turicibacter* in the OVX mice. At the genus level, there were positive correlations between the genera *Turicibacter* and cortical (or total) BMD. Fourth, there were correlations between several metabolites and cortical (or total) BMD. Collectively, these data suggest that gut microbiota and microbiome-derived metabolites may play a role in the beneficial effects of (*R*)-ketamine in reduced BMD of OVX mice.

α-diversity (i.e., observed_OTUs, and ACE) of gut microbiota in OVX + (*R*)-ketamine group was significantly higher than that in OVX + saline group, indicating that (*R*)-ketamine had a significant effect on gut microbiota composition of OVX mice. Furthermore, β-diversity data among the three groups suggest that (*R*)-ketamine is a driving factor for the differential expression of structural similarity in microbial communities. Collectively, these results suggest that (*R*)-ketamine could lead to improvement of intestinal flora in OVX mice, and that normalization of abnormal composition of gut microbiota by (*R*)-ketamine may play a role in the beneficial effects on reduced BMD of OVX mice.

At the phylum level, the phylum *Tenericutes* was significantly reduced in OVX + (*R*)-ketamine group. The phylum *Tenericutes* was more abundant in treatment-resistant patients with depression (Fontana et al., 2020), suggesting that *Tenericutes* may be involved in the dysbiosis of the gut microbiota in severe depression. The abundance of *Tenericutes* was positively associated with pro-inflammatory cytokines (IL-6 and TNF-α), but negatively related with insulin treatment in diabetic mice (Li et al., 2019). Since bone loss is associated with inflammation, the potential mechanism for the hemophilic arthropathy induced bone loss may be the activation of TNF-α-dependent osteoclastogenesis (Haxaire et al., 2018). Taken together, (*R*)-ketamine may remodel the pro-inflammatory intestinal microenvironment, resulting in the maintenance of intestinal homeostasis. The genus *Anaeromassilibacillus* was initially isolated and identified from the stool of a child with kwashiorkor (Guilhot et al., 2016). Zinc deficiency has been associated with depression in humans and animal models of depression. In pregnant mice on a zinc inhibitor diet, the abundance of *Kiloniella* was significantly decreased, accompanied by activation of inflammatory signaling (Sauer and Grabrucker, 2019). In this study, we found that high abundance of *Kiloniella* was observed in (*R*)-ketamine + OVX group, suggesting that (*R*)-ketamine may suppress inflammatory processes by regulating the composition of intestinal flora. Changes in the genus *Turicibacter* abundance have been associated with diseases including inflammation and colon cancer (Zackular et al., 2013). Furthermore, *Turicibacter sanguinis* colonization has been reported to modulate intestinal lipid metabolism and systemic triglyceride profiles in mice, which may be related to the relationship between SSRI use and metabolic syndrome symptoms (Fung et al., 2019). Collectively, it seems that (*R*)-ketamine might regulate the gut microbiome dysbiosis of OVX mice although further study is needed.

We investigated potential differences in bacterial community structure at the OTU and genera levels between the groups, particularly in the OVX + saline group and OVX + (*R*)-ketamine group. We found that the relative abundance of the (*R*)-ketamine-depleted bacteria OTU00061 (*Kineothrix*) was significantly negatively correlated with cortical (or total) BMD. In contrast, the relative abundance of the (*R*)-ketamine-enriched bacteria OTU00021 (*Blautia*) was significantly positively correlated with cortical (or total) BMD. Of note, Liddicoat et al. (2020) reported that the relative abundance of *Kineothrix* was significantly higher in the group of mice exposed to a high biodiversity (trace-level dust) environment and was associated with a reduction in anxiety-like behavior in mice (Liddicoat et al., 2020). Furthermore, Wang et al. (2017) reported that the relative abundance of *Blautia* varied considerably between primary osteoporosis patients and control groups (Wang et al., 2017). In patients with ankylosing spondylitis, the relative abundance of *Blautia* was significantly upregulated (Zhang et al., 2019). Collectively, the alterations of gut microbiota in OVX + (*R*)-ketamine group are likely involved in the beneficial effects of (*R*)-ketamine on reduced BMD of OVX mice, although further studies are required to determine detailed mechanisms of gut microbiota in postmenopausal osteopenia.

Tannahill et al. (2013) reported that succinic acid is thought to be a deleterious metabolite in innate immune system that triggers HIF (hypoxia inducible factor)-1α-induced IL-1β expression during inflammation (Tannahill et al., 2013). In addition, Guo et al. (2017) demonstrated that stromal cell-derived succinic acid enhances osteoclastogenesis and bone resorption by upregulating SUCNR1 (succinate receptor 1) and stimulating NF-κB signaling in diabetic mice (Guo et al., 2017). In this study, we found that the concentration of succinic acid was significantly decreased in the OVX + (*R*)-ketamine group, compared to sham + saline group. Give the role of succinic acid as a metabolic signal in inflammation (Mills et al., 2014), it is likely that reduced levels of succinic acid by (*R*)-ketamine may be involved in the inflammatory process of osteoporosis of (*R*)-ketamine.

Circulating biomarkers are becoming clinically reliable indicators of the status of bone metabolism. Metabolomics provides a new platform for screening novel biomarkers for various metabolic diseases, such as osteoporosis and diabetes (Wang et al., 2011; Yang et al., 2020). (*R*)-ketamine-depleted metabolite 3-methylthiophene (HMDB0033119) was negatively associated with femoral neck BMD of mice, which belongs to a group of organic compounds known as heteroaromatic compounds, exhibited dose-dependent cytotoxic effects against breast cancer cell lines (Baig et al., 2016). De Preter et al. (De Preter et al., 2015) reported higher levels of 3,4-dimethylthiophene in stool samples from patients with Crohn's disease than in healthy controls, indicating that it is an important metabolic biomarker of the changes associated with inflammatory bowel disease. In our study, we detected lower plasma levels of 3-methylthiophene in OVX + (*R*)-ketamine mice than in OVX mice, and it was significantly negatively correlated with total BMD of the mice femoral neck, suggesting that (*R*)-ketamine may play a role in regulating plasma metabolites to improve the inflammatory state. In addition, we found (*R*)-ketamine-depleted plasma metabolite dihydrouracil (HMDB0000076), an intermediate decomposition product of uracil. Altered levels of dihydrouracil are usually associated with metabolic disorders. Patients with dihydropyrimidine enzyme deficiency have elevated levels of dihydrouracil and exhibit various neurological abnormalities, autistic behavior, and gastrointestinal dysfunction (gastroesophageal reflux, recurrent vomiting) (Liu et al., 2014). Furthermore, Wikoff et al. (2015) reported that overexpression of 5, 6-dihydrouracil is a unique metabolic characteristics of early lung adenocarcinoma, suggesting that there is a direct relationship between elevated 5, 6-dihydrouracil and reduced glucose levels (Wikoff et al., 2015). In this study, we observed a significant decrease in plasma expression levels of dihydrouracil in OVX + (*R*)-ketamine group, and we also found a negative correlation between reduced dihydrouracil and cancellous BMD in mice. Collectively, these metabolites might play a role in the beneficial effects of (*R*)-ketamine in OVX mice.

From a multi-omics perspective, *Eisenbergiella* was found to be 400-fold enriched in the OVX + (*R*)-ketamine group compared to the OVX + saline group. Amir et al. (2014) initially discovered that *Eisenbergiella* can produce metabolites such as butyric acid, acetic acid, lactic acid, and succinic acid (Amir et al., 2014). *Eisenbergiella* exhibits correlations with energy metabolism, amino acid, nucleotide and SCFA utilization, and its reduction is associated with gastrointestinal disorders (functional dyspepsia), which characterized by impaired energy metabolism and dysbiosis of the intestinal microbiota (Luo et al., 2018). In this study, we found that *Eisenbergiella* showed a positive correlation with bone mass index (i.e., cortical BMD and total BMD) in OVX mice. Moreover, our integrative network analysis indicated that *Eisenbergiella* had a negative correlation with *N*-valeric acid and *N*-carbamoylglutamic acid. Nishida et al. (2019) reported significantly increased concentrations of *N*-valeric acid in participants who received the antidepressant *Lactobacillus agalactiae (CP2305)*, compared to placebo group (Nishida et al., 2019). As arginine precursor, *N*-carbamoylglutamic acid, an essential amino acid for juvenile animals, also plays an important role in animal growth. Sun et al. (2019) have described the important effects of *N*-carbamoylglutamic acid on growth, metabolism, immunity and organ morphology in the small intestine of juvenile rabbits. Specifically, intake of *N*-carbamoylglutamic acid plays an important role in nitrogen metabolism, weight gain, and expression of the immunoglobulins IgG and IgA (Sun et al., 2019). In our study, we observed a significant reduction of *N*-carbamoyl glutamate in OVX mice after administration of (*R*)-ketamine, and this decrease was negatively correlated with total BMD. Collectively, beneficial effects of (*R*)-ketamine on reduced BMD in OVX mice might be modulated by gut microbes, microbiome-derived SCFAs and metabolites although future longitudinal mechanistic studies are needed.

Genomics focusing on the whole gene transcriptional and translational levels has identified serval validated biomarkers for osteoporosis and provided elucidation from the perspective of relevant biological pathways (Yang et al., 2020). The present study identifies the metabolic pathways involved in the beneficial effect of (*R*)-ketamine on bone loss in OVX mice from a genome-wide perspective. Vijayan et al. (2014) reported that ʟ-methionine alleviates bone loss in OVX rats through inactivation of NF-κB signaling pathway in OVX rats (Vijayan et al., 2014). Of note, ʟ-methionine is one of the proteinogenic amino acids and involved in many important cellular functions including phospholipid synthesis and DNA methylation. Our study showed that the ʟ-methionine biosynthesis III pathway was significantly enriched in the OVX + (*R*)-ketamine group. Therefore, it seems that increased biosynthesis of ʟ-methionine by (*R*)-ketamine may play a role in its beneficial effects of reduced BMD in OVX mice.

Several genera have been shown to utilize ʟ-lysine as the sole source of carbon and nitrogen for fermentation, with butyric acid and acetic acid as the end products. ʟ-lysine administration had been proved to promote intestinal Ca absorption and in turn improves renal Ca retention in human, suggesting that ʟ-lysine products are considered to have great potential for the prevention and treatment of osteoporosis (Civitelli et al., 1992). Mineo et al. (2001) noted that SCFAs, specifically acetic acid and butyric acid, increased net Ca absorption in the rat cecum and colon *in vitro* (Mineo et al., 2001). It is known that calcium supplementation helps to restore disorders of calcium metabolism in postmenopausal women and that improvement in calcium homeostasis may be associated with recovery of bone loss (Avioli, 1984). In this study, we observed a significant increase in the enrichment of metabolic pathway named ʟ-lysine fermentation to acetate and butyrate in the OVX + (*R*)-ketamine group, compared to the OVX + saline group. The MetaCyc pathway analysis provides insights into several metabolic molecular pathways in which (*R*)-ketamine may play a role in alleviate OVX-mediated bone loss.

Patients with major depression are associated with low BMD, suggesting a risk for osteoporosis (Cizza et al., 2010). A study using a population-based sample demonstrated that depression score was a significant predictor of BMD at the lumbar spine and total hip in older participants (Hlis et al., 2018). Although decreased BMD in patients with depression is well recognized, bone loss in patients with depression is not treated adequately. It is well known that dietary supplementation with calcium and vitamin D could reduce bone loss in elderly people (Dawson-Hughes et al., 1997). In addition of dietary intake of calcium and vitamin D, it is likely that (*R*)-ketamine may ameliorate reduced BMD in elderly people with depression.

This study has one limitation. Although we did not examine depression-like behaviors in OVX mice in this study, it is reported that OVX mice show depression-like behaviors such as increased immobility times of tail suspension test and forced swimming test (Tantipongpiradet et al., 2019). Therefore, it is likely that (*R*)-ketamine may improve depression-like behaviors as well as reduced BMD in OVX mice although further study is needed.

5. Conclusion

Our study shows that repeated intermittent administration of (*R*)-ketamine could attenuate OVX-induced reduction of BMD in mice. Furthermore, this study suggests that gut microbiota, microbes-derived metabolites and SCFAs may be involved in the beneficial effects of (*R*)-ketamine. Therefore, it is of great interest whether (*R*)-ketamine could improve reduced BMD and depressive symptoms in patients with osteoporosis or depression.

Declaration of competing interest

Dr. Hashimoto is the inventor of filed patent applications on "The use of *R*-ketamine in the treatment of psychiatric diseases", "(*S*)-norketamine and salt thereof as pharmaceutical", "*R*-ketamine and derivative thereof as prophylactic or therapeutic agent for neurodegeneration disease or recognition function disorder", "Preventive or therapeutic agent and pharmaceutical composition for inflammatory diseases or bone diseases", "*R*-ketamine and its derivatives as a preventive or therapeutic agent for a neurodevelopmental disorder", and "TGF-β1 in the treatment of depression" by the Chiba University. Dr. Hashimoto also declares that he has received research support and consultant from Dainippon Sumitomo, Otsuka, Taisho, Murakami Farm, and Perception Neuroscience. Other authors have no conflict of interest.

Appendix A. Supplementary data

Supplementary data to this article can be found online at https://doi.org/10.1016/j.neuropharm.2022.109139.

References

Agus, A., Clément, K., Sokol, H., 2021. Gut microbiota-derived metabolites as central regulators in metabolic disorders. Gut 70, 1174–1182.

Amir, I., Bouvet, P., Legeay, C., Gophna, U., Weinberger, A., 2014. *Eisenbergiella tayi* gen. nov., sp. nov., isolated from human blood. International journal of systematic and evolutionary microbiology. Int. J. Syst. Evol. Microbiol. 64, 907–914.

Avioli, L.V., 1984. Calcium and osteoporosis. Annu. Rev. Nutr. 4, 471–491.

Bahji, A., Vazquez, G.H., Zarate Jr., C.A., 2021. Comparative efficacy of racemic ketamine and esketamine for depression: a systematic review and meta-analysis. J. Affect. Disord. 278, 542–555.

Baig, U., Gondal, M.A., Alam, M.F., Wani, W.A., Younus, H., 2016. Pharmacological evaluation of poly(3-methylthiophene) and its titanium(IV)phosphate nanocomposite: DNA interaction, molecular docking, and cytotoxic activity. J. Photochem. Photobiol., B 164, 244–255.

Civitelli, R., Villareal, D.T., Agnusdei, D., Nardi, P., Avioli, L.V., Gennari, C., 1992. Dietary L-lysine and calcium metabolism in humans. Nutrition 8, 400–405.

Cizza, G., Primma, S., Csako, G., 2009. Depression as a risk factor for osteoporosis. Trends Endocrinol. Metabol. 20, 367–373.

Cizza, G., Primma, S., Coyle, M., Gourgiotis, L., Csako, G., 2010. Depression and osteoporosis: a research synthesis with meta-analysis. Horm. Metab. Res. 42, 467–482.

Dalile, B., Van Oudenhove, L., Vervliet, B., Verbeke, K., 2019. The role of short-chain fatty acids in microbiota-gut-brain communication. Nat. Rev. Gastroenterol. Hepatol. 16, 461–478.

Dawson-Hughes, B., Harris, S.S., Krall, E.A., Dallal, G.E., 1997. Effect of calcium and vitamin D supplementation on bone density in men and women 65 years of age or older. N. Engl. J. Med. 337, 670–676.

De Preter, V., Machiels, K., Joossens, M., Arijs, I., Matthys, C., Vermeire, S., Rutgeerts, P., Verbeke, K., 2015. Faecal metabolite profiling identifies medium-chain fatty acids as discriminating compounds in IBD. Gut 64, 447–458.

Douglas, G.M., Maffei, V.J., Zaneveld, J.R., Yurgel, S.N., Brown, J.R., Taylor, C.M., Huttenhower, C., Langille, M., 2020. PICRUSt2 for prediction of metagenome functions. Nat. Biotechnol. 38 (6), 685–688.

Fan, Y., Pedersen, O., 2021. Gut microbiota in human metabolic health and disease. Nat. Rev. Microbiol. 19, 55–71.

Fontana, A., Manchia, M., Panebianco, C., Paribello, P., Arzedi, C., Cossu, E., Garzilli, M., Montis, M.A., Mura, A., Pisanu, C., Congiu, D., Copetti, M., Pinna, F., Carpiniello, B., Squassina, A., Pazienza, V., 2020. Exploring the role of gut microbiota in major depressive disorder and in treatment resistance to antidepressants. Biomedicines 8, 311.

Fujita, Y., Hashimoto, K., 2020. Decreased bone mineral density in ovariectomized mice is ameliorated after subsequent repeated intermittent administration of (*R*)-ketamine, but not (*S*)-ketamine. Neuropsychopharmacol. Rep. 40, 401–406.

Fung, T.C., Vuong, H.E., Luna, C., Pronovost, G.N., Aleksandrova, A.A., Riley, N.G., Vavilina, A., McGinn, J., Rendon, T., Forrest, L.R., Hsiao, E.Y., 2019. Intestinal serotonin and fluoxetine exposure modulate bacterial colonization in the gut. Nat. Microbiol. 4, 2064–2073.

Guilhot, E., Tidjani Alou, M., Diallo, A., Raoult, D., Khelaifia, S., 2016. *Anaeromassilibacillus senegalensis* gen. nov., sp. nov., isolated from the gut of a child with kwashiorkor. New Microbes New Infect. 12, 59–60.

Guo, W., Wan, X., Ma, L., Zhang, J., Hashimoto, K., 2021. Abnormalities in the composition of the gut microbiota in mice after repeated administration of DREADD ligands. Brain Res. Bull. 173, 66–73.

Guo, Y., Xie, C., Li, X., Yang, J., Yu, T., Zhang, R., Zhang, T., Saxena, D., Snyder, M., Wu, Y., Li, X., 2017. Succinate and its G-protein-coupled receptor stimulates osteoclastogenesis. Nat. Commun. 8, 15621.

Hashimoto, K., 2019. Rapid-acting antidepressant ketamine, its metabolites and other candidates: a historical overview and future perspective. Psychiatr. Clin. Neurosci. 73, 613–627.

Hashimoto, K., 2020. Molecular mechanisms of the rapid-acting and long-lasting antidepressant actions of (*R*)-ketamine. Biochem. Pharmacol. 177, 113935.

Hashimoto, K., 2022. Ketamine: anesthetic, psychotomimetic, antidepressant, or anthelmintic? Mol. Psychiatr. https://doi.org/10.1038/s41380-022-01587-7, 2022 Apr 27.

Haxaire, C., Hakobyan, N., Pannellini, T., Carballo, C., McIlwain, D., Mak, T.W., Rodeo, S., Acharya, S., Li, D., Szymonifka, J., Song, X., Monette, S., Srivastava, A., Salmon, J.E., Blobel, C.P., 2018. Blood-induced bone loss in murine hemophilic arthropathy is prevented by blocking the iRhom2/ADAM17/TNF-α pathway. Blood 132, 1064–1074.

Hernandez, C.J., Moeller, A.H., 2022. The microbiome: a heritable contributor to bone morphology? Semin. Cell Dev. Biol. 123, 82–87.

Hlis, R.D., McIntyre, R.S., Maalouf, N.M., Enkevort, E.V., Brown, E.S., 2018. Association between bone mineral density and depressive symptoms in a Population-based sample. J. Clin. Psychiatr. 79, 16m11276.

Kindilien, S., Goldberg, E.M., Roberts, M.H., Gonzales-Pacheco, D., 2018. Nutrition status, bone mass density, and selective serotonin reuptake inhibitors. Prev. Med. 113, 62–67.

Li, K., Zhang, L., Xue, J., Yang, X., Dong, X., Sha, L., Lei, H., Zhang, X., Zhu, L., Wang, Z., Li, X., Wang, H., Liu, P., Dong, Y., He, L., 2019. Dietary inulin alleviates diverse stages of type 2 diabetes mellitus via anti-inflammation and modulating gut microbiota in db/db mice. Food Funct. 10, 1915–1927.

Liddicoat, C., Sydnor, H., Cando-Dumancela, C., Dresken, R., Liu, J., Gellie, N., Mills, J. G., Young, J.M., Weyrich, L.S., Hutchinson, M.R., Weinstein, P., Breed, M.F., 2020. Naturally-diverse airborne environmental microbial exposures modulate the gut microbiome and may provide anxiolytic benefits in mice. Sci. Total Environ. 701, 134684.

Liu, X.Q., Zhuang, M., Wang, Z., Huber, R.M., 2014. Correlation between dihydropyrimidine dehydrogenase and efficacy and toxicity of fluoropyrimidine drugs. Eur. Rev. Med. Pharmacol. Sci. 18, 2772–2776.

Lu, L., Chen, X., Liu, Y., Yu, X., 2021. Gut microbiota and bone metabolism. Faseb. J. 35, e21740.

Luo, L., Hu, M., Li, Y., Chen, Y., Zhang, S., Chen, J., Wang, Y., Lu, B., Xie, Z., Liao, Q., 2018. Association between metabolic profile and microbiomic changes in rats with functional dyspepsia. RSC Adv. 8, 20166–20181.

Mills, E., O'Neill, L.A., 2014. Succinate: a metabolic signal in inflammation. Trends Cell Biol. 24, 313–320.

Mineo, H., Hara, H., Tomita, F., 2001. Short-chain fatty acids enhance diffusional ca transport in the epithelium of the rat cecum and colon. Life Sci. 69, 517–526.

Morrison, D.J., Preston, T., 2016. Formation of short chain fatty acids by the gut microbiota and their impact on human metabolism. Gut Microb. 7, 189–200.

Nishida, K., Sawada, D., Kuwano, Y., Tanaka, H., Rokutan, K., 2019. Health benefits of *Lactobacillus gasseri* CP2305 tablets in young adults exposed to chronic stress: a randomized, double-blind, placebo-controlled study. Nutrients 11, 1859.

Parks, D.H., Tyson, G.W., Hugenholtz, P., Beiko, R.G., 2014. STAMP: statistical analysis of taxonomic and functional profiles. Bioinformatics 30, 3123–3124.

Qu, Y., Yang, C., Ren, Q., Ma, M., Dong, C., Hashimoto, K., 2017. Comparison of (*R*)-ketamine and lanicemine on depression-like phenotype and abnormal composition of gut microbiota in a social defeat stress model. Sci. Rep. 7, 15725.

Rizzoli, R., Cooper, C., Reginster, J.Y., Abrahamsen, B., Adachi, J.D., Brandi, M.L., Bruyère, O., Compston, J., Ducy, P., Ferrari, S., Harvey, N.C., Kanis, J.A., Karsenty, G., Laslop, A., Rabenda, V., Vestergaard, P., 2012. Antidepressant medications and osteoporosis. Bone 51, 606–613.

Sauer, A.K., Grabrucker, A.M., 2019. Zinc deficiency during pregnancy leads to altered microbiome and elevated inflammatory markers in mice. Front. Neurosci. 13, 1295.

Schweiger, J.U., Schweiger, U., Hüppe, M., Kahl, K.G., Greggersen, W., Fassbinder, E., 2016. Bone density and depressive disorder: a meta-analysis. Brain Behav. 6, e00489.

Schymanski, E.L., Jeon, J., Gulde, R., Fenner, K., Ruff, M., Singer, H.P., Hollender, J., 2014. Identifying small molecules via high resolution mass spectrometry: communicating confidence. Environ. Sci. Technol. 48, 2097–2098.

Seely, K.D., Kotelko, C.A., Douglas, H., Bealer, B., Brooks, A.E., 2021. The human gut microbiota: a key mediator of osteoporosis and osteogenesis. Int. J. Mol. Sci. 22, 9452.

Sun, X., Shen, J., Liu, C., Li, S., Peng, Y., Chen, C., Yuan, B., Gao, Y., Meng, X., Jiang, H., Zhang, J., 2019. L-Arginine and N-carbamoylglutamic acid supplementation enhance young rabbit growth and immunity by regulating intestinal microbial community. Asian-Australas. J. Anim. Sci. 33, 166–176.

Tannahill, G.M., Curtis, A.M., Adamik, J., Palsson-McDermott, E.M., McGettrick, A.F., Goel, G., Frezza, C., Bernard, N.J., Kelly, B., Foley, N.H., Zheng, L., Gardet, A., Tong, Z., Jany, S.S., Corr, S.C., Haneklaus, M., Caffrey, B.E., Pierce, K., Walmsley, S., Beasley, F.C., Cummins, E., Nizet, V., Whyte, M., Taylor, C.T., Lin, H., Masters, S.L., Gottlieb, E., Kelly, V.P., Clish, C., Auron, P.E., Xavier, R.J., O'Neill, L.A., 2013. Succinate is an inflammatory signal that induces IL-1β through HIF-1α. Nature 496, 238–242.

Tantipongpiradet, A., Monthakantirat, O., Vipatpakpaiboon, O., Khampukdee, C., Umehara, K., Noguchi, H., Fujiwara, H., Matsumoto, K., Sekeroglu, N., Kijjoa, A., Chulikhit, Y., 2019. Effects of puerarin on the ovariectomy-induced depressive-like behavior in ICR mice and its possible mechanism of action. Molecules 24 (24), 4569.

Tsugawa, H., Cajka, T., Kind, T., Ma, Y., Higgins, B., Ikeda, K., Kanazawa, M., VanderGheynst, J., Fiehn, O., Arita, M., 2015. MS-DIAL: data-independent MS/MS deconvolution for comprehensive metabolome analysis. Nat. Methods 12, 523–526.

Tu, Y., Yang, R., Xu, X., Zhou, X., 2021. The microbiota-gut-bone axis and bone health. J. Leukoc. Biol. 110, 525–537.

Vijayan, V., Khandelwal, M., Manglani, K., Gupta, S., Surolia, A., 2014. Methionine down-regulates TLR4/MyD88/NF-κB signalling in osteoclast precursors to reduce bone loss during osteoporosis. Br. J. Pharmacol. 171, 107–121.

Wadhwa, R., Kumar, M., Talegaonkar, S., Vohora, D., 2017. Serotonin reuptake inhibitors and bone health: a review of clinical studies and plausible mechanisms. Osteoporos. Sarcopenia 3, 75–81.

Wang, J., Wang, Y., Gao, W., Wang, B., Zhao, H., Zeng, Y., Ji, Y., Hao, D., 2017. Diversity analysis of gut microbiota in osteoporosis and osteopenia patients. PeerJ 5, e3450.

Wang, T.J., Larson, M.G., Vasan, R.S., Cheng, S., Rhee, E.P., McCabe, E., Lewis, G.D., Fox, C.S., Jacques, P.F., Fernandez, C., O'Donnell, C.J., Carr, S.A., Mootha, V.K., Florez, J.C., Souza, A., Melander, O., Clish, C.B., Gerszten, R.E., 2011. Metabolite profiles and the risk of developing diabetes. Nat. Med. 17, 448–453.

Wei, M., Li, C., Dai, Y., Zhou, H., Cui, Y., Zeng, Y., Huang, Q., Wang, Q., 2021. High-throughput absolute quantification sequencing revealed osteoporosis-related gut microbiota alterations in Han Chinese elderly. Front. Cell. Infect. Microbiol. 11, 630372.

Wei, Y., Chang, L., Hashimoto, K., 2022. Molecular mechanisms underlying the antidepressant actions of arketamine: beyond the NMDA receptor. Mol. Psychiatr. 27, 559–573.

Wikoff, W.R., Grapov, D., Fahrmann, J.F., DeFelice, B., Rom, W.N., Pass, H.I., Kim, K., Nguyen, U., Taylor, S.L., Gandara, D.R., Kelly, K., Fiehn, O., Miyamoto, S., 2015. Metabolomic markers of altered nucleotide metabolism in early stage adenocarcinoma. Cancer Prev. Res. 8, 410–418.

Wu, Q., Magnus, J.H., Liu, J., Bencaz, A.F., Hentz, J.G., 2009. Depression and low bone mineral density: a meta-analysis of epidemiologic studies. Osteoporos. Int. 20, 1309–1320.

Xiong, Z., Fujita, Y., Zhang, K., Pu, Y., Chang, L., Ma, M., Chen, J., Hashimoto, K., 2019. Beneficial effects of (*R*)-ketamine, but not its metabolite (2*R*,6*R*)-hydroxynorketamine, in the depression-like phenotype, inflammatory bone markers, and bone mineral density in a chronic social defeat stress model. Behav. Brain Res. 368, 111904.

Xu, Z., Xie, Z., Sun, J., Huang, S., Chen, Y., Li, C., Sun, X., Xia, B., Tian, L., Guo, C., Li, F., Pi, G., 2020. Gut microbiome reveals specific dysbiosis in primary osteoporosis. Front. Cell. Infect. Microbiol. 10, 160.

Yang, C., Qu, Y., Fujita, Y., Ren, Q., Ma, M., Dong, C., Hashimoto, K., 2017. Possible role of the gut microbiota-brain axis in the antidepressant effects of (*R*)-ketamine in a social defeat stress model. Transl. Psychiatry 7, 1294.

Yang, C., Shirayama, Y., Zhang, J.C., Ren, Q., Yao, W., Ma, M., Dong, C., Hashimoto, K., 2015. *R*-ketamine: a rapid-onset and sustained antidepressant without psychotomimetic side effects. Transl. Psychiatry 5, e632.

Yang, T.L., Shen, H., Liu, A., Dong, S.S., Zhang, L., Deng, F.Y., Zhao, Q., Deng, H.W., 2020. A road map for understanding molecular and genetic determinants of osteoporosis. Nat. Rev. Endocrinol. 16, 91–103.

Yirmiya, R., Bab, I., 2009. Major depression is a risk factor for low bone mineral density: a meta-analysis. Biol. Psychiatr. 66, 423–432.

Zackular, J.P., Baxter, N.T., Iverson, K.D., Sadler, W.D., Petrosino, J.F., Chen, G.Y., Schloss, P.D., 2013. The gut microbiome modulates colon tumorigenesis. mBio 4, e00692–13.

Zhang, J., Fujita, Y., Chang, L., Pu, Y., Qu, Y., Wang, S., Hashimoto, K., 2020. Beneficial effects of anti-RANKL antibody in depression-like phenotype, inflammatory bone markers, and bone mineral density in male susceptible mice after chronic social defeat stress. Behav. Brain Res. 379, 112397.

Zhang, J.C., Li, S.X., Hashimoto, K., 2014. *R* (-)-ketamine shows greater potency and longer lasting antidepressant effects than *S* (+)-ketamine. Pharmacol. Biochem. Behav. 116, 137–141.

Zhang, K., Hashimoto, K., 2019. An update on ketamine and its two enantiomers as rapid-acting antidepressants. Expert Rev. Neurother. 19, 83–92.

Zhang, K., Ma, M., Dong, C., Hashimoto, K., 2018. Role of inflammatory bone markers in the antidepressant actions of (*R*)-ketamine in a chronic social defeat stress model. Int. J. Neuropsychopharmacol. 21, 1025–1030.

Zhang, L., Han, R., Zhang, X., Fang, G., Chen, J., Li, J., Xu, S., Qian, L., Chen, W., Pan, F., 2019. Fecal microbiota in patients with ankylosing spondylitis: correlation with dietary factors and disease activity. Clin. Chim. Acta 497, 189–196.

Zhang, L., Zhan, H., Xu, W., Yan, S., Ng, S.C., 2021. The role of gut mycobiome in health and diseases. Therap. Adv. Gastroenterol. 14, 17562848211047130.

Zhong, X., Zhang, F., Yin, X., Cao, H., Wang, X., Liu, D., Chen, J., Chen, X., 2021. Bone homeostasis and gut microbial-dependent signaling pathways. J. Microbiol. Biotechnol. 31, 765–774.

RESEARCH PAPER

Long-lasting beneficial effects of maternal intake of sulforaphane glucosinolate on gut microbiota in adult offspring

Yan Wei [a,b,#], Lijia Chang [a,#], Guoqi Liu [c], Xingming Wang [a], Yong Yang [a], Kenji Hashimoto [a,*]

[a] *Division of Clinical Neuroscience, Chiba University Center for Forensic Mental Health, Chiba, 260-8670, Japan*
[b] *Key Laboratory of Medical Electrophysiology of Ministry of Education and Medical Electrophysiological Key Laboratory of Sichuan Province, Collaborative Innovation Center for Prevention and Treatment of Cardiovascular Disease, Institute of Cardiovascular Research, Southwest Medical University, Luzhou, 646000, Sichuan, China*
[c] *Center for Bioinformatics, Mingke Biotechnology (Hangzhou) Co. Ltd, Hangzhou, 311100, Zhejiang, China*

Abstract

Mounting evidence suggests the impact of maternal diet on the health of offspring. We reported that maternal diet of sulforaphane glucosinolate (SGS) could prevent behavioral abnormalities in offspring after maternal immune activation. The present study was designed to investigate whether the dietary intake of SGS during pregnancy and lactation influences the composition of gut microbiota in the offspring. The dietary intake of SGS during pregnancy and lactation caused significant changes in the α-diversity and β-diversity of gut microbiota in 3-week-old offspring (SGS-3W group) and 10-week-old offspring (SGS-10W group). The LEfSe algorithm identified several microbes as important phylotypes in the SGS-3W or SGS-10W groups. Predictive functional metagenomes showed that the maternal intake of SGS caused several KEGG pathways alterations with respect to the genetic information processing and metabolism. Furthermore, the plasma levels of interleukin-6 (IL-6) and tumor necrosis factor-α (TNF-α) in the SGS-10W group after the injection of lipopolysaccharide (LPS: 0.5 mg/kg) were significantly lower than those of the CON-10W group. It is noteworthy that there were positive correlations between the relative abundance of the genus *Blautia* and IL-6 (or TNF-α) in adult offspring. Moreover, there were sex differences of gut microbiota composition in offspring. In conclusion, these data suggest that the dietary intake of SGS during pregnancy and lactation might produce long-lasting beneficial effects in adult offspring through the persistent modulation of gut microbiota. It is likely that the modulation of gut microbiota by maternal nutrition may confer resilience versus vulnerability to stress-related psychiatric disorders in the offspring.
© 2022 The Author(s). Published by Elsevier Inc.
This is an open access article under the CC BY license (http://creativecommons.org/licenses/by/4.0/)

Keywords: Brain–gut–microbiota axis; Inflammation; Maternal diet; Offspring; Sex difference; Sulforaphane.

1. Introduction

The research of the Developmental Origins of Health and Disease has consolidated the hypothesis that certain components of a woman's diet during pregnancy exert a long-lasting impact on the disease vulnerability of offspring [1–5]. Nutritional changes, including caloric restriction, macronutrient intake, and micronutrient intake, cause early life adaptations that can produce long-term effects in the offspring [5,6]. For example, a recent national birth cohort study on 19,582 mother-offspring pairs demonstrated that maternal diet quality during pregnancy was associated with the diet quality of the offspring at 14 years of age [7]. Collectively, it is possible that maternal diet during pregnancy and lactation plays a crucial role in the health and disease of the offspring. However, the precise mechanisms underlying the long-term impact of maternal nutrition in the offspring's health remain poorly understood.

The brain–gut–microbiota axis is a complex multiorgan bidirectional signaling system between the brain and the gastrointestinal tract that plays a crucial role in the host homeostasis [8–11]. Accumulating evidence has demonstrated that maternal diet is associated with the composition of the gut microbiota of the offspring [6,12–19]. However, it is unclear how maternal diet can influence the composition of gut microbiota and disease vulnerability in the offspring.

The Nuclear factor erythroid 2-related 2 (Nrf2) is the transcription factor that plays a key role in redox homeostasis [20–22]. The isothiocyanate sulforaphane, an inducer of the Nrf2, is known to produce potent cytoprotective effects [23,24]. Pretreatment with sulforaphane is reported to prevent schizophrenia-like behavioral changes in rodents following the administration of methamphetamine or phencyclidine [25,26]. Furthermore, pretreatment with sulforaphane prevented depression-like phenotypes in adult mice after repeated social defeat stress, lipopolysaccharide (LPS) injection, or spared nerve injury [27–30]. In addition, the level of Nrf2 protein is lower in the brain of rodents with depression-like phenotypes or patients with major depression than in the brain of controls; further, *Nrf2* knockout mice showed depression-like phenotypes [27,31,32]. Thus, it appears that sulforaphane has potent neuroprotective effects in several animal models via Nrf2 activation [21,33,34].

Sulforaphane glucosinolate (SGS: glucoraphanin), a precursor of sulforaphane, is found in cruciferous vegetables [34–36]. SGS can convert to sulforaphane via the catalytic actions of plant myrosinase or β-thioglucosidases in the gut microflora [37]. Dietary intake of food pellets, including SGS during juvenile and adolescent stages, prevented schizophrenia-like behavioral abnormalities in adult mice after repeated phencyclidine administration or maternal immune activation [38,39]. Furthermore, the dietary intake of SGS food pellets did not cause depression-like behaviors in mice that were exposed to repeated social defeat stress or LPS injection, indicating stress resilience [27,29]. It is noteworthy that the dietary intake of SGS food pellets during pregnancy and lactation could prevent behavioral abnormalities in the juvenile and adult offspring following maternal immune activation [40]. Collectively, it is likely that dietary intake of SGS during pregnancy and lactation could induce long-lasting prophylactic effects in the offspring. However, it is unclear how maternal intake of SGS in pregnant rodents influences the resilience and vulnerability in the offspring.

This study was performed to investigate whether the dietary intake of SGS food pellets during pregnancy and lactation affects the composition of the gut microbiota of juvenile and adult offspring. Furthermore, we examined the effects of maternal diet of SGS food pellets on systemic inflammation in adult offspring following LPS administration.

2. Methods and materials

2.1. Animals and diet

Pregnant female ddY mice (*n*=10, embryo at the 5th day [E5], aged 9–10 weeks, body weight 30–35 g) were purchased from Japan SLC, Inc (Hamamatsu, Shizuoka, Japan). Male ddY mice (aged 8–15 weeks) were used in the company for mating. Mice were housed under controlled conditions for temperature (23±1°C) and humidity (55±5%) with a 12-h light–dark cycle (lights on from 7:00 to 19:00). At the beginning (E5), 10 pregnant mice were randomly allocated to two groups (*n*=5). During the experiment, four pregnant mice of SGS group and three pregnant mice of CON group delivered. The original number of the SGS offspring and the control offspring enrolled after birth were 42 and 40, respectively. One female mouse and one male mouse died before 3-week-old in SGS offspring, respectively. Furthermore, one female mouse in SGS group died between 3-week-old and 10-week-old. There was no pup died in the control group. At last, the numbers of offspring were as follows: SGS-3W group (*n*=40; male *n*=18, female *n*=22), CON-3W group (*n*=40; male *n*=22, female *n*=18), SGS-10W group (*n*=39; male *n*=18, female *n*=21), and CON-10W group (*n*=40; male *n*=22, female *n*=18).

We previously reported that dietary intake of 0.1% SGS food pellet showed prophylactic effects in several animal models including depression, schizophrenia, and autism spectrum disorder [27,29,38–40]. Therefore, we used 0.1% SGS food pellets in this study. Food pellets (CE-2; Japan CLEA, Ltd.) containing 0.1% SGS were prepared as reported previously [27,29,38–40]. In brief, broccoli sprout was grown from specially selected seeds (Brassica Protection Products LLC., Baltimore, MD, USA) for 1 day after the germination. Then, broccoli sprout was plunged into boiling water and maintained at 95°C for 30 min, and the sprout residues was removed by filtration. The boiling water extract was mixed with a waxy corn starch dextrin and then spray dried to yield the broccoli sprout extract powder containing 135 mg (approx.

0.31 mmol) of SGS per gram. For preparing the animal diet containing 0.1% SGS (approx. 2.3 mmol SGS per 1 kg-diet), the extract powder was mixed with a basal diet CE-2 (CLEA Japan Inc., Tokyo, Japan), and then pelletized at a processing facility (Oriental Yeast Co., ltd., Tokyo, Japan). The basic nutrients composition of CE-2 was shown in the supplemental Tables S1 and S2. The SGS content in the diet was determined by high performance liquid chromatography, and 0.1% SGS was used as reported previously [27,29,38–40]. Normal food pellets or 0.1% SGS food pellets were given to female mice during pregnancy and lactation (from E5 to P21 [weaning]). All the pregnant female mice were randomly divided into two groups: maternal SGS group was given 0.1% SGS food pellets; maternal control group was given normal food pellets.

Throughout the period of gestation and lactation (3 weeks), maternal SGS group (SGS) consumed 0.1% SGS food pellets, whereas maternal control group (CON) consumed normal food pellets. Subsequently, pups were delivered through the vagina and the body weight was recorded weekly until 10 weeks. After weaning at 3 weeks of age, pups were separated from the dams. All pups received control food pellets and drinking water ad libitum until 10 weeks. The study was approved by the Chiba University Institutional Animal Care and Use Committee (permission number: 2-388).

2.2. Collection of fecal samples, DNA extraction, 16S rRNA analysis

Fresh fecal samples of mothers were collected at weaning (P21). Fresh fecal samples of offspring (male and female) were also collected on day 21 (postnatal 3 weeks) and day 70 (postnatal 10 weeks). Fresh fecal samples were collected in the morning (9:00–10:00) to avoid the effects of circadian rhythm on the microbiome. The fecal samples were placed into sterilized screw-cap microtubes immediately after defecation and stored at −80°C until analysis. The detailed methods of DNA extraction and 16S rRNA analysis were shown in the Supplemental methods.

2.3. Concordance and co-occurrence analysis, and functional analysis of bacterial composition

The detailed methods of concordance and co-occurrence analysis, and functional analysis of bacterial composition were shown in the Supplemental methods.

2.4. LPS administration, collection of blood samples, and ELISA

Lipopolysaccharide (LPS: 0.5 mg/kg, Sigma-Aldrich, Tokyo, Japan) and saline (control: 10 ml/kg) were administered intraperitoneally (i.p.) into mice (Fig. 1A). The dose of LPS (0.5 mg/kg) was selected from the previous reports [29,41,42]. Blood samples were collected 24 hours after LPS or saline administration. All mice were not fasted prior to blood collection. Plasma samples were prepared by the previous method [42], and stored at −80°C before further ELISA measurement (Supplemental methods).

2.5. Statistical analysis

Data was shown as mean ± standard error of mean (S.E.M.). Box plots or violin plot (plot showing the median, and the 25% and 75%, and the whiskers of the graph show the largest and smallest values) were also used to express the data. Mann–Whitney *U* test or Wilcoxon test was performed when comparison between two groups. Ordinary or repeated measures one-way or two-way analysis of variance (ANOVA) followed by Fisher's least significant difference (LSD) test were performed. Correlations were conducted using Spearman correlation analysis between the relative abundance of gut microbiota and IL-6 (or TNF-α). $P<.05$ was considered significant difference.

3. Results

3.1. Effects of dietary intake of SGS on body weight of pregnant mice and their offspring

We investigated the effects of dietary intake of SGS food pellets during pregnancy and lactation (from E5 to P21) on the composition of gut microbiota in the offspring (Fig. 1A). There were no differences in body weight of mother mice between SGS group and CON group during pregnancy and lactation (from E5 to P21; Fig. S1A). There were also no differences in body weight of the offspring from postnatal 3 weeks until postnatal 10 weeks (Fig. S1B). The data showed that dietary intake of SGS food pellets during pregnancy and lactation did not affect the body weight changes between the two groups of offspring.
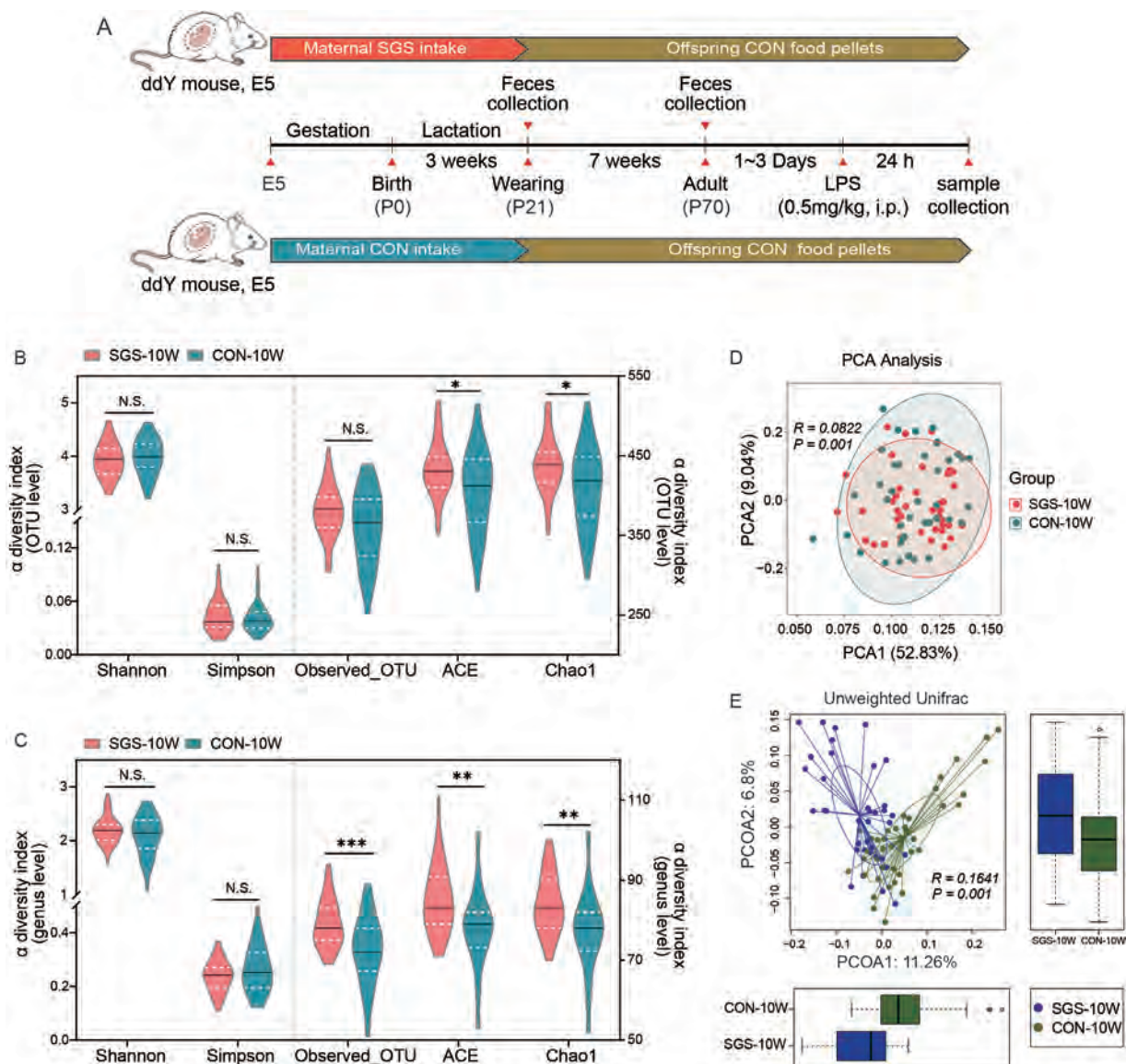
Fig. 1. Effects of maternal SGS intake on the α-diversity and β-diversity of gut microbiota in 10-week-old offspring. **(A)** Schematic diagram of sulforaphane glucosinolate (SGS) food intervention and experiments. Dietary 0.1% SGS food or CON food pellets were given to pregnant mice from E5 to postnatal 21 days (P21). CONT food pellets were given to all offspring from P21 to sample collection. Fresh fecal samples were collected at P21 and P70 for 16S rRNA gene analysis. Saline (10 ml/kg) or LPS (0.5mg/kg) was injected i.p. to adult offspring. Blood samples were collected 24 hours after a single injection. **(B)** Changes in α-diversity at OTU level of Shannon (U=688.5, Z=−0.897, P=0.370), Simpson (U=713.5, Z=−0.652, P=0.514), Observed_OTU (U=600, Z=−1.765, P=0.078), ACE (U=548.5, Z=−2.270, P=0.023) and Chao1 (U=529.5, Z=−2.457, P=0.014). **(C)** Changes in α-diversity at genus level of Shannon (U=699.5, Z=−0.790, P=0.430), Simpson (U=660, Z=−1.177, P=0.239), Observed_OTU (U=421, Z=−3.525, P=0.000), ACE (U=436, Z=−3.377, P=0.001) and Chao1 (U=435.5, Z=−3.382, P=0.001) between the two groups. **(D)** PCA analysis of the β-diversity change in the offspring's gut microbiota between the two groups based on the OTU level (ANOSIM, R=0.0822, P=.001). **(E)** PCoA analysis of the β-diversity change in the offspring's gut microbiota between the two groups based on the Unweighted Unifrac distance (ANOSIM, R=0.1641, P=.001), PCoA1: U=255, Z=−5.148, P=0.000; PCoA2: U=578, Z=−1.981, P=0.048. *P<.05, **P<.01, ***P<.001 (Mann–Whitney U test). N.S.: not significant. The numbers of 10-week-old offspring were SGS-10W group (n=39) and CON-10W group (n=40).

3.2. Effects of maternal SGS intake on the α-diversity, β-diversity, and composition of gut microbiota in 3-week-old offspring

α-diversity and β-diversity represent global changes in the gut microbiota. There were no differences in α-diversity at OTU level of Shannon, Simpson, Observed_OTU, ACE, and Chao1 between the two groups (SGS-3W and CON-3W;Fig. S2A). In contrast, there were significant changes in the all α-diversity (i.e., Shannon, Simpson, Observed_OTU, ACE, Chao1) at genus level (Fig. S2B). The association between maternal SGS diet and gut microbiota of offspring was assessed by PCA and PCoA for β-diversity. Based on the OTU level, PCA evaluated by ANOSIM (R=0.1473, P=.001) displayed a

significant separation of gut microbiota composition between the two groups (Fig. S2C). Based on the unweighted Unifrac distance, PCoA (ANOSIM, R=0.2045, P=.001) gave a conspicuous demonstration of separation distances in gut microbiota between the two groups (Fig. S2D). These data suggest an early consequence of maternal SGS intake in the composition of gut microbiota in 3-week-old offspring.

Figure S3 listed the top 60 of microbiota taxa (left) and top 24 significant differences microbial taxa (right) between the two groups at the genus level (Fig. S3). The data showed that maternal intake of SGS food pellets during pregnancy and lactation can affect the microbiota development in offspring at early stage.

3.3. Identification of gut microbiota contributing to difference in 3-week-old offspring

The LEfSe on the gut microbiota in offspring was distinct in abundant taxa between the two groups (Fig. S4). The colors displayed that their distribution for several taxa between the two groups was different by the Cladogram representation (LDA score >2.0, P<.05; Fig. S4A). Different abundant taxa based on LDA score (LDA score >2.0, P<.05) were shown in histogram between the two groups (Fig. S4B). Several microbes such as the genus *Clostridium sensu stricto 1, Prevotellaceae UCG 001,* the genus *Parabacteroides,* the genus *Prevotellaceae NK3B31 group,* the genus *Mucispirillum,* and the genus *Escherichia Shigella* were significantly enriched in the SGS-3W group compared with CON-3W group (Fig. S4B).

3.4. Effects of maternal SGS intake on the α-diversity, β-diversity of gut microbiota in 10-week-old offspring

Both of the α-diversity and β-diversity representing the global changes were still significant differences between the two groups (SGS-10W and CON-10W) at postnatal age of 10 weeks (Fig. 1B). Although there were no changes in α-diversity at OTU level of Shannon, Simpson, Observed_OTU between the two groups, two indices such as ACE and Chao1 were significant differences between the two groups (Fig. 1B). At genus level, two indices of Shannon and Simpson were not different between the two groups (Fig. 1C). However, three indices such as Observed_OTU, ACE, and Chao1 were significant differences between the two groups (Fig. 1C). Based on the OTU level, PCA evaluated by ANOSIM (R=0.0822, P=.001) displayed a significant separation of gut microbiota composition between the two groups (Fig. 1D). Based on the Unweighted Unifrac distance, β-diversity in PCoA changes (ANOSIM, R=0.2045, P=.001) revealed a clear separation distance in gut microbiota between the two groups (Fig. 1E). These results suggest a long-term consequence of maternal diet of SGS food pellets on the diversity of gut microbiota in the adult offspring (10-week-old).

3.5. Effects of maternal intake of SGS food pellet on composition of gut microbiota in adult offspring

At postnatal age of 10 weeks, the most composition alterations of the microbiota in adult offspring were shown at the genus level (Fig. 2A). Top 25 significant difference was listed with bar chart between the two groups (Fig. 2B). Those of them were higher in SGS-10W group than in the CON-10W group (Fig. 2B). These include *Lactobacillus, Bifidobacterium, Ruminococcaceae UCG-014, Intestinibacter, Anaerostipes, Rikenella, [Eubacterium] coprostanoligenes group, [Eubacterium] nodatum group, Candidatus Saccharimonas, Christensenellaceae R-7 group.* In contrast, several microbes including *Oscillibacter, Enterorhabdus, Blautia, Lachnospiraceae* and *Ruminococcaceae* were lower in the SGS-10W group than those of which in CON-10W group (Fig. 2B). The data revealed a long-term consequence of maternal intake of SGS food pellets on gut microbiota in adult offspring.

At postnatal age of 10 weeks, LEfSe results on the gut microbiota of adult offspring was distinct changes in abundant taxa between the two groups (Fig. S5). The colors displayed that their distribution for several taxa between the two groups was different by the Cladogram representation (LDA score >2.0, P<.05; Fig. S5A). Different abundant taxa based on LDA score (LDA score >2.0, P<.05) were shown in histogram between the two groups (Fig. S5B). Several microbes such as the genus *Lactobacillus,* the genus *Ruminococcaceae UCG 014,* the genus *Bifidobacterium* were signif-

icantly enriched in the SGS-10W group compared with control CON-10W group (Fig. S5B).

3.6. Predictive functional profiles of gut microbiota contributing to difference in the adult offspring at postnatal age of 10 weeks

The functional alterations of gut microbiota in early life intervention by the maternal diet, following by the control diet during development to adult, were predicted by the PICRUSt for the KEGG pathway (Fig. S6). Compared to the CON-10W group, the predominant KEGG pathways from SGS-10W group showed distinct function alteration, including 13 pathways on KEGG level 2, respectively related to 5 pathways on KEGG level 1 (Fig. S6), indicating a high abundance of predicted functions associated with genetic information processing and metabolism. Alterations in these pathways were similar to the previous report on the sulforaphane-related genes of transcriptome analyses showing the changes in KEGG analysis of functional annotation [41].

Moreover, significant differences between the two groups were displayed in 77 pathways on KEGG level 3 (Fig. S7), suggesting that many functions of adult offspring could be affected by maternal SGS diet.

3.7. Similar microbial shifts from mother to offspring of gut microbiota associated with dietary intake of SGS

The indices of α-diversity, including Observed_OTU, ACE, and Chao1, were significant different between the SGS-3W group and SGS-10W group (Fig. S8A), while there was no change between CON-3W group and CON-10W group (Fig. S8B). Moreover, β-diversity of gut microbiota among the mother, 3-week-old and 10-week-old offspring were also analyzed. Based on the Unweighted or Weighted Unifrac distance, ANOSIM algorithm showed an evident separation of gut microbiota composition among the three groups (Fig. S9A–S9C). Bray–Curtis distance analysis revealed an obviously different between the SGS-mother group and SGS-3W group, or between the SGS-mother group and SGS-10W group. In contrast, there were no differences for maternal CONT food groups (Fig. S9D–S9F). Taken together, these data suggest that α-diversity of gut microbiota is clearly increasing with the developmental progress in offspring, while higher distance between mother and offspring (3 weeks and 10 weeks old) was appreciable in β-diversity, those of which were associated with maternal SGS diet.

Using the Bray-Curtis distances, we analyzed the interactive effects of microbial shifts from mother to offspring's microbiota (Fig. 3A). The distances between gut microbiota of any two groups were significantly higher in SGS group than those in CON group (P<.001, Wilcoxon test; Fig. 3A). Next, we sought to identify concordance in top 100 most abundant OTU variations among mother, 3-week-old and 10-week-old offspring microbiota. First, we calculated the number of OTUs enriched or depleted in offspring with SGS group and then focused on those shared in maternal samples. OTUs variation with same (enriched or depleted in both maternal and offspring) or opposite trend (enriched or depleted in one side of maternal or offspring) were used to assess correlations with SGS. Unexpectedly, the number of OTUs in the same trend were almost equal compared with the opposite trend between the offspring at 10 weeks age and mother (Figs. 3B, S11A and S11B), which could be explained by the CON food intake after weaning at the age of 3 weeks. In addition, a large number of high abundant OTUs were found to vary with the same trend between mother and offspring at 3 weeks age (Fig. S10), or offspring between 3 and 10 weeks old (Fig. S12). Moreover, the most prevalent taxa showing
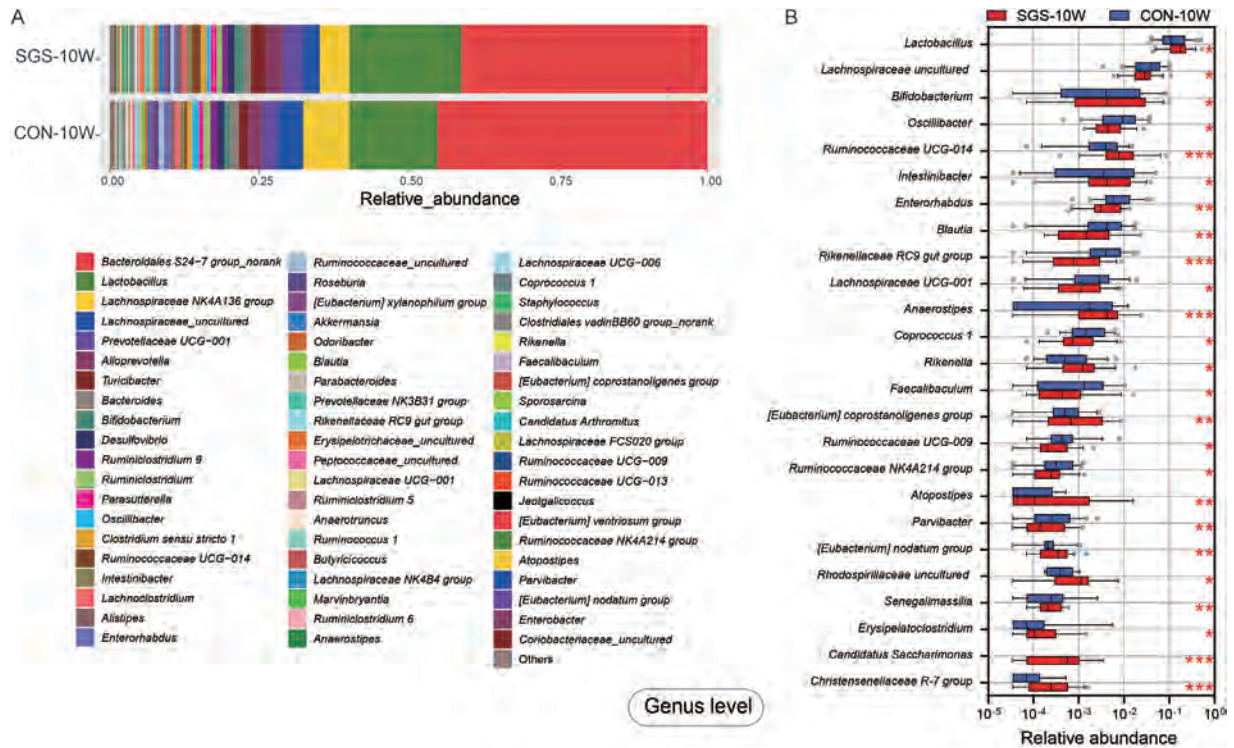
Fig. 2. Effects of maternal SGS intake on microbiota composition in the offspring at postnatal age of 10-week-old. **(A)** Average gut microbiota composition between the two groups at postnatal age of 10-week-old. **(B)** Statistical significance is denoted with box plot at genus level of relative abundance between the two groups. *$P<.05$, **$P<.01$, ***$P<.001$ (Mann–Whitney U test). The numbers of 10-week-old offspring were SGS-10W group ($n=39$) and CON-10W group ($n=40$).

the concordance of microbial variation between mother and offspring were denoted in any of two compared groups (Fig. 3C–E).

The variable importance in projection (VIP) taxa associated with SGS that is shared between mother and 3-week-old offspring were *Ruminococcaceae UCG-014, Candidatus Arthromitus, Clostridium sensu stricto-1,* and *Turicibacter* (Fig. 3C). Furthermore, VIP taxa associated with SGS that is shared between mother and 10-week-old offspring were *Lactobacillus, Parasutterella, Blautia, Ruminiclostridium, Bifidobacterium, Ruminococcaceae UCG-014,* and *Turicibacter* (Fig. 3D). Moreover, VIP taxa associated with SGS that is shared between 3-week-old and 10-week-old offspring were *Staphylococcus, Candidatus Arthromitus, Ruminococcaceae UCG-014, Blautia, Turicibacter,* and *Prevotellaceae NK3B31 group* (Fig. 3E). Thus, the two taxa of *Ruminococcaceae_UCG-014* and *Turicibacter* may be important VIP genera for the shifts from mother to offspring influenced by maternal SGS diet. Additionally, *Blautia, Turicibacter* and *Ruminococcaceae_UCG-014* were consistent with the shared VIP genera between offspring at 3-week-old and 10-week-old.

After exploring concordance of gut microbiota shifts from mother to the offspring, the maternal and offspring (3-week-old and 10-week-old) gut microbiota taxa were calculated for the co-occurrence networks of SGS group compared with those of CON group. The taxa including several VIP taxonomic notes were also distinctively differentiated according to the topographical network maps in mother group and offspring group (Fig. 4A–C). The detail difference among the groups were counted by the edges and nodes among the mother and offspring co-occurrence networks with or without SGS. There were also a different number of edges, and specific distribution of nodes, although there were overlapped edges and nodes between SGS group and CON group (Fig. 4D and E). Moreover, the gut microbiota correlations were also difference between SGS group and CON group (Fig. 4F–H). The number of

dots representing the significant correlations were higher in SGS group than those of which in the CON group, either at 3-week-old or 10-week-old of offspring (Fig. 4F–G). However, discrepancies of the gut microbiota in mother group and the correlations between SGS and CON did not reveal noticeable difference (Fig. 4H), possibly due to limited sample size ($n=4$ in SGS-mother group, $n=3$ in CON-mother group) and low power to identify the marked changes.

Furthermore, the correlation was showed by the co-occurrence pattern for assessing the gut microbiota shifts from mother to offspring associated with SGS (Fig. 4I). About 72.9% of all taxa connections had the same co-occurrence trend between the generations, and 54.2% were only detected in SGS group but not in CON group (Fig. 4I).

There was positive correlation between *Ruminiclostridium* and *Odoribacter,* while there was negative correlation between *Odoribacter* and *Erysipelatoclostridium.* There were also negative correlations between *Escherichia Shigella* and several VIP taxa, including *Ruminiclostridium* and *Odoribacter,* among the mother and offspring. Besides, the connections containing *Ruminiclostridium, Candidatus Soleaferrea,* and *Erysipelatoclostridium,* showed high frequencies of co-occurrence across multiple sample types, suggesting their universal attributions to microbiota associated with SGS (Fig. S13). It was suggested that the microbiota correlations were highly conserved between mothers and offspring gut samples associated with SGS.

3.8. A long-lasting protective effect of maternal SGS food intake against LPS induced inflammation in 10-weeks old offspring and its correlations with gut microbiota genera

Finally, we investigated the effects of maternal intake of SGS on systemic inflammation in adult offspring after LPS administration.
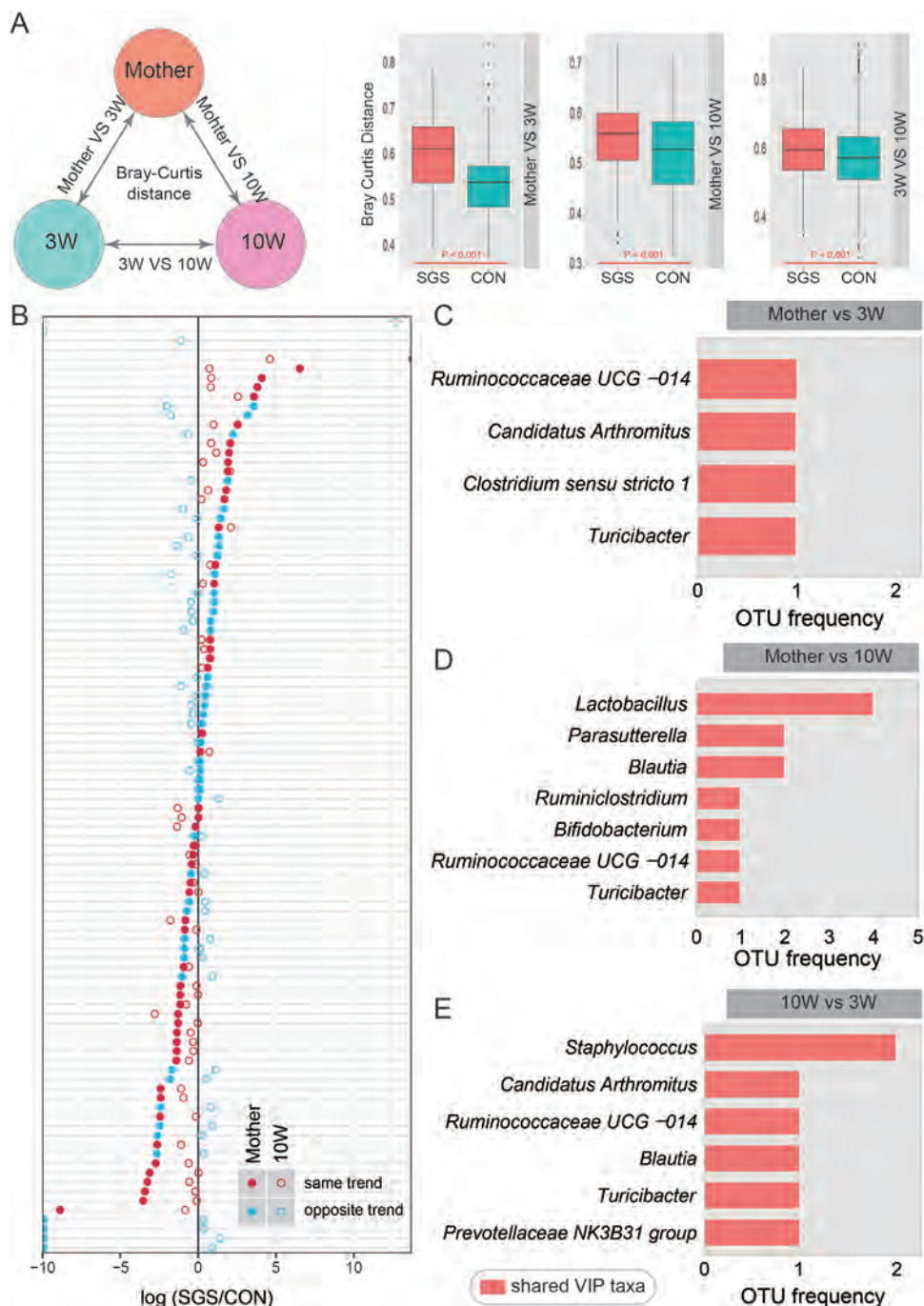
Fig. 3. Similar microbial shifts between mother and offspring of gut microbiota associated with SGS. **(A)** Gut microbiota variations of mother, offspring at 3-week-old and 10-week-old influenced by maternal SGS intake. Bacterial community dissimilarities between any two groups among mother, 3-week-old offspring and 10-week-old offspring. Wilcoxon test was used for analyzing the Bray-Curtis distance for SGS and CON group, independently. **(B)** Concordance of OTU variations between mother and 10-week-old offspring at the top 100 most abundant of gut microbiota average relative abundance. Solid points denoted maternal gut microbiota, while hollow points represented 10-week-old offspring's microbiota. Red or blue color showed the same or opposite trend of varied OTUs between mother and 10-week-old offspring. **(C–E)** The most predominant microbial variance concordance between mothers and offspring. Bar charts displayed OTU frequency of a specific variable importance for the projection (VIP) genus taxa associated with SGS. Between maternal and offspring, shared VIP taxa denoted that a certain genus was appearance between two groups. The numbers of offspring were SGS-3W group (*n*=40), CON-3W group (*n*=40), SGS-10W group (*n*=39) and CON-10W group (*n*=40). The numbers of mother were SGS group (*n*=4) and CON group (*n*=3).

A single injection of LPS (0.5 mg/kg, i.p.) increased plasma levels of IL-6 (Fig. 5A) and TNF-α (Fig. 5B) in both groups. However, plasma levels in these cytokines of SGS-10W group treated with LPS were significantly lower compared to those of CON-10W group treated with LPS (Fig. 5A and B). The data suggest that maternal SGS intake during pregnancy and lactation can induce an anti-inflammatory effect for LPS-induced systemic inflammation in adult offspring.

To explore the relationship between the relative abundance of microbes and cytokines levels, we adopted Spearman's rank-order correlation. There were significant negative correlations between the relative abundance of *[Eubacterium] nodatum*
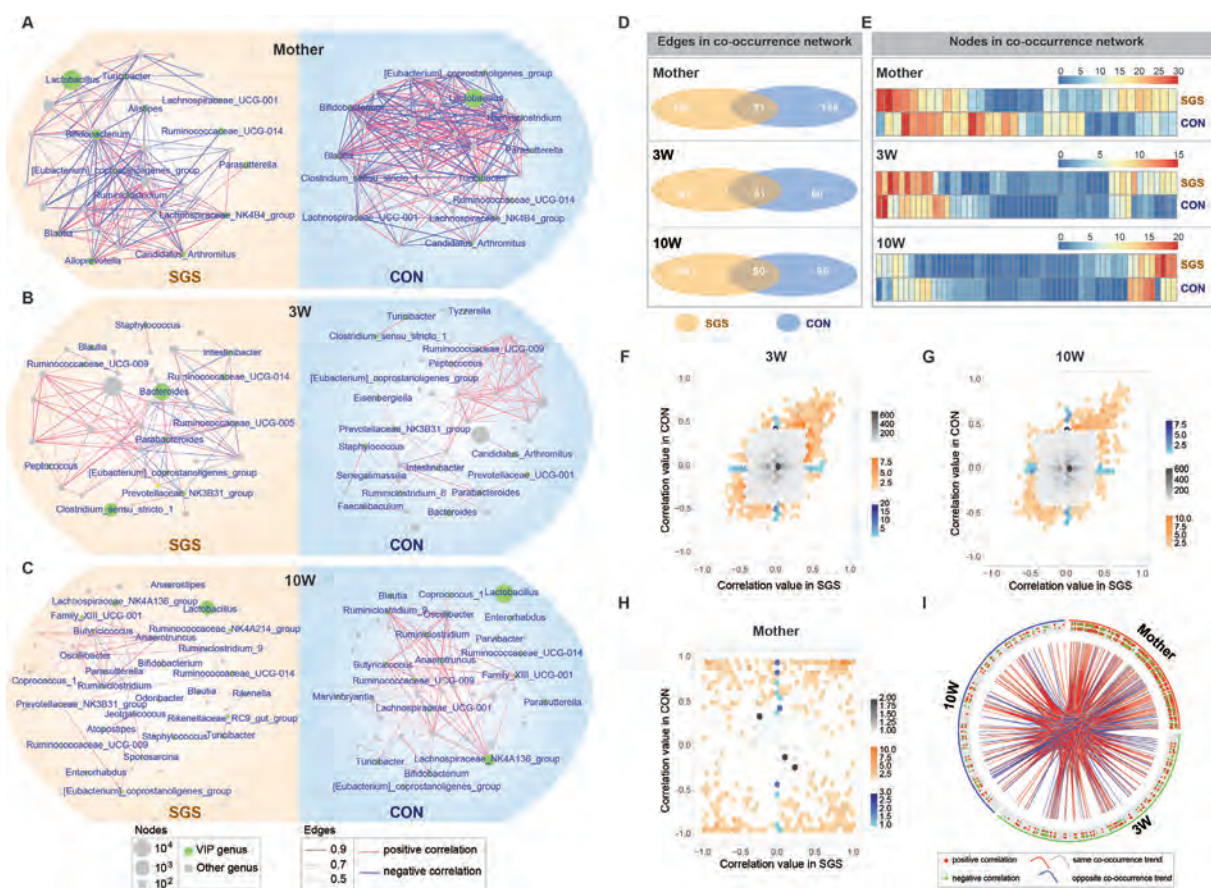
Fig. 4. Gut microbiota taxa co-occurrence network and concordance between maternal and offspring associated with SGS. **(A–C)** The co-occurrence network plots showed the gut microbiota relative abundance at the genus level between mothers **(A)**, between 3-week-old offspring **(B)** and between 10-week-old offspring **(C)**, respectively related to the SGS group (left panel) or CON group (right panel). The results were calculated by a pairwise correlation of all gut microbiota genera relative abundance in each sample. In the network, each node represented taxa-specific gut microbiota, node size indicated the average relative abundance of taxa-specific gut microbiota at genus level. Variable importance of projection (VIP) taxa-specific gut microbiota was displayed with green color in the nodes, linking with each other by the edge of red (positive) or blue (negative) color, respectively. The cut off value more than 0.4 was set for the gut microbiota connections (edges) in the co-occurrence network plots. **(D-E)** Statistical analysis for the number of edges and nodes in the co-occurrence network between mothers, between 3-week-old offspring and between 10-week-old offspring, respectively with maternal SGS or CON. **(F–H)** Gut microbiota interactive relationship between SGS and CON in mothers, 3-week-old offspring and 10-week-old offspring, displayed by the number of the same pair of gut microbiota taxa correlations. The horizontal and vertical coordinates showed that the same pair number of gut microbiota taxa accumulated in four quadrants, respectively in relation with SGS or CON. The color changes represented weak (gray) or strong (blue and yellow) correlations, respectively. **(I)** Concordance variation between maternal and offspring microbiota associated with SGS. The cut off value more than 0.4 was set for counting the same bacterial correlations among mother, offspring at 3-week-old and 10-week-old. In the outer cycle, dots were connected with each other from different group, representing one connection of two gut microbiota taxa (at least one is VIP genera). Red or green dot is a representative positive or negative relation, following with the same or opposite co-occurrence trend indicated by the red (occurred only in SGS) and grey curve (occurred in both SGS and CON), or vice versa by blue curve. The numbers of offspring were SGS-3W group (n=40), CON-3W group (n=40), SGS-10W group (n=39), and CON-10W group (n=40). The numbers of mother were SGS group (n=4) and CON group (n=3).

group, *Erysipelatoclostridium* and IL-6, while there was a positive correlation between *Blautia* and IL-6 (Fig. 5C). Moreover, there were significant negative correlations of the relative abundance of *Ruminococcaceae UCG-014, Anaerostipes, [Eubacterium] coprostanoligenes group, [Eubacterium] nodatum group, Erysipelatoclostridium, Christensenellaceae R-7 group, Coriobacteriaceae UCG-002, Christensenellaceae_uncultured* and *Candidatus Soleaferrea* with TNF-α, while *Blautia* and TNF-α was a positive correlation (Fig. 5C). These data suggest that several microbes might be associated with systemic inflammation after LPS administration.

3.9. Sex differences on gut microbiota at juvenile and adult offspring after maternal intake of SGS food pellet

We examined the effects of sex on α-diversity and β-diversity of the offspring of 3-week-old (Fig. S14). α-diversity indices includ-

ing Shannon, Simpson, Observed_OTU, ACE and Chao1 were not differences between the SGS-3W/male group and CON-3W/male group (Fig. S14A). However, α-diversity indices including Observed_OTU, ACE, and Chao1 were higher in SGS-3W/female group than that in CON-3W/female group (Fig. S14C). Interestingly, β-diversity of Unweighted Unifrac distance indicated a significant separation distance between the SGS-3W group and CON-3W group for male and female offspring (Fig. S14B and S14D).

Next, we examined the effects of sex on α-diversity and β-diversity of the offspring of 10-week-old (Fig. 6). α-diversity indices of Shannon and Simpson were significant differences between the SGS-10W/male group and CON-10W/male group, while other indices did not show significant differences (Fig. 6A). Furthermore, maternal diet of SGS affected the α-diversity indices of Observed_OTU, ACE, and Chao1 between SGS-10W/female group and CON-10W/female group (Fig. 6C). β-diversity of gut
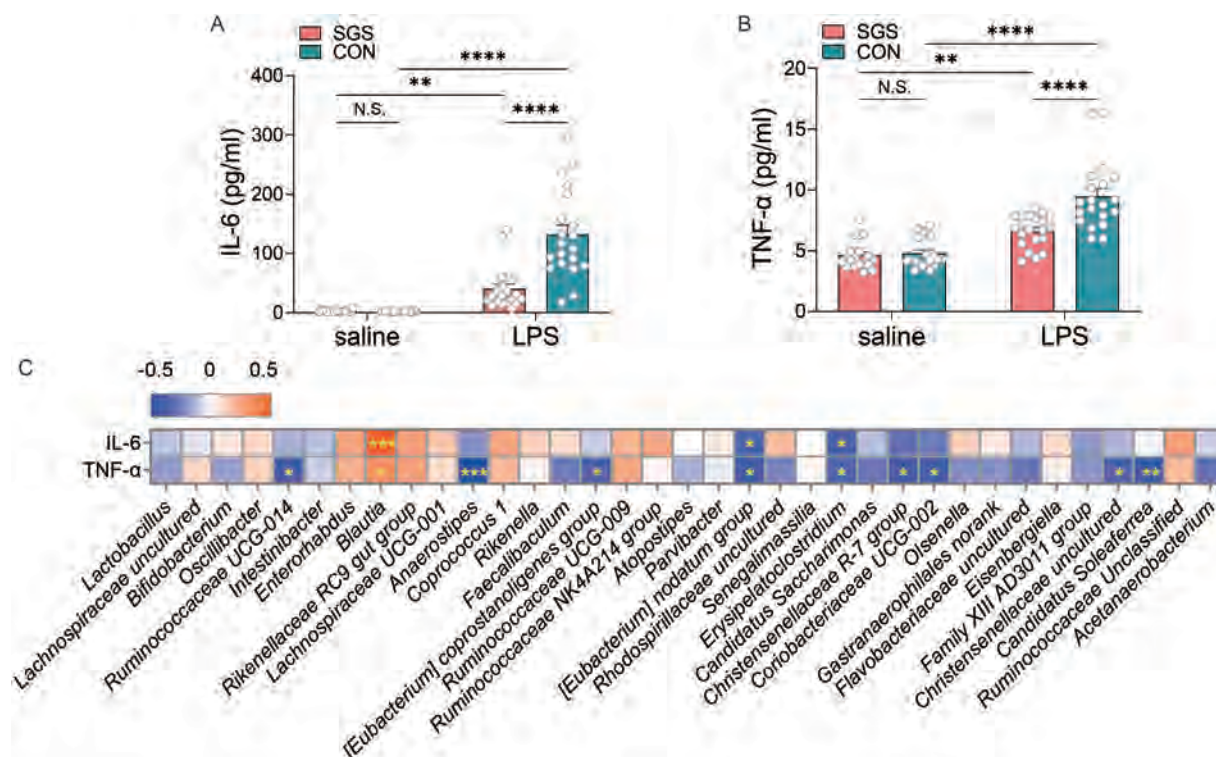
Fig. 5. Anti-inflammatory effect of maternal SGS intake on LPS-induced inflammation in 10-week-old offspring and correlations between microbiota genera. **(A)** Plasma levels of IL-6 in adult offspring 24 hours after saline or LPS administration (two-way ANOVA, $F_{(1,75)}=24.394$, $P<.001$). The data were expressed as mean±S. E.M ($n=19$ or 20). **$P<.01$, ****$P<.0001$. N.S.: no significant. **(B)** Plasma levels of TNF-α in adult offspring 24 hours after saline or LPS administration (two-way ANOVA, $F_{(1,75)}=11.223$, $P=.001$). The data were expressed as mean±S. E.M ($n=19$ or 20). **$P<.01$, ****$P<.0001$. N.S.: no significant. **(C)** Heatmaps showing correlations between microbes at genus level and plasma levels of IL-6 (or TNF-α) in the 10-week-old offspring with Spearman's correlation. The number of mice was saline treated group (SGS, $n=19$; CON, $n=20$) and LPS treated group (SGS, $n=20$; CON, $n=20$). *$P<.05$, **$P<.01$, ***$P<.001$.

microbiota in the male and female offspring were affected by maternal diet of SGS compared with the CON-10W/male group and CON-10W/female group, respectively (Fig. 6B and D). These data suggest that maternal diet of SGS may affect the gut microbiota of offspring, in a sex-specific manner.

Next, the relative abundance of gut microbiota in male offspring at 3-week-old was examined (Fig. S15). We found the top 60 of microbiota taxa (left) and 20 significant differences microbial taxa (right) between SGS-3W/male group and CON-3W/male group at the genus level (Fig. S15A and S15B). Furthermore, the relative abundance of gut microbiota in female offspring at 3-week-old was also analyzed (Fig. S16). We found the top 60 of microbiota taxa (left) and top 25 significant differences microbial taxa (right) between SGS-3W/female group and CON-3W/female group at the genus level (Fig. S16A and S16B). The data showed that maternal intake of SGS can affect the gut microbiota composition at 3-week-old, in a sex-dependent manner.

The relative abundance of gut microbiota of male offspring at 10-week-old was examined (Fig. S17). We found the top 60 of microbiota taxa (left) and top 25 significant differences microbial taxa (right) between SGS-10W/male group and CON-10W/male group at the genus level (Fig. S17A and S17B). Furthermore, the relative abundance of gut microbiota in female offspring at 10-week-old was also examined (Fig. S18). We found the top 60 of microbiota taxa (left) and 16 significant differences microbial taxa (right) between SGS-10W/female and CON-10W/female at the genus level (Fig. S18A and S18B). The data showed that maternal intake of SGS can affect the gut microbiota development at 10-week-old, in a sex dependent manner.

4. Discussion

The major findings of the current study were as follows. First, the dietary intake of SGS food pellets during pregnancy and lactation caused significant changes in the α-diversity and β-diversity of the gut microbiota at genus level in 3-week-old offspring (SGS-3W group). In addition, β-diversity analyzed using Bray-Curtis distance showed significant differences between the SGS-mother group and SGS-3W group although there was no difference between the CON-mother group and the CON-3W group. Second, the dietary intake of SGS food pellets during pregnancy and lactation caused significant changes in the α-diversity and β-diversity of the gut microbiota at OTU or genus level in 10-week-old offspring (SGS-10W group). Predictive functional metagenomes using PICRUSt showed that maternal dietary intake of SGS food pellets caused several KEGG pathways alterations in terms of genetic information processing and metabolism. Third, the plasma levels of IL-6 and TNF-α of the SGS-10W group treated with LPS were significantly lower than those of the CON-10W group, suggesting that SGS-10W mice exert anti-inflammatory effects for LPS-induced inflammation. It is noteworthy that there were correlations between the relative abundance of several microbes and IL-6 (or TNF-α) in adult offspring, suggesting that several microbes might contribute to the inflammatory (or anti-inflammatory) effects for LPS-induced systemic inflammation. Finally, we found sex differences in gut microbiota of offspring after maternal SGS intake. In sum, the current data suggest that the dietary intake of SGS food pellets during pregnancy and lactation causes long-lasting beneficial effects in adult offspring via persistent modulation of gut microbiota (Fig. 7).
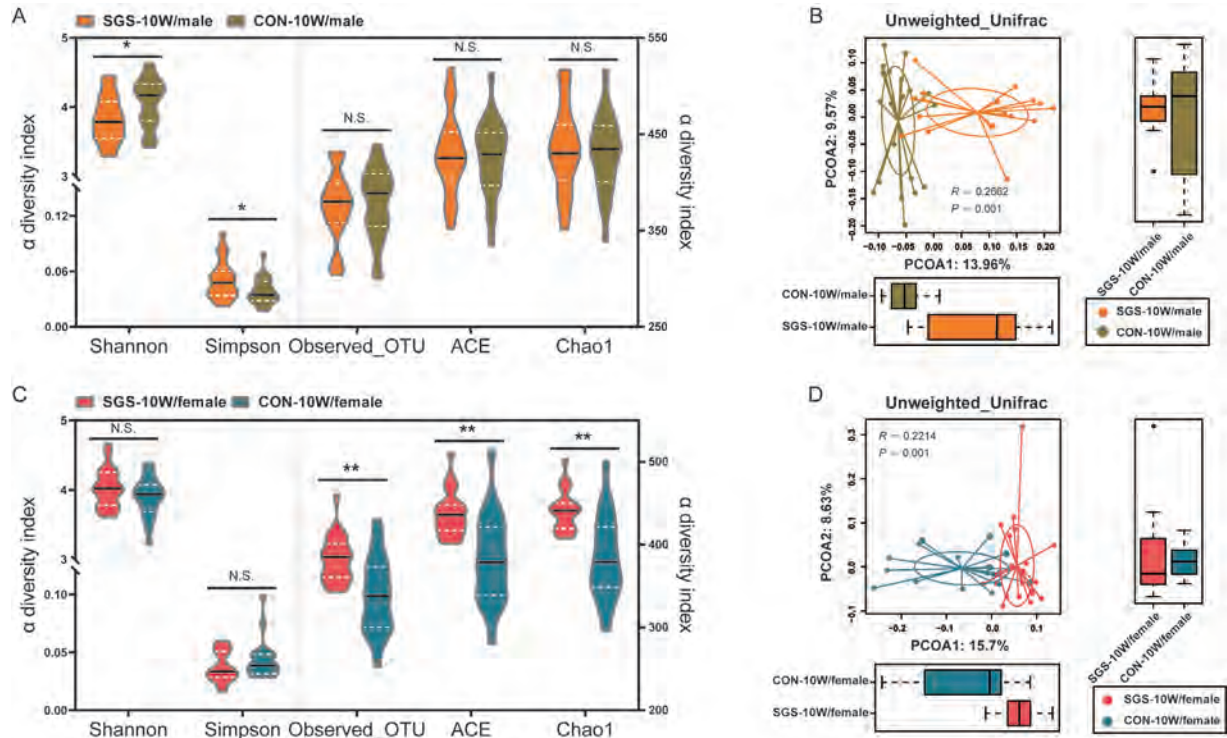
Fig. 6. Sex effects of maternal SGS intake on the α-diversity and β-diversity of gut microbiota of offspring at 10-week-old. **(A)** Changes in α-diversity at OTU level of Shannon (U=124.0, Z=−2.013, P=.044), Simpson (U=120.5, Z=−2.107, P=.035), Observed_OTU (U=192.0, Z=−0.163, P=.870), ACE (U=198.0, Z=−0.000, P=1.000) and Chao1 (U=194.0, Z=−0.109, P=.913) between SGS-10W/male group and CON-10W/male group. **(B)** PCoA analysis of the β-diversity change in the offspring's gut microbiota between SGS-10W/male group and CON-10W/male group based on the Unweighted Unifrac distance (ANOSIM, R=0.2662, P=.001), PCoA1: U=27.0, Z=−4.649, P=.000; PCoA2: U=180.0, Z=−0.489, P=.625. **(C)** Changes in α-diversity at OTU level of Shannon (U=155.0, Z=−0.958, P=0.338), Simpson (U=146.5, Z=−1.197, P=.231), Observed_OTU (U=81.0, Z=−3.043, P=.002), ACE (U=69.5, Z=−3.367, P=.001) and Chao1 (U=68.0, Z=−3.410, P=.001) between the SGS-10W/female and CON-10W/female. **(D)** PCoA analysis of the β-diversity change in the offspring's gut microbiota between SGS-10W/female and CON-10W/female based on the Unweighted Unifrac distance (ANOSIM, R=0.2214, P=.001), PCoA1: U=41.0, Z=−4.169, P=.000; PCoA2: U=161.0, Z=−0.789, P=.430. *P<.05, **P<.01, ***P<.001 (Mann–Whitney U test). N.S.: not significant. The numbers of mice in two groups were male (SGS-10W, n=18; CON-10W, n=22) and female (SGS-10W, n=21; CON-10W, n=18).

A recent study showed positive correlations between the relative abundance of the genus *Blautia* and plasma levels of IL-6 (or TNF-α) in rats treated with streptozotocin-nicotinamide [43]. In this study, we found positive correlations between the relative abundance of *Blautia* and the plasma levels of IL-6 (or TNF-α), suggesting that *Blautia* may be associated with the production of these pro-inflammatory cytokines. Given the crucial role of *Balutia* in inflammatory actions [44], our data suggest that lower abundance of *Balutia* in the SGS-10W group may contribute to its anti-inflammatory effects in adult offspring; however, further study on the different species *Blautia* is required. Moreover, there were negative correlations between several microbes and the plasma levels of IL-6 (or TNF-α), suggesting that these microbes might be related to the expression of anti-inflammatory effects. In sum, it is likely that maternal SGS intake during pregnancy and lactation produces long-lasting beneficial effects against stressful events in adult offspring via the modulation of gut microbiota. Nonetheless, further research is needed to investigate the precise relationship between these microbes and anti-inflammatory (or inflammatory) actions in adult offspring.

Several population-based studies have shown that inadequate nutrition during pregnancy exerts long-term negative effects on the health of the offspring [6,45], suggesting the crucial role of nutrition during pregnancy. SGS food pellet included a potent anti-inflammatory compound sulforaphane with a potent Nrf2 activator. Given the key role of Nrf2 in inflammation and oxidative stress [20–24], it is likely that dietary intake of SGS food pellet during pregnancy and lactation may contribute to long-term prophylactic effects in offspring through anti-inflammatory actions. Moreover, diet-induced alterations in the mother's gut microbiome can influence the gut microbiota of the offspring and the initial microbial colonization of the offspring originates from the mother's microbiota [46]. Given the role of maternal diet on the gut microbiome of the offspring [6,17], the dietary intake of SGS during pregnancy and lactation may contribute to resilience in the offspring via the modulation of gut microbiota.

It is reported that treatment of SGS or sulforaphane may have beneficial effects in patients with schizophrenia and autism spectrum disorder [47,48]. A previous study showed that dietary intake of 0.1% SGS food pellets during pregnancy and lactation could prevent the onset of behavioral abnormalities in offspring after maternal immune activation [40]. The dosage of 0.1% SGS used in this study is reasonable dose for human use. Collectively, it is possible that dietary intake of SGS in pregnant women may produce long-lasting beneficial effects in offspring although further clinical study is needed. For example, it is of interest to investigate whether supplementation of SGS in pregnant women with COVID-19 can affect the onset of neuropsychiatric disorders in offspring [49,50].

This study has some limitations. First, we did not investigate the mechanistic insight into how dietary intake of SGS during pregnancy and lactation modulates gut microbial communities in offspring. Second, using the PICRUSt, we found several signaling
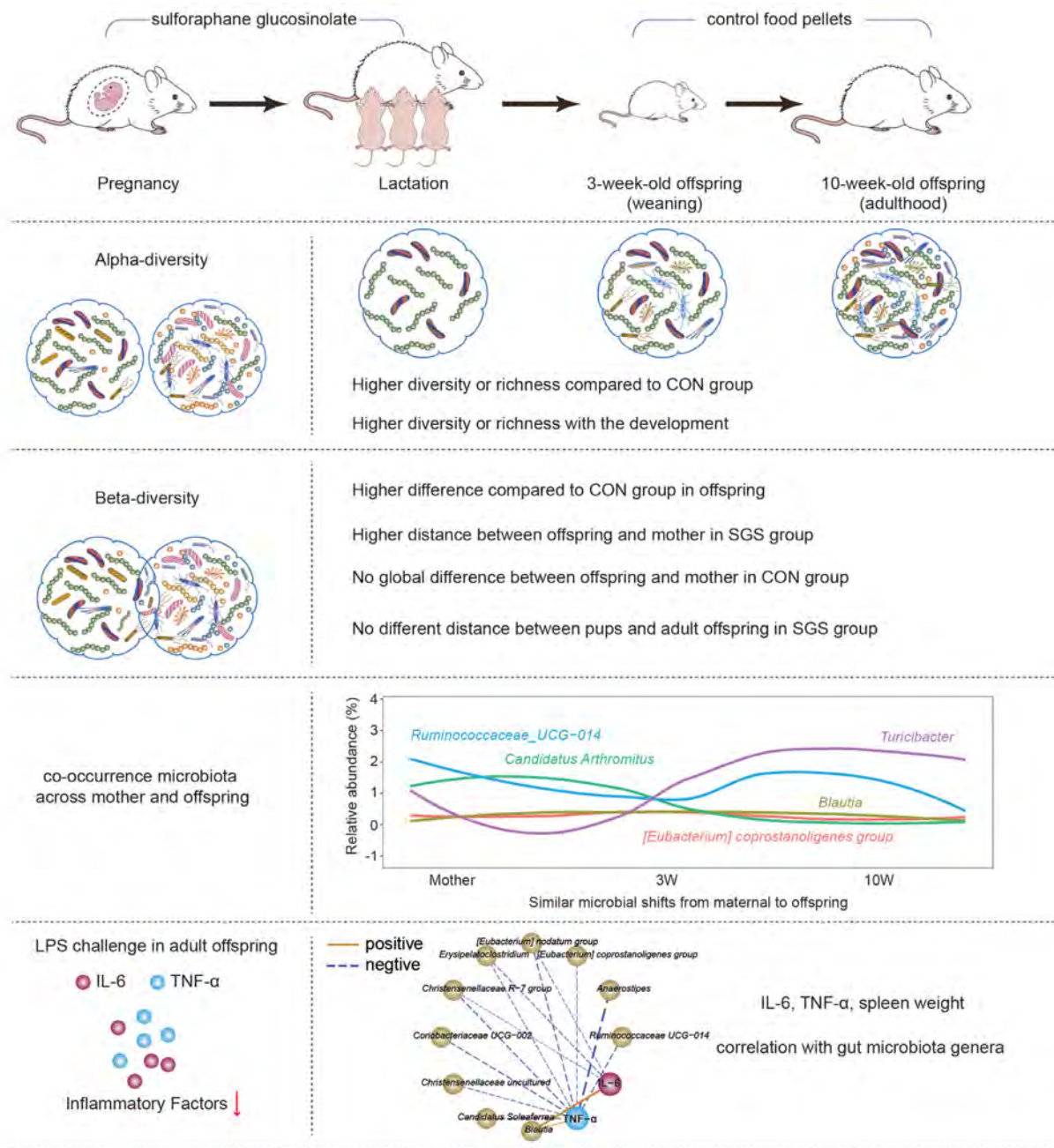
Fig. 7. Summary of major findings of the current study. Effects of maternal diet of SGS on the gut microbiota variation from mother to offspring, and the possible relationship between relative abundance of gut microbiota taxa and plasma levels of IL-6 (or TNF-α) in the adult offspring with LPS challenge. Dietary intake of SGS food pellets during pregnancy and lactation causes long-lasting beneficial effects in adult offspring via persistent modulation of gut microbiota.

pathways in the beneficial effects of SGS food pellet. Further study of the role of maternal intake of SGS food in these pathways is needed. Finally, we did not investigate the mechanisms of relationship between maternal intake of SGS and long-term anti-inflammatory action in the adult offspring. Further detailed study including epigenetic modification is needed.

In conclusion, the present data suggest that the dietary intake of SGS during pregnancy and lactation could produce long-lasting beneficial effects in adult offspring via the persistent modulation of gut microbiota. Therefore, the long-term modulation of gut microbiota by maternal nutrition could exert a strong impact on the health and disease vulnerability of the offspring.

Author statement

Disclosure statement

Authors' contributions

K.H. planned the study and formulated the working hypothesis. Y.W. and L.C. conducted the experiments and analyzed the results. X.W. and Y.Y. conducted collection of samples. Y.W., L.C., and K.H. wrote the manuscript. G.L. contributed intellectually to the analysis of the data. All authors critically proof-read the manuscript and approved for publication.

Data and code availability

The 16s rRNA sequencing data have been deposited to the NCBI Sequence Read Archive and are available at the accession number PRJNA744623.

Acknowledgments

Declaration of Competing Interest

The authors declare that there are no conflicts of interest.

Supplementary materials

Supplementary material associated with this article can be found, in the online version, at doi:10.1016/j.jnutbio.2022.109098.

References

[1] Yajnik CS, Deshmukh US. Maternal nutrition, intrauterine programming and consequential risks in the offspring. Rev Endocr Metab Disord 2008;9:203–11. doi:10.1007/s11154-008-9087-z.

[2] Hanson M. The birth and future health of DOHaD. J Dev Orig Health Dis 2015;6:434–7. doi:10.1017/S2040174415001129.

[3] Suzuki K. The developing world of DOHaD. J Dev Orig Health Dis 2018;9:266–9. doi:10.1017/S2040174417000691.

[4] Hanson MA, Poston L, Gluckman PD. DOHaD - the challenge of translating the science to policy. J Dev Orig Health Dis 2019;10:263–7. doi:10.1017/S2040174419000205.

[5] Jazwiec PA, Sloboda DM. Nutritional adversity, sex and reproduction: 30 years of DOHaD and what have we learned? J Endocrinol 2019;242:T51–68. doi:10.1530/JOE-19-0048.

[6] Bodden C, Hannan AJ, Reichelt AC. Of 'junk food' and 'brain food': how parental diet influences offspring neurobiology and behaviour. Trends Endocrinol Metab 2021;32:566–78. doi:10.1016/j.tem.2021.04.001.

[7] Bjerregaard AA, Halldorsson TI, Tetens I, Olsen SF. Mother's dietary quality during pregnancy and offspring's dietary quality in adolescence: Follow-up from a national birth cohort study of 19,582 mother-offspring pairs. PLoS Med 2019;16:e1002911. doi:10.1371/journal.pmed.1002911.

[8] Carabotti M, Scirocco A, Maselli MA, Severi C. The gut-brain axis: interactions between enteric microbiota, central and enteric nervous systems. Ann Gastroenterol 2015;28:203–9.

[9] Rogers GB, Keating DJ, Young RL, Wong ML, Licinio J, Wesselingh S. From gut dysbiosis to altered brain function and mental illness: mechanisms and pathways. Mol Psychiatry 2016;21:738–48. doi:10.1038/mp.2016.50.

[10] Cryan JF, O'Riordan KJ, Cowan CSM, Sandhu KV, Bastiaanssen TFS, Boehme M, et al. The Microbiota-gut-brain axis. Physiol Rev 2019;99:1877–2013. doi:10.1152/physrev.00018.2018.

[11] Wei Y, Chang L, Hashimoto K. Molecular mechanisms underlying the antidepressant actions of arketamine: beyond the NMDA receptor. Mol Psychiatry 2022;27(1):559–73. doi:10.1038/s41380-021-01121-1.

[12] Chu DM, Meyer KM, Prince AL, Aagaard KM. Impact of maternal nutrition in pregnancy and lactation on offspring gut microbial composition and function. Gut Microbes 2016;7:459–70. doi:10.1080/19490976.2016.1241357.

[13] Paul HA, Bomhof MR, Vogel HJ, Reimer RA. Diet-induced changes in maternal gut microbiota and metabolomic profiles influence programming of offspring obesity risk in rats. Sci Rep 2016;6:20683. doi:10.1038/srep20683.

[14] Robertson RC, Kaliannan K, Strain CR, Ross RP, Stanton C, Kang JX. Maternal omega-3 fatty acids regulate offspring obesity through persistent modulation of gut microbiota. Microbiome 2018;6:95. doi:10.1186/s40168-018-0476-6.

[15] Kimura I, Miyamoto J, Ohue-Kitano R, Watanabe K, Yamada T, Onuki M, et al. Maternal gut microbiota in pregnancy influences offspring metabolic phenotype in mice. Science 2020;367. doi:10.1126/science.aaw8429.

[16] Nettleton JE, Cho NA, Klancic T, Nicolucci AC, Shearer J, Borgland SL, et al. Maternal low-dose aspartame and stevia consumption with an obesogenic diet alters metabolism, gut microbiota and mesolimbic reward system in rat dams and their offspring. Gut 2020;69:1807–17. doi:10.1136/gutjnl-2018-317505.

[17] Al Rubaye H, Adamson CC, Jadavji NM. The role of maternal diet on offspring gut microbiota development: a review. J Neurosci Res 2021;99:284–93 Doi:. doi:10.1002/jnr.24605.

[18] Dawson SL, O'Hely M, Jacka FN, Ponsonby AL, Symeonides C, Loughman A, et al. Maternal prenatal gut microbiota composition predicts child behaviour. EBioMedicine 2021;68:103400. doi:10.1016/j.ebiom.2021.103400.

[19] Mirpuri J. Evidence for maternal diet-mediated effects on the offspring microbiome and immunity: implications for public health initiatives. Pediatr Res 2021;89:301–6. doi:10.1038/s41390-020-01121-x.

[20] Yamamoto M, Kensler TW, Motohashi H. The KEAP1-NRF2 system: a thiol-based sensor-effector apparatus for maintaining redox homeostasis. Physiol Rev 2018;98:1169–203. doi:10.1152/physrev.00023.2017.

[21] Hashimoto K. Essential role of Keap1-Nrf2 signaling in mood disorders: overview and future perspective. Front Pharmacol 2018;9:1182. doi:10.3389/fphar.2018.01182.

[22] Yu C, Xiao JH. The Keap1-Nrf2 system: a mediator between oxidative stress and aging. Oxid Med Cell Longev 2021;2021:6635460. doi:10.1155/2021/6635460.

[23] Dinkova-Kostova AT, Fahey JW, Kostov RV, Kensler TW. KEAP1 and done? Targeting the NRF2 pathway with sulforaphane. Trends Food Sci Technol 2017;69:257–69. doi:10.1016/j.tifs.2017.02.002.

[24] Kubo E, Chhunchha B, Singh P, Sasaki H, Singh DP. Sulforaphane reactivates cellular antioxidant defense by inducing Nrf2/ARE/Prdx6 activity during aging and oxidative stress. Sci Rep 2017;7:14130. doi:10.1038/s41598-017-14520-8.

[25] Chen H, Wu J, Zhang J, Fujita Y, Ishima T, Iyo M, et al. Protective effects of the antioxidant sulforaphane on behavioral changes and neurotoxicity in mice after the administration of methamphetamine. Psychopharmacology (Berl) 2012;222:37–45. doi:10.1007/s00213-011-2619-3.

[26] Shirai Y, Fujita Y, Hashimoto K. Effects of the antioxidant sulforaphane on hyperlocomotion and prepulse inhibition deficits in mice after phencyclidine administration. Clin Psychopharmacol Neurosci 2012;10:94–8. doi:10.9758/cpn.2012.10.2.94.

[27] Yao W, Zhang JC, Ishima T, Dong C, Yang C, Ren Q, et al. Role of Keap1-Nrf2 signaling in depression and dietary intake of glucoraphanin confers stress resilience in mice. Sci Rep 2016;6:30659. doi:10.1038/srep30659.

[28] Yao W, Lin S, Su J, Cao Q, Chen Y, Chen J, et al. Activation of BDNF by transcription factor Nrf2 contributes to antidepressant-like actions in rodents. Transl Psychiatry 2021;11:140. doi:10.1038/s41398-021-01261-6.

[29] Zhang JC, Yao W, Dong C, Yang C, Ren Q, Ma M, et al. Prophylactic effects of sulforaphane on depression-like behavior and dendritic changes in mice after inflammation. J Nutr Biochem 2017;39:134–44. doi:10.1016/j.jnutbio.2016.10.004.

[30] Li S, Yang C, Fang X, Zhan G, Huang N, Gao J, et al. Role of Keap1-Nrf2 signaling in anhedonia symptoms in a rat model of chronic neuropathic pain: Improvement with sulforaphane. Front Pharmacol 2018;9:887. doi:10.3389/fphar.2018.00887.

[31] Zhang JC, Yao W, Dong C, Han M, Shirayama Y, Hashimoto K. Keap1-Nrf2 signaling pathway confers resilience versus susceptibility to inescapable electric stress. Eur Arch Psychiatry Clin Neurosci 2018;268:865–70. doi:10.1007/s00406-017-0848-0.

[32] Qu Y, Shan J, Wang S, Chang L, Pu Y, Wang X, et al. Rapid-acting and long-lasting antidepressant-like action of (R)-ketamine in Nrf2 knock-out mice: a role of TrkB signaling. Eur Arch Psychiatry Clin Neurosci 2021;271:439–46. doi:10.1007/s00406-020-01208-w.

[33] Hashimoto K. Recent advances in the early intervention in schizophrenia: future direction from preclinical findings. Curr Psychiatry Rep 2019;21:75. doi:10.1007/s11920-019-1063-7.

[34] Mahn A, Castillo A. Potential of sulforaphane as a natural immune system enhancer: a review. Molecules 2021;26. doi:10.3390/molecules26030752.

[35] Fahey JW, Wade KL, Wehage SL, Holtzclaw WD, Liu H, Talalay P, et al. Stabilized sulforaphane for clinical use: phytochemical delivery efficiency. Mol Nutr Food Res 2017;61. doi:10.1002/mnfr.201600766.

[36] Cardozo L, Alvarenga LA, Ribeiro M, Dai L, Shiels PG, Stenvinkel P, et al. Cruciferous vegetables: rationale for exploring potential salutary effects of sulforaphane-rich foods in patients with chronic kidney disease. Nutr Rev 2021;79(11):1204–24. doi:10.1093/nutrit/nuaa129.

[37] Fahey JW, Kensler TW. The challenges of designing and implementing clinical trials with broccoli sprouts... and turning evidence into public health action. Front Nutr 2021;8:648788. doi:10.3389/fnut.2021.648788.

[38] Shirai Y, Fujita Y, Hashimoto R, Ohi K, Yamamori H, Yasuda Y, et al. Dietary intake of sulforaphane-rich broccoli sprout extracts during juvenile and adolescence can prevent phencyclidine-induced cognitive deficits at adulthood. PLoS One 2015;10:e0127244. doi:10.1371/journal.pone.0127244.

[39] Matsuura A, Ishima T, Fujita Y, Iwayama Y, Hasegawa S, Kawahara-Miki R, et al. Dietary glucoraphanin prevents the onset of psychosis in the adult offspring after maternal immune activation. Sci Rep 2018;8:2158. doi:10.1038/s41598-018-20538-3.

[40] Fujita Y, Fujita A, Ishima T, Hirai A, Suzuki S, Suganuma H, et al. Dietary intake of glucoraphanin during pregnancy and lactation prevents the behavioral abnormalities in the offspring after maternal immune activation. Neuropsychopharmacol Rep 2020;40:268–74. doi:10.1002/npr2.12112.

[41] Zhang JC, Wu J, Fujita Y, Yao W, Ren Q, Yang C, et al. Antidepressant effects of TrkB ligands on depression-like behavior and dendritic changes in mice after inflammation. Int J Neuropsychopharmacol 2014;18. doi:10.1093/ijnp/pyu077.

[42] Zhang J, Ma L, Chang L, Pu Y, Qu Y, Hashimoto K. A key role of the subdiaphragmatic vagus nerve in the depression-like phenotype and abnormal composition of gut microbiota in mice after lipopolysaccharide administration. Transl Psychiatry 2020;10:186. doi:10.1038/s41398-020-00878-3.

[43] Zhu L, Sha L, Li K, Wang Z, Wang T, Li Y, et al. Dietary flaxseed oil rich in omega-3 suppresses severity of type 2 diabetes mellitus via anti-inflammation and modulating gut microbiota in rats. Lipids Health Dis 2020;19:20. doi:10.1186/s12944-019-1167-4.

[44] Liu X, Mao B, Gu J, Wu J, Cui S, Wang G, et al. Blautia-a new functional genus with potential probiotic properties? Gut Microbes 2021;13:1–21. doi:10.1080/19490976.2021.1875796.

[45] Marx W, Lane M, Hockey M, Aslam H, Berk M, Walder K, et al. Diet and depression: exploring the biological mechanisms of action. Mol Psychiatry. 2021;26:134–50. doi:10.1038/s41380-020-00925-x.

[46] Stinson LF, Payne MS, Keelan JA. Planting the seed: Origins, composition, and postnatal health significance of the fetal gastrointestinal microbiota. Crit Rev Microbiol 2017;43:352–69. doi:10.1080/1040841X.2016.1211088.

[47] Shiina A, Kanahara N, Sasaki T, Oda Y, Hashimoto T, Hasegawa T, et al. An open-label study of sulforaphane-rich broccoli sprout extract in patients with schizophrenia. Clin Psychopharmacol Neurosci 2015;13:62–7. doi:10.9758/cpn.2015.13.1.62.

[48] Singh K, Connors SL, Macklin EA, Smith KD, Fahey JW, Talalay P, et al. Sulforaphane treatment of autism spectrum disorder (ASD). Proc Natl Acad Sci USA 2014;111:15550–5. doi:10.1073/pnas.1416940111.

[49] Hashimoto K. Risk of neuropsychiatric disorders in offspring of COVID-19-infected pregnant women and nutritiional intervention. Eur Arch Psychiatry Clin Neurosci 2021;271:387–9. doi:10.1007/s00406-020-01148-5.

[50] Hashimoto Y, Suzuki T, Hashimoto K. Mechanisms of action of fluvoxamine for COVID-19: a historical review. Mol Psychiatry 2022;27(4):1898–907. doi:10.1038/s41380-021-01432-3.
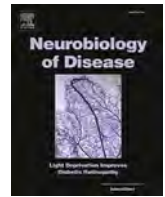
Key role of the gut–microbiota–brain axis via the subdiaphragmatic vagus nerve in demyelination of the cuprizone-treated mouse brain

Xingming Wang [a,b], Akifumi Eguchi [c], Yong Yang [a], Lijia Chang [a], Xiayun Wan [a], Jiajing Shan [a], Youge Qu [a], Li Ma [a], Chisato Mori [c,d], Jianjun Yang [b], Kenji Hashimoto [a,*]

[a] Division of Clinical Neuroscience, Chiba University Center for Forensic Mental Health, Chiba 260-8670, Japan
[b] Department of Anesthesiology, Pain and Perioperative Medicine, The First Affiliated Hospital of Zhengzhou University, Zhengzhou 450052, Henan, China
[c] Department of Sustainable Health Science, Chiba University Center for Preventive Medical Sciences, Chiba 263-8522, Japan
[d] Department of Bioenvironmental Medicine, Graduate School of Medicine, Chiba University, Chiba 260-8670, Japan

ABSTRACT

Multiple sclerosis (MS) is the most common demyelinating disease that attacks the central nervous system. Dietary intake of cuprizone (CPZ) produces demyelination resembling that of patients with MS. Given the role of the vagus nerve in gut–microbiota–brain axis in development of MS, we performed this study to investigate whether subdiaphragmatic vagotomy (SDV) affects demyelination in CPZ-treated mice. SDV significantly ameliorated demyelination and microglial activation in the brain compared with sham-operated CPZ-treated mice. Furthermore, 16S ribosomal RNA analysis revealed that SDV significantly improved the abnormal gut microbiota composition of CPZ-treated mice. An untargeted metabolomic analysis demonstrated that SDV significantly improved abnormal blood levels of metabolites in CPZ-treated mice compared with sham-operated CPZ-treated mice. Notably, there were correlations between demyelination or microglial activation in the brain and the relative abundance of several microbiome populations, suggesting a link between gut microbiota and the brain. There were also correlations between demyelination or microglial activation in the brain and blood levels of metabolites. Together, these data suggest that CPZ produces demyelination in the brain through the gut–microbiota–brain axis via the subdiaphragmatic vagus nerve.

1. Introduction

Multiple sclerosis (MS) can affect any part of the central nervous system (CNS) and is characterized by chronic neuroinflammation and the destruction of myelin sheaths. The symptoms of MS cause physical and psychological problems and have an important economic burden (Dahham et al., 2021; Nicholas et al., 2021; Wang et al., 2022a). An increasing body of evidence suggests that the gut–microbiota–brain axis plays a crucial role in the pathogenesis of MS (Cantarel et al., 2015; Farshbafnadi et al., 2021; Ghezzi et al., 2021; Maghzi and Weiner, 2020; Parodi and Kerlero de Rosbo, 2021; Wang et al., 2022b). Moreover, a recent meta-analysis revealed the abnormal composition of gut microbiota in MS patients, although α-diversity was not altered (Plassais et al., 2021). A role of gut microbiota in the cognitive impairment of MS patients has also been suggested (Ghadiri et al., 2022). However, the precise mechanisms underlying the role of the gut–microbiota–brain axis in MS remain elusive.

The vagus nerve–the principal component of the parasympathetic nervous system–plays an important role in the interface between the gut microbiota and the brain (Bonaz et al., 2018; Bravo et al., 2011; Cawthon and de La Serre, 2018; Chang et al., 2022; Cryan et al., 2019; Forsythe et al., 2014; Wei et al., 2022). We have previously reported that, after lipopolysaccharide (LPS) administration, the onset of depression-like behaviors and the abnormal composition of gut microbiota in mice can be blocked by subdiaphragmatic vagotomy (SDV) (Zhang et al., 2020). Furthermore, SDV also reportedly blocks the onset of depression-like behaviors in mice who have received fecal microbiota transplantation from mice with depression-like behaviors (Pu et al., 2021; Wang et al., 2020; Wang et al., 2021a). Collectively, it is likely that the gut–microbiota–brain axis via the subdiaphragmatic vagus

---

nerve plays a crucial role in depression-like behaviors in rodents (Chang et al., 2022; Wei et al., 2022).

Two animal models of MS have been widely used: experimental encephalomyelitis (EAE) and cuprizone (CPZ; bis-cyclohexanone-oxalyldihydrazone) treatment. The EAE model is mostly relevant for relapse-remitting MS (Kipp et al., 2017; Palumbo and Pellegrini, 2017). In contrast, CPZ has been applied to study the process of demyelination in the CNS (Procaccini et al., 2015; Torkildsen et al., 2008; Zhan et al., 2020); CPZ-treated animal models may thus be useful for identifying potential therapeutic methods of blocking demyelination (Franklin and Ffrench-Constant, 2017; Torkildsen et al., 2008; Wang et al., 2022a). However, no studies have yet reported the role of the subdiaphragmatic vagus nerve in demyelination using animal models of MS.

The CPZ model mostly mimics the acute and chronic disease courses of MS; it is likely to be a useful model for developing novel therapeutic candidates that protect against demyelination and stimulate remyelination in the CNS (Lubrich et al., 2022; Palumbo and Pellegrini, 2017; Salinas Tejedor et al., 2015; Skripuletz et al., 2011). In the present study, we investigated whether SDV affects demyelination in the brains of CPZ-treated mice. We also performed a 16S ribosomal RNA analysis of fecal samples and conducted an untargeted metabolomic analysis of blood samples because the gut–microbiota–brain axis may contribute to the pathogenesis of CPZ-treated mice (Moles et al., 2021; Wang et al., 2022a).

2. Materials and methods

2.1. Animals

Adult male C57BL/6 J mice (8–9 weeks old, body weight 20–25 g, Japan SLC, Inc., Hamamatsu, Japan) were used. Mice were housed under controlled temperatures and 12 h light/dark cycles (lights on between 07:00 and 19:00) with access to food (CE-2; CLEA Japan, Inc., Tokyo, Japan) and water ad libitum (Wang et al., 2022a). The experimental protocol was approved by the Chiba University Institutional Animal Care and Use Committee (permission number: 3–042). This study was carried out in strict accordance with the recommendations in the Guide for the Care and Use of Laboratory Animals of the National Institutes of Health, USA. Animals were deeply anesthetized with isoflurane before being killed by cervical dislocation. All efforts were made to minimize suffering.

2.2. SDV procedure

Bilateral SDV or sham surgery was performed under continuous inhalation anesthesia with 2%–3.5% isoflurane using an inhalation small animal anesthesia apparatus (KN-1071 NARCOBIT-E; Natsume Seisakusho, Tokyo, Japan), as previously reported (Pu et al., 2021; Wang et al., 2020; Wang et al., 2021a; Zhang et al., 2020). Briefly, each mouse was placed in the right-side decubitus position and the skin was disinfected with iodophor disinfectant. Starting from the midline alba of the abdomen, an incision of approximately 1 cm was made parallel to the costal arch at 0.5 cm below the left costal arch. A mini incision spreader was then used to expose the underlying liver tissue. The liver tissue was carefully pushed upward using a small sterilized cotton ball moistened with physiological saline solution. With the aid of an animal surgical microscope (Leica, Heidelberg, Germany), the fascia between the caudate lobe and the left lobe of the liver was cut to fully expose the esophagus and the surrounding surgical field of view. The dorsal and ventral branches of the vagus nerve, which run along the esophagus under the diaphragm, were then able to be identified, carefully separated, and severed. If no bleeding was detected and no additional injury of the esophagus, liver, or other organs had occurred, the liver tissue was then returned to its original position and 0.5 mL physiological saline solution was injected into the abdominal cavity. Next, 5–0 surgical silk sutures were used to suture the muscle and skin layers of the abdominal

incision layer by layer, ensuring an aseptic operation. The successful implementation of SDV was confirmed by a significant increase in stomach volume on postoperative day 14, caused by the loss of vagus nerve innervation.

For the sham operation, an abdominal wall incision of the same size as that in the SDV procedure was made in the same way at the same site. After the dorsal and ventral branches of the subdiaphragmatic vagus nerve were gently exposed but not severed, the animals were checked to ensure no bleeding and no additional damage to any other organs. Once the abdominal organs were restored to their original positions, 0.5 mL normal saline was injected into the abdominal cavity and the incision was sutured layer by layer using the same method as for the SDV surgery.

2.3. CPZ model

After 1 week of recovery from the SDV or sham operation, mice received 0.2% weight/weight CPZ (Cat# B0476; Tokyo Chemical Industry Co., Ltd., Tokyo, Japan) or control (CON) food pellets for 6 weeks, as previously reported (Wang et al., 2022a). Chow was replaced three times per week. Based on the operation (SDV or sham) that the mice underwent and the presence or absence of CPZ in their food pellets, the mice were divided into four groups: sham + CON group ($n = 9$), sham + CPZ group ($n = 9$), SDV + CON group (n = 10), and SDV + CPZ group (n = 10). The body weight of each mouse was measured every week.

2.4. Fecal sample collection

Fresh fecal samples of mice were collected at around 9:00 a.m. and placed into sterilized screw-cap microtubes, as previously reported (Wang et al., 2022a). They were then immediately frozen in liquid nitrogen and stored at −80 °C until use.

2.5. Plasma and brain sample collection

Mice were anesthetized under continuous inhalation anesthesia with 5% isoflurane. Blood was collected using a 1 mL syringe and centrifuged at 4 °C before the supernatant was collected and stored at −80 °C. The mice were then transcardially perfused with isotonic saline and ice-cold 4% paraformaldehyde in 0.1 mM phosphate buffer (30 mL per mouse, pH 7.4). Next, the brain was collected and post-fixed overnight at 4 °C. The brain from one mouse in the SDV + CON group was not used because it was abnormal (it had a hole in it).

2.6. Histopathology and immunofluorescence

Post-fixed brains were serially sectioned at 30 μm using a vibratome (VT1000S, Leica Microsystems AG, Wetzlar, Germany). Sections from bregma 1.10 to −0.58 were selected. For LFB (luxol fast blue) staining, four sections were collected per mouse (except for one mouse in the sham + CON group, for which just three sections were used); every third section was selected. The LFB staining was performed using an LFB staining kit (Cat# LBC-1; ScyTek Laboratories, Inc., USA). Immunofluorescence was performed as reported previously (Wang et al., 2021b; Wang et al., 2022a). Briefly, sections were washed three times for 15 min with 0.1 mM phosphate buffer before being blocked in 3% bovine serum albumin with 0.3% Triton X-100 for 2 h. Incubation with primary antibody (mouse, anti-myelin basic protein [MBP], Cat# sc-271,524, Santa Cruz Biotechnology, Inc., CA, USA, 1:100; rabbit, anti-ionized calcium-binding adapter molecule 1 [IBA1], Cat# 019–19,741, Fuji-Film Wako Pure Chemical Corporation, Tokyo, Japan, 1:250) was conducted overnight at 4 °C; the sections were then incubated with secondary antibody (Alexa Fluor 546 goat anti-mouse IgG$_1$, 1:1000; Alexa Fluor 488 donkey anti-rabbit IgG, 1:1000) for 2 h at room temperature. Next, the sections were washed three times for 15 mins with

0.1 mM phosphate buffer with 0.1% Tween-20, and analyzed using a Keyence BZ-900 microscope (Tokyo, Japan) and ImageJ software, in a blind manner. Furthermore, we did not apply the threshold for data analysis. The percentage area of demyelination was determined using both LFB and MBP staining as follows: (corpus callosum area − MBP/LFB-positive area)/corpus callosum area × 100% (Wang et al., 2022a). The percentage of IBA1-positive area was determined as follows: (IBA1-positive area/corpus callosum area) × 100% (Wang et al., 2022a).

2.7. 16S ribosomal RNA analysis of feces

Both the extraction of DNA from fecal samples and the 16S ribosomal RNA analysis were performed at MyMetagenome Co., Ltd. (Tokyo, Japan), as previously described (Pu et al., 2021; Wang et al., 2020; Wang et al., 2021a; Wang et al., 2022a). Briefly, the common primers 27Fmod (5′-AGRGTTTGATYMTGGCTCAG-3′) and 338R (5′-TGCTGCCTCCCGTAGGAGT-3′) were used to amplify the V1–V2 region of the bacterial 16S ribosomal RNA gene by polymerase chain reaction.

The α-diversity was measured using Chao1, observed operational taxonomic units (OTUs), and Shannon. In contrast, β-diversity was analyzed using principal component analysis (PCA) and principal co-ordinates analysis (PCoA). Significance was evaluated using analysis of similarities (ANOSIM). Linear discriminant analysis effect size (LEfSe) (Segata et al., 2011) was performed based on bacterial abundance to explore significant differential biomarkers between groups with different taxonomic levels (http://huttenhower.sph.harvard.edu/galaxy/). Only taxa with linear discriminant analysis scores >4.0 and *P*-values <0.05 were considered significantly enriched. The results were visualized using taxonomic bar charts and cladograms.

2.8. Untargeted metabolomic analysis of plasma samples

The untargeted metabolomic analysis of plasma samples was performed using ultra-performance liquid chromatography-tandem quadruple time-of-flight mass spectrometry, as previously reported (Wan et al., 2022a, 2022b; Yang et al., 2023). Acquisition was performed using an ExionLC™ AD system (SCIEX, Tokyo, Japan) coupled to a X500R QTOF system (SCIEX). Metabolomic data were analyzed using R statistical software version 4.0.5 and MS-DIAL version 4.60 (Tsugawa et al., 2015). Metabolites were detected from at least 50% of the analyzed samples and the coefficient of variation values of 30% of metabolites in the pooled quality control samples; annotation level 2, proposed by Schymanski et al. (2014), was used for the data analysis.

Orthogonal partial least squares discriminant analysis (OPLS-DA), which is a multivariate analysis model, was implemented in SIMCA-P version 14.0. Significant peaks were determined by the combination of variable importance in projection values >1 and Wilcox signed-rank test *P*-values <0.05.

2.9. Statistical analysis

Data are presented as the mean ± standard error of the mean. Body weight data were analyzed using repeated-measures two-way analysis of variance (ANOVA) followed by the Bonferroni post-hoc test. We used the log-transformation for data of LFB and IBA1, since these data were not normally distributed (Feng et al., 2014). The demyelination area in LFB staining/MBP immunofluorescence and the IBA1-positive area data were analyzed using two-way ANOVA followed by the Bonferroni post-hoc test.

The Kruskal–Wallis test was used to analyze the α-diversity of gut microbiota and the relative bacterial abundance at different levels. For the β-diversity of gut microbiota, the PCA of OTU levels, PCoA, and unweighted or weighted UniFrac phylogenetic distance were analyzed using ANOSIM with the vegan package in R (2.5.4) (Xia and Sun, 2017).

For the plasma metabolite analysis, we used orthogonal partial least squares discriminant analysis as the multivariate analysis model,

implemented in SIMCA-P (version 14.0). Significant peaks were determined by the combination of variable importance in projection values >1, Wilcox signed-rank test P-values <0.05, and false discovery rate < 0.076 between the sham + CPZ and SDV + CPZ groups. Two-way ANOVA followed by the Bonferroni post-hoc test was used to analyze differences among the four groups.

Correlations among the demyelination area, IBA1-positive area, plasma metabolites, and the relative abundances of bacteria were analyzed using Spearman's rank test. The integrative network of associations between differentially abundant taxa, plasma metabolites, IBA1-positive areas, and demyelination areas were assessed using Spearman's analysis and visualized with Cytoscape (version 3.8.1). For all analyses, the level of significance was set as *P* < 0.05.

3. Results

3.1. Effects of SDV on demyelination and body weight in CPZ-treated mice

One week after the SDV or sham operation, the mice received chow with or without CPZ for 6 weeks (Fig. 1A). Body weight gain compared with baseline (week −1) was significantly higher in the SDV + CPZ group than in the sham + CPZ group (Fig. 1B). The demyelination area in the brain was assessed by LFB staining and MBP immunostaining. Six weeks of CPZ treatment produced demyelination in the corpus callosum of mice; SDV significantly alleviated this CPZ-induced demyelination (Fig. 1C, D, F, G). Collectively, these findings indicate that SDV can ameliorate CPZ-induced body weight gain and demyelination in mice.

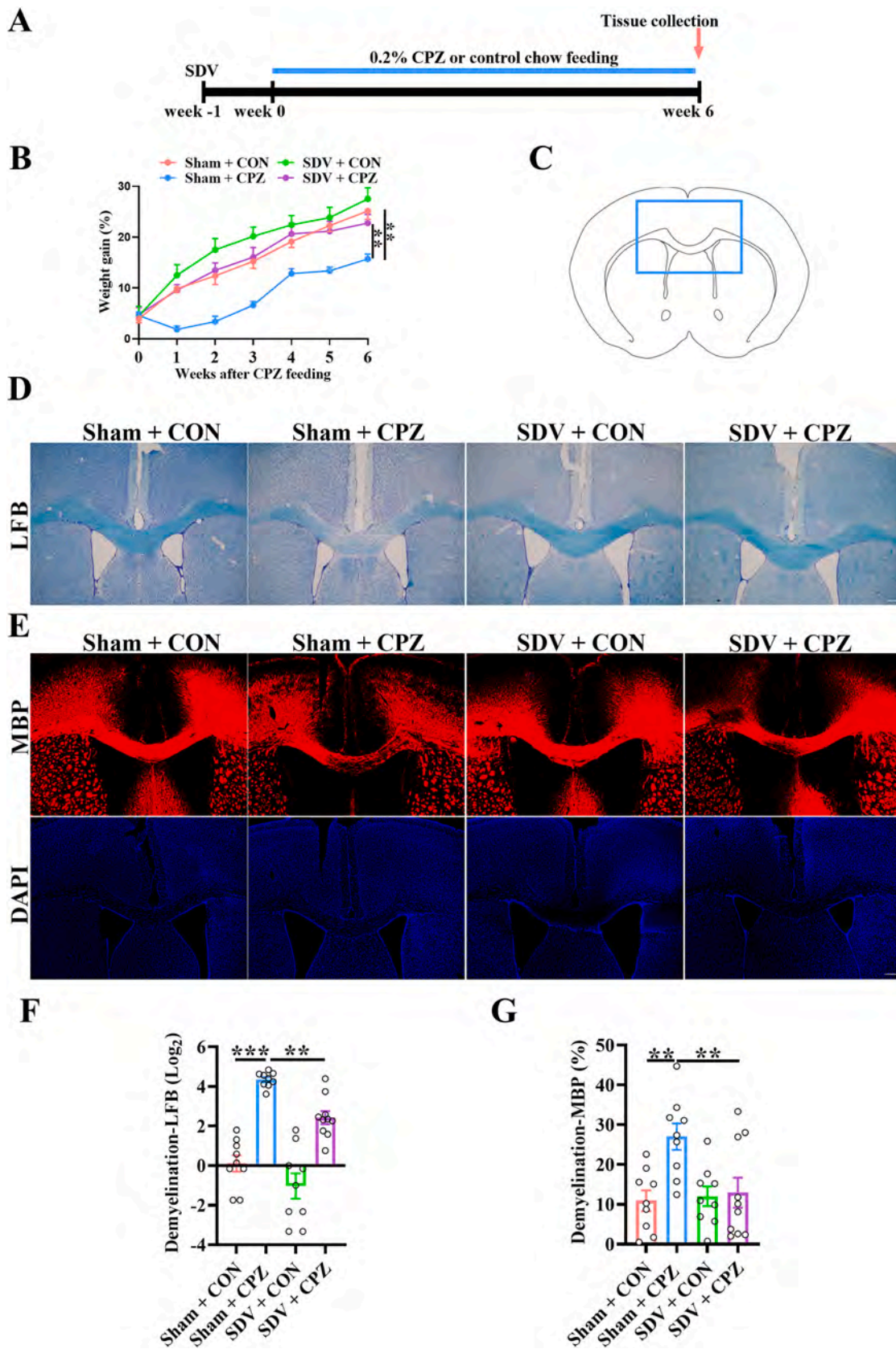### 3.2. Effects of SDV on microglial activation in CPZ-treated mice

Multiple evidence suggests that microglial activation contributes to MS development (Deng and Sriram, 2005; Kalafatakis and Karagogeos, 2021; Mayrhofer et al., 2021). We therefore investigated microglial activation in the corpus callosum of CPZ-treated mice by immunostaining for the microglial marker IBA1. In the sham + CON group, microglia were distributed broadly and evenly throughout the corpus callosum of mice; they were small and ramified, which is the typical morphology of resting microglia (Wang et al., 2022a). In the sham + CPZ group, there was a robust increase in the IBA1-positive area of the corpus callosum compared with the sham + CON group. SDV significantly alleviated this CPZ-induced increase in IBA1-positive area (Fig. 2A–C). Together, these results suggest that SDV can ameliorate CPZ-induced microglial activation in the mouse corpus callosum.

3.3. Gut microbiota composition

The α- and β-diversity were used to analyze gut microbiota composition in the four groups. Regarding α-diversity, there were no differences in Chao1, observed OTUs, or Shannon among the four groups (Fig. 3A–C). To determine the similarity (i.e., β-diversity) between microbiota communities in the four groups, PCA and PCoA were performed. The compositions of microbiota communities were significantly separated using PCA as evaluated by ANOSIM ($R = 0.5259$, $P = 0.001$) (Fig. 3D) based on OTU levels. Furthermore, the PCoA with unweighted and weighted UniFrac distance showed significant differences in the four groups using ANOSIM ($R = 0.4157$, P = 0.001) (Fig. 3E, F). These findings indicate that SDV can restore CPZ-induced β-diversity abnormalities in the gut microbiota.

3.4. Altered gut microbiota composition at different levels

At the phylum level, the relative abundances of *Firmicutes* and *Candidatus Saccharibacteria* were significantly higher in the SDV + CPZ group than in the sham + CPZ group (Supplemental Fig. S1). At the genus level, the relative abundances of the following 14 microbiota were

A

Tissue collection

SDV

0.2% CPZ or control chow feeding

week -1   week 0   week 6

B

Sham + CON   SDV + CON
Sham + CPZ   SDV + CPZ

Weight gain (%)

Weeks after CPZ feeding

C

D

| Sham + CON | Sham + CPZ | SDV + CON | SDV + CPZ |

LFB

E

| Sham + CON | Sham + CPZ | SDV + CON | SDV + CPZ |

MBP

DAPI

F

Demyelination-LFB (Log$_2$)

***   **

Sham + CON
Sham + CPZ
SDV + CON
SDV + CPZ

G

Demyelination-MBP (%)

**   **

Sham + CON
Sham + CPZ
SDV + CON
SDV + CPZ

(caption on next page)

Fig. 1. Effects of SDV on the body weight change and demyelination of CPZ-treated mice.
A: The protocol of the experiment. B: The body weight gain compared with baseline (week −1) (repeated measures two-way ANOVA, time: $F_{1,\ 34} = 71,327$. $P < 0.001$. group: $F_{1,\ 34} = 10.084$, $P < 0.001$. interaction: $F_{1,\ 34} = 3.825$, $P < 0.001$). C: The LFB (luxol fast blue) and MBP (myelin basic protein) staining images were taken of the area outlined by the blue line box. D: The representative photos of LFB in the corpus callosum of brain from sham + CON, sham + CPZ, SDV + CON, and SDV + CPZ groups. E: The representative photos of MBP and DAPI (4′,6′-diamino-2-phenylindole) in the corpus callosum of brain from sham + CON, sham + CPZ, SDV + CON, and SDV + CPZ groups. F: Quantitative data of demyelination area in the corpus callosum using LFB staining (two-way ANOVA: CPZ: $F_{1,33} = 85.477$, P < 0.001. SDV: $F_{1,33} = 13.687$, P < 0.001. interaction: $F_{1,33} = 0.880$, $P = 0.355$). G: Quantitative data of demyelination area in the corpus callosum using MBP staining (two-way ANOVA: CPZ: $F_{1,33} = 7.256$, $P = 0.011$. SDV: $F_{1,33} = 4.228$, $P = 0.048$. interaction: $F_{1,33} = 5.843$, $P = 0.021$). The data are the mean ± SEM ($n = 9$ or 10). **$P < 0.01$, ***$P < 0.001$. Scale bar: 200 μm. CPZ, cuprizone; SDV, subdiaphragmatic vagotomy. (For interpretation of the references to colour in this figure legend, the reader is referred to the web version of this article.)
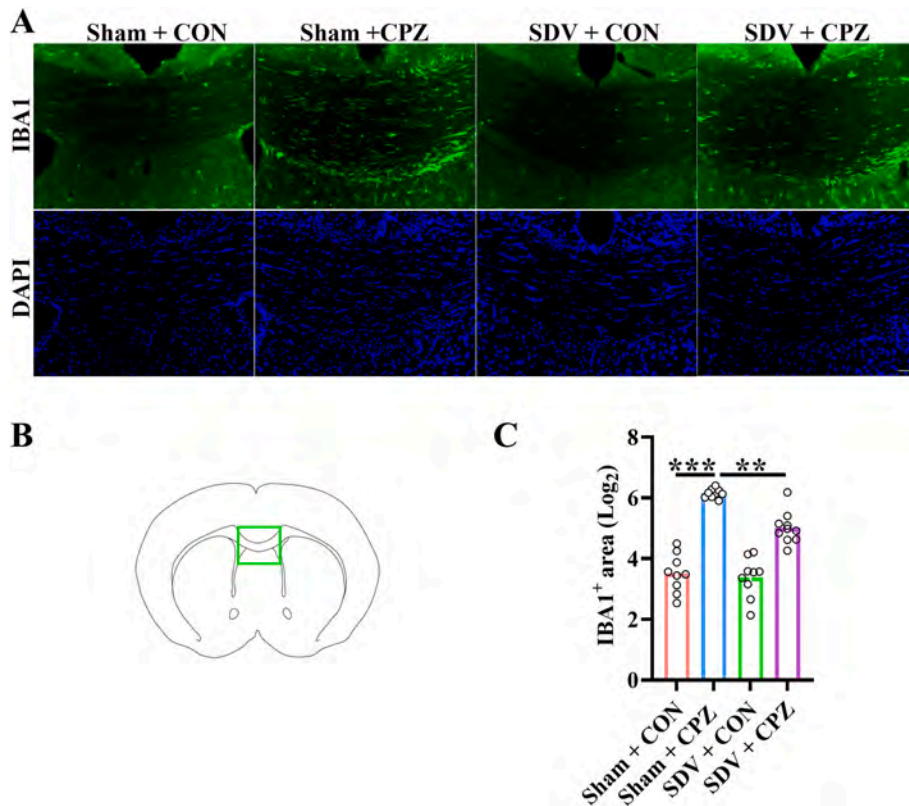
Fig. 2. Effects of SDV on the microglia activation of CPZ-treated mice.
A: The representative photos of IBA1 and DAPI in the corpus callosum of brain from sham + CON, sham + CPZ, SDV + CON, and SDV + CPZ groups. B: The IBA1 staining images were taken of the area outlined by the green line box. C: Quantitative data of IBA1-positive area in the corpus callosum (two-way ANOVA: CPZ: $F_{1,33} = 78.963$, P < 0.001. SDV: $F_{1,33} = 4.347$, $P = 0.045$. interaction: $F_{1,33} = 4.968$, $P = 0.033$). The data are the mean ± SEM (n = 9 or 10). ***P < 0.001. Scale bar: 50 μm. CPZ, cuprizone; SDV, subdiaphragmatic vagotomy. (For interpretation of the references to colour in this figure legend, the reader is referred to the web version of this article.)

significantly different in the four groups: *Prevotella, Bacteroides, Gabonia, Eubacterium, G_undefined_Bacteroidia, G_undefined_Bacteroidaceae, Dorea, Anaerocolumna, G_undefined_Acholeplasmatales, Parvibacter, G_undefined_Burkholderiales, Beduini, Acetoanaerobium,* and *Erysipelatoclostridium* (Supplemental Fig. S2).

At the species level, the relative abundances of the following 23 microbiota were significantly different in the four groups: *Lactobacillus johnsonii, Lactobacillus hominis, Lachnospiraceae bacterium A4, Gabonia massiliensis, Prevotella sp. CA17, Bacteroidia bacterium canine oral taxon 387, Eubacterium sp. oral clone BU014, Bacteroidaceae bacterium DJF_B220, Clostridiales bacterium CIEAF 030, Prevotella sp. oral taxon 317, Clostridium sp. ASF502, Clostridium sp. Clone-45, [Eubacterium] siraeum, Candidatus Dorea massiliensis, Bacteroides caecimuris, Anaerocolumna jejuensis, Bacteroides sp. Smarlab 3,302,398, Ruminococcus sp. M-1, Lachnospiraceae bacterium 6–1, Clostridiales bacterium oral taxon F32, Prevotella conceptionensis, Enterorhabdus muris,* and *Parvibacter caecicola* (Fig. 4).

3.5. LEfSe analysis

Changes in the abundance of taxa in the four groups were analyzed using the LEfSe algorithm (Kwak et al., 2020). Compared with sham surgery, SDV had significantly different effects on gut microbiota

(Fig. 5A). Four species-level phylotypes were identified as potential gut microbial markers for the sham + CON group: *Clostridiumsp clone27, Lachnospiraceae bacteriumRM29, Lachnospiraceae bacteriumA4,* and *Clostridiales bacterium CIEAF020* (Fig. 5B). In addition, three species-level phylotypes were identified as potential gut microbial markers for the sham + CPZ group: *Porphyromonadaceae bacterium_C941, Gabonia massiliensis,* and *Lactobacillus johnsonii,* (Fig. 5B). Similarly, three species-level phylotypes were identified as potential gut microbial markers for the SDV + CON group: *Lachnospiraceae bacterium 607, Lactobacillus murinus,* and *Lactobacillus hominis,* (Fig. 5B). Finally, the species *Lactobacillus sp. NBRC14512,* and *Turicibacter sp. LA62* were identified as potential gut microbial markers for the SDV + CPZ group (Fig. 5B).

3.6. Plasma metabolites

To explore the underlying mechanisms of the beneficial effects of SDV on demyelination in CPZ-treated mice, we performed an untargeted metabolomic analysis of plasma samples because gut microbiota can synthesize many metabolites. After quality control and the removal of low-abundance peaks, 161 ion pattern features were identified. The OPLS-DA model was used to analyze the distribution of plasma metabolic components between the sham + CPZ and SDV + CPZ groups
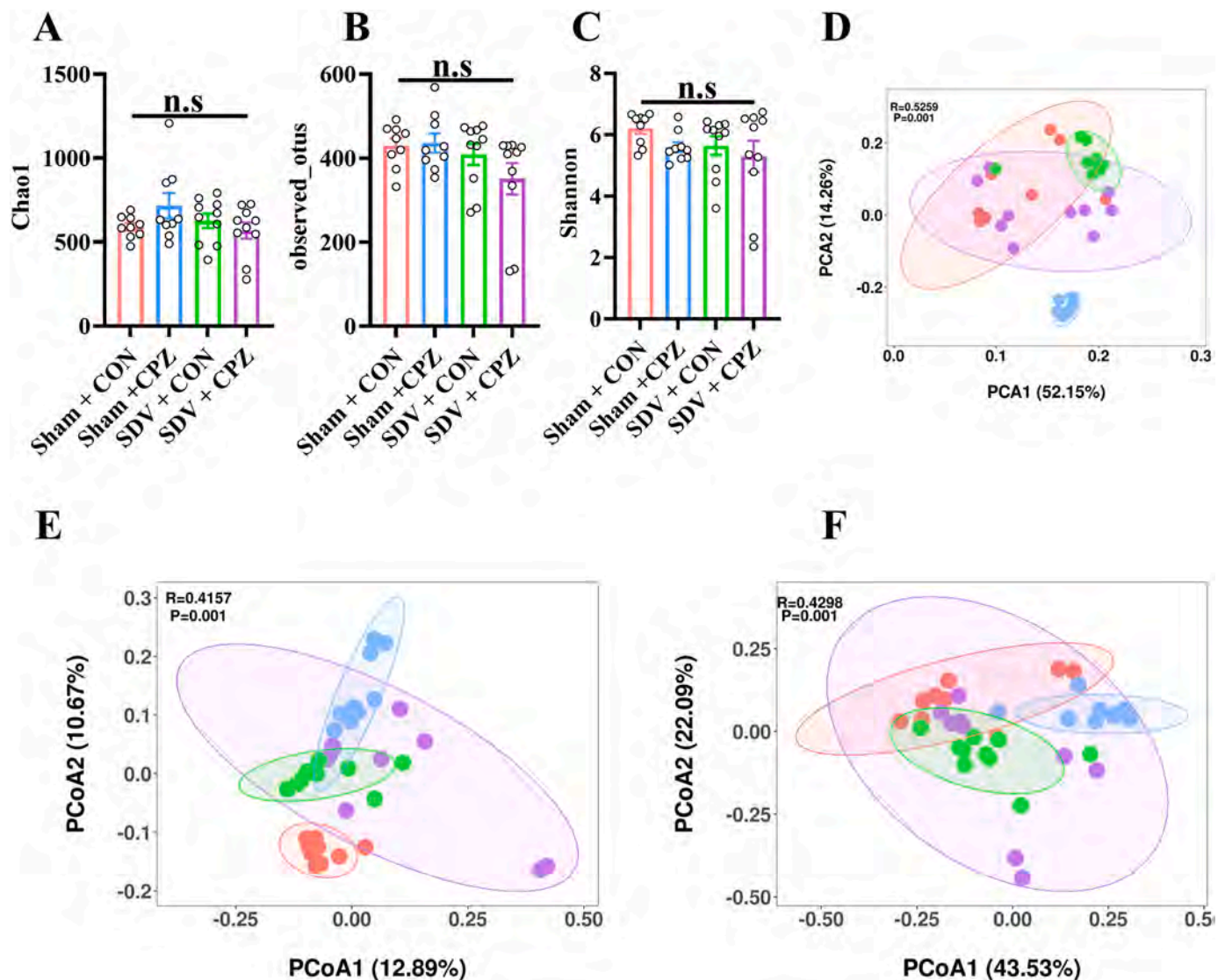
Fig. 3. α-diversity and β-diversity of gut microbiota.

A: α-diversity index of Chao1 (Kruskal-Wallis test, H = 2.376, P = 0.498). B: α-diversity index of observed_OTUs (Kruskal-Wallis test, H = 3.840, P = 0.279). C: α-diversity index of shannon (Kruskal-Wallis test, H = 4.929, P = 0.177) D: Principal component analysis (PCA) of β-diversity based on the OTU level, where each point represents a single sample colored by group circle, indicated by the second principal component of 14.25% on the Y- axis and the first principal component of 52.15% on the X-axis (ANOSIM, R = 0.5259, P = 0.001). E: Principal Coordinates Analysis (PCoA) plot based upon unweighted UniFrac distance (ANOSIM, R = 0.4157, P = 0.001). Each dot represents a single sample indicated by a principal component of 12.89% on the X-axis and another principal component of 10.67% on the Y- axis, contributing to discrepancy among the three groups. E: Principal Coordinates Analysis (PCoA) plot based upon weighted UniFrac distance (ANOSIM, *R* = 0.4298, *P* = 0.001). Each dot represents a single sample indicated by a principal component of 43.53% on the X-axis and another principal component of 22.09% on the Y- axis, contributing to discrepancy among the three groups. The data are the mean ± SEM (n = 9 or 10). CPZ, cuprizone; SDV, subdiaphragmatic vagotomy.

(Fig. 6A). Scatter plots of the scores between the sham + CPZ and SDV + CPZ groups are shown in Fig. 6A. After thresholding the metabolites (variable importance in projection values >1, Wilcoxon signed-rank test *P*-values <0.05 and FDR < 0.076), 27 metabolites were identified as having significant differences in abundance between the sham + CPZ and SDV + CPZ groups (Fig. 6B). Of these, the following 26 metabolites were upregulated in the SDV + CPZ group: 1,2-dichloroethane, 1,5-anhydro-D-sorbitol, 1-phenylethylamine, 1-pyrroline, 2-(methylthio) ethanol, 2-aminoacetophenone, 3-aminohexanoic acid, atrazine-desethyl, C9H11NO2, DL-arginine, DL-malic acid, glucosereductone, histidine, isocitric acid, leucine, L-phenylalanine, L-valine, maleic acid, monoethyl carbonate, pentaethylene glycol, piperidine, proline, pyrro-lidine, triflumuron, tryptophan, and tyrosine (Fig. 6B). In contrast, D-glucose was downregulated in the SDV + CPZ group compared with the sham + CPZ group (Fig. 6B). Notably, SDV significantly improved the

plasma levels of six of these 27 metabolites (DL-arginine, DL-malic acid, maleic acid, isocitric acid, glucosereductone, and monoethyl carbonate) in CPZ-treated mice (Fig. 6C).

The correlations among demyelination and IBA1-positive areas and these six plasma metabolites were then examined. Both the demyelin-ation area (with LFB staining) and the IBA1-positive area were nega-tively correlated with all six compounds (Fig. 6D). The demyelination area (with MBP staining) was negatively correlated with glucoser-eductone and monoethyl carbonate only (Fig. 6D).

3.7. Correlations among bacterial relative abundance, plasma metabolites, and demyelination and IBA1-positive areas

Heat maps were used to demonstrate the correlations among demyelination and IBA1-positive areas, plasma metabolites, and relative
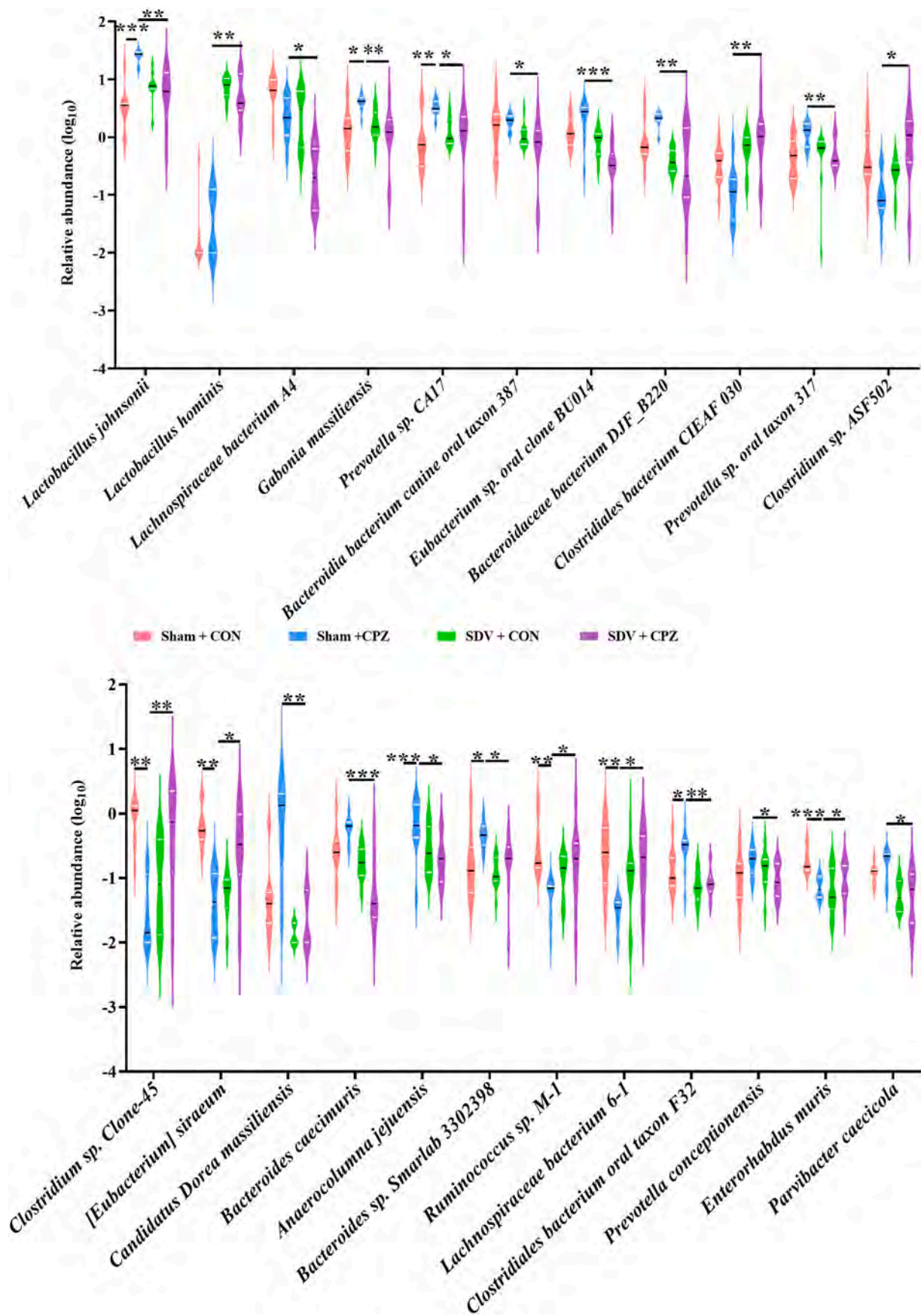
Fig. 4. Altered composition in the gut microbiota at species.
There are significantly changed bacteria among the four groups. Statistical analysis data were shown in the Supplemental Table 1. The data are the median and interquartile range (n = 9 or 10). CPZ, cuprizone; SDV, subdiaphragmatic vagotomy.
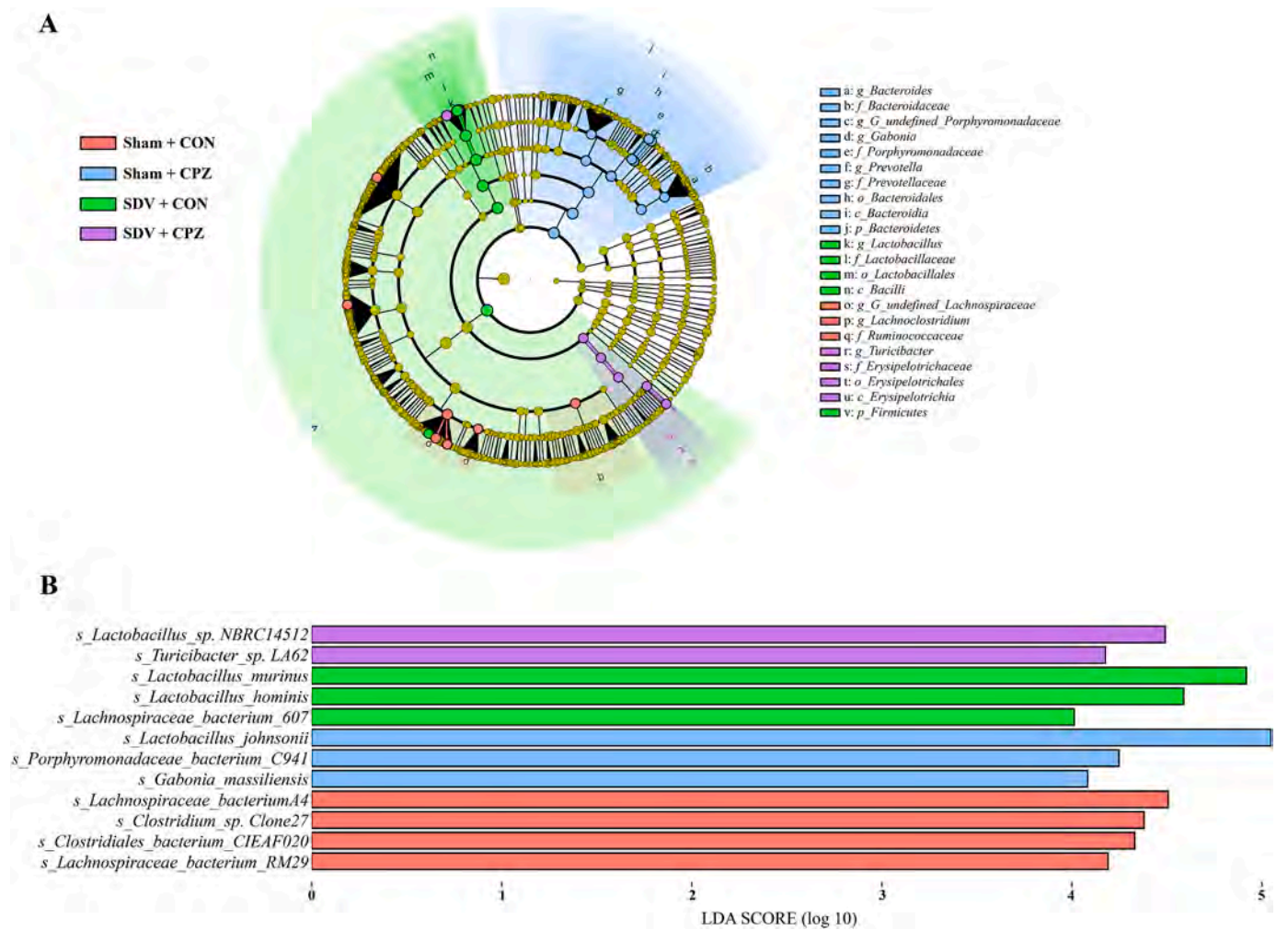
Fig. 5. The LEfSe algorithm of gut microbiota.

A: Cladogram (LDA score > 4.0, P < 0.05) showed the taxonomic distribution difference among sham + CON, sham + CPZ, SDV + CON, and SDV + CPZ groups, indicating with different colour region. Each successive circle represents a differentially abundant taxonomic clades at phylum, class, order, family, genus and species level from the inner to outer rings. B: Histograms of the different abundant taxa based on the cutoff value of LDA score (log_{10}) > 4.0 and P < 0.05 among the four groups. p, phylum; c, class; o, order; f, family; g, genus; s, species. CPZ, cuprizone; SDV, subdiaphragmatic vagotomy.

bacterial abundances that differed significantly at the species level (Fig. 7A). Spearman's correlations between the microbiome and plasma metabolites were also analyzed. Twenty-three bacteria were significantly associated with 27 plasma metabolites, which were further related to demyelination and IBA1-positive areas (Fig. 7A).

The demyelination area (LFB staining) was positively correlated with the relative abundances of *Prevotella* sp. *oral taxon 317, Bacteroides* sp. *Smarlab 3,302,398, Gabonia massiliensis, Prevotella* sp. *CA17, Lactobacillus johnsonii, Anaerocolumna jejuensis, Candidatus Dorea massiliensis, Parvibacter caecicola,* and *Bacteroidaceae bacterium DJF_B220*. Furthermore, the demyelination area (MBP staining) was positively correlated with the relative abundances of *Prevotella conceptionensis, Prevotella* sp. *oral taxon 317, Bacteroides* sp. *Smarlab 3,302,398, Gabonia massiliensis, Prevotella* sp. *CA17, Lactobacillus johnsonii, Anaerocolumna jejuensis, Candidatus Dorea massiliensis, Bacteroidaceae bacterium DJF_B220,* and *Bacteroides caecimuris* (Fig. 7A). In contrast, the demyelination area (LFB staining) was negatively correlated with the relative abundances of *Enterorhabdus muris, Lachnospiraceae bacterium 6–1,* and *Ruminococcus* sp. *M-1*. The demyelination area (MBP staining) was negatively correlated with the relative abundances of *Clostridiales bacterium CIEAF 030, [Eubacterium] siraeum, Clostridium* sp. *Clone-45, Clostridium* sp. *ASF502, Lachnospiraceae bacterium 6–1,* and *Ruminococcus* sp. *M-1*. (Fig. 7A).

There were positive correlations between the IBA1-positive area and

the relative abundances of *Prevotella* sp. *oral taxon 317, Bacteroides* sp. *Smarlab 3,302,398, Gabonia, massiliensis, Prevotella* sp. *CA17, Lactobacillus johnsonii, Anaerocolumna jejuensis, Candidatus Dorea massiliensis,* and *Bacteroidaceae bacterium DJF_B220*. There were negative correlations between the IBA1-positive area and the relative abundances of *Enterorhabdus muris, Lachnospiraceae bacterium 6–1, Ruminococcus* sp. *M-1, Clostridiales bacterium CIEAF 030,* and *Clostridium* sp. *Clone-45* (Fig. 7A).

More specifically, the relative abundance of *Lactobacillus johnsonii* (the relative abundance is >25% in sham + CPZ group) was negatively correlated with maleic acid, DL-malic acid, monoethyl carbonate, DL-arginine, tyrosine, proline, 1-pyrroline, tryptophan, 1,2-dichloroethane, triflumuron, isocitric acid, and glucosereductone levels, and positively correlated with D-glucose levels (Fig. 7A).

A correlation network revealed that the correlations (Spearman's analysis, R > 0.5, P < 0.05) among plasma metabolites, demyelination area, IBA1-positive area, and bacterial relative abundances differed significantly between any two groups (Fig. 7B). There were also correlations among the relative abundances of significant microbiomes at the species level and significantly different plasma metabolites between the sham + CPZ and SDV + CPZ groups (Fig. 7 B).

(caption on next page)

4. Discussion

The major findings of the present study are as follows. First, compared with sham surgery, SDV ameliorated both demyelination and microglial activation in the corpus callosum of CPZ-treated mice. Second, SDV partially restored the abnormal β-diversity of gut microbiota in CPZ-treated mice. Two phylum—*Firmicutes* and *Candidatus Saccharibacteria*—were different between the sham + CPZ and SDV + CPZ groups. Furthermore, several genera and species were altered among the four groups. The LEfSe algorithm identified two species, *Lactobacillus_sp_NBRC14512* and *Turicibacter_sp_LA62*, as specific microbial biomarkers for the SDV + CPZ group. Third, 27 metabolites were identified as having significant differences in abundance between the sham + CPZ and SDV + CPZ groups. Of these 27 metabolites, SDV significantly improved the reduced levels of six metabolites (DL-arginine, DL-malic acid, maleic acid, isocitric acid, glucosereductone, and monoethyl carbonate) in CPZ-treated mice. Notably, there were negative correlations between demyelination or microglial activation and plasma metabolites. Fourth, the relative abundances of some species of bacteria were correlated with demyelination or microglial activation in the brain as well as with plasma metabolites. Taken together, our findings indicate that the gut–microbiota–brain axis might play a role in the demyelination of CPZ-treated mice via the subdiaphragmatic vagus nerve.

Several lines of evidence suggest that microglial activation plays a crucial role in MS development (Chu et al., 2018; Deng and Sriram, 2005; Gao and Tsirka, 2011; Guerrero and Sicotte, 2020; Rawji and Yong, 2013; Voet et al., 2019). Microglial activation can lead to neuroinflammation and myelin and axonal damage in both CPZ-treated mice and MS patients (Clarner et al., 2012). Recently, we reported that microglial activation is positively correlated with demyelination in the corpus callosum of CPZ-treated mice, suggesting a link between demyelination and microglial activation (Wang et al., 2022a). In the present study, we found that SDV alleviated demyelination and microglial activation in the corpus callosum of CPZ-treated mice. Collectively, it is therefore possible that the subdiaphragmatic vagus nerve contributes to microglial activation and demyelination in the corpus callosum of CPZ-treated mice.

Accumulating evidence has highlighted the essential role of abnormal gut microbiota in the pathogenesis of MS (Cantarel et al., 2015; Chen et al., 2019; Farshbafnadi et al., 2021; Ghezzi et al., 2021; Maghzi and Weiner, 2020; Parodi and Kerlero de Rosbo, 2021). In the current study, many species of bacteria were altered between the sham + CPZ and SDV + CPZ groups. Among these species, there was a strong positive correlation between the relative abundance of *Bacteroides* sp. *Smarlab 3,302,398* and demyelination in the brain. Although the precise functions of this bacterial species remain unclear, it is possible that *Bacteroides* sp. *Smarlab 3,302,398* is involved in demyelination via neuroinflammation. Furthermore, there was a positive correlation between the relative abundances of both *Bacteroides caecimuris* and *Gabonia massiliensis* and microglial markers in the brain. These two bacteria might play a role in inflammation (Behary et al., 2021;

Kishikawa et al., 2020; Osaka et al., 2017; Sanchis-Artero et al., 2021), and may therefore contribute to neuroinflammation in CPZ-treated mice. Nonetheless, it is noteworthy that SDV was able to alleviate the CPZ-induced increased relative abundances of both *Gabonia massiliensis* and *Bacteroides caecimuris*, as well as those of *Lactobacillus johnsonii* and *Provotella* sp. *CA17*. We have recently reported that SDV can block depression-like behaviors in mice after LPS administration (Zhang et al., 2020) or after fecal microbiota transplantation from mice with depression-like behaviors (Pu et al., 2021; Wang et al., 2020; Wang et al., 2021a; Wang et al., 2021b). In addition, it was reported that SDV can abolish the increased hippocampal expression of IBA1 and the cognitive deficits that occur after LPS (5 mg/kg) treatment in mice, thus indicating a role of the subdiaphragmatic vagus nerve in LPS-induced neuroinflammation (Wu et al., 2021). Together with the present results, these findings suggest that the subdiaphragmatic vagus nerve contributes to demyelination in CPZ-treated mice.

A number of previous studies have indicated that gut microbiota is linked to microglial activation in the brain (Abdel-Haq et al., 2019; Cryan et al., 2019; Erny and Prinz, 2020; Lynch et al., 2021; Ma et al., 2019; Mossad and Erny, 2020; Wang et al., 2018; Yang et al., 2022). Similarly, we identified correlations between IBA1 expression in the corpus callosum and the relative abundances of several bacteria; this finding indicates that microglial activation may be regulated by gut microbiota. Furthermore, there was a positive correlation between the relative abundance of *Lactobacillus johnsonii* and microglial activation, suggesting that this bacterial species may contribute to inflammation in CPZ-treated mice. Taken together, microbiome–microglia crosstalk might play a crucial role in demyelination in the brains of CPZ-treated mice through the gut–microbiota–brain axis.

Six plasma metabolites (malic acid, maleic acid, arginine, glucosereductone, isocitric acid, and monoethyl carbonate) were increased in the SDV + CPZ group compared with the sham + CPZ group. Notably, all six of these plasma metabolites were decreased in the sham + CPZ group compared with the sham + CON group. Malic acid is a saturated dicarboxylic acid, whereas maleic acid is an unsaturated dicarboxylic acid. Interestingly, we identified negative correlations between plasma levels of malic acid or maleic acid and demyelination or microglial activation in the corpus callosum of CPZ-treated mice. Furthermore, the plasma levels of the other four metabolites (arginine, glucosereductone, isocitric acid, and monoethyl carbonate) were negatively correlated with demyelination or microglial activation in the brain. Although the detailed functions of these six metabolites are unknown, they may contribute to the beneficial effects of SDV on demyelination in the brains of CPZ-treated mice. However, further study of these six metabolites is needed to confirm their roles in the protective effects of SDV on CPZ-treated mice. Furthermore, there were positive correlations between the relative abundance of *Lactobacillus hominis* and many plasma metabolites in the current study, suggesting that this bacterial species may have a role in the production of these metabolites.

Vagus nerve stimulation is a form of neuromodulation that stimulates the vagus nerve. It is currently an alternative therapy for both refractory epilepsy and treatment-resistant depression (Badran and
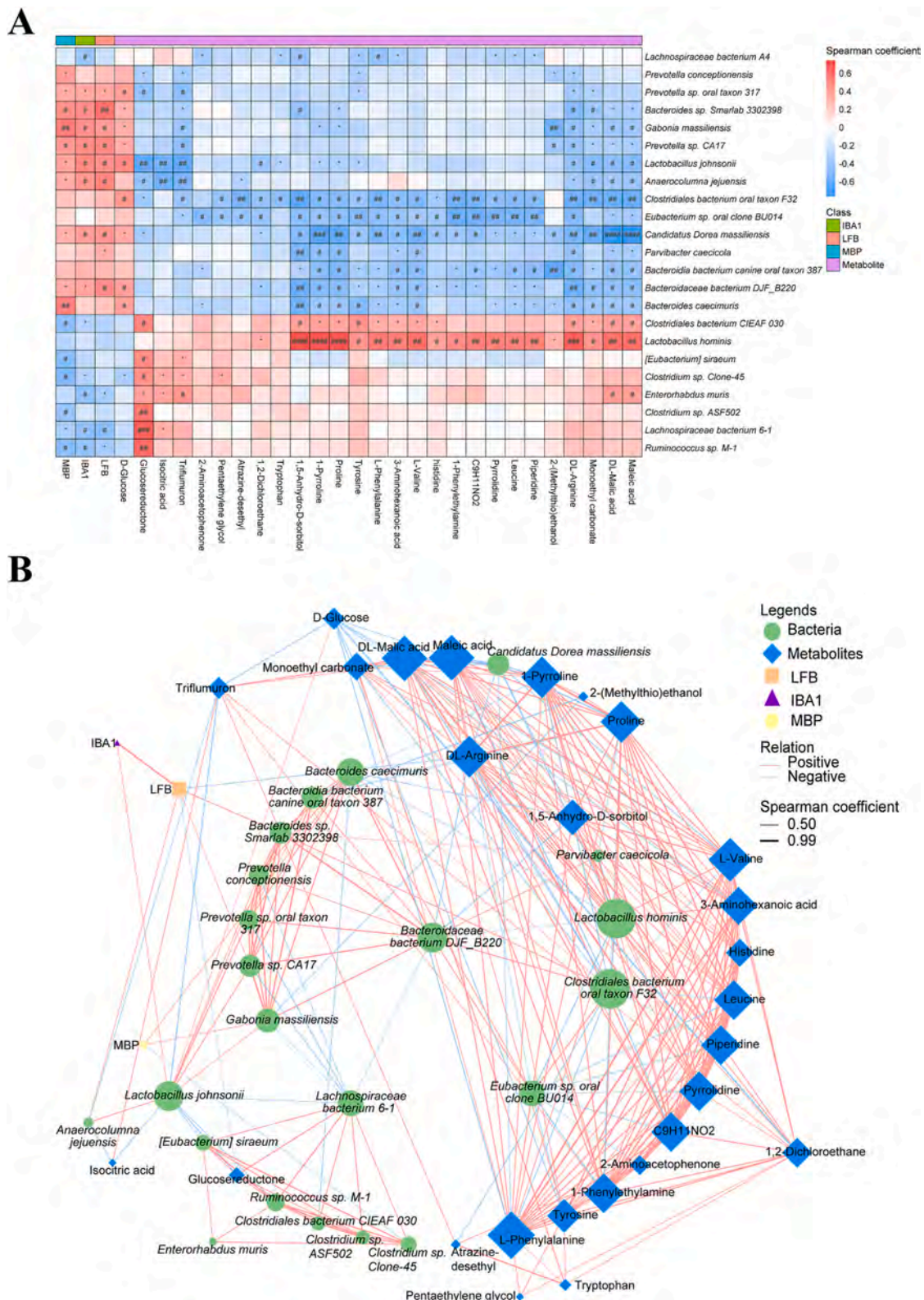
Fig. 7. Correlations among plasm metabolites, bacterial relative abundance, demyelination area, or IBA1-positive area.
A: Spearman correlations among gut microbiome and metabolites, demyelination area (LFB staining or MBP staining), and IBA1-positive area. B: A: Network plots were used to investigate plasm metabolites correlation (P < 0.05, VIP >1, sham + CPZ group vs. SDV + CPZ group), and the interrelationship of significant different bacterial relative abundance with demyelination area, or IBA1-positive area. Red connections indicate positive correlations, blue connections indicate negative correlations, and thicker connection lines indicate larger correlation coefficients (Spearman correlation analysis, absolute value of correlation coefficient > 0.5, P < 0.05). (For interpretation of the references to colour in this figure legend, the reader is referred to the web version of this article.)

Austelle, 2022; Rosson et al., 2022; Wang et al., 2021c). Our data suggest that the vagus nerve may play a role in demyelination and microglial activation in the brains of MS patients. It has also been reported that vagus nerve stimulation can improve cerebellar tremor and dysphagia in MS patients (Marrosu et al., 2005, 2007). Given the comorbidity of depression in MS patients (Jones et al., 2021; Skokou et al., 2012), it will be of great interest to investigate whether vagus nerve stimulation can improve clinical symptoms, including depression, in MS patients.

The present study has some limitations. First, we did not identify the specific species of bacteria and metabolites that contribute to the beneficial effects of SDV in CPZ-treated mice. Further research is therefore needed to confirm the specific microbiome and microbe-derived metabolites that underlie the beneficial effects of SDV. Second, because the EAE model reproduces different patterns of MS from the CDZ-treated model (Palumbo and Pellegrini, 2017), we need to investigate the effects of SDV on demyelination in other animal models—such as the EAE model—of MS (Wang et al., 2021b).

In conclusion, the findings of the current study suggest that SDV can ameliorate demyelination and microglial activation in the brains of CPZ-treated mice through the gut–microbiota–brain axis. Given the crucial role of the vagus nerve in the gut–microbiota–brain axis, vagus nerve stimulation may be a promising therapeutic option for MS patients.

Data and code availability

The 16 s rRNA sequencing data have been deposited to the NCBI Sequence Read Archive and are available at the accession number PRJNA868498.

CRediT authorship contribution statement

Xingming Wang: Conceptualization, Investigation, Writing – original draft, Writing – review & editing. **Akifumi Eguchi:** Investigation, Writing – review & editing. **Yong Yang:** Writing – review & editing. **Lijia Chang:** Investigation, Writing – review & editing. **Xiayun Wan:** Investigation, Writing – review & editing. **Jiajing Shan:** Investigation, Writing – review & editing. **Youge Qu:** Investigation, Writing – review & editing. **Li Ma:** Investigation, Writing – review & editing. **Chisato Mori:** Investigation, Funding acquisition, Writing – review & editing. **Jianjun Yang:** Investigation, Writing – review & editing. **Kenji Hashimoto:** Conceptualization, Funding acquisition, Writing – original draft, Writing – review & editing.

Declaration of Competing Interest

Dr. Hashimoto is the inventor of filed patent applications on "The use of *R*-Ketamine in the treatment of psychiatric diseases", "(*S*)-norketamine and salt thereof as pharmaceutical", "*R*-Ketamine and derivative thereof as prophylactic or therapeutic agent for neurodegeneration disease or recognition function disorder", "Preventive or therapeutic agent and pharmaceutical composition for inflammatory diseases or bone diseases", "*R*-Ketamine and its derivatives as a preventive or therapeutic agent for a neurodevelopmental disorder", and "Preventive or therapeutic agent and pharmaceutical composition for inflammatory diseases" by the Chiba University. Dr. K. Hashimoto has also received speakers' honoraria, consultant fee, or research support from Abbott, Boehringer Ingelheim, Daiichi-Sankyo, Meiji Seika Pharma, Seikagaku Corporation, Sumitomo-Pharma, Taisho, Otsuka, Murakami Farm and Perception Neuroscience. Other authors declare no conflict of interest.

Data availability

Data will be made available on request.

Appendix A. Supplementary data

Supplementary data to this article can be found online at https://doi.org/10.1016/j.nbd.2022.105951.

References

Abdel-Haq, R., Schlachetzki, J., Glass, C.K., Mazmanian, S.K., 2019. Microbiome-microglia connections via the gut-brain axis. J. Exp. Med. 216, 41–59. https://doi.org/10.1084/jem.20180794.

Badran, B.W., Austelle, C.W., 2022. The future is noninvasive: a brief review of the evolution and clinical utility of vagus nerve stimulation. Focus (Am. Psychiatr. Publ.) 20 (1), 3–7. https://doi.org/10.1176/appi.focus.20210023.

Behary, J., Amorim, N., Jiang, X.T., Raposo, A., Gong, L., McGovern, E., Ibrahim, R., Chu, F., Stephens, C., Jebeili, H., Fragomeli, V., Koay, Y.C., Jackson, M., O'Sullivan, J., Weltman, M., McCaughan, G., El-Omar, E., Zekry, A., 2021. Gut microbiota impact on the peripheral immune response in non-alcoholic fatty liver disease related hepatocellular carcinoma. Nat. Commun. 212 (1), 187. https://doi.org/10.1038/s41467-020-20422-7.

Bonaz, B., Bazin, T., Pellissier, S., 2018. The vagus nerve at the interface of the microbiota-gut-brain axis. Front. Neurosci. 12, 49. https://doi.org/10.3389/fnins.2018.00049.

Bravo, J.A., Forsythe, P., Chew, M.V., Escaravage, E., Savignac, H.M., Dinan, T.G., Bienenstock, J., Cryan, J.F., 2011. Ingestion of *Lactobacillus* strain regulates emotional behavior and central GABA receptor expression in a mouse via the vagus nerve. Proc. Natl. Acad. Sci. U. S. A. 108 (38), 16050–16055. https://doi.org/10.1073/pnas.1102999108.

Cantarel, B.L., Waubant, E., Chehoud, C., Kuczynski, J., DeSantis, T.Z., Warrington, J., Venkatesan, A., Fraser, C.M., Mowry, E.M., 2015. Gut microbiota in multiple sclerosis: possible influence of immunomodulators. J. Investig. Med. 63 (5), 729–734. https://doi.org/10.1097/JIM.0000000000000192.

Cawthon, C.R., de La Serre, C.B., 2018. Gut bacteria interaction with vagal afferents. Brain Res. 1693, 134–139. https://doi.org/10.1016/j.brainres.2018.01.012.

Chang, L., Wei, Y., Hashimoto, K., 2022. Brain-gut-microbiota axis in depression: a historical overview and future directions. Brain Res. Bull. 182, 44–56. https://doi.org/10.1016/j.brainresbull.2022.02.004.

Chen, T., Noto, D., Hoshino, Y., Mizuno, M., Miyake, S., 2019. Butyrate suppresses demyelination and enhance remyelination. J. Neuroinflammation 16 (1), 165. https://doi.org/10.1186/s12974-019-1552-y.

Chu, F., Shi, M., Zheng, C., Shen, D., Zhu, J., Zheng, X., Cui, L., 2018. The roles of macrophages and microglia in multiple sclerosis and experimental autoimmune encephalomyelitis. J. Neuroimmunol. 318, 1–7. https://doi.org/10.1016/j.jneuroim.2018.02.015.

Clarner, T., Diederichs, F., Berger, K., Denecke, B., Gan, L., van der Valk, P., Beyer, C., Amor, S., Kipp, M., 2012. Myelin debris regulates inflammatory responses in an experimental demyelination animal model and multiple sclerosis lesions. Glia 60 (10), 1468–1480. https://doi.org/10.1002/glia.22367.

Cryan, J.F., O'Riordan, K.J., Cowan, C.S.M., Sandhu, K.V., Bastiaanssen, T.F.S., Boehme, M., Codagnone, M.G., Cussotto, S., Fulling, C., Golubeva, A.V., Guzzetta, K. E., Jaggar, M., Long-Smith, C.M., Lyte, J.M., Martin, J.A., Molinero-Perez, A., Moloney, G., Morelli, E., Morillas, E., O'Connor, R., Cruz-Pereira, J.S., Peterson, V.L., Rea, K., Ritz, N.L., Sherwin, E., Spichak, S., Teichman, E.M., van de Wouw, M., Ventura-Silva, A.P., Wallace-Fitzsimons, S.E., Hyland, N., Clarke, G., Dinan, T.G., 2019. The microbiota-gut-brain axis. Physiol. Rev. 99, 1877–2013. https://doi.org/10.1152/physrev.00018.2018.

Dahham, J., Rizk, R., Kremer, I., Evers, S., Hiligsmann, M., 2021. Economic burden of multiple sclerosis in low- and middle-income countries: a systematic review. PharmacoEconomics 39 (7), 789–807. https://doi.org/10.1007/s40273-021-01032-7.

Deng, X., Sriram, S., 2005. Role of microglia in multiple sclerosis. Curr. Neurol. Neurosci. Rep. 5 (3), 239–244. https://doi.org/10.1007/s11910-005-0052-x.

Erny, D., Prinz, M., 2020. How microbiota shape microglial phenotypes and epigenetics. Glia 68, 1655–1672. https://doi.org/10.1002/glia.23822.

Farshbafnadi, M., Agah, E., Rezaei, N., 2021. The second brain: the connection between gut microbiota composition and multiple sclerosis. J. Neuroimmunol. 360, 577700. https://doi.org/10.1016/j.jneuroim.2021.577700.

Feng, C., Wang, H., Lu, N., Chen, T., He, H., Lu, Y., Tu, X.M., 2014. Log-transformation and its implications for data analysis. Shanghai Arch. Psychiatry 26 (2), 105–109. https://doi.org/10.3969/j.issn.1002-0829.2014.02.009.

Forsythe, P., Bienenstock, J., Kunze, W.A., 2014. Vagal pathways for microbiome-brain-gut axis communication. Adv. Exp. Med. Biol. 817, 115–133. https://doi.org/10.1007/978-1-4939-0897-4_5.

Franklin, R.J.M., Ffrench-Constant, C., 2017. Regenerating CNS myelin–from mechanisms to experimental medicines. Nat. Rev. Neurosci. 18 (12), 753–769. https://doi.org/10.1038/nrn.2017.136.

Gao, Z., Tsirka, E.S., 2011. Animal models of MS reveal multiple roles of microglia in disease pathogenesis. Neurol. Res. Int. 2011 https://doi.org/10.1155/2011/383087, 383087.

Ghadiri, F., Ebadi, Z., Asadollahzadeh, E., Naser Moghadasi, A., 2022. Gut microbiome in multiple sclerosis-related cognitive impairment. Mult. Scler. Relat. 67 https://doi.org/10.1016/j.msard.2022.104165, 104165.

Ghezzi, L., Cantoni, C., Pinget, G.V., Zhou, Y., Piccio, L., 2021. Targeting the gut to treat multiple sclerosis. J. Clin. Invest. 131 (13) https://doi.org/10.1172/JCI143774 e143774.

Guerrero, L.B., Sicotte, L.N., 2020. Microglia in multiple sclerosis: friend or foe? Front. Immunol. 11, 374. https://doi.org/10.3389/fimmu.2020.00374.

Jones, C.D., Motl, R., Sandroff, B.M., 2021. Depression in multiple sclerosis: is one approach for its management enough? Mult. Scler. Relat. Disord. 51, 102904 https://doi.org/10.1016/j.msard.2021.102904.

Kalafatakis, I., Karagogeos, D., 2021. Oligodendrocytes and microglia: key players in myelin development, damage and repair. Biomolecules 11 (7), 1058. https://doi.org/10.3390/biom11071058.

Kipp, M., Nyamoya, S., Hochstrasser, T., Amor, S., 2017. Multiple sclerosis animal models: a clinical and histopathological perspective. Brain Pathol. 27 (2), 123–137. https://doi.org/10.1111/bpa.12454.

Kishikawa, T., Ogawa, K., Motooka, D., Hosokawa, A., Kinoshita, M., Suzuki, K., Yamamoto, K., Masuda, T., Matsumoto, Y., Nii, T., Maeda, Y., Nakamura, S., Inohara, H., Mochizuki, H., Okuno, T., Okada, Y., 2020. A metagenome-wide association study of gut microbiome in patients with multiple sclerosis revealed novel disease pathology. Front. Cell. Infect. Microbiol. 10 https://doi.org/10.3389/fcimb.2020.585973, 585973.

Kwak, M.S., Cha, J.M., Shin, H.P., Jeon, J.W., Yoon, J.Y., 2020. Development of a novel metagenomic biomarker for prediction of upper gastrointestinal tract involvement in patients with Crohn's disease. Front. Microbiol. 11, 1162. https://doi.org/10.3389/fmicb.2020.01162.

Lubrich, C., Giesler, P., Kipp, M., 2022. Motor behavioral deficits in the cuprizone model: validity of the rotarod test paradigm. Int. J. Mol. Sci. 23 (19), 11342. https://doi.org/10.3390/ijms231911342.

Lynch, C.M.K., Clarke, G., Cryan, J.F., 2021. Powering up microbiome-microglia interactions. Cell Metab. 33 (11), 2097–2099. https://doi.org/10.1016/j.cmet.2021.10.006.

Ma, Q., Xing, C., Long, W., Wang, H.Y., Liu, Q., Wang, R.F., 2019. Impact of microbiota on central nervous system and neurological diseases: the gut-brain axis. J. Neuroinflammation 16, 53. https://doi.org/10.1186/s12974-019-1434-3.

Maghzi, A.H., Weiner, H.L., 2020. A one-two punch in the gut may trigger multiple sclerosis. Immunity 53 (4), 707–709. https://doi.org/10.1016/j.immuni.2020.09.016.

Marrosu, F., Maleci, A., Cocco, E., Puligheddu, M., Marrosu, M.G., 2005. Vagal nerve stimulation effects on cerebellar tremor in multiple sclerosis. Neurology 65 (3), 490. https://doi.org/10.1212/01.wnl.0000172343.45110.79.

Marrosu, F., Maleci, A., Cocco, E., Puligheddu, M., Barberini, L., Marrosu, M.G., 2007. Vagal nerve stimulation improves cerebellar tremor and dysphagia in multiple sclerosis. Mult. Scler. 13 (9), 1200–1202. https://doi.org/10.1177/1352458507078399.

Mayrhofer, F., Dariychuk, Z., Zhen, A., Daugherty, D.J., Bannerman, P., Hanson, A.M., Pleasure, D., Soulika, A., Deng, W., Chechneva, O.V., 2021. Reduction in CD11c+ microglia correlates with clinical progression in chronic experimental autoimmune demyelination. Neurobiol. Dis. 161 https://doi.org/10.1016/j.nbd.2021.105556, 105556.

Moles, L., Egimendia, A., Osorio-Querejeta, I., Iparraguirre, L., Alberro, A., Suárez, J., Sepúlveda, L., Castillo-Triviño, T., Muñoz-Culla, M., Ramos-Cabrer, P., Otaegui, D., 2021. Gut microbiota changes in experimental autoimmune encephalomyelitis and cuprizone mice models. ACS Chem. Neurosci. 12 (5), 893–905. https://doi.org/10.1021/acschemneuro.0c00695.

Mossad, O., Erny, D., 2020. The microbiota-microglia axis in central nervous system disorders. Brain Pathol. 30 (6), 1159–1177. https://doi.org/10.1111/bpa.12908.

Nicholas, J., Zhou, H., Deshpande, C., 2021. Annual cost burden by level of relapse severity in patients with multiple sclerosis. Adv. Ther. 38 (1), 758–771. https://doi.org/10.1007/s12325-020-01570-0.

Osaka, T., Moriyama, E., Arai, S., Date, Y., Yagi, J., Kikuchi, J., Tsuneda, S., 2017. Meta-analysis of fecal microbiota and metabolites in experimental colitic mice during the inflammatory and healing phases. Nutrients. 9 (12), 1329. https://doi.org/10.3390/nu9121329.

Palumbo, S., Pellegrini, S., 2017. Chapter 11. Experimental in vivo models of multiple sclerosis: state of the art. In: Zagon, I.S., McLaughlin, P.J. (Eds.), Multiple Sclerosis: Perspectives in Treatment and Pathogenesis.

Parodi, B., Kerlero de Rosbo, N., 2021. The gut-brain axis in multiple sclerosis. Is it dysfunction a pathological trigger or a consequence of the disease? Front. Immunol. 12, 718220 https://doi.org/10.3389/fimmu.2021.718220.

Plassais, J., Gbikpi-Benissan, G., Figarol, M., Scheperjans, F., Gorochov, G., Derkinderen, P., Cervino, A.C.L., 2021. Gut microbiome alpha-diversity is not a

marker of Parkinson's disease and multiple sclerosis. Brain Commun. 3 (2) https://doi.org/10.1093/braincomms/fcab113 fcab113.

Procaccini, C., De Rosa, V., Pucino, V., Formisano, L., Matarese, G., 2015. Animal models of multiple sclerosis. Eur. J. Pharmacol. 759, 182–191. https://doi.org/10.1016/j.ejphar.2015.03.042.

Pu, Y., Tan, Y., Qu, Y., Chang, L., Wang, S., Wei, Y., Wang, X., Hashimoto, K., 2021. A role of the subdiaphragmatic vagus nerve in depression-like phenotypes in mice after fecal microbiota transplantation from *Chrna7* knock-out mice with depression-like phenotypes. Brain Behav. Immun. 94, 318–326. https://doi.org/10.1016/j.bbi.2020.12.032.

Rawji, K.S., Yong, V.W., 2013. The benefits and detriments of macrophages/microglia in models of multiple sclerosis. Clin. Dev. Immunol. 2013 https://doi.org/10.1155/2013/948976, 948976.

Rosson, S., de Filippis, R., Croatto, G., Collantoni, E., Pallottino, S., Guinart, D., Brunoni, A.R., Dell'Osso, B., Pigato, G., Hyde, J., Brandt, V., Cortese, S., Fiedorowicz, J.G., Petrides, G., Correll, C.U., Solmi, M., 2022. Brain stimulation and other biological non-pharmacological interventions in mental disorders: an umbrella review. Neurosci. Biobehav. Rev. 139 https://doi.org/10.1016/j.neubiorev.2022.104743, 104743.

Salinas Tejedor, L., Gudi, V., Kucman, V., Pul, R., Gingele, S., Sühs, K.W., Stangel, M., Skripuletz, T., 2015. Oligodendroglial markers in the cuprizone model of CNS de- and remyelination. Histol. Histopathol. 30 (12), 1455–1464. https://doi.org/10.14670/HH-11-640.

Sanchis-Artero, L., Martínez-Blanch, J.F., Manresa-Vera, S., Cortés-Castell, E., Valls-Gandia, M., Iborra, M., Paredes-Arquiola, J.M., Boscá-Watts, M., Huguet, J.M., Gil-Borrás, R., Rodríguez-Morales, J., Cortés-Rizo, X., 2021. Evaluation of changes in intestinal microbiota in Crohn's disease patients after anti-TNF alpha treatment. Sci. Rep. 11 (1), 10016. https://doi.org/10.1038/s41598-021-88823-2.

Schymanski, E.L., Jeon, J., Gulde, R., Fenner, K., Ruff, M., Singer, H.P., Hollender, J., 2014. Identifying small molecules via high resolution mass spectrometry: communicating confidence. Environ. Sci. Technol. 48 (4), 2097–2098. https://doi.org/10.1021/es5002105.

Segata, N., Izard, J., Waldron, L., Gevers, D., Miropolsky, L., Garrett, W.S., Huttenhower, C., 2011. Metagenomic biomarker discovery and explanation. Genome Biol. 12, R60. https://doi.org/10.1186/gb-2011-12-6-r60.

Skokou, M., Soubasi, E., Gourzis, P., 2012. Depression in multiple sclerosis: a review of assessment and treatment approaches in adult and pediatric populations. ISRN Neurol. 2012, 427102 https://doi.org/10.5402/2012/427102.

Skripuletz, T., Gudi, V., Hackstette, D., Stangel, M., 2011. De- and remyelination in the CNS white and grey matter induced by cuprizone: the old, the new, and the unexpected. Histol. Histopathol. 26 (12), 1585–1597. https://doi.org/10.14670/HH-26.1585.

Torkildsen, O., Brunborg, L.A., Myhr, K.M., Bø, L., 2008. The cuprizone model for demyelination. Acta Neurol. Scand. 188, 72–76. https://doi.org/10.1111/j.1600-0404.2008.01036.x.

Tsugawa, H., Cajka, T., Kind, T., Ma, Y., Higgins, B., Ikeda, K., Kanazawa, M., VanderGheynst, J., Fiehn, O., Arita, M., 2015. MS-DIAL: data-independent MS/MS deconvolution for comprehensive metabolome analysis. Nat. Methods 12 (6), 523–526. https://doi.org/10.1038/nmeth.3393.

Voet, S., Prinz, M., Loo, V.G., 2019. Microglia in central nervous system inflammation and multiple sclerosis pathology. Trends Mol. Med. 25 (2), 112–123. https://doi.org/10.1016/j.molmed.2018.11.005.

Wan, X., Eguchi, A., Fujita, Y., Ma, L., Wang, X., Yang, Y., Qu, Y., Chang, L., Zhang, J., Mori, C., Hashimoto, K., 2022a. Effects of (*R*)-ketamine on reduced bone mineral density in ovariectomized mice: a role of gut microbiota. Neuropharmacol. 213 https://doi.org/10.1016/j.neuropharm.2022.109139, 109139.

Wan, X., Eguchi, A., Qu, Y., Yang, Y., Chang, L., Shan, J., Mori, C., Hashimoto, K., 2022b. Gut–microbiota–brain axis in the vulnerability to psychosis in adulthood after repeated cannabis exposure during adolescence. Eur. Arch. Psychiatry Clin. Neurosci. https://doi.org/10.1007/s00406-022-01437-1, 2022 Jun 6.

Wang, Y., Wang, Z., Wang, Y., Li, F., Jia, J., Song, X., Qin, S., Wang, R., Jin, F., Kitazato, K., Wang, Y., 2018. The gut-microglia connection: implications for central nervous system diseases. Front. Immunol. 9, 2325. https://doi.org/10.3389/fimmu.2018.02325.

Wang, S., Ishima, T., Zhang, J., Qu, Y., Chang, L., Pu, Y., Fujita, Y., Tan, Y., Wang, X., Hashimoto, K., 2020. Ingestion of *Lactobacillus intestinalis* and *Lactobacillus reuteri* causes depression- and anhedonia-like phenotypes in antibiotic-treated mice via the vagus nerve. J. Neuroinflammation 17 (1), 241. https://doi.org/10.1186/s12974-020-01916-z.

Wang, S., Ishima, T., Qu, Y., Shan, J., Wei, Y., Chang, L., Qu, Y., Zhang, J., Pu, Y., Fujita, Y., Tan, Y., Wang, X., Ma, L., Wan, X., Hammock, B.D., Hashimoto, K., 2021a. Ingestion of *Faecalibacterium rodentium* causes depression-like phenotypes in resilient *Ephx2* knock-out mice: a role of brain–gut–microbiota axis via the subdiaphragmatic vagus nerve. J. Affect. Disord. 292, 565–573. https://doi.org/10.1016/j.jad.2021.06.006.

Wang, X., Chang, L., Tan, Y., Qu, Y., Shan, J., Hashimoto, K., 2021b. (R)-ketamine ameliorates the progression of experimental autoimmune encephalomyelitis in mice. Brain Res. Bull. 177, 316–323. https://doi.org/10.1016/j.brainresbull.2021.10.013.

Wang, Y., Zhan, G., Cai, Z., Jiao, B., Zhao, Y., Li, S., Luo, A., 2021c. Vagus nerve stimulation in brain diseases: therapeutic applications and biological mechanisms. Neurosci. Biobehav. Rev. 127, 37–53. https://doi.org/10.1016/j.neubiorev.2021.04.018.

Wang, X., Chang, L., Wan, X., Tan, Y., Qu, Y., Shan, J., Yang, Y., Ma, L., Hashimoto, K., 2022a. (R)-ketamine ameliorates demyelination and facilitates remyelination in cuprizone-treated mice: a role of gut-microbiota-brain axis. Neurobiol. Dis. 165, 105635 https://doi.org/10.1016/j.nbd.2022.105635.

Wang, X., Yang, J., Hashimoto, K., 2022b. (R)-ketamine as prophylactic and therapeutic drug for neurological disorders: beyond depression. Neurosci. Biobehav. Rev. 139, 104762 https://doi.org/10.1016/j.neubiorev.2022.104762.

Wei, Y., Wang, T., Liao, L., Fan, X., Chang, L., Hashimoto, K., 2022. Brain-spleen axis in health and diseases: a review and future perspective. Brain Res. Bull. 182, 130–140. https://doi.org/10.1016/j.brainresbull.2022.02.008.

Wu, Y., Zhang, Y., Xie, B., Abdelgawad, A., Chen, X., Han, M., Shang, Y., Yuan, S., Zhang, J., 2021. RhANP attenuates endotoxin-derived cognitive dysfunction through subdiaphragmatic vagus nerve-mediated gut microbiota-brain axis. J. Neuroinflammation 18 (1), 300. https://doi.org/10.1186/s12974-021-02356-z.

Xia, Y., Sun, J., 2017. Hypothesis testing and statistical analysis of microbiome. Genes Dis. 4, 138–148. https://doi.org/10.1016/j.gendis.2017.06.001.

Yang, Y., Ishima, T., Wan, X., Wei, Y., Chang, L., Zhang, J., Qu, Y., Hashimoto, K., 2022. Microglial depletion and abnormalities in gut microbiota composition and short-chain fatty acids in mice after repeated administration of colony stimulating factor 1 receptor inhibitor PLX5622. Eur. Arch. Psychiatry Clin. Neurosci. 272 (3), 483–495. https://doi.org/10.1007/s00406-021-01325-0.

Yang, Y., Eguchi, A., Wan, X., Chang, L., Wang, X., Qu, Y., Mori, C., Hashimoto, K., 2023. A role of gut-microbiota-brain axis via subdiaphragmatic vagus nerve in depression-like phenotypes in *Chrna7* knock-out mice. Prog. Neuro-Psychopharmacol. Biol. Psychiatry 120, 110652. https://doi.org/10.1016/j.pnpbp.2022.110652.

Zhan, J., Mann, T., Joost, S., Behrangi, N., Frank, M., Kipp, M., 2020. The cuprizone model: dos and do nots. Cells 9 (4), 843. https://doi.org/10.3390/cells9040843.

Zhang, J., Ma, L., Chang, L., Pu, Y., Qu, Y., Hashimoto, K., 2020. A key role of the subdiaphragmatic vagus nerve in the depression-like phenotype and abnormal composition of gut microbiota in mice after lipopolysaccharide administration. Transl. Psychiatry 10 (1), 186. https://doi.org/10.1038/s41398-020-00878-3.

Update

Neurobiology of Disease
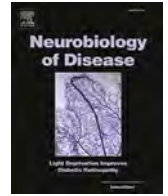
Corrigendum to "Key role of the gut–microbiota–brain axis via the subdiaphragmatic vagus nerve in demyelination of cuprizone-treated mouse brain" [Neurobiology of Disease 176 (2023); 105961. doi: 10.1016/j.nbd.2022.105951]

X. Wang, A. Eguchi, Y. Yang, L. Chang, X. Wan, J. Shan, Y. Qu, L. Ma, C. Mori, J. Yang, K. Hashimoto [*]

Chiba University, Japan and Zhengzhou University, China

The authors regret the errors in the legend of Fig. 1B. The original version of Fig. 1B legend is "B: The body weight gain compared with baseline (week -1) (repeated measures two-way ANOVA, time: $F_{1, 34} = 71,327$. P < 0.001. group: $F_{1, 34} = 10.084$, P < 0.001. interaction: $F_{1, 34} = 3.825$, P < 0.001)". The corrected version of Fig. 1B legend is "B: The body weight gain compared with baseline (week -1) (repeated measures two-way ANOVA, time: $F_{6, 29} = 71.327$. P < 0.001. group: $F_{3, 34} = 10.084$, P < 0.001. interaction: $F_{18, 93} = 3.825$, P < 0.001)". These mistakes do not affect the results of this article. The authors would like to apologise for any inconvenience caused.

A role of gut–microbiota–brain axis via subdiaphragmatic vagus nerve in depression-like phenotypes in *Chrna7* knock-out mice

Yong Yang [a], Akifumi Eguchi [b], Xiayun Wan [a], Lijia Chang [a], Xingming Wang [a], Youge Qu [a], Chisato Mori [b,c], Kenji Hashimoto [a,*]

[a] *Division of Clinical Neuroscience, Chiba University Center for Forensic Mental Health, Chiba 260-8670, Japan*
[b] *Department of Sustainable Health Science, Chiba University Center for Preventive Medical Sciences, Chiba 263-8522, Japan*
[c] *Department of Bioenvironmental Medicine, Graduate School of Medicine, Chiba University, Chiba 260-8670, Japan*

ARTICLE INFO

ABSTRACT

The α7 subtype of the nicotinic acetylcholine receptor (α7 nAChR: coded by *Chrna7*) is known to regulate the cholinergic ascending anti-inflammatory pathway. We previously reported that *Chrna7* knock-out (KO) mice show depression-like behaviors through abnormal composition of gut microbiota and systemic inflammation. Given the role of subdiaphragmatic vagus nerve in gut–microbiota–brain axis, we investigated whether sub-diaphragmatic vagotomy (SDV) could affect depression-like behaviors, abnormal composition of gut microbiota, and microbes-derived metabolites in *Chrna7* KO mice. SDV blocked depression-like behaviors and reduced expression of synaptic proteins in the medial prefrontal cortex (mPFC) of *Chrna7* KO mice. LEfSe (linear discriminant analysis effect size) analysis revealed that the species *Lactobacillus* sp. *BL302*, the species *Lactobacillus hominis*, and the species *Lactobacillus reuteri*, were identified as potential microbial markers in the KO + SDV group. There were several genus and species altered among the three groups [wild-type (WT) + sham group, KO + sham group, KO + SDV group]. Furthermore, there were several plasma metabolites altered among the three groups. Moreover, there were correlations between relative abundance of several microbiome and behavioral data (or synaptic proteins). Network analysis showed correlations between relative abundance of several microbiome and plasma metabolites (or behavioral data). These data suggest that *Chrna7* KO mice produce depression-like behaviors and reduced expression of synaptic proteins in the mPFC through gut–microbiota–brain axis via subdiaphragmatic vagus nerve.

1. Introduction

Depression is the most prevalent mental disorder with an estimated 5.0% of adults and 5.7% of elderly adults (>60 years old) worldwide. Furthermore, depression is a leading cause of disability worldwide, and it is a major contributor to the overall global burden of disease (WHO, 2021). Although the precise neurobiology underlying depression remains unclear, inflammation is known to play an important role in depression (Brydges et al., 2022; Haroon et al., 2012; Hashimoto, 2009; Hashimoto, 2015; Liu et al., 2020; Lucido et al., 2021; Mac Giollabhui et al., 2021; Miller and Raison, 2016; Shan and Hashimoto, 2022; Toenders et al., 2022; Zhang et al., 2016a).

Nicotinic acetylcholine receptor (nAChR) is a kind of ionotropic ligand-gated ion channels widely distributed in various cells of the central nervous system (CNS), peripheral nervous system (PNS), enteric nervous system, neuromuscular junction and immune system, which is consist of pentameric combinations of α and/or β subunits (Dani, 2015; Dani and Bertrand, 2007). Among its many subtypes, α7 nAChRs, encoded by the *Chrna7* gene, mediates systemic inflammatory homeostasis between the CNS and the immune system through a vagus nerve mediated way known as the "cholinergic anti-inflammatory pathway" (Andersson and Tracey, 2012; Lei and Duan, 2021; Martelli et al., 2014; Olofsson et al., 2012; Piovesana et al., 2021; Ulloa, 2005; Wang et al., 2003; Wu et al., 2021). We previously reported that *Chrna7* KO mice show depression-like phenotypes through systemic inflammation (Pu et al., 2021b; Zhang et al., 2016b).

---

* Corresponding author.
E-mail address: hashimoto@faculty.chiba-u.jp (K. Hashimoto).

Increasing evidence suggests altered composition of intestinal microbiota in rodents with depressive-like phenotypes (Chang et al., 2022; Hashimoto, 2020; Huang et al., 2019; Park et al., 2013; Qu et al., 2017; Wang et al., 2020a, 2020b; Wong et al., 2016; Yang et al., 2017, 2019; Zhang et al., 2017; Zhang et al., 2019), and patients with depression (Caso et al., 2021; Jiang et al., 2015; Li et al., 2022; Nikolova et al., 2021; Sanada et al., 2020; Wei et al., 2022a, 2022b; Wong et al., 2016; Zheng et al., 2016). Fecal microbiota transplantation (FMT) of certain intestinal microbiota from depressed patients or rodents with depressive-like phenotypes causes depression-like phenotypes in mice (Kelly et al., 2016; Pu et al., 2021b; Pu et al., 2022; Wang et al., 2020a; Yang et al., 2019; Zheng et al., 2016). Furthermore, microbial-derived metabolites, including short-chain fatty acids (SCFAs), tryptophan-derived metabolites, bile acids and D-amino acids, could regulate a number of physiological functions such as behaviors (Bartoli et al., 2021; Chang et al., 2022; Hashimoto, 2022; Li et al., 2022; Pu et al., 2021a; Tran and Mohajeri, 2021; Wan et al., 2022a, 2022b). Vagus nerve is known to play a key role in the bi-directional communication between the gut microbiota and the brain (Bonaz et al., 2018; Cawthon and de La Serre, 2018; Chang et al., 2022; Cryan et al., 2019; Forsythe et al., 2014). We reported that subdiaphragmatic vagotomy (SDV) blocked the onset of depression-like behavior and altered composition of intestinal microbiota in mice after lipopolysaccharide (LPS) administration (Zhang et al., 2020). Subsequently, we reported that SDV blocked the onset of depression-like behaviors in mice after FMT from mice with depression-like behaviors (Pu et al., 2021a; Wang et al., 2020a; Wang et al., 2021). Collectively, it is likely that subdiaphragmatic vagus nerve plays a key role in depression-like behaviors (Chang et al., 2022; Wei et al., 2022b). However, there are no reports showing the role of subdiaphragmatic vagus nerve in depression-like phenotypes in *Chrna7* KO mice.

The aim of present study was to evaluate whether SDV could affect depression-like phenotypes and reduced expression of synaptic proteins in the medial prefrontal cortex (mPFC) of *Chrna7* KO mice. Furthermore, we performed 16S rRNA analysis for gut microbiota composition and untargeted metabolomics analysis of plasma samples.

2. Materials and methods

2.1. Animals

Mice deficient in α7 nAChR (coded by *Chrna7* gene, C57BL/6 background) were purchased from the Jackson Laboratory (Bar Harbor, ME, USA) (Zhang et al., 2016b). Adult male wild-type (WT) and *Chrna7* KO mice used in this study were littermates. All the experimental mice were aged 9 weeks, body weight 21–27 g. All the experimental mice were acclimatized to standard laboratory conditions (3 or 4/ cage), maintain alternating cycles of 12 h of light and 12 h of darkness (lights on from 7:00–19:00), and under constant room temperature of $23 \pm 1\ °C$ and controlled humidity of $55 \pm 5\%$. Animals were given free admittance to chow and water. The experimental protocol of present study was approved by the Chiba University Institutional Animal Care and Use Committee (Permission number 3–399). The experimental mice were all firstly deeply anesthetized with inhaled isoflurane and then rapidly sacrificed by cervical dislocation. All efforts were made to minimize animals suffering.

2.2. Bilateral subdiaphragmatic vagotomy (SDV)

Bilateral SDV or sham surgery was performed under continuous inhalation anesthesia with 4–5% isoflurane by using an inhalation small animal anesthesia apparatus (KN-1071 NARCOBIT-E; Natsume Seisakusho, Tokyo, Japan), as previously method (Pu et al., 2021a; Wang et al., 2020a, 2021; Zhang et al., 2020) with a slight modification. Briefly, each mouse was placed in the right-side decubitus position, the skin is disinfected with iodophor disinfectant and sterile tissue is laid.

Starting from the midline alba of the abdomen, about 1 cm incision parallel to the costal arch was made at 0.5 cm below the left costal arch. The incision was gently opened with Mini incision spreader to expose the underlying liver tissue. The liver tissue was carefully pushed upward using a small sterilized cotton ball moistened with physiological saline solution and with the aid of an animal surgical microscope (Leica, Heidelberg, Germany), the fascia between the caudate lobe and the left lobe of the liver was sharply cut to fully expose the esophagus and the surrounding surgical field of view. In this case, the dorsal and ventral branches running along the esophagus under the diaphragm of the vagus nerve can be clearly identified and can be severed after careful separation. After that, no bleeding was detected, and no additional injury of esophagus, liver and other organs was checked, the liver tissue was returned to its original normal position, and 0.5 ml physiological saline solution was injected into the abdominal cavity. Then 5–0 surgical silk sutures were used to suture the abdominal incision muscle and skin layers layer by layer, ensuring aseptic operation throughout the operation. The successful implementation of SDV was confirmed by a significant increase in stomach volume on the 14th postoperative day due to loss of vagus nerve innervation.

During the sham operation, the abdominal wall incision of the same size was made in the same way at the same site. After the dorsal and ventral branches of the subdiaphragmatic vagus nerve were also softly exposed but not cut off, no bleeding and no additional damage of other organs was checked. After the abdominal organs were restored to their normal positions, 0.5 ml normal saline was also injected into the abdominal cavity, then the incision was sutured layer by layer using the same method.

2.3. Behavioral tests

Male WT and *Chrna7* KO mice born in the same litter were subjected to behavioral tests, as previously method (Pu et al., 2021a; Wang et al., 2020a, 2021). Behavioral tests including locomotion test (LMT), forced swimming test (FST), and 1% sucrose preference test (1% SPT) (Fig. 1A).

In order to monitor the locomotor activity of the mice, we adopted an automatic animal movement analysis system (SCANET MV-40; MELQUEST Co., Ltd., Toyama, Japan). The cumulative ambulatory activity counts were automatic document continuously over a total stage of 60 min (10 min × 6 times) after the mice were placed into the experimental cube boxes [33 cm (height) × 56 cm (width) × 56 cm (length)]. To avoid experimental interference, the cube boxes were cleaned up during the test interval.

A mouse automated forced-swim apparatus (SCANET MV-40; MELQUEST Co., Ltd., Toyama, Japan) was used to perform FST. Mice were placed into an inescapable transparent tank [31 cm (height) × 23 cm (diameter)] that is filled with tap water at a temperature of $23 \pm 1\ °C$ and a depth of 15 cm. Then their escape related mobility behavior was measured immediately. The immobility times were automatic document and calculated using the analytical software of the apparatus over a total stage of 6 min (1 min × 6 times).

For 1% SPT, which was carried out in the separate animal's home cage. Each mouse was presented with two dual bearing sipper bottles, one bottle contained tap water, and the second contained a 1% sucrose solution. After 24 h of every mouse exposed to the respective two bottles containing different solution, replaced the positions of two bottles for each other to lower any confound produced by a side bias. After another 24 h, all food and bottles were deprived lasting 4 h, then performed 1 h exposure to two identical bottles (containing tap water and 1% sucrose solution), which were weighed before and after the exposure period. The 1% sucrose preference was calculated as a percentage of 1% sucrose solution intake weight over the total liquid intake weight.

2.4. Western blotting analysis of synaptic proteins (PSD-95 and GluA1)

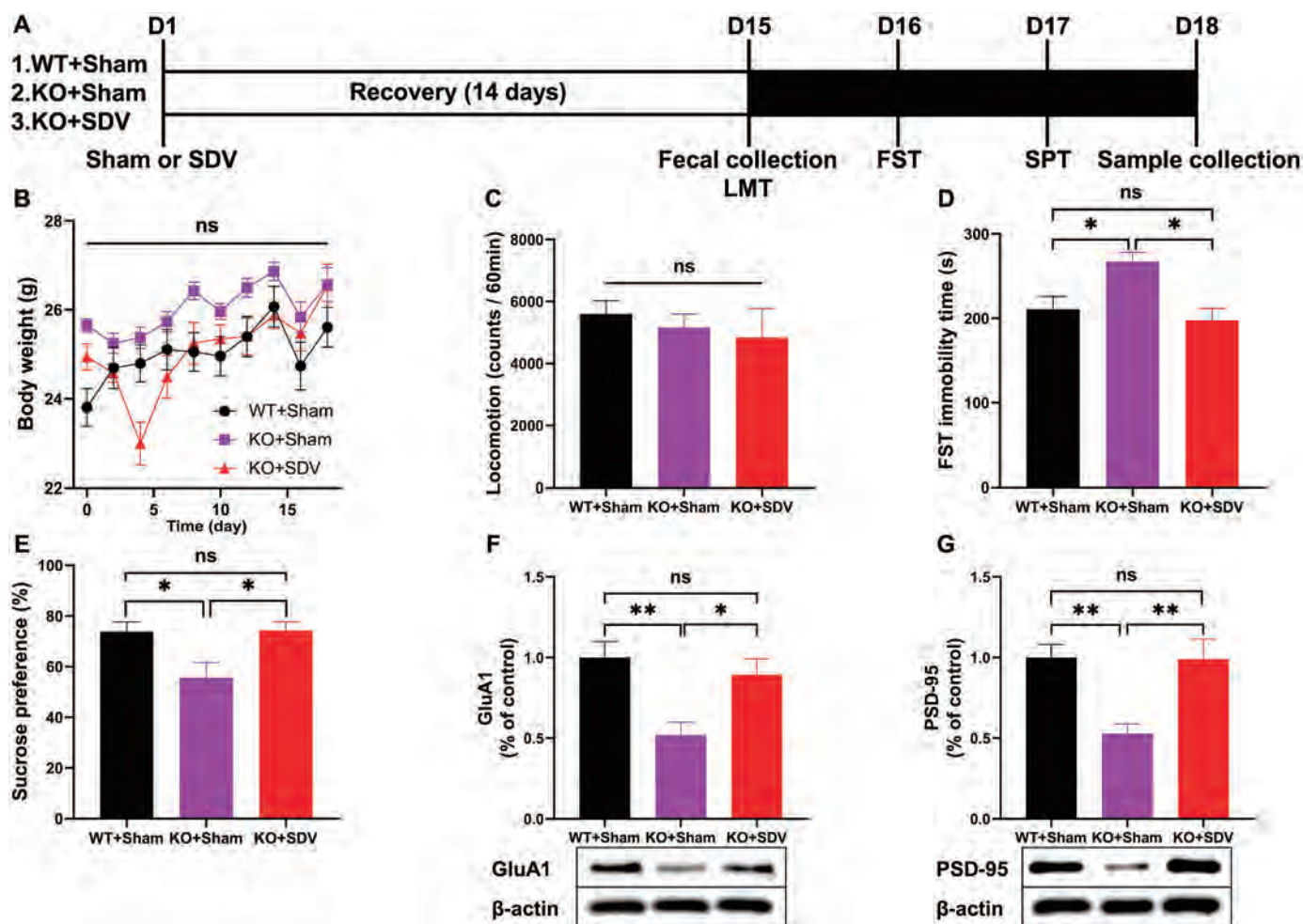Western blotting analysis was performed as previously method (Pu

2

Fig. 1. Effects of bilateral SDV on depression-like phenotypes and reduced expression of synaptic proteins in *Chrna7* KO mice.
(A): Experimental schedule. On day 1, bilateral SDV or sham was performed, and they were recovered 14 days. On day 15, fresh feces samples were collected, and subsequently LMT was performed. FST and SPT were performed on day 16 and day 17, respectively. On day 18, medial prefrontal cortex (mPFC) and plasma samples were collected. (B): Body weight (repeated measure ANOVA, $F_{(2, 21)} = 2.424$, $P = 0.1129$). (C): LMT (one-way ANOVA, $F_{(2,21)} = 0.4278$, $P = 0.6575$). (D): FST (one-way ANOVA, $F_{(2, 21)} = 6.050$, $P = 0.0084$). (E): SPT (one-way ANOVA, $F_{(2, 21)} = 5.312$, $P = 0.0136$). (F): Western blot analysis of GluA1 in the mPFC (one-way ANOVA, $F_{(2, 21)} = 6.805$, $P = 0.0053$) and the representative bands. (G): Western blot analysis of PSD-95 in the mPFC (one-way ANOVA, $F_{(2, 21)} = 8.191$, $P = 0.0023$) and the representative bands. The data are shown as means ± S.E.M (WT + sham group: $n = 10$, KO + sham group: $n = 7$, KO + SDV group: n = 7). ANOVA: analysis of variance. ns: not significant; *P<0.05; **P<0.01; ***P<0.001.

et al., 2021a; Wang et al., 2020a, 2021; Yang et al., 2022b). The mPFC tissues were mechanical homogenized just right in ice-cold Laemmli lysis buffer. To avoid cross-contamination, each specimen was prepared separately, liquid supernatants were collected after centrifugation at 3000 ×g (RCF) at 4 °C for 5 min. The total protein concentration extracted from each sample was detected on a spectrophotometer (Molecular Devices Emax Precision Microplate Reader; Molecular Devices., San Jose, CA, USA) using a DC protein assay kit (Bio-Rad, Hercules, CA, USA). By adding a quarter volume of sample buffer (125 mM Tris-HCl, pH 6.8; 0.1% bromophenol blue; 4% sodium dodecyl sulfate; and 10% β-mercaptoethanol and 20% glycerol) and Laemmili Lysis buffer in appropriate proportions to balance the total protein concentration of each sample, then incubate them at 95 °C for 10 min.

Considering the size of target protein, we chose 10% sodium dodecyl sulfate–polyacrylamide gel electrophoresis (SDS-PAGE) (catalog #: 4568125, Mini-PROTEAN TGX™ Stain-Free Gels; Bio-Rad, USA) separated the proteins by gel electrophoresis. Then a Trans-Blot Mini Cell apparatus (Bio-Rad) was used to electrotransfer the target protein onto polyvinylidene difluoride membranes.

For immunodetection, the polyvinylidene difluoride membranes were blocked with blocker [5% skim milk in TBS + 0.1% Tween-20 (TBST)] at room temperature for 1 h, the membranes for detecting postsynaptic density protein 95 (PSD-95) were incubated with the recommended dilution of the primary antibody against PSD-95 (1:1000, Catalog No.: 51–6,900, 1 μg/mL, Invitrogen, Camarillo, CA, USA) and β-actin (1:10,000; Cat number: A5441 Sigma-Aldrich Co., Ltd., St Louis, MO, USA) at 4 °C overnight. The next day, wash the polyvinylidene difluoride membranes in three washes of TBST, 10 min each. Then the polyvinylidene difluoride membranes were selectively incubated with a recommended dilution of labeled secondary antibody [anti-mouse antibody (1:5000, catalog No.: NA931, GE Healthcare) or a horseradish peroxidase-conjugated anti-rabbit antibody (1:5000, catalog No.: NA934, GE Healthcare)] in 5% blocking buffer in TBST at room temperature for 1 h. After three final washes in TBST, 10 min each. The bands in the polyvinylidene difluoride membranes were detected using enhanced chemiluminescence plus a Western Blotting Detection system (GE Healthcare Bioscience).

The membranes for detecting anti-glutamate receptor 1 (AMPA subtype: GluA1) were incubated in elution buffer (62.5 mM Tris–HCl, pH 6.8, 2% sodium dodecyl sulfate, and 100 mM β-mercaptoethanol) (preheat in incubator at 60 °C for 10 min, shake 50 times /min) at 60 °C for 30 min and then washed three times (10 min at a time) in TBST. The

3

stripped membranes were blocked with blocker [5% skim milk in TBS + 0.1% Tween-20 (TBST)] at room temperature for 1 h and then were incubated with the recommended dilution of primary antibody directed against GluA1 (1:1,000; Cat No.: ab31232, Abcam, Cambridge, MA, USA) at 4 °C overnight. The following day, washing the membranes for three times (10 min at a time) in TBST and were incubated with a recommended dilution of horseradish peroxidase-conjugated anti-rabbit antibody (1:5000, catalog No.: NA934, GE Healthcare) for 1 h at room temperature. After three final washes in TBST, 10 min each. The bands in the polyvinylidene difluoride membranes were detected using enhanced chemiluminescence plus a Western Blotting Detection system (GE Healthcare Bioscience). Images were produced using a ChemiDoc™ Touch Imaging System (170–01401; Bio-Rad Laboratories, Hercules, CA, USA), and immunoreactive bands were quantified using Image Lab™3.0 software (Bio-Rad Laboratories).

2.5. Collection of fresh fecal samples and 16S ribosome RNA sequencing

We collected fresh fecal samples from mice before behavioral test LMT (Fig. 1A). To avoid cross-contamination, fecal samples from each mouse were collected separately. After the mice defecated, fresh fecal samples were collected immediately and were quickly intromitted into individual sterilized screw cap microtubes and then were stored at −80 °C until use.

Extraction of total DNA from mouse feces samples and subsequent 16S rRNA analysis were performed at MyMetagenome Co., Ltd. (Tokyo, Japan). The specific operation scheme can be carried out according to the procedure previously reported (Pu et al., 2021b; Wang et al., 2020a, 2021; Yang et al., 2022b). In brief, in order to amplify the V1-V2 hypervariable region of the bacterial 16S ribosome RNA gene, the universal primers 27F-mod (5′-AGRGTTTGATYMTGGCTCAG-3′) and 338R (5′-TGCTGCCTCCCGTAGGAGT-3′) have been used in the process of PCR. Then used an Illumina MiSeq Platform to sequence the 16S amplicons. The similarities between the genome database of the National Center for Biotechnology Information (NCBI) and the Ribosome Database Project were searched by using the GLSEARCH program. Finally, OTUs were classified and identified.

α-diversity analysis such as Observed_otus, Chao1, Ace, Shannon, and Shannon_e was used to reflect the abundance and diversity of intestinal microbial communities. β-diversity analysis including Principal Co-ordinates Analysis (PCoA) was used to access similarity or dissimilarity of the three intestinal microbial communities. Linear discriminant analysis (LDA) effect size (LEfSe) was used for identifying certain bacteria as potential microbial biomarkers discovery. Microbiota-based potential biomarker discoveries were performed with LEfSe using the online galaxy platform (Segata et al., 2011). The LDA scores (LDA > 4.0 and $P < 0.05$) derived from LEfSe analysis were considered significantly to be enriched or deficient bacterial taxa in the intestinal microbiota among the three groups.

2.6. Untargeted metabolomics analysis of plasma samples and data preprocessing

Untargeted metabolomics profiles from plasm samples were analysis by using ultra-performance liquid chromatography-tandem quadruple time-of-flight mass spectrometry (UPLC-QTOF/MS) technique. The acquisition was operated on an ExionLC™ AD system (SCIEX, Tokyo, Japan) coupled to a X500R QTOF system (SCIEX, Tokyo, Japan), as previously reported (Wan et al., 2022a, 2022b). With the help of R statistical environment Ver 4.0.5. and Mass Spectrometry-Data Independent AnaLysis (MS-DIAL) software version 4.60 (Tsugawa et al., 2015), metabolomics profiles data was analyzed. Metabolites were detected at least 50% from the analyzed samples and the coefficient of variation (CV) values of 30% of metabolites in pooled quality control (QC) samples, and annotation level 2 proposed by Schymanski et al. (2014) were used for data analysis.

2.7. Statistical analysis

Statistical analysis of the data was performed using SPSS version 20.0 software (SPSS, Tokyo, Japan). The data were shown as the mean ± standard error of the mean (S.E.M.). Data for behavioral tests and the expression levels of synaptic proteins were analyzed using one-way analysis of variance (ANOVA), followed by Fisher's least significant difference (LSD) test. The data of body weight were analyzed using repeated measure ANOVA, followed by Fisher's LSD test. Metabolites, the α-diversity of intestinal microbiota, and the abundance of gut microbiota at the phylum level, genus level, and species level among the three groups were analyzed using the Kruskal-Wallis test, followed by the Dunn's test for post-hoc analysis. Pairwise comparison of metabolomics data among the three groups were analyzed by Wilcoxon rank sum test. Bioinformatic analysis of PCoA, LEfSe algorithm of intestinal microbiota, Volcanic plot analysis of metabolomics and Correlation networks were all performed by using the OmicStudio tools (https://www.omicstudio.cn/tool).

Correlations between the plasma metabolites and the intestinal microbiota at species level, depression-like phenotypes and the expression of synaptic proteins in the brain, and correlations between the relative abundance of species bacteria and the expression levels of synaptic proteins in the mPFC and depression-like phenotypes were analyzed using Spearman's correlation analysis. *P*-value for comparison <0.05 was regarded as significant.

3. Results

3.1. Effects of bilateral SDV on depression-like phenotypes, and the expression of synaptic proteins in the brain

Effects of bilateral SDV in depression-like phenotypes in *Chrna7* KO mice were investigated (Fig. 1A). Body weight after surgery was not different among the three groups (Fig. 1B). There were no changes in locomotion among the three groups (Fig. 1C). The immobility time of FST in the KO + sham group was significantly higher than that of WT + sham group and KO + SDV group (Fig. 1D). In the SPT, sucrose preference of KO + sham group was significantly lower than that of WT + sham and KO + SDV groups (Fig. 1E). There were no differences in FST immobility time and sucrose preference of SPT between WT + sham group and KO + SDV group (Fig. 1D and E).

It is well known that synaptic proteins such as PSD-95 and GluA1 are decreased in the mPFC of rodents with depression-like phenotypes (Pu et al., 2021b; Wang et al., 2020a, 2020b, 2021; Yang et al., 2015; Zhang et al., 2014). Western blotting analysis showed that the expressions of PSD-95 and GluA1 in the mPFC of the KO + sham group were significantly lower than those of WT + sham group and KO + SDV group (Fig. 1F and G). There were no differences in expressions of GluA1 and PSD-95 in the mPFC between WT + sham group and KO + SDV group (Fig. 1F and G).

These data suggest that bilateral SDV significantly blocked depression-like phenotypes and reduced expression of synaptic proteins in the mPFC of *Chrna7* KO mice.

3.2. Effects of bilateral SDV on the composition diversity of intestinal microbiota

For α-diversity, Kruskal-Wallis test revealed no statistically significant differences in the Observed_otus, Chao1, Ace, Shannon, and Shannon_e indices among the three group (Fig. 2A-E). Regarding β-diversity, the bacterial population composition of intestine microbiota in the three groups was analyzed by PCoA. Based on the OUT level, PCoA analysis showed a significant separation in the bacterial population composition through Analysis of similarities (ANOSIM) assessment ($R = 0.3500, P = 0.001$) (Fig. 2F).
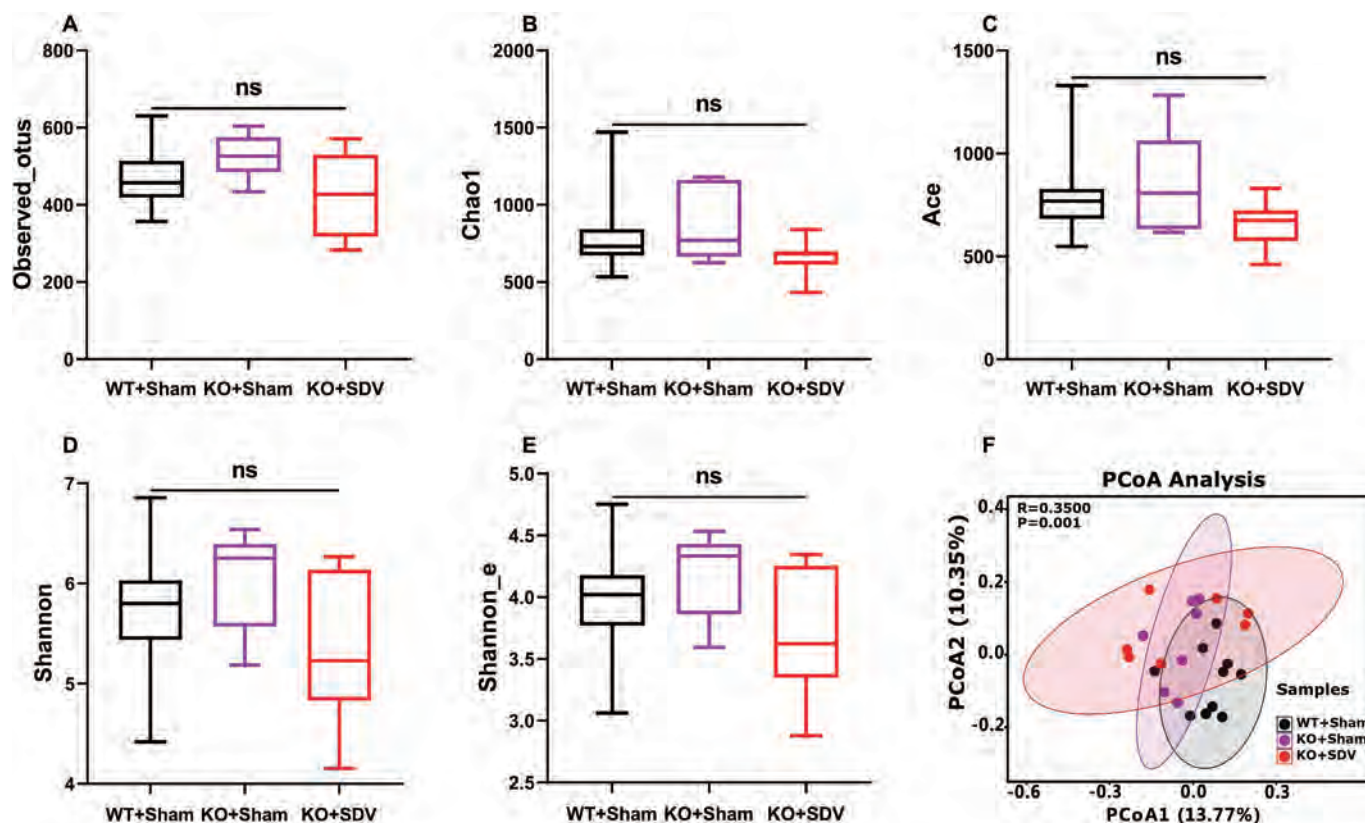
4

Fig. 2. Effects of bilateral SDV on the diversity of gut microbiota composition.
(A): Observed_otus (Kruskal-Wallis test, $P = 0.2028$). (B): Chao1 (Kruskal-Wallis test, $P = 0.1920$). (C): Ace (Kruskal-Wallis test, $P = 0.2305$). (D): Shannon (Kruskal-Wallis test, $P = 0.1941$). (E): Shannon_e (Kruskal-Wallis test, $P = 0.1941$). (F): PCoA based on OTU level (ANOSIM, Bray-Curtis dissimilarity matrix) ($R = 0.3500$, $P = 0.001$). For all box plots, the middle line in the box addresses the median, the box addresses the interquartile range, and the whisker addresses the most extreme and least values. ns: not significant.

3.3. Effects of bilateral SDV on the LEfSe algorithm of intestinal microbiota

Cladogram presented the relationship between biomarker taxa (layers of the cladogram represent different levels, with phylum, class, order, family, genus, and species from inside to outside) generated by LEfSe analysis (Fig. 3A). Furthermore, we identified 5 taxonomic biomarkers, the species *Porphyromonadaceae bacteriumC941*, the genus *G_undefined_Porphyromonadaceae*, the species *Gabonibacter massiliensis*, the genus *Gabonibacter*, and the species *Prevotella* sp. *oral taxon 317* for the WT + sham group. Furthermore, we identified 6 taxonomic biomarkers, the species *Gabonia massiliensis*, the genus *Gabonia*, the family *Porphyromonadaceae*, the order *Bacteroidales*, the class *Bacteroidia*, and the phylum *Bacteroidetes* for the KO + sham group. Moreover, we identified 8 taxonomic biomarkers, the species *Lactobacillus hominis*, the species *Lactobacillus reuteri*, the species *Lactobacillus* sp. *BL302*, the genus *Lactobacillus*, the family *Lactobacillaceae*, the order *Lactobacillales*, the class *Bacilli*, and the phylum *Firmicutes* for the KO + SDV group (Fig. 3B).

3.4. Effects of bilateral SDV on the intestinal microbiota at the levels of phylum, genus, and species

At the phylum level, the composition of the intestinal microbiota in *Chrna7* KO mice was altered after SDV (Fig. 4A). Compared with WT + sham group and KO + sham group, the relative abundance of *Firmicutes* in the KO + SDV group were significantly higher, although there were no significant differences between WT + sham group and KO + sham group (Fig. 4B). Although there were no significant differences in the relative

abundance of *Tenericutes* between KO + SDV group and KO + sham group, the relative abundance of *Tenericutes* in the KO + SDV group were significantly lower than that in the WT + sham group (Fig. 4C).

At the genus level, the composition of the gut microbiota in *Chrna7* KO mice was altered after SDV (Fig. 5A). The relative abundance of *Faecalibaculum* in the KO + SDV group were statistically significantly lower than in the WT + sham group and KO + sham group (Fig. 5B). The relative abundance of *Candidatus Arthromitus*, *Bifidobacterium*, *G_undefined_Burkholderiales*, and *Muribaculum* in the KO + SDV group was lower than that in the WT + sham group, whereas the relative abundance of *Ihubacter* in the KO + SDV group was higher than that in the WT + sham group (Fig. 5C, F, and I-5J). The relative abundance of *Turicibacter* in the KO + SDV group were lower than in the KO + sham group (Fig. 5D). The relative abundance of *Lactobacillus* in the KO + SDV group were higher than in the KO + sham group (Fig. 5G). The relative abundance of *Lactococcus* in the KO + sham group and the KO + SDV group were lower than that in the WT + sham group (Fig. 5E).

At the species level, we screened out 15 bacteria with statistical differences based on their relative abundance (Fig. 6A). There were significant differences in the relative abundance of *Lactobacillus intestinalis*, *Lactobacillus hominis*, *Faecalibaculum rodentium*, *Lactobacillus* sp. *BL302*, *Bacteroides* sp. *TP-5*, *Candidatus Arthromitus* sp. *SFB-mouse*, *Turicibacter* sp. *LA62*, *Lactobacillus reuteri*, *Lactococcus lactis*, *Lactobacillus* sp. *NBRC 14512*, *Clostridium* sp. *Culture Jar-56*, *Lachnospiraceae bacterium 607*, *Clostridiales bacterium CIEAF 030*, *Bifidobacterium pseudolongum* and *Muribaculum intestinale* (Fig. 6B-6P). Among these microbes, the relative abundance of three microbiome (*Lactobacillus intestinalis*, *Lactobacillus* sp. *BL302*, *Turicibacter* sp. *LA62*) was significantly different between KO + sham group and KO + SDV group (Fig. 6B, E, and H).
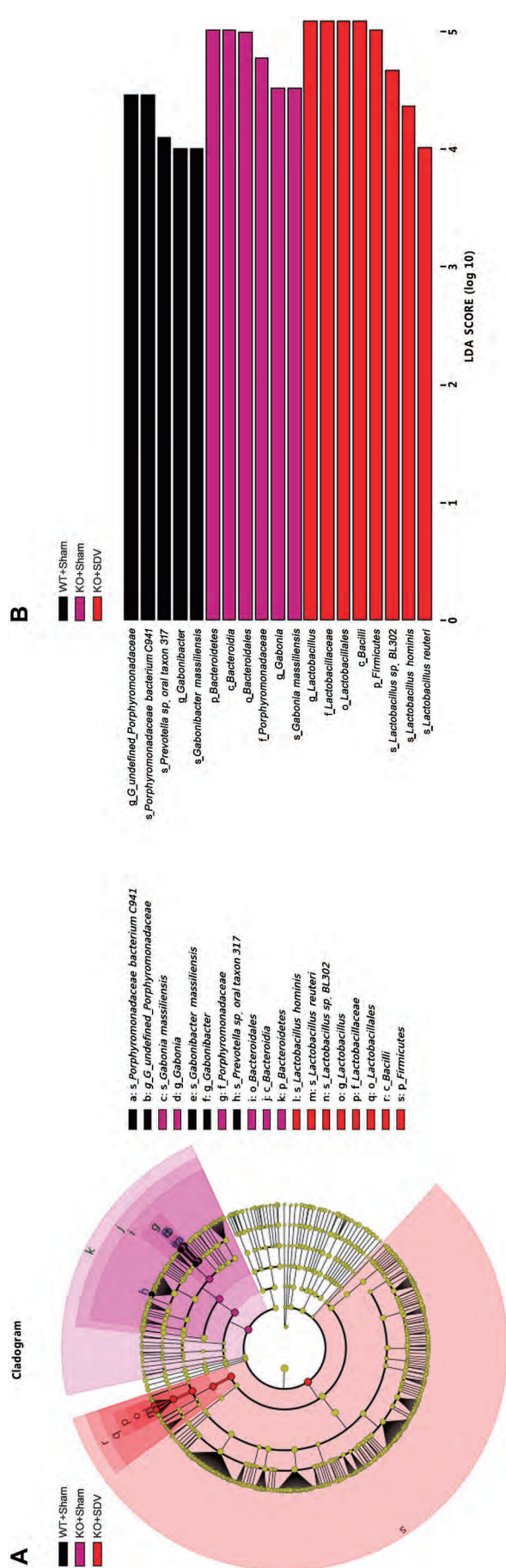
5

Fig. 3. LEfSe analysis for potential bacteria biomarkers of gut microbiota. (A): Functional branching diagram generated from LEfSe showing the differences of the three groups at different taxonomic levels. (B): Histogram representing the enriched taxa with LDA score > 4.0 and $P < 0.05$ obtained from LEfSe of the three groups.

3.5. Untargeted metabolomic profiles analysis of plasma samples

Considering the close interaction between intestinal microbiome and host metabolism, we conducted untargeted metabolomics profiles analysis from plasma samples. After the quality control and removal of low-abundance peaks, a subset of 175 metabolites was annotated. After log10 transformation of the concentration of metabolomics data, Kruskal-Wallis test was performed among the three groups. We identified 24 metabolites with statistical differences (Fig. 7A-D).

Then we conducted pairwise comparison of metabolomics data among the three groups, and screened out the metabolites with significant up-regulation and down-regulation obtained in each two groups through the form of Volcano plot [the threshold was set as: $P < 0.05$ and fold change (FC) > 2]. When comparing the WT + sham group with the KO + sham group, we confirmed that 3 annotation metabolites were significantly up-regulated and 7 annotation metabolites were significantly down-regulated (Fig. 8A). When comparing the WT + sham group with the KO + SDV group, we confirmed that 9 annotation metabolites were significantly up-regulated and 8 annotation metabolites were significantly down-regulated (Fig. 8B). When the KO + sham group compared with the KO + SDV group, we confirmed 9 significantly up-regulated annotated metabolites and 4 significantly down-regulated metabolites (Fig. 8C).

Finally, we further used UpSet plot listed out that there were 11 kinds of annotated metabolites with statistical differences between WT + sham group and KO + sham group, 17 kinds of annotated metabolites with statistical differences between the KO + sham group and KO + SDV group, and 27 kinds of annotated metabolites with statistical differences between WT + sham group and KO + SDV group. In addition, 6 kinds of annotated metabolites showed significant differences between the WT + sham group and the KO + sham group, and between the WT + sham group and the KO + SDV group. Furthermore, 9 kinds of annotated metabolites showed significant differences between the KO + sham group and the KO + SDV group, and between the WT + sham group and the KO + SDV group (Fig. 8D).

3.6. Correlations between the gut microbiota and plasma metabolites (or FST, synapse proteins)

There was a widely correlation between the plasma metabolites and the gut microbiota of the three groups, indicating the existence of a close relationship between the plasma metabolites and the gut microbiota. Furthermore, we evaluated the association between plasma metabolites and the gut microbiota at the species level. After screening the data by setting the threshold of $P < 0.05$ and the absolute value of $R \geq 0.5$, a Correlation Network was developed to indicate the correlation between the plasma metabolites and the intestinal microbiota at species level, depression-like phenotypes and the expression of synaptic proteins in the brain, all of which significantly differences among the three groups in the present study (Fig. 9A).

Two differentially relative abundant of gut bacteria (*Lactobacillus intestinalis* and *Bacteroides* sp. *TP-5*) were positively correlated with 1,5-anhydro-D-sorbitol (Fig. 9A). Three differentially relative abundant of gut bacteria (*Faecalibaculum rodentium*, *Turicibacter* sp. *LA62* and *Muribaculum intestinale*) were negatively correlated with 1,5-anhydro-D-sorbitol (Fig. 9A). There were positive correlations between the relative abundance of species *Lactobacillus intestinalis*, *Lactobacillus hominis*, *Lactobacillus* sp. *BL302*, *Lactobacillus* sp. *NBRC 14512,* and *Clostridiales bacterium CIEAF 030* and L-citrulline. In contrast, there were negative correlations between the relative abundance of species *Faecalibaculum rodentium* and L-citrulline (Fig. 9A).

The relative abundance of species *Lachnospiraceae bacterium 607* was positively correlated with succinic anhydride while the relative abundances of species *Lactobacillus hominis*, *Lactobacillus* sp. *BL302*, *Bacteroides* sp. *TP-5*, *Lactobacillus reuteri*, and *Clostridiales bacterium CIEAF 030* were negatively correlated with succinic anhydride (Fig. 9A). The
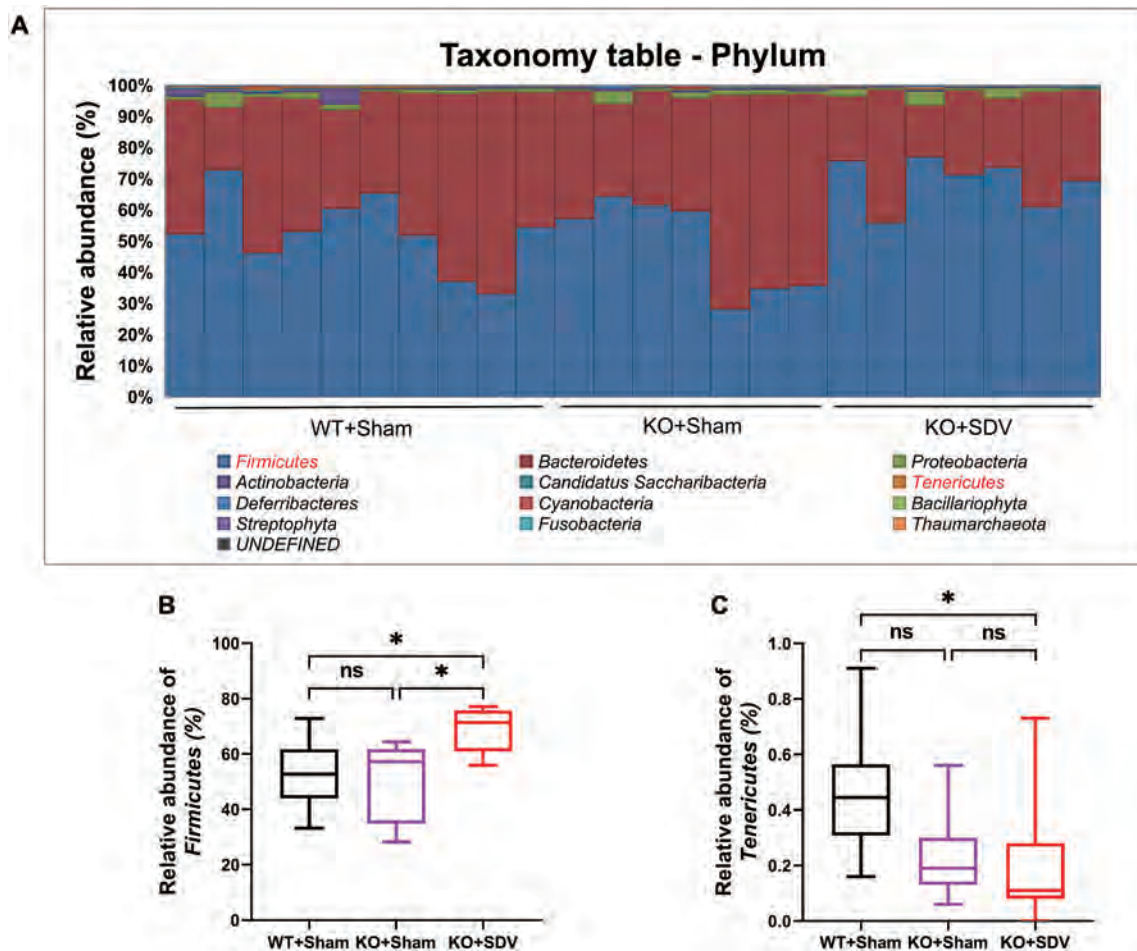
Fig. 4. Effects of bilateral SDV on gut microbiota at the phylum levels.
(A): Gut bacteria composition at the phylum level in the three groups. (B): Relative abundance of the phylum *Firmicutes* (Kruskal-Wallis test, $P = 0.0126$). (C): Relative abundance of the phylum *Tenericutes* (Kruskal-Wallis test, $P = 0.0258$). For all box plots, the middle line in the box addresses the median, the box addresses the interquartile range, and the whisker addresses the most extreme and least values. *$P < 0.05$. ns: not significant.

species *Lactobacillus intestinalis*, *Lactobacillus hominis*, *Lactobacillus* sp. *BL302*, *Lactobacillus reuteri* and *Lactobacillus* sp. *NBRC 14512* were positively correlated with taurocholic acid. In contrast, the species *Faecalibaculum rodentium* and *Turicibacter* sp. *LA62* were negatively correlated with taurocholic acid (Fig. 9A).

There was only a significant positive correlation between the FST data and the concentration of ethyl hydrogen sulfate (Fig. 9A). There was no correlation between changes in SPT and changes in metabolite concentration (data not shown). There was a positive correlation between GluA1 expression levels in mPFC and the concentration of 2-oxindole (Fig. 9A). Furthermore, there were positive correlations between PSD-95 expression levels in mPFC and the concentration of L-citrulline, D-ornithine, 2,6-dihydroxybenzoic acid or resorcinol. In contrast, there were no negative correlations between expressions of GluA1 and PSD-95 in the mPFC and plasma metabolites (Fig. 9A).

Similarly, we used a Correlation Network to investigate correlations between the relative abundance of the gut bacteria that differed significantly at the species levels among the three groups and depression-like phenotypes or the expression of synaptic proteins (Fig. 9B). After screening the data by setting the threshold of P < 0.05 and the absolute value of $R \geq 0.5$. There were significant negative correlations between the FST data and the relative abundance of the species *Lactobacillus intestinalis*, *Lactobacillus* sp. *BL302*, *Bacteroides* sp. *TP-5*, and *Lactobacillus* sp. *NBRC 14512* in the three groups (Fig. 9B), suggesting a role of these species in behavioral despair. There were statistically significant positive correlations between the SPT data and the relative abundance of

species *Bacteroides* sp. *TP-5* in the three experimental groups (Fig. 9B), suggesting a role of *Bacteroides* sp. *TP-5* in anhedonia-like behavior. Furthermore, there were positive or negative correlation between expression levels of synaptic proteins in the mPFC and the relative abundance of species bacteria (Fig. 9B).

4. Discussion

The major findings of this study are as follows: First, SDV blocked depression-like behaviors and reduced expression of synaptic proteins (i. e., GluA1 and PSD-95) in the mPFC of *Chrna7* KO mice. Second, there were no changes in α-diversity among the three groups. However, there was a significant difference in β-diversity among the three groups. LEfSe analysis revealed that the species *Lactobacillus* sp. *BL302*, the species *Lactobacillus hominis*, and the species *Lactobacillus reuteri*, were identified as potential microbial markers in the KO + SDV group. Furthermore, there were several genus and species altered among the three groups. Third, there were several metabolites altered among the three groups. Fourth, there were correlations between relative abundance of several microbiome and behavioral data (or synaptic proteins). Network analysis showed correlations between several microbiome and blood metabolites or behavioral data. Collectively, these data suggest that subdiaphragmatic vagus nerve plays a crucial role in depression-like phenotypes in *Chrna7* KO mice through gut–microbiota–brain axis including microbiome-derived metabolites.

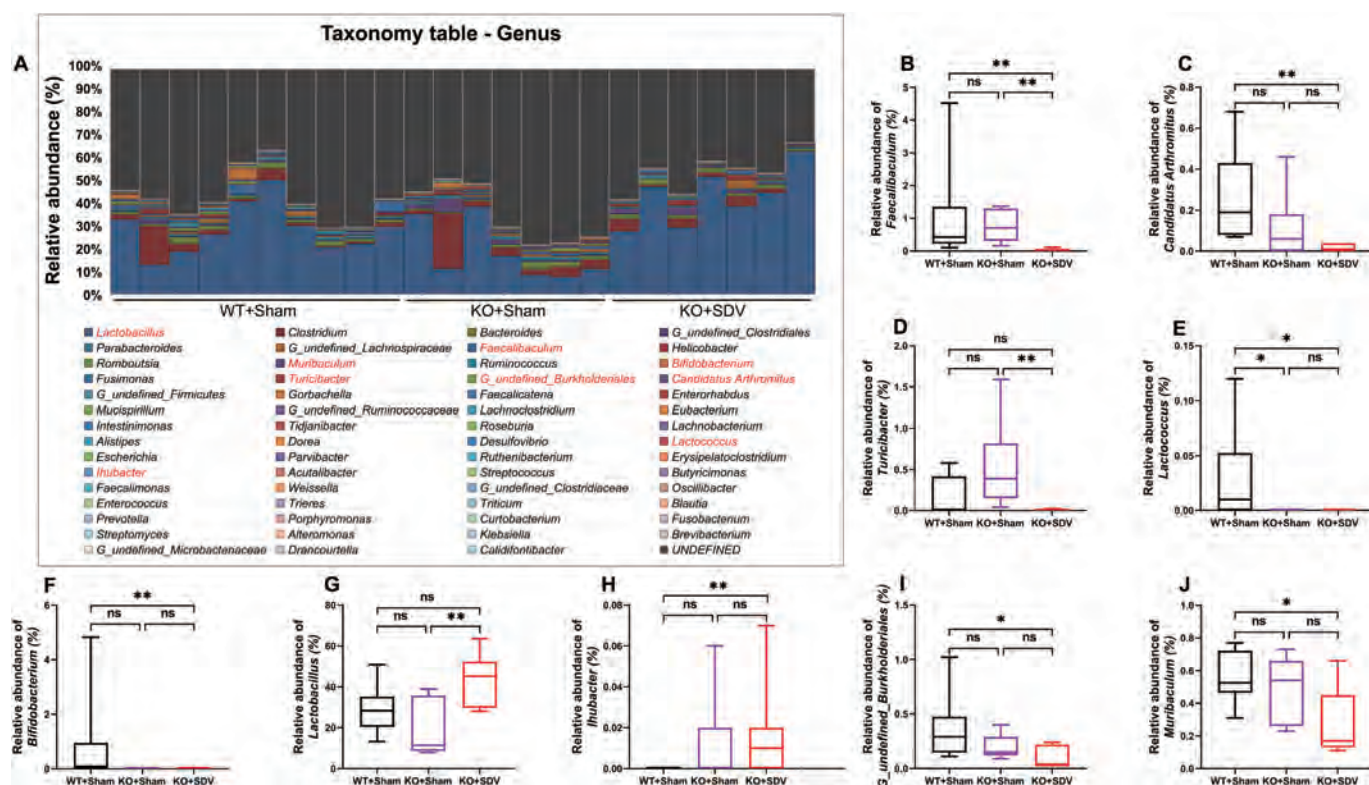β-diversity data among the three groups suggest that SDV is a driving

Fig. 5. Effects of bilateral SDV on gut microbiota at the genus levels.
(A): Gut bacteria composition at the genus level in the three groups. (B): Relative abundance of the genus *Faecalibaculum* (Kruskal-Wallis test, *P* = 0.0009). (C): Relative abundance of the genus *Candidatus Arthromitus* (Kruskal-Wallis test, *P* = 0.0021). (D): Relative abundance of the genus *Turicibacter* (Kruskal-Wallis test, *P* = 0.0030). (E): Relative abundance of the genus *Lactococcus* (Kruskal-Wallis test, P = 0.0053). (F): Relative abundance of the genus *Bifidobacterium* (Kruskal-Wallis test, *P* = 0.0086). (G): Relative abundance of the genus *Lactobacillus* (Kruskal-Wallis test, *P* = 0.0102). (H): Relative abundance of the genus *Ihubacter* (Kruskal-Wallis test, *P* = 0.0131). (I): Relative abundance of the genus *G_undefined_Burkholderiales* (Kruskal-Wallis test, *P* = 0.0132). (J): Relative abundance of the genus *Muribaculum* (Kruskal-Wallis test, *P* = 0.0395). For all box plots, the middle line in the box addresses the median, the box addresses the interquartile range, and the whisker addresses the most extreme and least values. *P < 0.05; **P < 0.01. ns: not significant.
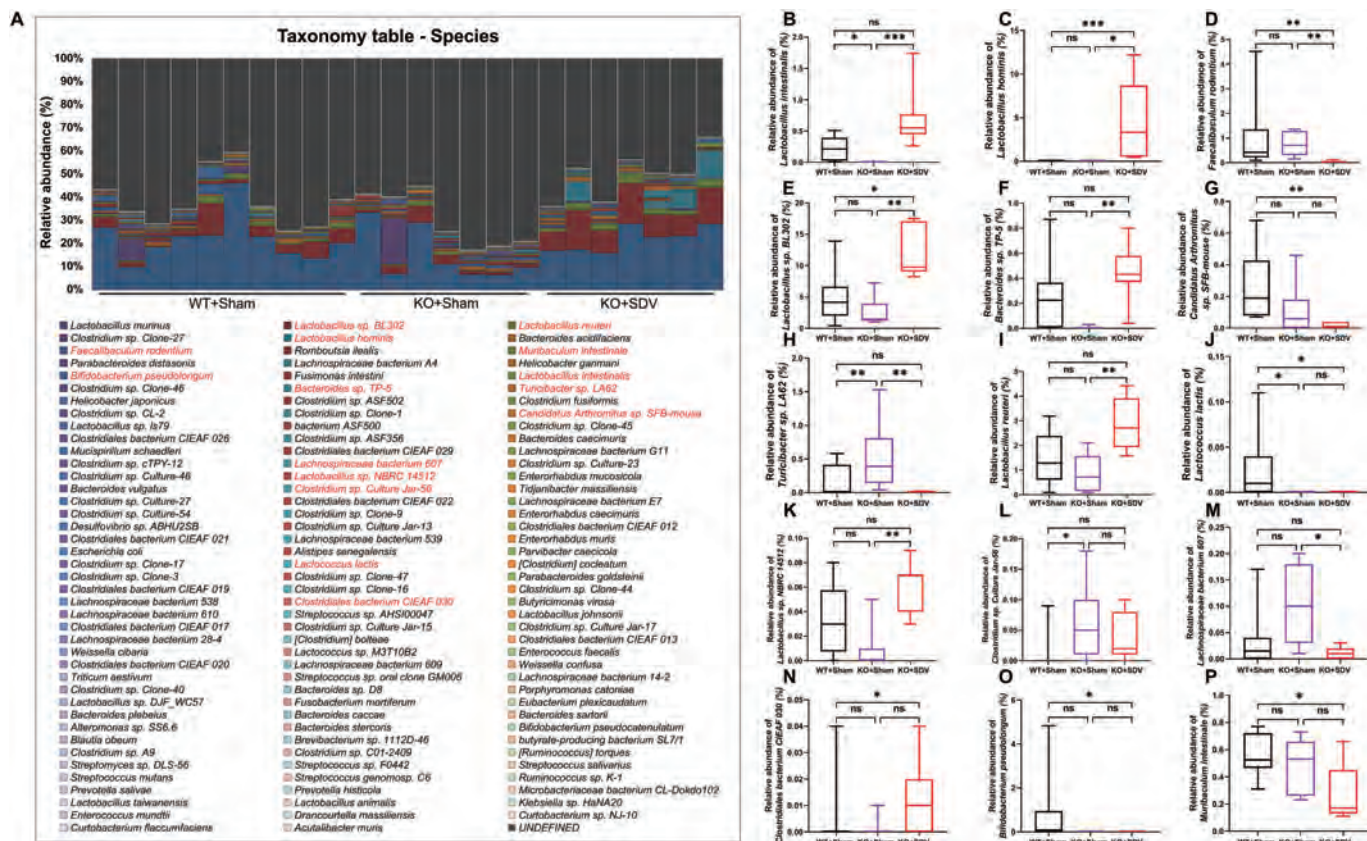
Fig. 6. Effects of bilateral SDV on gut microbiota at the species levels.
(A): Gut bacteria composition at the species level in the three groups. (B): Relative abundance of the species *Lactobacillus intestinalis* (Kruskal-Wallis test, *P* = 0.0001). (C): Relative abundance of the species *Lactobacillus hominis* (Kruskal-Wallis test, *P* = 0.0002). (D): Relative abundance of the species *Faecalibaculum rodentium* (Kruskal-Wallis test, P = 0.0009). (E): Relative abundance of the species *Lactobacillus* sp. BL302 (Kruskal-Wallis test, *P* = 0.0012). (F): Relative abundance of the species *Bacteroides* sp. *TP-5* (Kruskal-Wallis test, *P* = 0.0018). (G): Relative abundance of the species *Candidatus Arthromitus* sp. *SFB-mouse* (Kruskal-Wallis test, P = 0.0023). (H): Relative abundance of the species *Turicibacter* sp. *LA62* (Kruskal-Wallis test, *P* = 0.0030). (I): Relative abundance of the species *Lactobacillus reuteri* (Kruskal-Wallis test, *P* = 0.0047). (J): Relative abundance of the species *Lactococcus lactis* (Kruskal-Wallis test, *P* = 0.0053). (K): Relative abundance of the species *Lactobacillus* sp. *NBRC 14512* (Kruskal-Wallis test, *P* = 0.0088). (L): Relative abundance of the species *Clostridium* sp. *Culture Jar-56* (Kruskal-Wallis test, *P* = 0.0155). (M): Relative abundance of the species *Lachnospiraceae bacterium 607* (Kruskal-Wallis test, *P* = 0.0155). (N): Relative abundance of the species *Clostridiales bacterium CIEAF 030* (Kruskal-Wallis test, *P* = 0.0214). (O): Relative abundance of the species *Bifidobacterium pseudolongum* (Kruskal-Wallis test, *P* = 0.0245). (P): Relative abundance of the species *Muribaculum intestinale* (Kruskal-Wallis test, P = 0.0395). For all box plots, the middle line in the box addresses the median, the box addresses the interquartile range, and the whisker addresses the most extreme and least values. *P < 0.05; **P < 0.01; ***P < 0.001. ns: not significant.
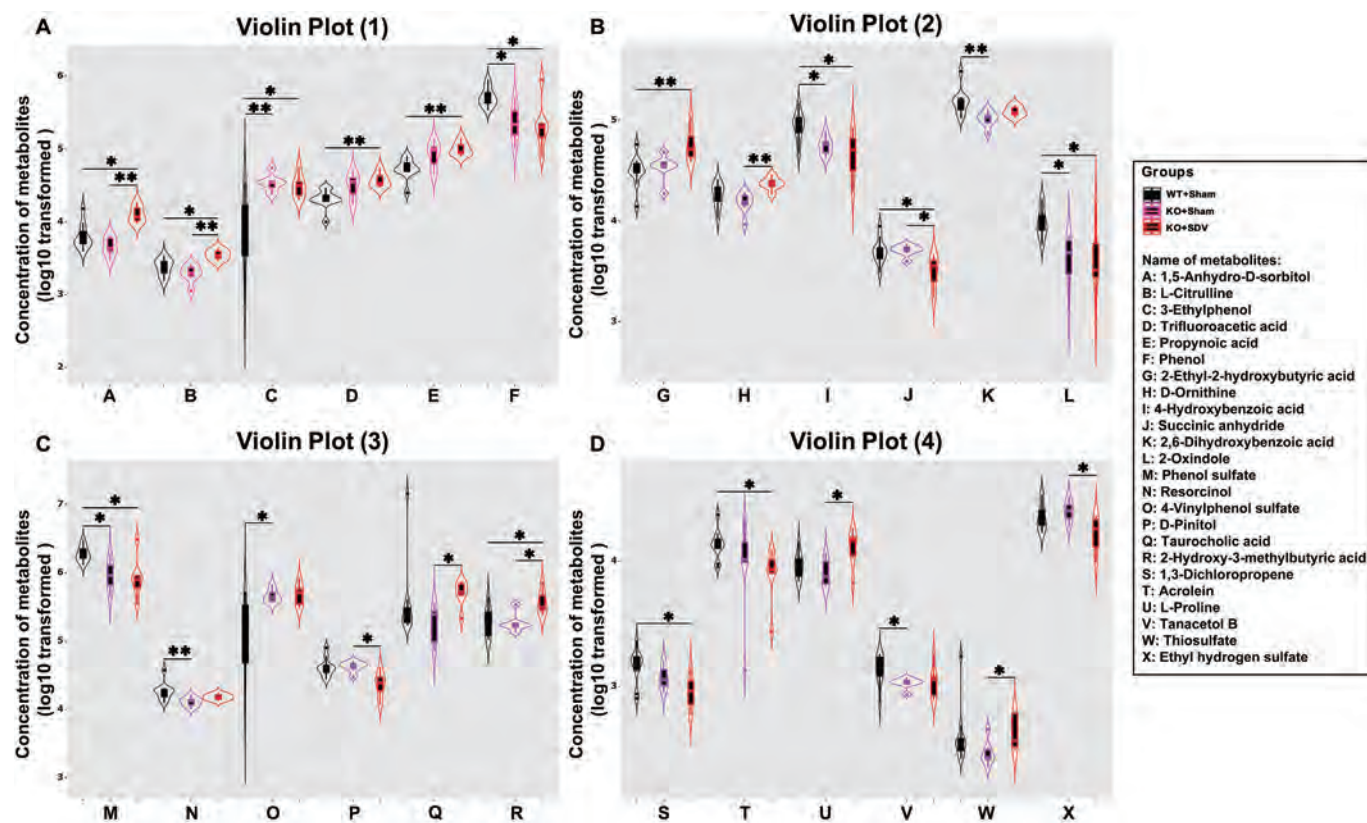
Fig. 7. Effect of bilateral SDV on plasma metabolites.

(A): Violin plot showing the changes of 6 kinds of metabolites [1,5-anhydro-D-sorbitol (Kruskal-Wallis test, $P = 0.0016$), L-citrulline (Kruskal-Wallis test, P = 0.0018), 3-ethylphenol (Kruskal-Wallis test, $P = 0.0019$), trifluoroacetic acid (Kruskal-Wallis test, $P = 0.0046$), propynoic acid (Kruskal-Wallis test, P = 0.0046), phenol (Kruskal-Wallis test, $P = 0.0055$)] among the three groups. (B): Violin plot showing the changes of 6 kinds of metabolites [2-ethyl-2-hydroxybutyric acid (Kruskal-Wallis test, $P = 0.0059$), D-ornithine (Kruskal-Wallis test, $P = 0.0065$), 4-hydroxybenzoic acid (Kruskal-Wallis test, $P = 0.0077$), succinic anhydride (Kruskal-Wallis test, $P = 0.0078$), 2,6-dihydroxybenzoic acid (Kruskal-Wallis test, $P = 0.0080$), 2-oxindole (Kruskal-Wallis test, P = 0.0080)] among the three groups. (C): Violin plot showing the changes of 6 kinds of metabolites [phenol sulfate (Kruskal-Wallis test, $P = 0.0080$), resorcinol (Kruskal-Wallis test, $P = 0.0111$), 4-vinylphenol sulfate (Kruskal-Wallis test, $P = 0.0113$), D-pinitol (Kruskal-Wallis test, $P = 0.0122$), taurocholic acid (Kruskal-Wallis test, $P = 0.0129$), 2-hydroxy-3-methylbutyric acid (Kruskal-Wallis test, $P = 0.0145$)] among the three groups. (D): Violin plot showing the changes of 6 kinds of metabolites [1,3-dichloropropene (Kruskal-Wallis test, $P = 0.0203$), acrolein (Kruskal-Wallis test, $P = 0.0209$), L-proline (Kruskal-Wallis test, P = 0.0245), tanacetol B (Kruskal-Wallis test, $P = 0.0321$), thiosulfate (Kruskal-Wallis test, $P = 0.0436$), ethyl hydrogen sulfate (Kruskal-Wallis test, $P = 0.0460$)] among the three groups. The X-axis using the letter symbol representing the names of different plasma metabolites, and the Y-axis represents the concentration of various plasma metabolites after log10 transformation. *P < 0.05; **P < 0.01; Different colors of violin plots represent the corresponding groups.

factor for the differential expression of structural similarity in microbial communities. We reported that LPS significantly decreased α-diversity and relative abundance of gut microbiota in mice, and that SDV did not cause LPS-induced alterations in α-diversity and relative abundance of gut microbiota in mice (Zhang et al., 2020), suggesting that LPS could cause depression-like behaviors in mice through gut–microbiota–brain axis via subdiaphragmatic vagus nerve. Furthermore, SDV blocked depression-like behaviors in mice after FMT from mice with depression-like behaviors (Pu et al., 2021b; Wang et al., 2020a; Wang et al., 2021). McVey Neufeld et al. (2019) reported that oral treatment with selective serotonin reuptake inhibitor (SSRI: fluoxetine or sertraline) leads to a significant increase in vagal fiber activity, and that blocking vagal signaling from the gut to the brain via SDV abolished antidepressant-like effect of SSRI, suggesting the role of vagus nerve dependent gut–brain axis in the antidepressant effects of SSRIs. From the current data, it is unclear whether subdiaphragmatic vagus nerve is responsible for depression-like phenotypes of *Chrna7* KO mice. A recent study demonstrated that SDV or genetic knock-out of α7 nAchRs abolished the anti-inflammatory actions of famotidine (a histamine 2 receptor antagonist) in mice with LPS-treated cytokine stream (Yang et al., 2022a), suggesting a role of vagus nerve anti-inflammation via α7 nAchRs. Given the crucial role of α7 nAchRs on vagus nerve inflammatory actions

(O'Mahony et al., 2009; Yang et al., 2022a), it is possible that sub-diaphragmatic vagus nerve may be responsible for depression-like phenotypes of *Chrna7* KO mice. Taken together, it is likely that gut–microbiota–brain axis via subdiaphragmatic vagus nerve plays an important role in depression-like phenotypes of *Chrna7* KO mice.

At the phylum level, the most abundant phylum *Firmicutes* was significantly increased in KO + SDV group compared to other two groups, suggesting that subdiaphragmatic vagus nerve may affect relative abundance of *Firmicutes* in gastrointestinal trait. At the species level, the relative abundance of *Lactobacillus intestinalis* and *Lactobacillus* sp. *BL302* in KO + SDV group was higher than that of KO + sham group. Furthermore, network analysis showed that these two bacteria were correlated with depression-like phenotypes and reduced synaptic proteins, suggesting a role of these two bacteria in depression. In contrast, the relative abundance of *Turicibacter* sp. *LA62* in KO + SDV group was lower than that of KO + sham group. A network analysis showed that *Turicibacter* sp. *LA62* was also correlated with depression-like phenotypes and reduced synaptic proteins. Collectively, it seems that *Lactobacillus intestinalis*, *Lactobacillus* sp. *BL302,* and *Turicibacter* sp. *LA62* might be associated with depression-like phenotypes although further study is needed.

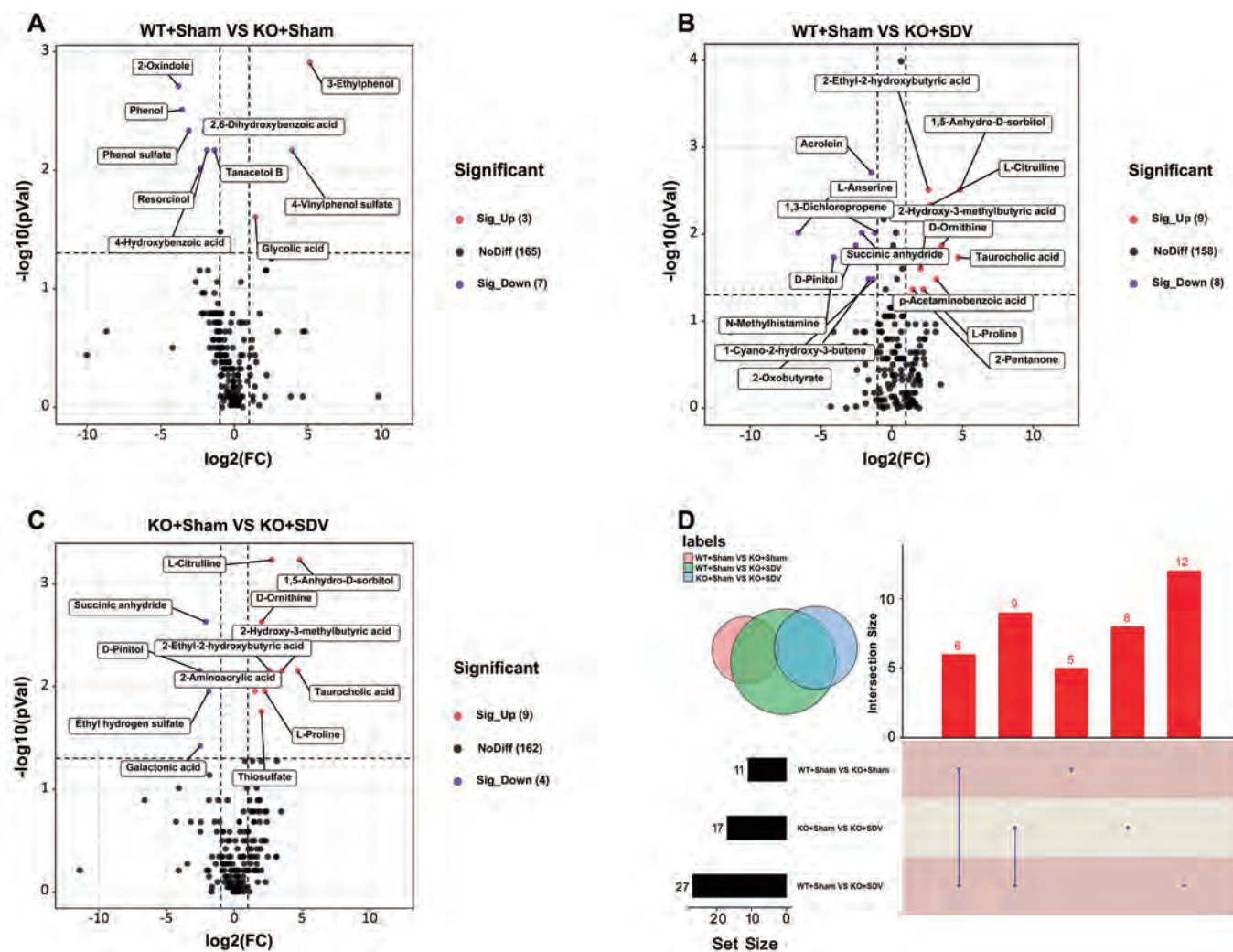Using untargeted metabolomics analysis, we found that plasma

Fig. 8. Differences of plasma metabolites between different experimental groups.

(A): Volcano plot indicating that 3 annotation metabolites were significantly up-regulated, 7 annotation metabolites were significantly down-regulated and 165 annotation metabolites were no differences when comparing the WT + sham group with the KO + sham group. (B): Volcano plot indicating that 9 annotation metabolites were significantly up-regulated, 8 annotation metabolites were significantly down-regulated and 158 annotation metabolites were no differences when comparing the WT + sham group with the KO + SDV group. (C): Volcano plot indicating that 9 annotation metabolites were significantly up-regulated, 4 annotation metabolites were significantly down-regulated and 162 annotation metabolites were no differences when comparing the KO + sham group with the KO + SDV group. The X-axis represents the log2-transformed values of the FC of plasma metabolite concentration, and the Y-axis represents the -log10-transformed values of P value using the Wilcoxon rank sum test. The horizontal dotted line indicates $P = 0.05$ and the vertical dotted line indicates FC = ± 2. Metabolites with up-regulated, down-regulated, and no difference were marked in red, purple, and black respectively. (D): UpSet plot listed out that there were 11 kinds of annotated metabolites with statistical differences between the WT + sham group and the KO + sham group, 17 kinds of annotated metabolites with statistical differences between the KO + sham group and the KO + SDV group, and 27 kinds of annotated metabolites with statistical differences between the WT + sham group and the KO + SDV group by using the Wilcoxon rank sum test (P<0.05). In addition, 6 kinds of annotated metabolites showed significant differences between the WT + Sham group and the KO + sham group and between the WT + sham group and the KO + SDV group, and 9 kinds of annotated metabolites showed significant differences between the KO + sham group and the KO + SDV group and between the WT + sham group and the KO + SDV group. Besides, 5 kinds of annotated metabolites showed significant differences only between the WT + sham group and the KO + sham group, 8 kinds of annotated metabolites showed significant differences only between the KO + sham group and the KO + SDV group, 12 kinds of annotated metabolites showed significant differences only between the WT + sham group and the KO + SDV group. (For interpretation of the references to colour in this figure legend, the reader is referred to the web version of this article.)

levels of 1,5-anhydro-D-sorbitol (also known as 1,5-anhydro-D-glucitol), L-citrulline, and taurocholic acid in the KO + SDV group were higher than those of KO + sham group. A network analysis showed that 1,5-anhydro-D-sorbitol was negatively correlated with *Faecalibaculum rodentium*, suggesting that *Faecalibaculum rodentium* may be involved in the synthesis of 1,5-anhydro-D-sorbitol. A report showed that low plasma levels of 1,5-anhydro-D-sorbitol are closely associated with impaired peripheral nerve function and diabetic peripheral neuropathy in patients with type 2 diabetes (Xu et al., 2022), suggesting that lower plasma levels of 1,5-anhydro-D-sorbitol may be a risk factor for diabetic

peripheral neuropathy. L-citrulline is a nitrogen end product produced from glutamine through urea cycle. Blood levels of L-citrulline and L-arginine in unmedicated patients with major depressive disorder (MDD) were significantly lower than healthy controls (Hess et al., 2017). MDD patients had a lower NOS (nitric oxide synthase) activity (L-citrulline/L-arginine ratio) than healthy controls at baseline (Loeb et al., 2020). NOS activity in MDD patients increased significantly after antidepressant treatment (Loeb et al., 2020), suggesting a state biomarker for depression. Furthermore, taurocholic acid (conjugation of cholic acid with taurine) was positively correlated with several bacteria including
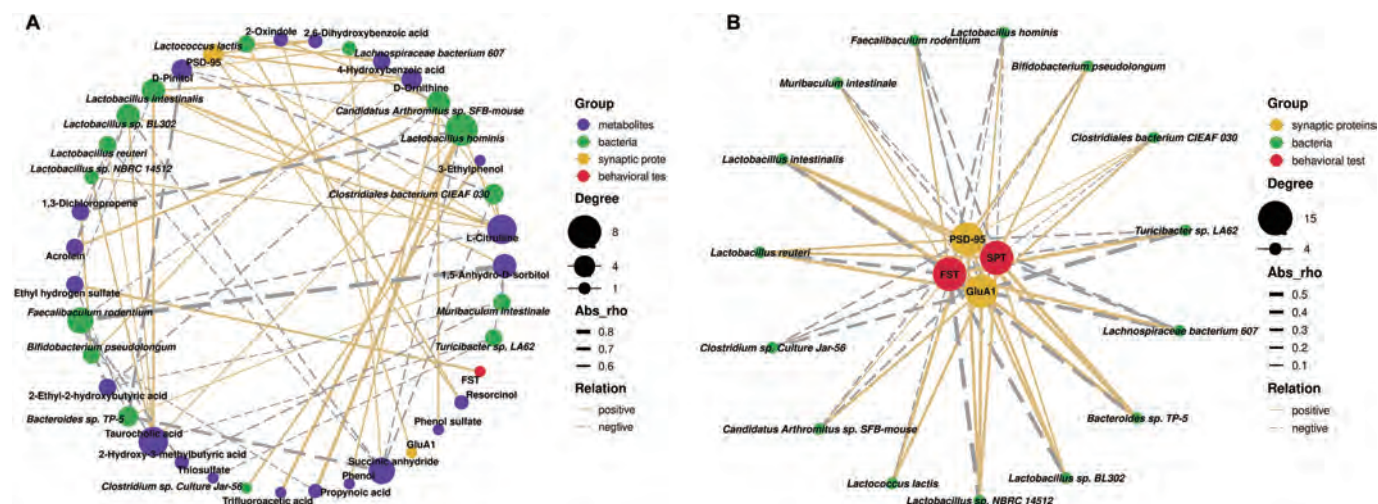
Fig. 9. Correlation network between behavioral data (or synaptic proteins) and microbiota (or metabolites).

(A): A Correlation Network indicating the correlations between the concentrations of plasma metabolites and the gut microbiota at the species level, the results of the behavioral test and the expression of synaptic proteins of mPFC (The threshold was set as P < 0.05 and the absolute value of $R \geq 0.5$. The different colors of nodes represent different groups. The sizes of node gradients represent varying degrees of correlation. The thickness of the line represents the absolute value of the correlation coefficient. Solid lines represent positive correlations, dotted lines represent negative correlations). (B): A Correlation Network showed correlations between the relative abundance of gut bacteria at the species level and the results of the behavioral test and the expression of synaptic proteins of mPFC (The threshold was set as P < 0.05. The different colors of nodes represent different groups. The sizes of node gradients represent varying degrees of correlation. The thickness of the line represents the absolute value of the correlation coefficient. Solid lines represent positive correlations, dotted lines represent negative correlations).

Lactobacillus intestinalis, suggesting that these bacteria may play a role in the production of taurocholic acid, major bile acid. Interestingly, there was a significant difference in blood levels of taurocholic acid between MDD patients and healthy controls (Bai et al., 2021). Given anti-inflammatory role of taurocholic acid, it is possible that higher levels of taurocholic acid may play a role in antidepressant-like effects of SDV in *Chrna7* KO mice. Succinic anhydride was negatively correlated with *Bacteroides* sp. *TP-5* which were associated with depression-like phenotypes. Collectively, it is likely that microbes-derived metabolites may play a role in the antidepressant-like effects of SDV in *Chrna7* KO mice.

A network analysis showed that *Lactobacillus intestinalis*, *Lactobacillus reuteri*, *Turicibacter* sp. *LA62*, and *Bacteroides* sp. *TP-5* were correlated with depression-like behaviors. There are no reports showing the role of *Turicibacter* sp. *LA62, and Bacteroides* sp. *TP-5* in depression. We reported that oral ingestion of *Lactobacillus intestinalis* and *Lactobacillus reuteri* caused depression-like phenotypes in antibiotic-treated mice through gut–microbiota–brain axis via subdiaphragmatic vagus nerve (Wang et al., 2020a). Furthermore, we reported that oral ingestion of *Faecalibaculum rodentium* caused depression-like phenotypes in resilient *Ephx2* KO mice through gut–microbiota–brain axis via subdiaphragmatic vagus nerve (Wang et al., 2021). Furthermore, *Faecalibaculum rodentium* was positively correlated with FST data, and negatively correlated with SPT data. These data suggest that *Faecalibaculum rodentium* might play a role in depression-like phenotypes. Collectively, it is likely that these bacteria might play a role in the antidepressant-like effects of SDV in *Chrna7* KO mice although further study is needed.

This study has the one limitation. The current data of this study do not show a direct role of gut microbiota in depression-like phenotypes of *Chrna7* KO mice although a previous study suggests a role of gut microbiota in depression-like phenotypes of *Chrna7* KO mice (Pu et al., 2021b). Further study to identify specific microbiomes which contribute to depression-like phenotypes of *Chrna7* KO mice is needed.

In conclusion, the current data show that SDV blocked depression-like behaviors and reduced synaptic proteins in the mPFC of *Chrna7* KO mice. Therefore, gut–microbiota–brain axis via subdiaphragmatic vagus nerve plays a role in depression-like phenotypes in *Chrna7* KO mice.

Data and code availability

The 16S rRNA sequencing data has been uploaded and saved in the NCBI Sequence Read Archive and is available at the accession number PRJNA845101.

Ethical statement

The experimental protocol of present study was approved by the Chiba University Institutional Animal Care and Use Committee (Permission number 3-399). The experimental mice were all firstly deeply anesthetized with inhaled isoflurane and then rapidly sacrificed by cervical dislocation. All efforts were made to minimize animals suffering.

CRediT authorship contribution statement

Yong Yang: Investigation, Data curation, Formal analysis, Writing – original draft, Writing – review Ā̀editing. **Akifumi Eguchi:** Investigation, Data curation, Formal analysis, Writing – review Ā̀editing. **Xiayun Wan:** Investigation, Writing – review Ā̀editing. **Lijia Chang:** Investigation, Writing – review Ā̀editing. **Xingming Wang:** Investigation, Writing – review Ā̀editing. **Youge Qu:** Investigation, Writing – review Ā̀ editing. **Chisato Mori:** Investigation, Funding acquisition, Writing – review Ā̀editing. **Kenji Hashimoto:** Conceptualization, Funding acquisition, Writing – original draft, Writing – review Ā̀editing.

Declaration of Competing Interest

Dr. Hashimoto is the inventor of filed patent applications on "The use of *R*-ketamine in the treatment of psychiatric diseases", "(*S*)-norketamine and salt thereof as pharmaceutical", "*R*-ketamine and derivative thereof as prophylactic or therapeutic agent for neurodegeneration disease or recognition function disorder", "Preventive or therapeutic agent and pharmaceutical composition for inflammatory diseases or bone diseases", and "*R*-ketamine and its derivatives as a preventive or therapeutic agent for a neurodevelopmental disorder" by the Chiba University. Dr. Hashimoto has also received speakers' honoraria, consultant fee, or research support from Abbott, Boehringer Ingelheim, Daiichi-Sankyo, Meiji Seika Pharma, Seikagaku Corporation, Dainippon-Sumitomo, Taisho, Otsuka, Murakami Farm and Perception Neuroscience. Other authors declare no conflict of interest.

Data availability

Data will be made available on request.

References

Andersson, U., Tracey, K.J., 2012. Reflex principles of immunological homeostasis. Annu. Rev. Immunol. 30, 313–335. https://doi.org/10.1146/annurev-immunol-020711-075015.

Bai, S., Xie, J., Bai, H., Tian, T., Zou, T., Chen, J.J., 2021. Gut microbiota-derived inflammation-related serum metabolites as potential biomarkers for major depressive disorder. J. Inflamm. Res. 14, 3755–3766. https://doi.org/10.2147/JIR.S324922.

Bartoli, F., Misiak, B., Callovini, T., Cavaleri, D., Cioni, R.M., Crocamo, C., Savitz, J.B., Carrà, G., 2021. The kynurenine pathway in bipolar disorder: a meta-analysis on the peripheral blood levels of tryptophan and related metabolites. Mol. Psychiatry 26 (7), 3419–3429. https://doi.org/10.1038/s41380-020-00913-1.

Bonaz, B., Bazin, T., Pellissier, S., 2018. The vagus nerve at the interface of the microbiota-gut-brain axis. Front. Neurosci. 12, 49. https://doi.org/10.3389/fnins.2018.00049.

Brydges, C.R., Bhattacharyya, S., Dehkordi, S.M., Milaneschi, Y., Penninx, B., Jansen, R., Kristal, B.S., Han, X., Arnold, M., Kastenmüller, G., Bekhbat, M., Mayberg, H.S., Craighead, W.E., Rush, A.J., Fiehn, O., Dunlop, B.W., Kaddurah-Daouk, R., Mood Disorders Precision Medicine Consortium, 2022. Metabolomic and inflammatory signatures of symptom dimensions in major depression. Brain Behav. Immun. 102, 42–52. https://doi.org/10.1016/j.bbi.2022.02.003.

Caso, J.R., MacDowell, K.S., González-Pinto, A., García, S., de Diego-Adeliño, J., Carceller-Sindreu, M., Sarramea, F., Caballero-Villarraso, J., Gracia-García, P., De la Cámara, C., Agüera, L., Gómez-Lus, M.L., Alba, C., Rodríguez, J.M., Leza, J.C., 2021. Gut microbiota, innate immune pathways, and inflammatory control mechanisms in patients with major depressive disorder. Transl. Psychiatry 11 (1), 645. https://doi.org/10.1038/s41398-021-01755-3.

Cawthon, C.R., de La Serre, C.B., 2018. Gut bacteria interaction with vagal afferents. Brain Res. 1693, 134–139. https://doi.org/10.1016/j.brainres.2018.01.012.

Chang, L., Wei, Y., Hashimoto, K., 2022. Brain-gut-microbiota axis in depression: a historical overview and future directions. Brain Res. Bull. 182, 44–56. https://doi.org/10.1016/j.brainresbull.2022.02.004.

Cryan, J.F., O'Riordan, K.J., Cowan, C.S.M., Sandhu, K.V., Bastiaanssen, T.F.S., Boehme, M., Codagnone, M.G., Cussotto, S., Fulling, C., Golubeva, A.V., Guzzetta, K.E., Jaggar, M., Long-Smith, C.M., Lyte, J.M., Martin, J.A., Molinero-Perez, A., Moloney, G., Morelli, E., Morillas, E., O'Connor, R., Cruz-Pereira, J.S., Peterson, V.L., Rea, K., Ritz, N.L., Sherwin, E., Spichak, S., Teichman, E.M., van de Wouw, M., Ventura-Silva, A.P., Wallace-Fitzsimons, S.E., Hyland, N., Clarke, G., Dinan, T.G., 2019. The microbiota-gut-brain axis. Physiol. Rev. 99 (4), 1877–2013. https://doi.org/10.1152/physrev.00018.2018.

Dani, J.A., 2015. Neuronal nicotinic acetylcholine receptor structure and function and response to nicotine. Int. Rev. Neurobiol. 124, 3–19. https://doi.org/10.1016/bs.irn.2015.07.001.

13

Dani, J.A., Bertrand, D., 2007. Nicotinic acetylcholine receptors and nicotinic cholinergic mechanisms of the central nervous system. Annu. Rev. Pharmacol. Toxicol. 47, 699–729. https://doi.org/10.1146/annurev.pharmtox.47.120505.105214.

Forsythe, P., Bienenstock, J., Kunze, W.A., 2014. Vagal pathways for microbiome-brain-gut axis communication. Adv. Exp. Med. Biol. 817, 115–133. https://doi.org/10.1007/978-1-4939-0897-4_5.

Haroon, E., Raison, C.L., Miller, A.H., 2012. Psychoneuroimmunology meets neuropsychopharmacology: translational implications of the impact of inflammation on behavior. Neuropsychopharmacology. 37 (1), 137–162. https://doi.org/10.1038/npp.2011.205.

Hashimoto, K., 2009. Emerging role of glutamate in the pathophysiology of major depressive disorder. Brain Res. Rev. 61 (2), 105–123. https://doi.org/10.1016/j.brainresrev.2009.05.005.

Hashimoto, K., 2015. Inflammatory biomarkers as differential predictors of antidepressant response. Int. J. Mol. Sci. 16 (4), 7796–7801. https://doi.org/10.3390/ijms16047796.

Hashimoto, K., 2020. Molecular mechanisms of the rapid-acting and long-lasting antidepressant actions of (*R*)-ketamine. Biochem. Pharmacol. 177, 113935 https://doi.org/10.1016/j.bcp.2020.113935.

Hashimoto, K., 2022. Gut–microbiota–brain by bile acids in depression. Psychiatry Clin. Neurosci. 76 (7), 281. https://doi.org/10.1111/pcn.13370.

Hess, S., Baker, G., Gyenes, G., Tsuyuki, R., Newman, S., Le Melledo, J.M., 2017. Decreased serum L-arginine and L-citrulline levels in major depression. Psychopharmacology 234 (21), 3241–3247. https://doi.org/10.1007/s00213-017-4712-8.

Huang, N., Hua, D., Zhan, G., Li, S., Zhu, B., Jiang, R., Yang, L., Bi, J., Xu, H., Hashimoto, K., Luo, A., Yang, C., 2019. Role of *Actinobacteria* and *Coriobacteriia* in the antidepressant effects of ketamine in an inflammation model of depression. Pharmacol. Biochem. Behav. 176, 93–100. https://doi.org/10.1016/j.pbb.2018.12.001.

Jiang, H., Ling, Z., Zhang, Y., Mao, H., Ma, Z., Yin, Y., Wang, W., Tang, W., Tan, Z., Shi, J., Li, L., Ruan, B., 2015. Altered fecal microbiota composition in patients with major depressive disorder. Brain Behav. Immun. 48, 186–194. https://doi.org/10.1016/j.bbi.2015.03.016.

Kelly, J.R., Borre, Y., O'Brien, C., Patterson, E., El Aidy, S., Deane, J., Kennedy, P.J., Beers, S., Scott, K., Moloney, G., Hoban, A.E., Scott, L., Fitzgerald, P., Ross, P., Stanton, C., Clarke, G., Cryan, J.F., Dinan, T.G., 2016. Transferring the blues: depression-associated gut microbiota induces neurobehavioural changes in the rat. J. Psychiatr. Res. 82, 109–118. https://doi.org/10.1016/j.jpsychires.2016.07.019.

Lei, W., Duan, Z., 2021. Advances in the treatment of cholinergic anti-inflammatory pathways in gastrointestinal diseases by electrical stimulation of vagus nerve. Digestion 102 (2), 128–138. https://doi.org/10.1159/000504474.

Li, Z., Lai, J., Zhang, P., Ding, J., Jiang, J., Liu, C., Huang, H., Zhen, H., Xi, C., Sun, Y., Wu, L., Wang, L., Gao, X., Li, Y., Fu, Y., Jie, Z., Li, S., Zhang, D., Chen, Y., Zhu, Y., Lu, S., Lu, J., Wang, D., Zhou, H., Yuan, X., Li, X., Pang, L., Huang, M., Yang, H., Zhang, W., Brix, S., Kristiansen, K., Song, X., Nie, C., Hu, S., 2022. Multi-omics analyses of serum metabolome, gut microbiome and brain function reveal dysregulated microbiota-gut-brain axis in bipolar depression. Mol. Psychiatry. https://doi.org/10.1038/s41380-022-01569-9.

Liu, J.J., Wei, Y.B., Strawbridge, R., Bao, Y., Chang, S., Shi, L., Que, J., Gadad, B.S., Trivedi, M.H., Kelsoe, J.R., Lu, L., 2020. Peripheral cytokine levels and response to antidepressant treatment in depression: a systematic review and meta-analysis. Mol. Psychiatry 25 (2), 339–350. https://doi.org/10.1038/s41380-019-0474-5.

Loeb, E., El Asmar, K., Trabado, S., Gressier, F., Colle, R., Rigal, A., Martin, S., Verstuyft, C., Fève, B., Chanson, P., Becquemont, L., Corruble, E., 2020. Nitric oxide synthase activity in major depressive episodes before and after antidepressant treatment: results of a large case-control treatment study. Psychol. Med. 1–10. https://doi.org/10.1017/S0033291720001749.

Lucido, M.J., Bekhbat, M., Goldsmith, D.R., Treadway, M.T., Haroon, E., Felger, J.C., Miller, A.H., 2021. Aiding and abetting anhedonia: impact of inflammation on the brain and pharmacological implications. Pharmacol. Rev. 73 (3), 1084–1117. https://doi.org/10.1124/pharmrev.120.000043.

Mac Giollabhui, N., Ng, T.H., Ellman, L.M., Alloy, L.B., 2021. The longitudinal associations of inflammatory biomarkers and depression revisited: systematic review, meta-analysis, and meta-regression. Mol. Psychiatry 26 (7), 3302–3314. https://doi.org/10.1038/s41380-020-00867-4.

Martelli, D., McKinley, M.J., McAllen, R.M., 2014. The cholinergic anti-inflammatory pathway: a critical review. Auton. Neurosci. 182, 65–69. https://doi.org/10.1016/j.autneu.2013.12.007.

McVey Neufeld, K.A., Bienenstock, J., Bharwani, A., Champagne-Jorgensen, K., Mao, Y., West, C., Liu, Y., Surette, M.G., Kunze, W., Forsythe, P., 2019. Oral selective serotonin reuptake inhibitors activate vagus nerve dependent gut-brain signalling. Sci. Rep. 9 (1), 14290. https://doi.org/10.1038/s41598-019-50807-8.

Miller, A.H., Raison, C.L., 2016. The role of inflammation in depression: from evolutionary imperative to modern treatment target. Nat. Rev. Immunol. 16 (1), 22–34. https://doi.org/10.1038/nri.2015.5.

Nikolova, V.L., Hall, M.R.B., Hall, L.J., Cleare, A.J., Stone, J.M., Young, A.H., 2021. Perturbations in gut microbiota composition in psychiatric disorders: a review and meta-analysis. JAMA Psychiatry 78 (12), 1343–1354. https://doi.org/10.1001/jamapsychiatry.2021.2573.

Olofsson, P.S., Rosas-Ballina, M., Levine, Y.A., Tracey, K.J., 2012. Rethinking inflammation: neural circuits in the regulation of immunity. Immunol. Rev. 248 (1), 188–204. https://doi.org/10.1111/j.1600-065X.2012.01138.x.

O'Mahony, C., van der Kleij, H., Bienenstock, J., Shanahan, F., O'Mahony, L., 2009. Loss of vagal anti-inflammatory effect: in vivo visualization and adoptive transfer. Am. J. Physiol. Regul. Integr. Comp. Physiol. 297 (4), R1118–R1126. https://doi.org/10.1152/ajpregu.90904.2008.

Park, A.J., Collins, J., Blennerhassett, P.A., Ghia, J.E., Verdu, E.F., Bercik, P., Collins, S.M., 2013. Altered colonic function and microbiota profile in a mouse model of chronic depression. Neurogastroenterol. Motil. 25 (9), 733–e575. https://doi.org/10.1111/nmo.12153.

Piovesana, R., Salazar Intriago, M.S., Dini, L., Tata, A.M., 2021. Cholinergic modulation of neuroinflammation: focus on α7 nicotinic receptor. Int. J. Mol. Sci. 22 (9), 4912. https://doi.org/10.3390/ijms22094912.

Pu, J., Liu, Y., Zhang, H., Tian, L., Gui, S., Yu, Y., Chen, X., Chen, Y., Yang, L., Ran, Y., Zhong, X., Xu, S., Song, X., Liu, L., Zheng, P., Wang, H., Xie, P., 2021a. An integrated meta-analysis of peripheral blood metabolites and biological functions in major depressive disorder. Mol. Psychiatry 26 (8), 4265–4276. https://doi.org/10.1038/s41380-020-0645-4.

Pu, Y., Tan, Y., Qu, Y., Chang, L., Wang, S., Wei, Y., Wang, X., Hashimoto, K., 2021b. A role of the subdiaphragmatic vagus nerve in depression-like phenotypes in mice after fecal microbiota transplantation from *Chrna7* knock-out mice with depression-like phenotypes. Brain Behav. Immun. 94, 318–326. https://doi.org/10.1016/j.bbi.2020.12.032.

Pu, Y., Zhang, Q., Tang, Z., Lu, C., Wu, L., Zhong, Y., Chen, Y., Hashimoto, K., Luo, Y., Liu, Y., 2022. Fecal microbiota transplantation from patients with rheumatoid arthritis causes depression-like behaviors in mice through abnormal T cells activation. Transl. Psychiatry 12 (1), 223. https://doi.org/10.1038/s41398-022-01993-z.

Qu, Y., Yang, C., Ren, Q., Ma, M., Dong, C., Hashimoto, K., 2017. Comparison of (*R*)-ketamine and lanicemine on depression-like phenotype and abnormal composition of gut microbiota in a social defeat stress model. Sci. Rep. 7 (1), 15725. https://doi.org/10.1038/s41598-017-16060-7.

Sanada, K., Nakajima, S., Kurokawa, S., Barceló-Soler, A., Ikuse, D., Hirata, A., Yoshizawa, A., Tomizawa, Y., Salas-Valero, M., Noda, Y., Mimura, M., Iwanami, A., Kishimoto, T., 2020. Gut microbiota and major depressive disorder: a systematic review and meta-analysis. J. Affect. Disord. 266, 1–13. https://doi.org/10.1016/j.jad.2020.01.102.

Schymanski, E.L., Jeon, J., Gulde, R., Fenner, K., Ruff, M., Singer, H.P., Hollender, J., 2014. Identifying small molecules via high resolution mass spectrometry: communicating confidence. Environ. Sci. Technol. 48 (4), 2097–2098. https://doi.org/10.1021/es5002105.

Segata, N., Izard, J., Waldron, L., Gevers, D., Miropolsky, L., Garrett, W.S., Huttenhower, C., 2011. Metagenomic biomarker discovery and explanation. Genome Biol. 12 (6), R60. https://doi.org/10.1186/gb-2011-12-6-r60.

Shan, J., Hashimoto, K., 2022. Soluble epoxide hydrolase as a therapeutic target for neuropsychiatric disorders. Int. J. Mol. Sci. 23 (9), 4951. https://doi.org/10.3390/ijms23094951.

Toenders, Y.J., Laskaris, L., Davey, C.G., Berk, M., Milaneschi, Y., Lamers, F., Penninx, B.W.J.H., Schmaal, L., 2022. Inflammation and depression in young people: a systematic review and proposed inflammatory pathways. Mol. Psychiatry 27 (1), 315–327. https://doi.org/10.1038/s41380-021-01306-8.

Tran, S.M., Mohajeri, M.H., 2021. The role of gut bacterial metabolites in brain development, aging and disease. Nutrients 13 (3), 732. https://doi.org/10.3390/nu13030732.

Tsugawa, H., Cajka, T., Kind, T., Ma, Y., Higgins, B., Ikeda, K., Kanazawa, M., VanderGheynst, J., Fiehn, O., Arita, M., 2015. MS-DIAL: data-independent MS/MS deconvolution for comprehensive metabolome analysis. Nat. Methods 12 (6), 523–526. https://doi.org/10.1038/nmeth.3393.

Ulloa, L., 2005. The vagus nerve and the nicotinic anti-inflammatory pathway. Nat. Rev. Drug Discov. 4 (8), 673–684. https://doi.org/10.1038/nrd1797.

Wan, X., Eguchi, A., Fujita, Y., Ma, L., Wang, X., Yang, Y., Qu, Y., Chang, L., Zhang, J., Mori, C., Hashimoto, K., 2022a. Effects of (*R*)-ketamine on reduced bone mineral density in ovariectomized mice: a role of gut microbiota. Neuropharmacol. 213, 109139 https://doi.org/10.1016/j.neuropharm.2022.109139.

Wan, X., Eguchi, A., Qu, Y., Yang, Y., Chang, L., Shan, J., Mori, C., Hashimoto, K., 2022b. Gut–microbiota–brain axis in the vulnerability to psychosis in adulthood after repeated cannabis exposure during adolescence. Eur. Arch. Psychiatry Clin. Neurosci. 272 (7), 1297–1309. https://doi.org/10.1007/s00406-022-01437-1.

Wang, H., Yu, M., Ochani, M., Amella, C.A., Tanovic, M., Susarla, S., Li, J.H., Wang, H., Yang, H., Ulloa, L., Al-Abed, Y., Czura, C.J., Tracey, K.J., 2003. Nicotinic acetylcholine receptor α7 subunit is an essential regulator of inflammation. Nature. 421 (6921), 384–388. https://doi.org/10.1038/nature01339.

Wang, S., Ishima, T., Zhang, J., Qu, Y., Chang, L., Pu, Y., Fujita, Y., Tan, Y., Wang, X., Hashimoto, K., 2020a. Ingestion of *Lactobacillus intestinalis* and *Lactobacillus reuteri* causes depression- and anhedonia-like phenotypes in antibiotic-treated mice via the vagus nerve. J. Neuroinflammation 17 (1), 241. https://doi.org/10.1186/s12974-020-01916-z.

Wang, S., Qu, Y., Chang, L., Pu, Y., Zhang, K., Hashimoto, K., 2020b. Antibiotic-induced microbiome depletion is associated with resilience in mice after chronic social defeat stress. J. Affect. Disord. 260, 448–457. https://doi.org/10.1016/j.jad.2019.09.064.

Wang, S., Ishima, T., Qu, Y., Shan, J., Chang, L., Wei, Y., Zhang, J., Pu, Y., Fujita, Y., Tan, Y., Wang, X., Ma, L., Wan, X., Hammock, B.D., Hashimoto, K., 2021. Ingestion of *Faecalibaculum rodentium* causes depression-like phenotypes in resilient *Ephx2* knock-out mice: a role of brain-gut-microbiota axis via the subdiaphragmatic vagus nerve. J. Affect. Disord. 292, 565–573. https://doi.org/10.1016/j.jad.2021.06.006.

Wei, Y., Chang, L., Hashimoto, K., 2022a. Molecular mechanisms underlying the antidepressant actions of arketamine: beyond the NMDA receptor. Mol. Psychiatry 27 (1), 559–573. https://doi.org/10.1038/s41380-021-01121-1.

14

Wei, Y., Wang, T., Liao, L., Fan, X., Chang, L., Hashimoto, K., 2022b. Brain-spleen axis in health and diseases: a review and future perspective. Brain Res. Bull. 182, 130–140. https://doi.org/10.1016/j.brainresbull.2022.02.008.

WHO, 2021. Depression. https://www.who.int.news-room/fact-sheets/default/depression.

Wong, M.L., Inserra, A., Lewis, M.D., Mastronardi, C.A., Leong, L., Choo, J., Kentish, S., Xie, P., Morrison, M., Wesselingh, S.L., Rogers, G.B., Licinio, J., 2016. Inflammasome signaling affects anxiety- and depressive-like behavior and gut microbiome composition. Mol. Psychiatry 21 (6), 797–805. https://doi.org/10.1038/mp.2016.46.

Wu, Y.J., Wang, L., Ji, C.F., Gu, S.F., Yin, Q., Zuo, J., 2021. The role of α7 nAChR-mediated cholinergic anti-inflammatory pathway in immune cells. Inflammation. 44 (3), 821–834. https://doi.org/10.1007/s10753-020-01396-6.

Xu, F., Zhao, L.H., Wang, X.H., Wang, C.H., Yu, C., Zhang, X.L., Ning, L.Y., Huang, H.Y., Su, J.B., Wang, X.Q., 2022. Plasma 1,5-anhydro-D-glucitol is associated with peripheral nerve function and diabetic peripheral neuropathy in patients with type 2 diabetes and mild-to-moderate hyperglycemia. Diabetol. Metab. Syndr. 14 (1), 24. https://doi.org/10.1186/s13098-022-00795-z.

Yang, C., Shirayama, Y., Zhang, J.C., Ren, Q., Yao, W., Ma, M., Dong, C., Hashimoto, K., 2015. R-ketamine: a rapid-onset and sustained antidepressant without psychotomimetic side effects. Transl. Psychiatry 5 (9), e632. https://doi.org/10.1038/tp.2015.136.

Yang, C., Qu, Y., Fujita, Y., Ren, Q., Ma, M., Dong, C., Hashimoto, K., 2017. Possible role of the gut microbiota-brain axis in the antidepressant effects of (R)-ketamine in a social defeat stress model. Transl. Psychiatry 7 (12), 1294. https://doi.org/10.1038/s41398-017-0031-4.

Yang, C., Fang, X., Zhan, G., Huang, N., Li, S., Bi, J., Jiang, R., Yang, L., Miao, L., Zhu, B., Luo, A., Hashimoto, K., 2019. Key role of gut microbiota in anhedonia-like phenotype in rodents with neuropathic pain. Transl. Psychiatry 9 (1), 57. https://doi.org/10.1038/s41398-019-0379-8.

Yang, H., George, S.J., Thompson, D.A., Silverman, H.A., Tsaava, T., Tynan, A., Pavlov, V.A., Chang, E.H., Andersson, U., Brines, M., Chavan, S.S., Tracey, K.J., 2022a. Famotidine activates the vagus nerve inflammatory reflex to attenuate cytokine storm. Mol. Med. 28 (1), 57. https://doi.org/10.1186/s10020-022-00483-8.

Yang, Y., Ishima, T., Wan, X., Wei, Y., Chang, L., Zhang, J., Qu, Y., Hashimoto, K., 2022b. Microglial depletion and abnormalities in gut microbiota composition and short-chain fatty acids in mice after repeated administration of colony stimulating factor 1 receptor inhibitor PLX5622. Eur. Arch. Psychiatry Clin. Neurosci. 272 (3), 483–495. https://doi.org/10.1007/s00406-021-01325-0.

Zhang, J.C., Wu, J., Fujita, Y., Yao, W., Ren, Q., Yang, C., Li, S.X., Shirayama, Y., Hashimoto, K., 2014. Antidepressant effects of TrkB ligands on depression-like behavior and dendritic changes in mice after inflammation. Int. J. Neuropsychopharmacol. 18 (4), pyu077. https://doi.org/10.1093/ijnp/pyu077.

Zhang, J.C., Yao, W., Hashimoto, K., 2016a. Brain-derived neurotrophic factor (BDNF)-TrkB signaling in inflammation-related depression and potential therapeutic targets. Curr. Neuropharmacol. 14 (7), 721–731. https://doi.org/10.2174/1570159x14666160119094646.

Zhang, J.C., Yao, W., Ren, Q., Yang, C., Dong, C., Ma, M., Wu, J., Hashimoto, K., 2016b. Depression-like phenotype by deletion of α7 nicotinic acetylcholine receptor: role of BDNF-TrkB in nucleus accumbens. Sci. Rep. 6, 36705. https://doi.org/10.1038/srep36705.

Zhang, J.C., Yao, W., Dong, C., Yang, C., Ren, Q., Ma, M., Hashimoto, K., 2017. Blockade of interleukin-6 receptor in the periphery promotes rapid and sustained antidepressant actions: a possible role of gut-microbiota-brain axis. Transl. Psychiatry 7 (5), e1138. https://doi.org/10.1038/tp.2017.112.

Zhang, K., Fujita, Y., Chang, L., Qu, Y., Pu, Y., Wang, S., Shirayama, Y., Hashimoto, K., 2019. Abnormal composition of gut microbiota is associated with resilience versus susceptibility to inescapable electric stress. Transl. Psychiatry 9 (1), 231. https://doi.org/10.1038/s41398-019-0571-x.

Zhang, J., Ma, L., Chang, L., Pu, Y., Qu, Y., Hashimoto, K., 2020. A key role of the subdiaphragmatic vagus nerve in the depression-like phenotype and abnormal composition of gut microbiota in mice after lipopolysaccharide administration. Transl. Psychiatry 10 (1), 186. https://doi.org/10.1038/s41398-020-00878-3.

Zheng, P., Zeng, B., Zhou, C., Liu, M., Fang, Z., Xu, X., Zeng, L., Chen, J., Fan, S., Du, X., Zhang, X., Yang, D., Yang, Y., Meng, H., Li, W., Melgiri, N.D., Licinio, J., Wei, H., Xie, P., 2016. Gut microbiome remodeling induces depressive-like behaviors through a pathway mediated by the host's metabolism. Mol. Psychiatry 21 (6), 786–796. https://doi.org/10.1038/mp.2016.44.

Repeated use of 3,4-methylenedioxymethamphetamine is associated with the resilience in mice after chronic social defeat stress: A role of gut–microbiota–brain axis

Youge Qu [a], Akifumi Eguchi [b], Xiayun Wan [a], Li Ma [a], Lijia Chang [a], Jiajing Shan [a], Yong Yang [a], Chisato Mori [b,c], Kenji Hashimoto [a,*]

[a] *Division of Clinical Neuroscience, Chiba University Center for Forensic Mental Health, Chiba 260-8670, Japan*
[b] *Department of Sustainable Health Science, Chiba University Center for Preventive Medical Sciences, Chiba 263-8522, Japan*
[c] *Department of Bioenvironmental Medicine, Graduate School of Medicine, Chiba University, Chiba 260-8670, Japan*

ARTICLE INFO

ABSTRACT

3,4-Methylenedioxymethamphetamine (MDMA), the most widely used illicit compound worldwide, is the most attractive therapeutic drug for post-traumatic stress disorder (PTSD). Recent observational studies of US adults demonstrated that lifetime MDMA use was associated with lower risk of depression. Here, we examined whether repeated administration of MDMA can affect resilience versus susceptibility in mice exposed to chronic social defeat stress (CSDS). CSDS produced splenomegaly, anhedonia-like phenotype, and higher plasma levels of interleukin-6 (IL-6) in the saline-treated mice. In contrast, CSDS did not cause these changes in the MDMA-treated mice. Analysis of gut microbiome found several microbes altered between saline + CSDS group and MDMA + CSDS group. Untargeted metabolomics analysis showed that plasma levels of N-epsilon-methyl-L-lysine in the saline + CSDS group were significantly higher than those in the control and MDMA + CSDS groups. Interestingly, there were positive correlations between plasma IL-6 levels and the abundance of several microbes (or plasma N-epsilon-methyl-L-lysine) in the three groups. Furthermore, there were also positive correlations between the abundance of several microbes and N-epsilon-methyl-L-lysine in the three groups. In conclusion, these data suggest that repeated administration of MDMA might contribute to stress resilience in mice subjected to CSDS through gut–microbiota–brain axis.

1. Introduction

3,4-Methylenedioxymetahmphetamine (MDMA; ecstasy), a synthetic ring-substituted methamphetamine, is one of the most widely used recreational drugs in the world since it can produce the subjective prosocial feeling, the enhancement of empathy and sociability (Boote, 2018; Dunlap et al., 2018; Nutt, 2019; Parrott et al., 2017). A recent observational study using a large nationally representative sample of US adults (n = 213,437) demonstrated that lifetime MDMA use was associated with lower risk of depression (Jones and Nock, 2022b). Furthermore, a new study using US adults (n = 484,732) demonstrated that lifetime MDMA use was associated with lowered odds of psychological distress and suicidal thoughts (Jones and Nock, 2022a).

Moreover, another study using US representative sample of noninstitutionalized adults (n = 241,675) from 2015 - 2020 National Survey on Drug Use and Health showed that MDMA use was associated with a decreased likelihood of serious psychological distress, major depressive episode, and suicidal thinking whereas the use of the hallucinogen LSD (lysergic acid diethylamide) was associated with an increased likelihood of major depressive episode and suicidal thinking (Yang et al., 2022). Taken together, it is likely that lifetime use of MDMA in adults is associated with lower risk of depression, although the reasons underlying the relationship between lifetime MDMA use and resilience remain unclear.

Therapeutic potential of MDMA for post-traumatic stress disorder (PTSD) has attracted a lot of interest from the scientific community (Feduccia et al., 2018; Hoskins et al., 2021; Reiff et al., 2020; Smith

et al., 2022; Tedesco et al., 2021). Mithoefer et al. (2011; 2018) demonstrated a significant efficacy of MDMA-assisted psychotherapy for chronic PTSD patients. A recent randomized, double-blind, placebo-controlled phase 3 trial showed that MDMA could produce significant and robust reduction in PTSD symptoms in severe PTSD patients compared with placebo (Mitchell et al., 2021). However, the precise mechanisms underlying MDMA's beneficial effects for PTSD symptoms remain to be elucidated.

Gut–microbiota–brain axis consists of bidirectional communication between the gastrointestinal (GI) tract and the brain (Chang et al., 2022; Cryan et al., 2019; Góralczyk-Bińkowska et al., 2022; Wei et al., 2022b). Multiple lines of evidence suggest that gut–microbiota–brain axis may contribute to resilience versus susceptibility in rodents after repeated stress (Bailey et al., 2011; Cathomas et al., 2019; Szyszkowicz et al., 2017; Wang et al., 2020a, 2021; ; Wei et al., 2022a, 2022b; Yang et al., 2017, 2019; Zhang et al., 2017, 2019). We previously reported higher levels of *Bifidobacterium* in the resilient mice compared with susceptible mice after chronic social defeat stress (CSDS), and oral supplementation with *Bifidobacterium* produced resilience in mice exposed to CSDS (Yang et al., 2017). Furthermore, antibiotic-induced microbiome depletion confers stress resilience in mice after CSDS, suggesting a role of microbiome in stress resilience (Wang et al., 2020a). Moreover, repeated oral administration of betaine produced stress resilience in mice after CSDS through gut–microbiota–brain axis (Qu et al., 2020). In addition, Zhang et al. (2019) reported that abnormal composition of gut microbiota is associated with resilience versus susceptibility to inescapable electric stress in a learned helplessness model. Taken all together, it is likely that gut–microbiota–brain axis might play a crucial role in resilience versus susceptibility in rodents exposed to stress. At present, there are no articles reporting a role of gut–microbiota–brain axis in beneficial effects of MDMA.

The serotonin (5-hydroxytryptamine: 5-HT) system in the body plays an important role in the mechanisms of action of MDMA (Green et al., 2003; Schenk and Highgate, 2021). In addition of inhibition for 5-HT transporter, MDMA causes excessive release of 5-HT, and it has less potent effects of other neurotransmitters such as dopamine and norepinephrine. Importantly, approximately 95% of 5-HT in the body is synthesized and secreted by enterochromaffin cells in the GI tract (Liu et al., 2021; Mawe and Hoffman, 2013; Shine et al., 2022). From the current findings, we have a hypothesis that 5-HT in the GI tract may play a role in beneficial actions of MDMA.

The present study was undertaken to examine whether repeated administration of MDMA contributes to resilience in mice after subsequent CSDS. First, we examined anhedonia-like phenotype using sucrose preference test since anhedonia is a core symptom of stress-related disorders such as depression (Pizzagalli, 2014). As the auxiliary analysis, we examined the role of gut–microbiota–brain axis including microbes-derived metabolites in the stress resilience after MDMA administration since gut microbiota might play a role in stress resilience.

2. Materials and methods

2.1. Animals

Both male adult CD1 (ICR) mice, aged 13 weeks (body weight >40 g), and male adult C57BL/6 mice, aged 7 weeks (body weight 20–25 g), were purchased from Japan SLC, Inc. (Hamamatsu, Japan). The animals were kept in controlled environments with water and food available at all times, as well as 12-hour light/dark cycles (lights on between 07:00 and 19:00 h). The Institutional Animal Care and Use Committee at Chiba University approved the experimental protocol of the study (Permission number: 4-349). The guidelines of the National Institutes of Health's Guide for the Care and Use of Laboratory Animals were strictly followed when conducting this investigation. Every attempt was made to reduce pain.

2.2. MDMA, CSDS, collection of fecal samples, behavioral test, and collection of samples

MDMA hydrochloride was synthesized from 3,4-methylenedioxy-phenyl-2-propanone and methylamine by the one (K.H.) of the authors. Three groups such as saline + control (no CSDS) group (n = 10), saline + CSDS group (n = 9), and MDMA + CSDS group (n = 7) were used in the experiment. Saline (10 ml/kg/day) or MDMA (10 mg/kg/day as hydrochloride salt) was administered intraperitoneally (i.p.) to mice for 14 days (day 1–day 14) (Fig. 1**A**). The dose (10 mg/kg) of MDMA was used as previous reported (Zhang et al., 2006). Subsequently, CSDS was carried out for 10 days (day 15–day 24) (Fig. 1**A**), as previously described (Qu et al., 2017, 2020; Wang et al., 2020a). The C57BL/6 mice were exposed to a different CD1 aggressor mouse for 10 min each day for a total of 10 days (day 15–day 24). The resident CD1 mouse and the invader mouse were kept in one half of the cage after the social defeat session concluded, separated by a perforated Plexiglas divider to allow visual, olfactory, and auditory interaction for the remaining 24 h.

At 24 h after the last session, all mice were housed individually. To minimize circadian impacts on the microbiota, we collected fecal samples from each mouse at around 10:00 on day 25 (Fig. 1**A**). When each mouse was put in a fresh and clean cage, we collected fecal samples. Immediately following defecation, the fecal samples were placed in a sterile screw-cap microtube, where they were kept until use at -80 °C.

On day 27, sucrose preference test (SPT: one % sucrose and water) was performed from 17:00 to 18:00, to examine anhedonia-like phenotype. Mice were given access to the sucrose solution 48 h before to the test in order to acclimate them to the 1% sucrose solution before verifying the change in sucrose solution consumption. Then, after going without food and water for 4 h, the subjects were exposed for an hour to either water or a 1% sucrose solution in one of two identical bottles. The bottles were weighed both before and just after the test. The ratio of sucrose solution ingestion to total liquid consumption was used to calculate the sucrose preference.

On day 28, blood was collected from heart under inhaled isoflurane (2–5%) anesthesia and placed into a tube containing ethylenediamine-*N,N,N',N'*-tetraacetic acid potassium salt dehydrate as an anticoagulant. Then plasma samples were collected after centrifugation, and stored at -80 °C before the use. In addition, mouse spleen was removed and weighted.

2.3. ELISA measurement of pro-inflammatory cytokine IL-6

Plasma levels of interleukin-6 (IL-6) were measured, since CSDS susceptible mice have higher blood levels of IL-6 (Qu et al., 2020; Wang et al., 2020a; Zhang et al., 2017). The mouse IL-6 ELISA kit (Invitrogen, Tokyo, Japan. catalog number: 88-7064-22) was used to measure the plasma levels of IL-6.

2.4. 16S rRNA analysis

NucleoSpin^{ÃÄ} DNA Stool (Macherey-Nagel. catalog number: U0472C) was used to extract DNA from fecal samples.16S rRNA analysis of fecal samples was performed at BGI Japan (Kobe, Japan). The FastPrep-24 5G homogenizer was used to dissolve the fecal samples while they were suspended in a solution containing 4M guanidium thiocyanate, 100 mM Tris-HCl (pH 9.0), and 40 mM EDTA (MP Biomedicals, Irvine, CA). Following that, GENE PREP STAR PI-480 was used to extract the DNA from the solution after bead treatment (KURABO, Tokyo, Japan). The DNA sample's final concentration was changed to 10 ng/L. One sample of control (saline + no CSDS) group was not used for subsequent 16S rRNA analysis since the DNA purity was not good. In a nutshell, PCR was used to amplify the V3-V4 hypervariable regions of the 16S rRNA from microbial genomic DNA using the dual-index approach and bacterial universal primers (341F/R806). Following an approach that has already been disclosed, bioinformatics analysis was
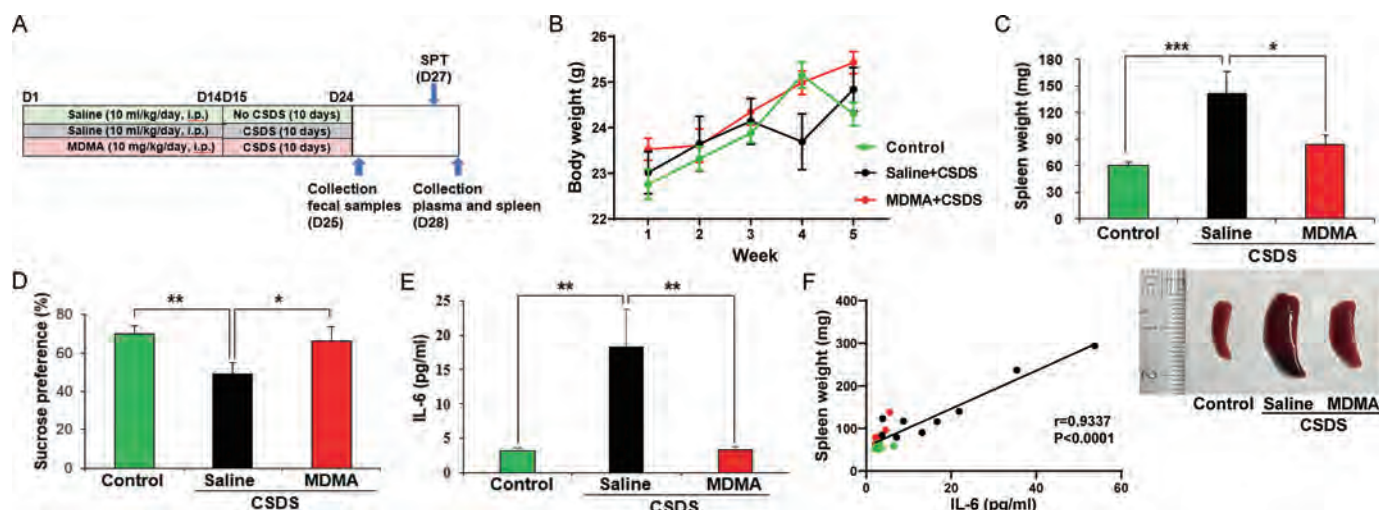
2

Fig. 1. Effects of MDMA on splenomegaly, anhedonia-like phenotype and blood levels of IL-6 in mice after CSDS. (**A**): The schedule of repeated administration of MDMA, CSDS model, feces collection, sucrose preference test, and collection of plasma and spleen. Saline (10 ml/kg/day) or MDMA (10 mg/kg/day) was given to adult mice from day 1 to day 14. Subsequently, CSDS was performed for 10 days (day 15–day 24). On day 25, fresh feces were collected. On day 26, one % SPT was performed, and plasma and spleen were collected on day 28. (**B**): Body weight (repeated measure two-way ANOVA, treatment: $F_{2,115} = 2.454$, P = 0.0904, time: $F_{4,115} = 10.28$, P < 0.0001, interaction: $F_{8,115} = 1.346$, P = 0.2282). (**C**): Spleen weight (one-way ANOVA, $F_{2,23} = 7.617$, P = 0.003). Representative photograph of spleen in the three groups. (**D**): One % SPT (one-way ANOVA, $F_{2,23} = 4.298$, P = 0.026). (**E**): Plasma IL-6 levels (one-way ANOVA, $F_{2,23} = 6.790$, P = 0.005). Data are shown as mean ± S.E.M (n = 7-10). *P < 0.05, **PP < 0.01, ***PP < 0.001. (**E**): There was a positive correlation (r = 0.9337, P < 0.0001) between spleen weight and plasma IL-6.

carried out. The fastq-join application was used to integrate the overlapping paired-end readings using its default parameters. The readings underwent the following quality and chimera screening processes. Usearch6.1 was used to eliminate chimeric sequences and only extract reads with quality value scores of 20 for >99% of the sequence. For 16S rDNA-based taxonomy analysis, non-chimeric data were submitted using the Ribosomal Database Project (RDP) Multiclassifier program. With an 80% confidence criterion, reads acquired in the multi-FASTA format were categorized at the genus or phylum level. α-diversity analyses, including Observed_OTU, Chao, Ace and Shannon, were used to reflect the abundance and diversity of the microbial community. The similarity or dissimilarity of three groups was assessed by β-diversity analysis including principal components analysis (PCA).

Linear discriminant analysis (LDA) effect size (LEfSe) was used for identifying certain bacteria as potential microbial biomarkers discovery. Microbiota-based potential biomarker discoveries were performed with LEfSe using the online galaxy platform (Segata et al., 2011). The LDA scores (LDA > 3.0 and P < 0.05) derived from LEfSe analysis were considered significantly to be enriched or deficient bacterial taxa in the intestinal microbiota among the three groups.

2.5. Untargeted metabolomics analysis

Untargeted metabolomics profiles from plasm samples were analyzed by using ultra-performance liquid chromatography-tandem quadruple time-of-flight mass spectrometry (UPLC-QTOF/MS) technique, as previously reported (Wan et al., 2022a; 2022b; Yang et al., 2023). With the help of R statistical environment Ver 4.0.5. and Mass Spectrometry-Data Independent AnaLysis (MS-DIAL) software version 4.60 (Tsugawa et al., 2015), metabolomics data were analyzed. Metabolites were detected at least 50% from the analyzed samples and the coefficient of variation (CV) values of 30% of metabolites in pooled quality control (QC) samples, and annotation level 2 proposed by Schymanski et al. (2014) was used for data analysis.

2.6. Statistical analysis

The data are shown as the mean ± standard error of the mean (S.E.

M.). Analysis was performed by using PASW Statistics 20 (formerly SPSS statistics; SPSS, Tokyo, Japan). Body weight data were analyzed using repeated measure two-way analysis of variance (ANOVA). Comparisons among the three groups were performed by one-way ANOVA, followed by post-hoc Fisher's Least Significant Difference (LSD) test. For the gut microbiota data, differences among the three groups were determined with a Kruskal-Wallis test. For plasma metabolite analysis, we used orthogonal partial least squares discriminant analysis (OPLS-DA) as a multivariate analysis model implemented in SIMCA-P (V.14.0). Significant peaks of metabolites were determined by combination of variable importance in projection (VIP) value > 1, Wilcoxon rank test P values < 0.05, false discovery rate (FDR) < 0.15. The P < 0.05 was considered statistically significant.

3. Results

3.1. Effects of CSDS on body weight, anhedonia-like phenotype, and plasma IL-6

There were no changes of body weight among the three groups (Fig. 1**B**). CSDS significantly increased the spleen weight in the saline-treated mice. In contrast, MDMA (10 mg/kg/day for 14 days) did not produce splenomegaly in mice after CSDS (Fig. 1**C**). In SPT, CSDS caused significant reduction in sucrose preference of the saline-treated group, but not the MDMA-treated group, indicating anhedonia-like phenotype in saline-treated mice (Fig. 1**D**). Furthermore, CSDS significantly increased plasma levels of IL-6 in the saline-treated group, whereas CSDS did not alter plasma IL-6 levels in the MDMA-treated group (Fig. 1**E**). There was a positive correlation (r = 0.9337, P < 0.001) between the spleen weight and plasma IL-6 levels in the three groups (Fig. 1**F**), suggesting that systemic inflammation is associated with splenomegaly in mice. The data suggest that MDMA-treated mice show stress resilience in the mice exposed to CSDS.

3.2. Composition of gut microbiota

As the auxiliary analysis, we examined the composition of gut microbiota among the three groups. For α-diversity, four indices such as

3

Observed_OUT, Chao, ACE, and Shannon were not different among the three groups (Fig. 2**A**-2**D**). The bacterial population composition of fecal microbiota was analyzed by PCA β-diversity. At the OUT level, PCA analysis showed a significant separation (R = 0.4301, P = 0.001) in the bacterial population composition among the three groups (Fig. 2**E**).

Cladograms presented the relationship between biomarker taxa were generated by LEfSe analysis (Fig. 3**A and** 3**B**). We identified the different distributions of fifteen bacteria (e.g., *Butyricimonas, Prevotella, Alistipes, Rikenellaceae, Gpl, Atopostipes, Carnobacteriaceae, Lactobacillaceae, Lactobacillales, Bacilli, Clostridium_XIVb, Flavonifractor, Oscillibacter, Akkermansia* among the three groups (Fig. 3**A**). Five mix-level phylotypes, including *Rikenellaceae, Oscillibacter, Alistipes, Flavonifractor,* and *Clostridium_XIVb* were identified as potential microbial makers for the saline + CSDS group (Fig. 3**B**). The genus Gpl was identified as a potential microbial maker for the MDMA + CSDS group (Fig. 3**B**).

At the genus level (Fig. 4**A**), CSDS significantly increased the relative abundance of *Oscillibacter* in the saline-treated group, but not the MDMA-treated group (Fig. 4**B**). Furthermore, CSDS significantly increased the relative abundance of *Flavonifractor* in the saline-treated group (not MDMA-treated group), although CSDS significantly decreased the relative abundance of *Lactobacillus* in the saline-treated group (not MDMA-treated group) (Fig. 4**C** and 4**D**).

At the species level (Fig. 4**E**), CSDS significantly increased the relative abundance of *Oscillibacter_valericigenes* in the saline-treated group, but not the MDMA-treated group (Fig. 4**F**). Furthermore, CSDS significantly increased the relative abundance of *Flavonifractor_plautii*, and *Alistipes_onderdonkii* in the saline-treated group (not MDMA-treated group), although CSDS significantly decreased the relative abundance of *Barnesiella_intestinihominis* in the saline-treated group (not MDMA-treated group) (Fig. 5**G**-5**I**).

3.3. Untargeted metabolomics analysis of plasma samples

To examine the interaction between gut microbiota and host metabolism at the plasma metabolic level, we performed untargeted metabolomics analysis of plasma samples. The OPLS-DA model scatter plots of the scores were employed to represent the distribution of plasma metabolic components in the control group and saline + CSDS group (Fig. 5**A**), and saline + CSDS group and MDMA + CSDS group (Fig. 5**B**). When saline + CSDS group compared with MDMA + CSDS group, five compounds including 3-ureidopropionic acid, N-epsilon-methyl-L-lysine, L-cysteine-glutathione disulfide, benzophenone, DL-3-phenyllactic acid were significantly up-regulated annotated metabolites. Seven compounds including 1-stearoyl-2-hydroxy-sn-glycero-3-phosphoethanolamine, PC (16:0/0:0) [1-hexadecanoyl-sn-glycero-3-phosphocholine], beta-D-allose, galactinol, lactose, 5-keto-D-gluconic acid were significantly down-regulated annotated metabolites (Fig. 5**C**). We identified 4 metabolites (4-imidazoleacetic acid, N-epsilon-methyl-L-lysine, 3-hydroxymethylglutaric acid, 3-methylhistamine) with statistical differences (Fig. 5**D**). Among these metabolites, plasma levels of N-epsilon-methyl-L-lysine in the saline + MDMA group were significantly altered compared to control group or MDMA + CSDS group. The data suggest that N-epsilon-methyl-L-lysine is the most attractive metabolite.

3.4. Correlations among plasma IL-6 levels and the relative abundance of bacteria (or plasma metabolites)

There was a positive correlation between plasma N-epsilon-methyl-L-lysine and plasma IL-6 (Fig. 6**A**). There were also positive correlations between the genus *Oscillibacter* (or the species *Flavonifractor_plautii*) and plasma IL-6 (Fig. 6**B and** 6**C**). Furthermore, there were positive correlations between N-epsilon-methyl-L-lysine and the relative abundance of the genus *Oscillibacter,* the genus *Flavonifractor*, the species *Flavonifractor_plautii,* or the species level *Alistipes_onderdonkii* (Fig. 6**D**-6**G**).

4. Discussion

The major findings of this study are as follows. First, repeated treatment with MDMA did not cause splenomegaly, anhedonia-like phenotype and increases of plasma IL-6 levels in mice after subsequent CSDS although CSDS caused splenomegaly, anhedonia-like phenotype and increase of plasma IL-6 levels in the saline-treated group. There was a positive correlation between spleen weight and plasma IL-6 levels. Second, repeated treatment with MDMA restored the marked alterations in the beta-diversity of microbiota in the host gut after CSDS. At the genus level, CSDS showed marked alterations in the several bacteria in host gut. Interestingly, MDMA significantly ameliorated higher abundance of *Oscillibacter* in the CSDS-exposed mice. At the species levels, MDMA significantly ameliorated higher abundance of
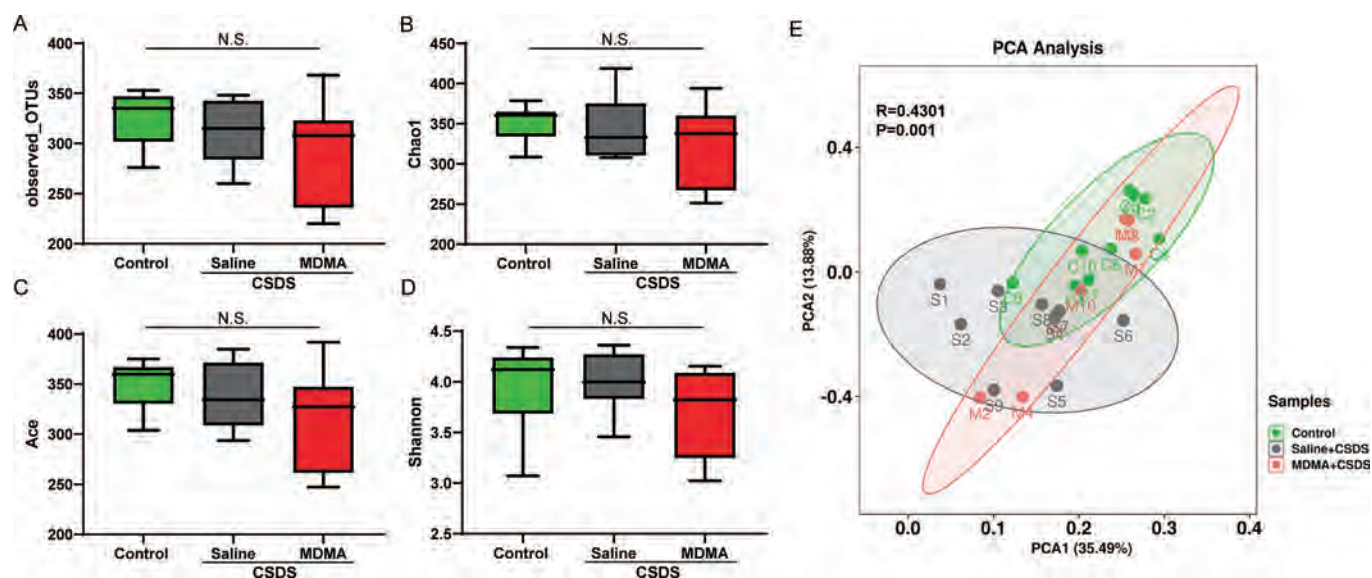

Fig. 2. Alpha-diversity and beta-diversity of gut microbiota, (**A**): Observed_OTU (Kruskal-Wallis test, H = 3.008, P = 0.222). (**B**): Chao (Kruskal-Wallis test, H = 2.234, P = 0.327). (**C**): Ace (Kruskal-Wallis test, H = 2.390, P = 0.303). (**D**): Shannon (Kruskal-Wallis test, H = 1.773, P = 0.412). (**E**): PCA based on OTU level (R = 0.4301, P = 0.001). For all box plots, the middle line in the box represents the median, the box represents the interquartile range, and the whisker represents the most extreme and least value (n = 7 or 9). N.S.: not significant.
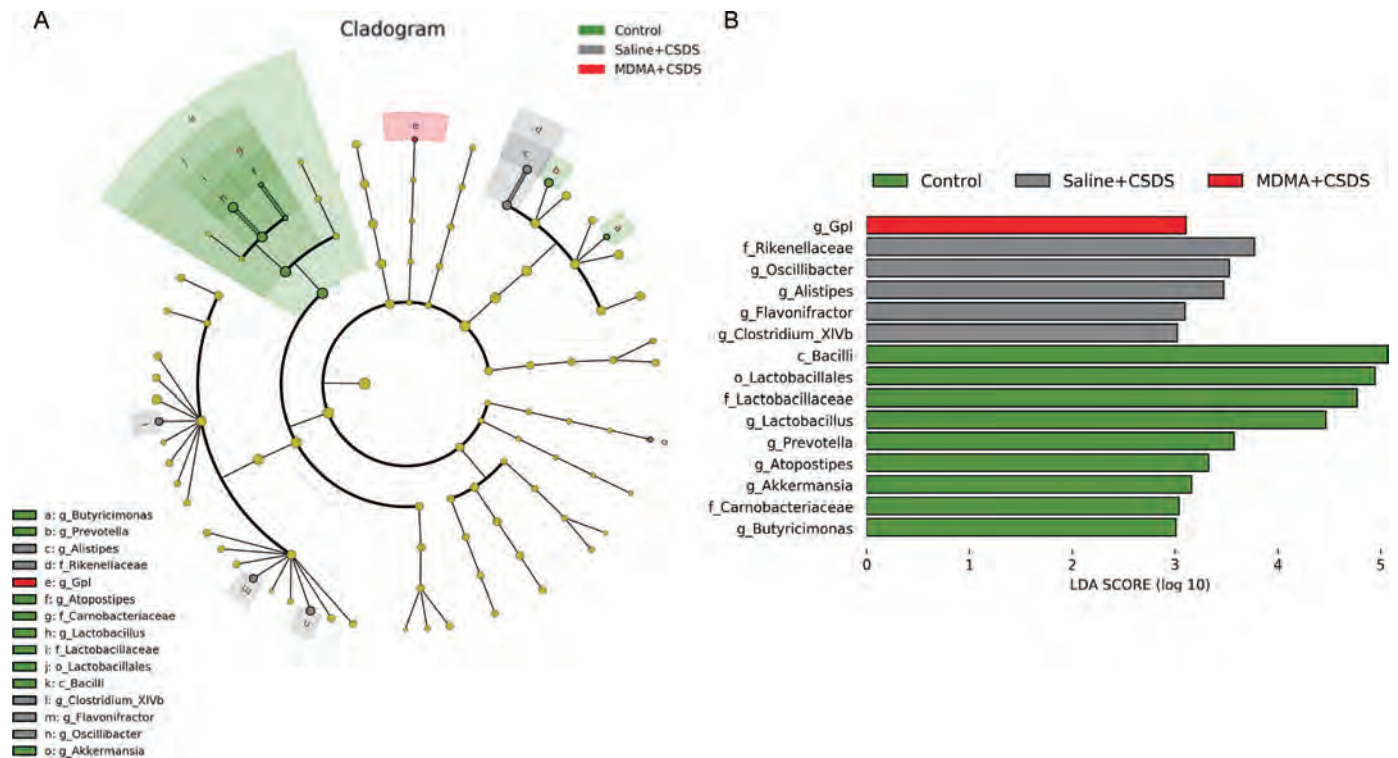
Fig. 3. LEfSe analysis, (**A**): Cladogram (LDA score >3.0, P < 0.05) indicated the taxonomic distribution difference among the three groups. (**B**): Histograms of the different abundant taxa based on the cutoff value of LDA score (log10) > 3.0 and P < 0.05 among the three groups. c: class. f: family. g: genus, o: order.

Oscillibacter_valericigenes in the CSDS-exposed mice. Third, we found 4 plasma metabolites altered among the three groups. Among the four metabolites, N-epsilon-methyl-L-lysine was the most attractive metabolite. Fourth, there was a positive correlation between plasma IL-6 levels and N-epsilon-methyl-L-lysine. Furthermore, there were positive correlations between plasma Il-6 levels and the relative abundance of the genus *Oscillibacter* (or the species *Flavonifractor_plautii*). Moreover, there were also positive correlations between plasma levels of N-epsilon-methyl-L-lysine and the relative abundance of the genus *Oscillibacter,* the genus *Flavonifractor*, the species *Flavonifractor_plautii,* or the species level *Alistipes_onderdonkii.* Collectively, these findings suggest that repeated treatment with MDMA might be associated with the resilience in mice after subsequent CSDS through anti-inflammatory action via gut–microbiota–brain axis.

We previously reported that CSDS causes splenomegaly in the susceptible mice with depression-like behaviors compared to CSDS resilient mice without depression-like behaviors and control (no CSDS) mice (Zhang et al., 2021b). Furthermore, a single dose of lipopolysaccharide (LPS) causes splenomegaly in mice, and spleen weight was positively correlated with blood levels of IL-6 (Ma et al., 2022a, 2022b; 2022c; Zhang et al., 2020, 2021a). In this study, we found a positive correlation between spleen weight and plasma Il-6 levels, suggesting that systemic inflammation was associated with splenomegaly in mice, consistent with previous reports (Ma et al., 2022a, 2022b, 2022c; Zhang et al., 2020, 2021a, 2021b). It has been reported that CSDS resilient mice had lower blood levels of IL-6 than CSDS susceptible mice in response to acute stress (Hodes et al., 2014). Furthermore, blockade of IL-6 receptor in the periphery promotes rapid and sustained antidepressant-like effects by normalizing the altered composition of gut microbiota in CSDS susceptible mice (Zhang et al., 2017). Moreover, antibiotic-induced microbiome depletion is associated with resilience and lower IL-6 levels in mice after subsequent CSDS (Wang et al., 2020a). Collectively, it seems that systemic inflammation such as higher IL-6 levels in the blood is associated with increases in spleen weight of mice with anhedonia-like phenotype after CSDS. It is noteworthy that repeated

treatment with MDMA could attenuate systemic inflammation in mice exposed to CSDS despite MDMA was not administered to mice during CSDS (10 days).

In this study, we found that MDMA significantly ameliorated the higher abundance of *Oscillibacter_valericigenes* in the CSDS-exposed mice. Although the precise functions of *Oscillibacter_valericigenes* are unclear, a recent study showed that *Oscillibacter_valericigenes* might cause inflammation through TLR2 (Toll-like receptor 2) ligands (Li et al., 2022). Thus, it is possible that reduction of the abundance of *Oscillibacter_valericigenes* by MDMA may play a role in long-lasting prophylactic effects of MDMA in mice exposed to CSDS although further study is needed.

N-epsilon-methyl-L-lysine is generated by metabolic transmethylation of the endogenous amino acid L-lysine, and methylation of L-lysine is implicated in transcriptional regulation (Levy, 2019). In this study, we found a positive correlation between plasma IL-6 levels and plasma levels of N-epsilon-methyl-L-lysine. Although the precise functions of N-epsilon-methyl-L-lysine are unknown, the current data suggest that it may play a role in inflammation. In addition, we found positive correlations between plasma levels of N-epsilon-methyl-L-lysine and the relative abundance of the genus *Oscillibacter,* the genus *Flavonifractor*, the species *Flavonifractor_plautii,* or the species *Alistipes_onderdonkii.* The data suggest that these microbes may contribute to production of N-epsilon-methyl-L-lysine. In addition, Wang et al. (2020) reported that the abundance of the genus *Oscillibacter* was associated with plasma N-epsilon-methyl-L-lysine in the Mongolian sheep. Thus, it seems that the genus *Oscillibacter* may play a role in the production of N-epsilon-methyl-L-lysine. Interestingly, we also found positive correlations between plasma IL-6 levels and the relative abundance of two microbes (the genus *Oscillibacter* and the species *Flavonifractor_plautii*), suggesting that these two microbes may play a role in systemic inflammation. Interestingly, N-epsilon-methyl-L-lysine was detected in human and rat urine (Kalász et al., 2005; Löwer et al., 1975), indicating production of this metabolite in the body. Collectively, it is likely that these microbes may contribute to production of N-epsilon-methyl-L-lysine in
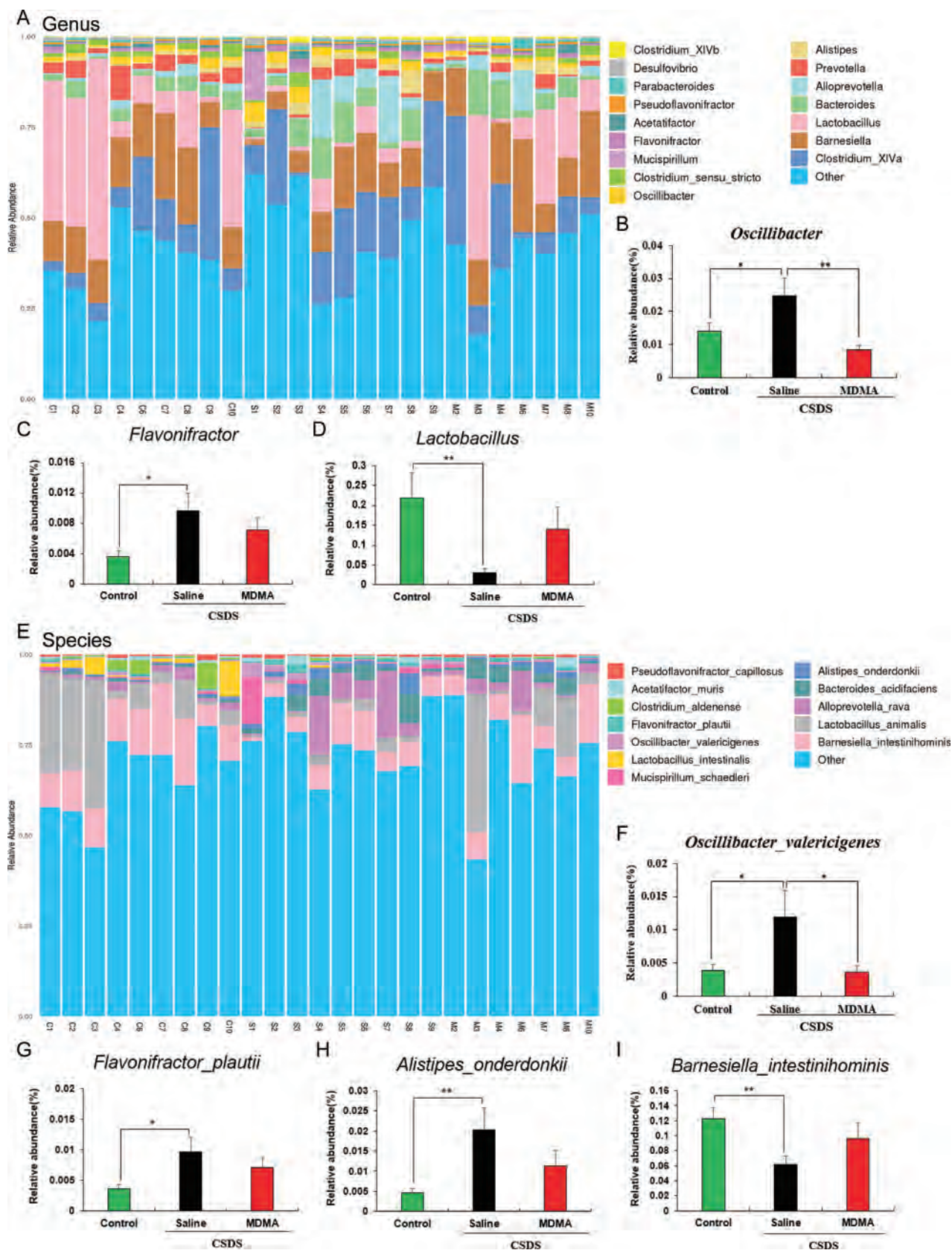
Fig. 4. Altered composition in the gut microbiota at different levels, (**A**): Relative abundance of microbiota at the genus level. (**B**): *Oscillibacter* (Kruskal-Wallis test, H = 6.733, P = 0.035). (**C**): *Flavonifractor* (Kruskal-Wallis test, H = 7.263, P = 0.026). (**D**): *Lactobacillus* (Kruskal-Wallis test, H = 7.028, P = 0.030). (**E**): Relative abundance of microbiota at the species level. (**F**): *Oscillibacter_valericigenes* (Kruskal-Wallis test, H = 6.400, P = 0.041). (**G**): *Flavonifractor_plautii* (Kruskal-Wallis test, H = 7.263, P = 0.026). (**H**): *Alistipes_onderdonkii* (Kruskal-Wallis test, H = 8.497, P = 0.014). (**I**): *Barnesiella_intestinihominis* (Kruskal-Wallis test, H = 7.767, P = 0.021). The number of mice (n = 7 or 9). *P < 0.05, **P < 0.01.
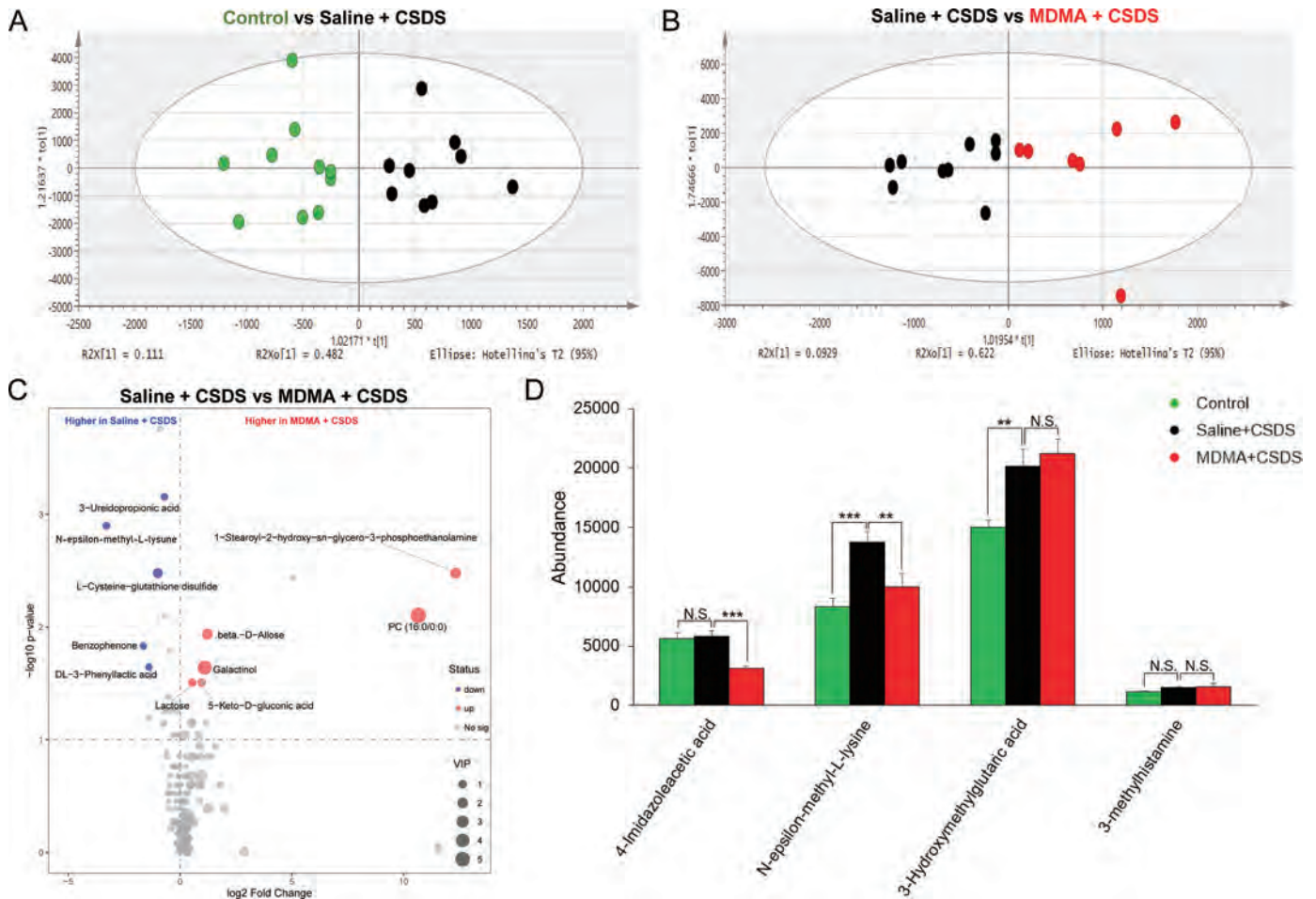
6

Fig. 5. Effect of MDMA and CSDS on plasma metabolites, (A): Scatter plot of mouse plasma metabolites based on orthogonal partial least square discriminant analysis (OPLS-DA) between control (no CSDS) group and saline + CSDS group. (B): Scatter plot of mouse plasma metabolites based on OPLS-DA between saline + CSDS group and MDMA + CSDS group. (C): Volcano plot indicating that 6 annotation metabolites were significantly up-regulated, 5 annotation metabolites were significantly down-regulated when comparing the saline + CSDS group with the MDMA + CSDS group. (D): Violin plot showing the changes of 4 kinds of metabolites [4-imidazoleacetic acid (Kruskal-Wallis test, FDR-corrected P = 0.11), N-epsilon-methyl-L-lysine (Kruskal-Wallis test, FDR-corrected P = 0.11), 3-hydroxymethylglu-taric acid (Kruskal-Wallis test, FDR-corrected P = 0.12), 3-methylhistamine (Kruskal-Wallis test, FDR-corrected P = 0.13)] among the three groups. The number of mice (n = 7 - 10). *P < 0.05, **P < 0.01, ***P < 0.001.

the GI tract, resulting in systemic inflammation. Nonetheless, further detailed study is needed to investigate the role of gut microbiome in the production of N-epsilon-methyl-L-lysine.

As mentioned in the introduction, the 5-HT system plays an important role in the mechanisms of action of MDMA in the body (Green et al., 2003; Schenk and Highgate, 2021). Since approximately 95% of 5-HT in the body is synthesized in the GI tract (Liu et al., 2021; Mawe and Hoffman, 2013; Shine et al., 2022), the data of this study suggest that gut–microbiota may play a role in long-lasting prophylactic effects of MDMA in CSDS model. Considering a major role of MDMA in the 5-HT system, it is likely that 5-HT system in the GI tract could contribute to resilience-enhancing effects of MDMA through gut–microbiota–brain axis. Further study is needed to ascertain the role of 5-HT system in the GI tract as well as gut microbiota and microbes-derived metabolites for resilience-enhancing effects of MDMA.

Accumulating evidence suggests that vagus nerve plays a key role in the gut–microbiota–brain axis (Chang et al., 2022; Wei et al., 2022b). It is reported that vagotomy blocked the beneficial effects of *Lactobacillus rhamnosus* on anxiety- and depression-like behaviors in mice exposed to stress (Bravo et al., 2011), suggesting the vagus nerve in the communication of brain and body. Furthermore, we reported a role of sub-diaphragmatic vagus nerve in depression-like behaviors in rodents after fecal microbiota transplantation of mice with depression-like behaviors

(Pu et al., 2021; Wang et al., 2020b, Wang et al., 2021). Given the role of vagus nerve in communication of brain and body (Chang et al., 2022; Pavlov and Tracey, 2022; Shine et al., 2022; Wei et al., 2022b), it is of great interest to investigate whether vagotomy could block MDMA-induced resilience in rodents exposed to stress.

As aforementioned in the introduction, combination of MDMA with psychotherapy for PTSD has attracted a lot of interest from the scientific community (Smith et al., 2022; Tedesco et al., 2021). A new US population-based survey study demonstrated that lifetime use of MDMA was associated with significantly lower risk of self-reported over-weightness and obesity, and lower odds of self-reported physical diseases such as heart condition and/or cancer, hypertension, and diabetes (Jones et al., 2022). Importantly, Price et al. (2022) reported that chronic SSRI (selective serotonin reuptake inhibitor) use dampens the response to MDMA-assisted therapy in the treatment of PTSD, suggesting a role of 5-HT system in the beneficial effects of MDMA for PTSD. Collectively, it is possible that lifetime MDMA use could have long-lasting beneficial effects in later life, although the precise mechanisms underlying MDMA's beneficial effects in PTSD remain to be elucidated. Further study on brain–body crosstalk is needed to ascertain the role of gut–microbiota–brain axis in the mechanisms of actions of MDMA on stress resilience. Collectively, it is of great interest to examine the role of gut–microbiota–brain axis on resilience and vulnerability in
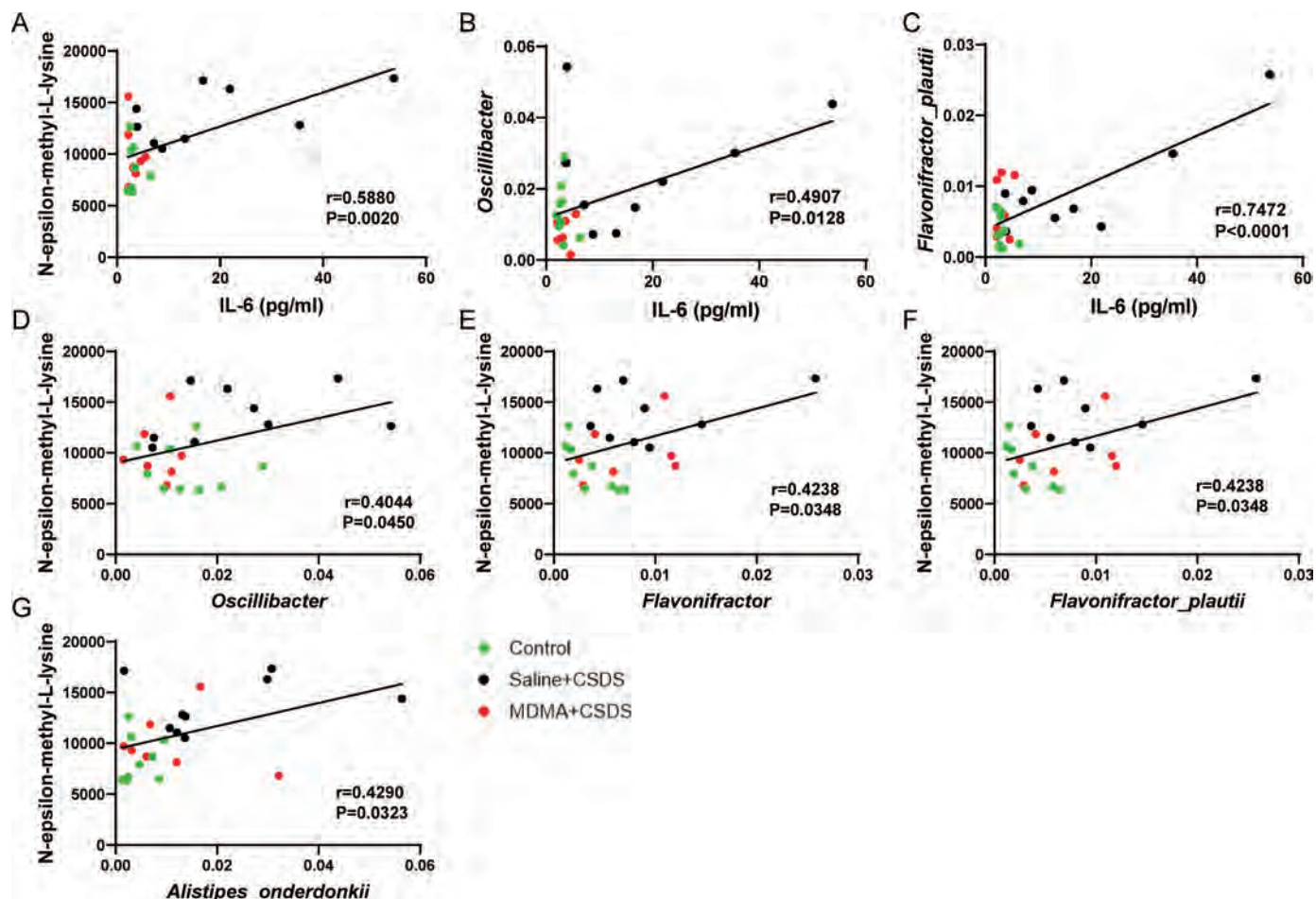
Fig. 6. Correlations among plasma IL-6, plasma N-epsilon-methyl-L-lysine, and the relative abundance of microbiome, (**A**): A positive correlation (r = 0.5880, P = 0.0020) between N-epsilon-methyl-L-lysine and plasma IL-6. (**B**): A positive correlation (r = 0.4907, P = 0.0128) between the relative abundance of *Oscillibacter* and plasma IL-6. (**C**): A positive correlation (r = 0.7472, P < 0.0001) between the relative abundance of *Flavonifractor_plautii* and plasma IL-6. (**D**): A positive correlation (r = 0.4044, P = 0.0450) between N-epsilon-methyl-L-lysine and the relative abundance of *Oscillibacter*. (**E**): A positive correlation (r = 0.4238, P = 0.0348) between N-epsilon-methyl-L-lysine and the relative abundance of *Flavonifractor*. (**F**): A positive correlation (r = 0.4238, P = 0.0348) between N-epsilon-methyl-L-lysine and the relative abundance of *Flavonifractor_plautii*. (**G**): A positive abundance of correlation (r = 0.4290, P = 0.0323) between N-epsilon-methyl-L-lysine and the relative abundance of *Alistipes_onderdonkii*.

MDMA users.

This study has some limitations. In this study, we did not identify the specific microbiome and metabolites which contribute to MDMA-induced resilience. Although higher levels of N-epsilon-methyl-L-lysine may play a role in the susceptibility in mice exposed to CSDS, we did not investigate the effects of N-epsilon-methyl-L-lysine in a CSDS model. Furthermore, we did not identify specific microbiome which can produce N-epsilon-methyl-L-lysine in the GI tract. Finally, we do not have strong evidence supporting the role of gut–microbiota–brain axis in stress resilience of MDMA from the current exploratory analysis. Therefore, further study is needed to confirm the role of gut–microbiota–brain axis in MDMA-induced stress resilience.

In conclusion, the present study suggests that repeated use of MDMA might be associated with resilience in mice subjected to CSDS through gut–microbiota–brain axis. It is likely that abnormalities in gut–microbiota–brain axis including microbes-derived metabolites may contribute to susceptibility to stress-related disorders. Finally, MDMA would be a prophylactic and therapeutic drug to prevent the onset of stress-related disorders.

Role of the Funding Source

This study was supported by the grants from Japan Society for the

CRediT authorship contribution statement

Youge Qu: Conceptualization, Methodology, Formal analysis, Investigation, Data curation, Writing – original draft, Writing – review À editing. **Akifumi Eguchi:** Conceptualization, Methodology, Formal analysis, Investigation, Resources, Data curation, Writing – review À editing. **Xiayun Wan:** Conceptualization, Methodology, Formal analysis, Investigation, Resources, Data curation, Writing – review Àediting. **Li Ma:** Conceptualization, Methodology, Formal analysis, Investigation, Resources, Data curation, Writing – review À editing. **Lijia Chang:** Conceptualization, Methodology, Formal analysis, Investigation, Resources, Data curation, Writing – review À editing. **Jiajing Shan:** Conceptualization, Methodology, Formal analysis, Investigation, Resources, Data curation, Writing – review À editing. **Yong Yang:** Conceptualization, Methodology, Formal analysis, Investigation, Resources, Data curation, Writing – review À editing. **Chisato Mori:** Conceptualization, Methodology, Formal analysis, Investigation, Resources, Data curation, Supervision, Project administration, Funding acquisition, Writing – review À editing. **Kenji Hashimoto:**

Conceptualization, Methodology, Formal analysis, Investigation, Resources, Data curation, Supervision, Project administration, Funding acquisition, Writing – original draft, Writing – review Ä editing.

Declaration of Competing Interest

Dr. Hashimoto is the inventor of filed patent applications on "The use of *R*-ketamine in the treatment of psychiatric diseases", "(*S*)-norketamine and salt thereof as pharmaceutical", "*R*-ketamine and derivative thereof as prophylactic or therapeutic agent for neurodegeneration disease or recognition function disorder", "Preventive or therapeutic agent and pharmaceutical composition for inflammatory diseases or bone diseases", and "*R*-ketamine and its derivatives as a preventive or therapeutic agent for a neurodevelopmental disorder" by the Chiba University. Dr. Hashimoto has also received speakers' honoraria, consultant fee, or research support from Abbott, Boehringer-Ingelheim, Daiichi-Sankyo, Meiji Seika Pharma, Seikagaku Corporation, Dainippon-Sumitomo, Taisho, Otsuka, Murakami Farm and Perception Neuroscience. Other authors declare no conflict of interest.

Data and code availability

: The 16S rRNA sequencing data has been uploaded and saved in the NCBI Sequence Read Archive and is available at the accession number PRJNA914843.

Acknowledgments

Supplementary materials

Supplementary material associated with this article can be found, in the online version, at doi:10.1016/j.psychres.2022.115020.

References

Bailey, M.T., Dowd, S.E., Galley, J.D., Hufnagle, A.R., Allen, R.G., Lyte, M., 2011. Exposure to a social stressor alters the structure of the intestinal microbiota: implications for stressor-induced immunomodulation. Brain Behav. Immun. 25, 397–407. https://doi.org/10.1016/j.bbi.2010.10.023.

Boote, T., 2018. Is the recreational use of 3,4-methyelenedioxy-methamphetamine safe? Med. Leg. J. 86 (2), 94–99. https://doi.org/10.1177/0025817217747203.

Bravo, J.A., Forsythe, P., Chew, M.V., Escaravage, E., Savignac, H.M., Dinan, T.G., Bienenstock, J., Cryan, J.F., 2011. Ingestion of *Lactobacillus* strain regulates emotional behavior and central GABA receptor expression in a mouse via the vagus nerve. Proc. Natl. Acad. Sci. USA. 108 (38), 16050–16055. https://doi.org/10.1073/pnas.1102999108.

Cathomas, F., Murrough, J.W., Nestler, E.J., Han, M.H., Russo, S.J., 2019. Neurobiology of resilience: interface between mind and body. Biol. Psychiatry 86 (6), 410–420. https://doi.org/10.1016/j.biopsych.2019.04.011.

Chang, L., Wei, Y., Hashimoto, K., 2022. Brain-gut-microbiota axis in depression: a historical overview and future directions. Brain Res. Bull. 182, 44–56. https://doi.org/10.1016/j.brainresbull.2022.02.004.

Cryan, J.F., O'Riordan, K.J., Cowan, C.S.M., Sandhu, K.V., Bastiaanssen, T.F.S., Boehme, M., Codagnone, M.G., Cussotto, S., Fulling, C., Golubeva, A.V., Guzzetta, K. E., Jaggar, M., Long-Smith, C.M., Lyte, J.M., Martin, J.A., Molinero-Perez, A., Moloney, G., Morelli, E., Morillas, E., O'Connor, R., Cruz-Pereira, J.S., Peterson, V.L., Rea, K., Ritz, N.L., Sherwin, E., Spichak, S., Teichman, E.M., van de Wouw, M., Ventura-Silva, A.P., Wallace-Fitzsimons, S.E., Hyland, N., Clarke, G., Dinan, T.G., 2019. The microbiota-gut-brain axis. Physiol. Rev. 99 (4), 1877–2013. https://doi.org/10.1152/physrev.00018.2018.

Dunlap, L.E., Andrews, A.M., Olson, D.E., 2018. Dark classics in chemical neuroscience: 3,4-methyelenedixoymethamphetamine. ACS Chem. Neurosci. 9 (10), 2408–2427. https://doi.org/10.1021/acschemneuro.8b00155.

Feduccia, A.A., Holland, J., Mithoefer, M.C., 2018. Progress and promise for the MDMA drug development program. Psychopharmacology (Berl.) 235 (2), 561–571. https://doi.org/10.1007/s00213-017-4779-2.

Góralczyk-Bińkowska, A., Szmajda-Krygier, D., Kozłowska, E., 2022. The microbiota-gut-brain axis in psychiatric disorders. Int. J. Mol. Sci. 23 (19), 11245 https://doi.org/10.3390/ijms231911245.

Green, A.R., Mechan, A.O., Elliott, J.M., O'Shea, E., Colado, M.I., 2003. The pharmacology and clinical pharmacology of 3,4-methylenedixoymethamphetamine. Pharmacol. Rev. 55 (3), 463–508. https://doi.org/10.1124/pr.55.3.3.

Hodes, G.E., Pfau, M.L., Leboeuf, M., Golden, S.A., Christoffel, D.J., Bregman, D., Rebusi, N., Heshmati, M., Aleyasin, H., Warren, B.L., Lebonté, B., Horn, S., Lapidus, K., Stelzhammer, V., Wong, E.H.F., Bahn, S., Krishnan, V., Bolaños-Guzman, C., Murrough, J.W., Merad, M., Russo, S.J., 2014. Individual differences in the peripheral immune system promote resilience versus susceptibility to social stress. Proc. Natl. Acad. Sci. USA. 111 (45), 16136–16141. https://doi.org/10.1073/pnas.1415191111.

Hoskins, M.D., Bridges, J., Sinnerton, R., Nakamura, A., Underwood, J.F.G., Slater, A., Lee, M.R.D., Clarke, L., Lewis, C., Roberts, N.P., Bisson, J.I., 2021. Pharmacological therapy for post-traumatic stress disorder: a systematic review and meta-analysis of monotherapy, augmentation and head-to-head approaches. Eur. J. Psychotraumatol. 12 (1), 1802920 https://doi.org/10.1080/20008198.2020.1802920.

Jones, G.M., Nock, M.K., 2022a. MDMA/ecstasy use and psilocybin use are associated with lowered odds of psychological distress and suicidal thoughts in a sample of US adults. J. Psychopharmacol. 36 (1), 46–56. https://doi.org/10.1177/02698811211058912.

Jones, G.M., Nock, M.K., 2022b. Lifetime use of MDMA/ecstasy and psilocybin is associated with reduced odds of major depressive episodes. J. Psychopharmacol. 36 (1), 57–65. https://doi.org/10.1177/02698811211066714.

Jones, G., Ricard, J.A., Hendricks, P., Simonsson, O., 2022. Associations between MDMA/ecstasy use and physical health in a U.S. population-based survey sample. J. Psychopharmacol. https://doi.org/10.1177/02698811221127318, 2022 Oct 3: 2698811221127318.

Kalász, H., Klebovich, I., Balogh-Nemes, K., Szilágyi, A., Tihanyi, M., Szarvas, T., Lengyel, J., 2005. Detection of N-monomethyl-lysine generated by metabolic transmethylation. Anal. Bioanal. Chem. 382 (3), 760–764. https://doi.org/10.1007/s00216-005-3089-4.

Levy, D., 2019. Lysine methylation signaling of non-histone proteins in the nucleus. Cell. Mol. Life Sci. 76, 2873–2883. https://doi.org/10.1007/s00018-019-03142-0.

Li, Z., Gurung, M., Rodrigues, R.R., Padiadpu, J., Newman, N.K., Manes, N.P., Pederson, J.W., Greer, R.L., Vasquez-Perez, S., You, H., Hioki, K.A., Moulton, Z., Fel, A., De Nardo, D., Dzutsev, A.K., Nita-Lazar, A., Trinchieri, G., Shulzhenko, N., Morgun, A., 2022. Microbiota and adipocyte mitochondrial damage in type 2 diabetes are linked by Mmp12$^+$ macrophages. J. Exp. Med. 219 (7), e20220017 https://doi.org/10.1084/jem.20220017.

Liu, N., Sun, S., Wang, P., Sun, Y., Hu, Q., Wang, X., 2021. The mechanism of secretion and metabolism of gut-derived 5-hydroxytryptamine. Int. J. Mol. Sci. 22 (15), 7931 https://doi.org/10.3390/ijms22157931.

Löwer, R., Lange, Hempel, K., 1975. Diagnostic meaning of the urinary output of Nepsilon-methylated lysines. Investigation of healthy individuals and patients with malignant diseases, myopathies or renal failure. Clin. Chim. Acta 58 (2), 155–164. https://doi.org/10.1016/s0009-9981(75)80007-6.

Ma, L., Wang, L., Chang, L., Shan, J., Qu, Y., Wang, X., Fujita, Y., Hashimoto, K., 2022a. A role of microRNA-149 in the prefrontal cortex for prophylactic actions of (*R*)-ketamine in inflammation model. Neuropharmacology 219, 109250. https://doi.org/10.1016/j.neuropharm.2022.109250.

Ma, L., Zhang, J., Fujita, Y., Qu, Y., Shan, J., Wan, X., Wang, X., Ishima, T., Kobayashi, K., Wang, L., Hashimoto, K., 2022b. Nuclear factor of activated T cells 4 in the prefrontal cortex is required for prophylactic actions of (*R*)-ketamine. Transl. Psychiatry 12 (1), 27. https://doi.org/10.1038/s41398-022-01803-6.

Ma, L., Zhang, J., Fujita, Y., Shinno-Hashimoto, H., Shan, J., Wan, X., Qu, Y., Chang, L., Wang, X., Hashimoto, K., 2022c. Effects of spleen nerve denervation on depression-like phenotype, systemic inflammation, and abnormal composition of gut microbiota in mice after administration of lipopolysaccharide: a role of brain-spleen axis. J. Affect. Disord. 317, 156–165. https://doi.org/10.1016/j.jad.2022.08.087.

Mawe, G.M., Hoffman, J.M., 2013. Serotonin signalling in the gut–functions, dysfunctions and therapeutic targets. Nat. Rev. Gastroenterol. Hepatol. 10 (8), 473–486. https://doi.org/10.1038/nrgastro.2013.105.

Mitchell, J.M., Bogenschutz, M., Lilienstein, A., Harrison, C., Kleiman, S., Parker-Guilbert, K., Ot'alora, G.M., Garas, W., Paleos, C., Gorman, I., Nicholas, C., Mithoefer, M., Carlin, S., Poulter, B., Mithoefer, A., Quevedo, S., Wells, G., Klaire, S. S., van der Kolk, B., Tzarfaty, K., Amiaz, R., Worthy, R., Shannon, S., Woolley, J.D., Marta, C., Gelfand, Y., Hapke, E., Amar, S., Wallach, Y., Brown, R., Hamilton, S., Wang, J.B., Coker, A., Matthews, R., de Boer, A., Yazar-Klosinski, B., Emerson, A., Doblin, R., 2021. MDMA-assisted therapy for severe PTSD: a randomized, double-blind, placebo-controlled phase 3 study. Nat. Med. 27 (6), 1025–1033. https://doi.org/10.1038/s41591-021-01336-3.

Mithoefer, M.C., Mithoefer, A.T., Feduccia, A.A., Jerome, L., Wagner, M., Wymer, J., Holland, J., Hamilton, S., Yazar-Klosinski, B., Emerson, A., Doblin, R., 2018. 3,4-methylenedioxymethamphetamine (MDMA)-assisted psychotherapy for post-traumatic stress disorder in military veterans, firefighters, and police officers: a randomised, double-blind, dose-response, phase 2 clinical trial. Lancet Psychiatry 5 (6), 486–497. https://doi.org/10.1016/S2215-0366(18)30135-4.

Mithoefer, M.C., Wagner, M.T., Mithoefer, A.T., Jerome, L., Doblin, R., 2011. The safety and efficacy of ± 3,4-methylenedioxymethamphetamine-assisted psychotherapy in subjects with chronic, treatment-resistant posttraumatic stress disorder: the first

9

randomized controlled pilot study. J. Psychopharmacol. 25 (4), 439–452. https://doi.org/10.1177/0269881110378371.

Nutt, D., 2019. Psychedelic drugs – a new era in psychiatry? Dialogues Clin. Neurosci. 21 (2), 139–147. https://doi.org/10.31887/DCNS.2019.21.2/dnutt, 2019.

Parrott, A.C., Downey, L.A., Roberts, C.A., Montgomery, C., Bruno, R., Fox, H.C., 2017. Recreational 3,4-methylenedioxymethamphetamine or 'ecstasy': Current perspective and future research prospects. J. Psychopharmacol. 31 (8), 959–966. https://doi.org/10.1177/0269881117711922.

Pavlov, V.A., Tracey, K.J., 2022. Bioelectronic medicine: Preclinical insights and clinical advances. Neuron 110 (21), 3627–3644. https://doi.org/10.1016/j.neuron.2022.09.003.

Pizzagalli, D., 2014. Depression, stress, and anhedonia: toward a synthesis and integrated model. Annu. Rev. Clin. Psychol. 10, 393–423. https://doi.org/10.1146/annurev-clinpsy-050212-185606.

Price, C.M., Feduccia, A.A., DeBonis, K., 2022. Effects of selective serotonin reuptake inhibitor use on 3,4-methylenedioxymethamphetamine-assisted therapy for posttraumatic stress disorder: A review of the evidence, neurobiological plausibility, and clinical significance. J. Clin. Psychopharmacol. 42 (5), 464–469. https://doi.org/10.1097/JCP.0000000000001595.

Pu, Y., Tan, Y., Qu, Y., Chang, L., Wang, S., Wei, Y., Wang, X., Hashimoto, K., 2021. A role of the subdiaphragmatic vagus nerve in depression-like phenotypes in mice after fecal microbiota transplantation from *Chrna7* knock-out mice with depression-like phenotypes. Brain Behav. Immun. 94, 318–326. https://doi.org/10.1016/j.bbi.2020.12.032.

Qu, Y., Yang, C., Ren, Q., Ma, M., Dong, C., Hashimoto, K., 2017. Comparison of (*R*)-ketamine and lanicemine on depression-like phenotype and abnormal composition of gut microbiota in a social defeat stress model. Sci. Rep. 7 (1), 15725 https://doi.org/10.1038/s41598-017-16060-7.

Qu, Y., Zhang, K., Pu, Y., Chang, L., Wang, S., Tan, Y., Wang, X., Zhang, J., Ohnishi, T., Yoshikawa, T., Hashimoto, K., 2020. Betaine supplementation is associated with the resilience in mice after chronic social defeat stress: a role of brain-gut-microbiota axis. J. Affect. Disord. 272, 66–76. https://doi.org/10.1016/j.jad.2020.03.095.

Reiff, C.M., Richman, E.E., Nemeroff, C.B., Carpenter, L.L., Widge, A.S., Rodriguez, C.I., Kalin, N.H., McDonald, W.M., the Work Group on Biomarkers and Novel Treatments, a Division of the American Psychiatric Association Council of Research, 2020. Psychedelics and psychedelic-assisted psychotherapy. Am. J. Psychiatry 177 (5), 391–410. https://doi.org/10.1176/appi.ajp.2019.19010035.

Schenk, S., Highgate, Q., 2021. Methylenedioxymethamphetamine (MDMA): Serotonergic and dopaminergic mechanisms related to its use and misuse. J. Neurochem. 157 (5), 1714–1724. https://doi.org/10.1111/jnc.15348.

Schymanski, E.L., Jeon, J., Gulde, R., Fenner, K., Ruff, M., Singer, H.P., Hollender, J., 2014. Identifying small molecules via high resolution mass spectrometry: communicating confidence. Environ. Sci. Technol. 48 (4), 2097–2098. https://doi.org/10.1021/es5002105.

Segata, N., Izard, J., Waldron, L., Gevers, D., Miropolsky, L., Garrett, W.S., Huttenhower, C., 2011. Metagenomic biomarker discovery and explanation. Genome. Biol. 12 (6), R60 https://doi.org/10.1186/gb-2011-12-6-r60.

Shine, J.M., O'Callaghan, C., Walpola, I.C., Wainstein, G., Taylor, N., Aru, J., Huebner, R., John, Y.J., 2022. Understanding the effects of serotonin in the brain through its role in the gastrointestinal tract. Brain 145 (9), 2967–2981. https://doi.org/10.1093/brain/awac256.

Smith, K.W., Sicignano, D.J., Hernandez, A.V., White, C.M., 2022. MDMA-assisted psychotherapy for treatment of posttraumatic stress disorder: a systematic review with meta-analysis. J. Clin. Pharmacol. 62 (4), 463–471. https://doi.org/10.1002/jcph.1995.

Szyszkowicz, J.K., Wong, A., Anisman, H., Merali, Z., Audet, M.C., 2017. Implications of the gut microbiota in vulnerability to the social avoidance effects of chronic social defeat in male mice. Brain Behav. Immun. 66, 45–55.

Tedesco, S., Gajaram, G., Chida, S., Ahmad, A., Pentak, M., Kelada, M., Lewis, L., Krishnan, D., Tran, C., Soetan, O.T., Mukona, L.T., Jolayemi, A., 2021. The efficacy of MDMA (3,4-methylenedioxymethamphetamine) for post-traumatic stress disorder in humans: a systematic review and meta-analysis. Cureus 13 (5), e15070. https://doi.org/10.7759/cureus.15070.

Tsugawa, H., Cajka, T., Kind, T., Ma, Y., Higgins, B., Ikeda, K., Kanazawa, M., VanderGheynst, J., Fiehn, O., Arita, M., 2015. MS-DIAL: data-independent MS/MS deconvolution for comprehensive metabolome analysis. Nat. Methods 12 (6), 523–526. https://doi.org/10.1038/nmeth.3393.

Wan, X., Eguchi, A., Fujita, Y., Ma, L., Wang, X., Yang, Y., Qu, Y., Chang, L., Zhang, J., Mori, C., Hashimoto, K., 2022a. Effects of (*R*)-ketamine on reduced bone mineral density in ovariectomized mice: A role of gut microbiota. Neuropharmacology 213, 109139. https://doi.org/10.1016/j.neuropharm.2022.109139.

Wan, X., Eguchi, A., Qu, Y., Yang, Y., Chang, L., Shan, J., Mori, C., Hashimoto, K., 2022b. Gut-microbiota-brain axis in the vulnerability to psychosis in adulthood after repeated cannabis exposure during adolescence. Eur. Arch. Psychiatry Clin. Neurosci. 272 (7), 1297–1309. https://doi.org/10.1007/s00406-022-01437-1.

Wang, S., Ishima, T., Qu, Y., Shan, J., Chang, L., Wei, Y., Zhang, J., Pu, Y., Fujita, Y., Tan, Y., Wang, X., Ma, L., Wan, X., Hammock, B.D., Hashimoto, K., 2021. Ingestion of *Faecalibaculum rodentium* causes depression-like phenotypes in resilient *Ephx2* knock-out mice: A role of brain-gut-microbiota axis via the subdiaphragmatic vagus nerve. J. Affect. Disord. 292, 565–573. https://doi.org/10.1016/j.jad.2021.06.006.

Wang, S., Ishima, T., Zhang, J., Qu, Y., Chang, L., Pu, Y., Fujita, Y., Tan, Y., Wang, X., Hashimoto, K., 2020b. Ingestion of *Lactobacillus intestinalis* and *Lactobacillus reuteri* causes depression- and anhedonia-like phenotypes in antibiotic-treated mice via the vagus nerve. J. Neuroinflammation 17 (1), 241. https://doi.org/10.1186/s12974-020-01916-z.

Wang, B., Luo, Y., Su, R., Yao, D., Hou, Y., Liu, C., Du, R., Jin, Y., 2020. Impact of feeding regimens on the composition of gut microbiota and metabolite profiles of plasma and feces from Mongolian sheep. J. Microbiol. 58 (6), 472–482. https://doi.org/10.1007/s12275-020-9501-0.

Wang, S., Qu, Y., Chang, L., Pu, Y., Zhang, K., Hashimoto, K., 2020a. Antibiotic-induced microbiome depletion is associated with resilience in mice after chronic social defeat stress. J. Affect. Disord. 260, 448–457. https://doi.org/10.1016/j.jad.2019.09.064.

Wei, Y., Chang, L., Liu, G., Wang, X., Yang, Y., Hashimoto, K., 2022a. Long-lasting beneficial effects of maternal intake of sulforaphane glucosinolate on gut microbiota in adult offspring. J. Nutr. Biochem. 109, 109098 https://doi.org/10.1016/j.jnutbio.2022.109098.

Wei, Y., Wang, T., Liao, L., Fan, X., Chang, L., Hashimoto, K., 2022b. Brain-spleen axis in health and diseases: a review and future perspective. Brain Res. Bull. 182, 130–140. https://doi.org/10.1016/j.brainresbull.2022.02.008.

Yang, C., Fang, X., Zhan, G., Huang, N., Li, S., Bi, J., Jiang, R., Yang, L., Miao, L., Zhu, B., Luo, A., Hashimoto, K., 2019. Key role of gut microbiota in anhedonia-like phenotype in rodents with neuropathic pain. Transl. Psychiatry 9, 57. https://doi.org/10.1038/s41398-019-0379-8.

Yang, C., Fujita, Y., Ren, Q., Ma, M., Dong, C., Hashimoto, K., 2017. *Bifidobacterium* in the gut microbiota confer resilience to chronic social defeat stress in mice. Sci. Rep. 7, 45942 https://doi.org/10.1038/srep45942.

Yang, K.H., Han, B.H., Palamar, J.J., 2022. Past-year hallucinogen use in relation to psychological distress, depression, and suicidality among US adults. Addict. Behav. 132, 107343 https://doi.org/10.1016/j.addbeh.2022.107343.

Yang, Y., Eguchi, A., Wan, X., Chang, L., Wang, X., Qu, Y., Mori, C., Hashimoto, K., 2023. A role of gut-microbiota-brain axis via subdiaphragmatic vagus nerve in depression-like phenotypes in *Chrna7* knock-out mice. Prog. Neuropsychopharmacol. Biol. Psychiatry 120, 110652. https://doi.org/10.1016/j.pnpbp.2022.110652.

Zhang, J., Ma, L., Chang, L., Pu, Y., Qu, Y., Hashimoto, K., 2020. A key role of the subdiaphragmatic vagus nerve in the depression-like phenotype and abnormal composition of gut microbiota in mice after lipopolysaccharide administration. Transl. Psychiatry 10 (1), 186. https://doi.org/10.1038/s41398-020-00878-3.

Zhang, J., Ma, L., Wan, X., Shan, J., Qu, Y., Hashimoto, K., 2021a. (*R*)-Ketamine attenuates LPS-induced endotoxin-derived delirium through inhibition of neuroinflammation. Psychopharmacology (Berl.) 238 (10), 2743–2753. https://doi.org/10.1007/s00213-021-05889-6.

Zhang, J.C., Yao, W., Dong, C., Yang, C., Ren, Q., Ma, M., Hashimoto, K., 2017. Blockade of interleukin-6 receptor in the periphery promotes rapid and sustained antidepressant actions: a possible role of gut-microbiota-brain axis. Transl. Psychiatry 7, e1138. https://doi.org/10.1038/tp.2017.112.

Zhang, K., Fujita, Y., Chang, L., Qu, Y., Pu, Y., Wang, S., Shirayama, Y., Hashimoto, K., 2019. Abnormal composition of gut microbiota is associated with resilience versus susceptibility to inescapable electric stress. Transl. Psychiatry 9, 231. https://doi.org/10.1038/s41398-019-0571-x.

Zhang, K., Sakamoto, A., Chang, L., Qu, Y., Wang, S., Pu, Y., Tan, Y., Wang, X., Fujita, Y., Ishima, T., Hatano, M., Hashimoto, K., 2021b. Splenic NKG2D confers resilience versus susceptibility in mice after chronic social defeat stress: beneficial effects of (*R*)-ketamine. Eur. Arch. Psychiatry Clin. Neurosci. 271 (3), 447–456. https://doi.org/10.1007/s00406-019-01092-z.

Zhang, L., Shirayama, Y., Shimizu, E., Iyo, M., Hashimoto, K., 2006. Protective effects of minocycline on 3,4-methylenedioxymethamphetamine-induced neurotoxicity in serotonergic and dopaminergic neurons of mouse brain. Eur. J. Pharmacol. 544 (1-3), 1–9. https://doi.org/10.1016/j.ejphar.2006.05.047.
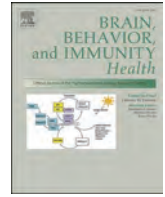
Impact of broad-spectrum antibiotics on the gut–microbiota–spleen–brain axis

Xiayun Wan [a], Akifumi Eguchi [b], Akemi Sakamoto [c], Yuko Fujita [a], Yong Yang [a], Youge Qu [a], Masahiko Hatano [c], Chisato Mori [b,d], Kenji Hashimoto [a,*]

[a] *Division of Clinical Neuroscience, Chiba University Center for Forensic Mental Health, Chiba, 260-8670, Japan*
[b] *Department of Sustainable Health Science, Chiba University Center for Preventive Medical Sciences, Chiba, 263-8522, Japan*
[c] *Department of Biomedical Science, Chiba University Graduate School of Medicine, Chiba, 260-8670, Japan*
[d] *Department of Bioenvironmental Medicine, Graduate School of Medicine, Chiba University, Chiba, 260-8670, Japan*

ARTICLE INFO

ABSTRACT

The spleen is a key immune-related organ that plays a role in communication between the brain and the immune system through the brain–spleen axis and brain–gut–microbiota axis. However, how the gut microbiota affects spleen and brain function remains unclear. Here, we investigated whether microbiome depletion induced by administration of an antibiotic cocktail (ABX) affects spleen and brain function. Treatment with ABX for 14 days resulted in a significant decrease in spleen weight and significant alterations in splenic functions, including the percentage of neutrophils, NK cells, macrophages, and CD8$^+$ T cells. Furthermore, ABX treatment resulted in the depletion of a large portion of the gut microbiota. Untargeted metabolomics analysis showed that ABX treatment caused alterations in the levels of certain compounds in the plasma, spleen, and brain. Moreover, ABX treatment decreased the expression of microglia marker Iba1 in the cerebral cortex. Interestingly, correlations were found between the abundance of different microbiome components and metabolites in various tissues, as well as splenic cell populations and spleen weight. These findings suggest that ABX-induced microbiome depletion and altered metabolite levels may affect spleen and brain function through the gut–microbiota–spleen–brain axis.

1. Introduction

Accumulating evidence demonstrates that the gut microbiota contributes to human health and disease. Dysbiosis (imbalance of the gut microbiota) is observed in patients with gastrointestinal (GI) disorders as well as patients with a variety of diseases, including metabolic, psychiatric, and neurological disorders (Aron-Wisnewsky and Clément, 2016; Cryan et al., 2020; Fan and Pedersen, 2021; Miyauchi et al., 2022; Sharon et al., 2016). Bidirectional communication takes place between the gut microbiota and the central nervous system (CNS) via neural, endocrine, immune, and humoral pathways, known as the brain–gut–microbiota axis (Chang et al., 2022; Cryan et al., 2019; Wei et al., 2022a, 2022b).

The spleen is a key immune-related organ that may mediate communication between the brain and the immune system through the brain–spleen axis (Bronte and Pittet, 2013; Lewis et al., 2019; Mebius and Kraal, 2005; Noble et al., 2018; Wei et al., 2022b). We previously demonstrated that the brain–spleen axis might play a role in stress-related psychiatric disorders such as depression (Hashimoto, 2020; Ma et al., 2022b; Wei et al., 2022a, 2022b; Yang et al., 2017; Zhang et al., 2020a, 2020b, 2021b).

The spleen contributes to brain–gut crosstalk and behavioral outcomes through the production of metabolites and immune factors (Buchmann Godinho et al., 2021; Rhee et al., 2009; Wei et al., 2021). Pathways involved in the gut–brain–spleen axis may include the cholinergic anti-inflammatory reflex and efficient activation of the vagus afferent fiber system by inflammatory intermediates (Borovikova et al., 2000; Huston et al., 2006; Rosas-Ballina et al., 2008). Previous studies suggest that a number of neuropsychiatric disorders, such as Alzheimer's disease, Parkinson's disease, schizophrenia, and depression, might be associated with the gut–brain–spleen axis (Breit et al., 2018; Buchmann Godinho et al., 2021; Mok et al., 2020). A dynamic,

pathological crosstalk among the brain, gut, and spleen manifests as internal metabolite disturbances and CNS inflammation (Buchmann Godinho et al., 2021). However, whether microbiome depletion induces alterations in the metabolic profile and in the function of organs, such as the brain, spleen, and blood, remains unclear.

Germ-free (GF) mouse models are generally considered to be the gold standard for microbiota studies. Importantly, GF mice exhibit a broad range of developmental impairments, including development of the early immune system (Kennedy et al., 2018), and as such are not suitable for studying development-related conditions such as psychiatric and neurological disorders. In contrast, treating adult mice with a broad-spectrum antibiotic cocktail (ABX) allows study of the role that the microbiota plays in maintaining cell functionality and signaling pathways after development (Kennedy et al., 2018). Therefore, the aim of the present study was to investigate whether ABX-induced microbiome depletion affects spleen and brain function and the metabolites present in the blood, spleen, and brain. We performed 16S rRNA sequencing analysis to analyze gut microbiota and untargeted metabolomics analysis to analyze the metabolites in the blood, spleen, and brain.

2. Material and methods

2.1. Animals

Male C57BL/6 mice (8 weeks old, body weight 20–25 g) were purchased from Japan SLC Corporation (Hamamatsu, Shizuoka, Japan). All mice were carefully housed in clear polycarbonate cages (21 × 30 × 22.5 cm), 4–5 per cage, on an automatically managed light/dark cycle of 12 h/12 h (7:00 a.m. to 7:00 p.m.), with a constant and stable ambient temperature of $23 \pm 1\ ^{\circ}C$ and a relative humidity of $55 \pm 5\%$. The experimental procedures used in this study were approved by the Animal Care and Use Committee of Chiba University Institution (License No. 4–237 and 4–407). Animals were promptly sacrificed by inducing deep anesthesia with inhaled isoflurane followed by skilled cervical dislocation. Animal suffering was minimized to the greatest extent possible.

2.2. Antibiotic cocktail therapy and sample collection

On days 1–14, mice were allowed *ad libitum* access to plain drinking water or drinking water containing the broad-spectrum antibiotic cocktail (ABX: ampicillin 1 g/L, FUJIFILM Wako Pure Chemical Corporation, Tokyo, Japan; neomycin sulfate 1 g/L, Sigma-Aldrich Co. Ltd, MO, USA; metronidazole 1 g/L, FUJIFILM Wako Pure Chemical Corporation, Tokyo, Japan) (Fig. 1A), as previously described (Hashimoto et al., 2022; Pu et al., 2019, 2021; Wang et al., 2020a, 2020b, 2021). Fresh mouse feces were collected on the morning of day 15 for 16S ribosomal RNA sequencing analysis as previously described (Hashimoto et al., 2022; Wan et al., 2022a, 2022b; Wang et al., 2022a, 2022b) (Fig. 1A). All mouse fecal samples were quickly frozen in liquid nitrogen after collection and then transferred to a −80 °C freezer for storage. Plasma, spleen, and cerebral cortex samples were also collected from each mouse on day 15 (Fig. 1A).

After anesthetization with 5% isoflurane, cardiac blood was collected from each mouse using a 1-mL syringe and placed into a tube containing ethylenediamine-*N,N,N′,N′*-tetraacetic acid (EDTA) potassium salt dehydrate as an anticoagulant. Then, blood samples were centrifuged at 4 °C, and the supernatant (containing the plasma) was collected and stored at −80 °C. Half of the spleen samples were immediately subject to fluorescence activated cell sorting (FACS) analysis, while the remaining spleen, plasma, and left cerebral cortex samples were subjected to untargeted metabolomics analysis. The right cerebral cortex was used for western blot analysis.

2.3. FACS analysis of spleen samples

Single-cell suspensions were prepared from the spleen samples and stained for FACS (fluorescence activated cell sorting) analysis as previously described (Shinno-Hashimoto et al., 2022; Zhang et al., 2021b). The following antibodies were used for immunofluorescence staining: anti-CD3-FITC (x40, cat# 100305: BioLegnd, San Diego, CA), anti-CD4-allophycocyanin (x100, cat# 17-0042-82: eBioscience, San Diego, CA), anti-CD8a-allophycocyanin (x100, cat# 553035: BD Bioscience), anti-NK1.1-PE (x100, cat# 553165: BD Bioscience), anti-Ly6c-FITC (x100, cat# 553104: BD Bioscience), anti-CD11b-PE (x400 diluted using FACS buffer, cat# 553312: BD Bioscience, Franklin Lakes, NJ), anti-CD11c-PE (x100, cat# 557401: BD Bioscience), anti-Ter119-PE (x40, cat# 12-5921-83: eBioscience, San Diego, CA), anti-F4/80-PE (x40, cat# 12-4801-80: Invitrogen), and anti-B220-PE (x200, cat# 553309: BD Bioscience). The stained cells were analyzed using a FACSCanto II and FlowJo software (BD Bioscience).

2.4. Western blot analysis

Western blotting was carried out to assess the expression levels of ionized calcium binding adaptor molecule 1 for microglia (Iba1) and glial fibrillary acidic protein for astrocyte (GFAP) in the cerebral cortex, as previously described (Ma et al., 2022b; Wan et al., 2022b). The cerebral cortex tissue was ground in frozen Laemmli lysis buffer, the ground sample was centrifuged at $3000 \times g$ (RCF) for 10 min at 4 °C, and the supernatant was collected. The protein concentration in each sample was determined using a DC protein assay kit (Bio-Rad, Hercules, CA). Then, the protein samples were boiled for 10 min at 95 °C in loading buffer (125 mM Tris/HCl (pH 6.8), 20% glycerol, 0.1% bromophenol blue, 10% β-mercaptoethanol, 4% sodium dodecyl sulfate). The proteins were separated on 10% sodium dodecyl sulfate-polyacrylamide gel electrophoresis (SDS-PAGE) gels (Mini-PROTEAN Ä TGX™ precast gels; Bio-Rad) and then electro-transferred to polyvinylidene difluoride (PVDF) membranes using a Trans Blot Mini Cell (Bio-Rad). The membranes were blocked with 5% skim milk powder dissolved in 0.1% Tween 20 in TBS solution for 60 min, followed by incubation with the corresponding primary antibodies (anti-Iba1 (1:1000, cat# 016–20001, 1 μg/mL, FUJIFILM, Tokyo, Japan), anti-GFAP (1:1000, cat# MA5-15086, Thermo Fisher Scientific, USA), and anti-β-actin (1:10,000; cat# A5441, Sigma-Aldrich Co., Ltd, St Louis, MO, USA)) overnight at 4 °C, followed by incubation with the corresponding secondary antibody (1:5000) for 1 h. Bands were visualized with an enhanced chemiluminescence (ECL) kit and quantified using a ChemiDoc™ Touch Imaging System (170–01,401; Bio-Rad Laboratories, Hercules, CA).

2.5. 16S rRNA sequencing analysis

DNA was extracted from mouse fecal samples using the NucleoSpin DNA Fecal Kit (REF: 740472.50, MACHEREY-NAGEL, Germany) following the manufacturer's protocol. The V3–V4 region of the 16S rRNA gene was amplified by polymerase chain reaction (PCR), and all PCR products were sequenced on a HiSeq2500 platform by BGI JAPAN K.K. (Kobe, Japan). The sequences were deposited with the National Center for Biotechnology Information (accession number: PR JNA887905).

We used the Observed species index, Chao index, Ace index, and Shannon index to measure α-diversity (species diversity within each sample). The Observed species index, Chao index, and ACE index reflect the species richness of the microbial community. The Shannon index reflects the species diversity of the community, which is influenced by species richness and species evenness. Principal component analysis (PCA) was performed to assess differences in β-diversity, or species complexity, among samples (Caporaso et al., 2010). Linear discriminant analysis (LDA) effect size (LEfSe) was employed using LEfSe Software to

2
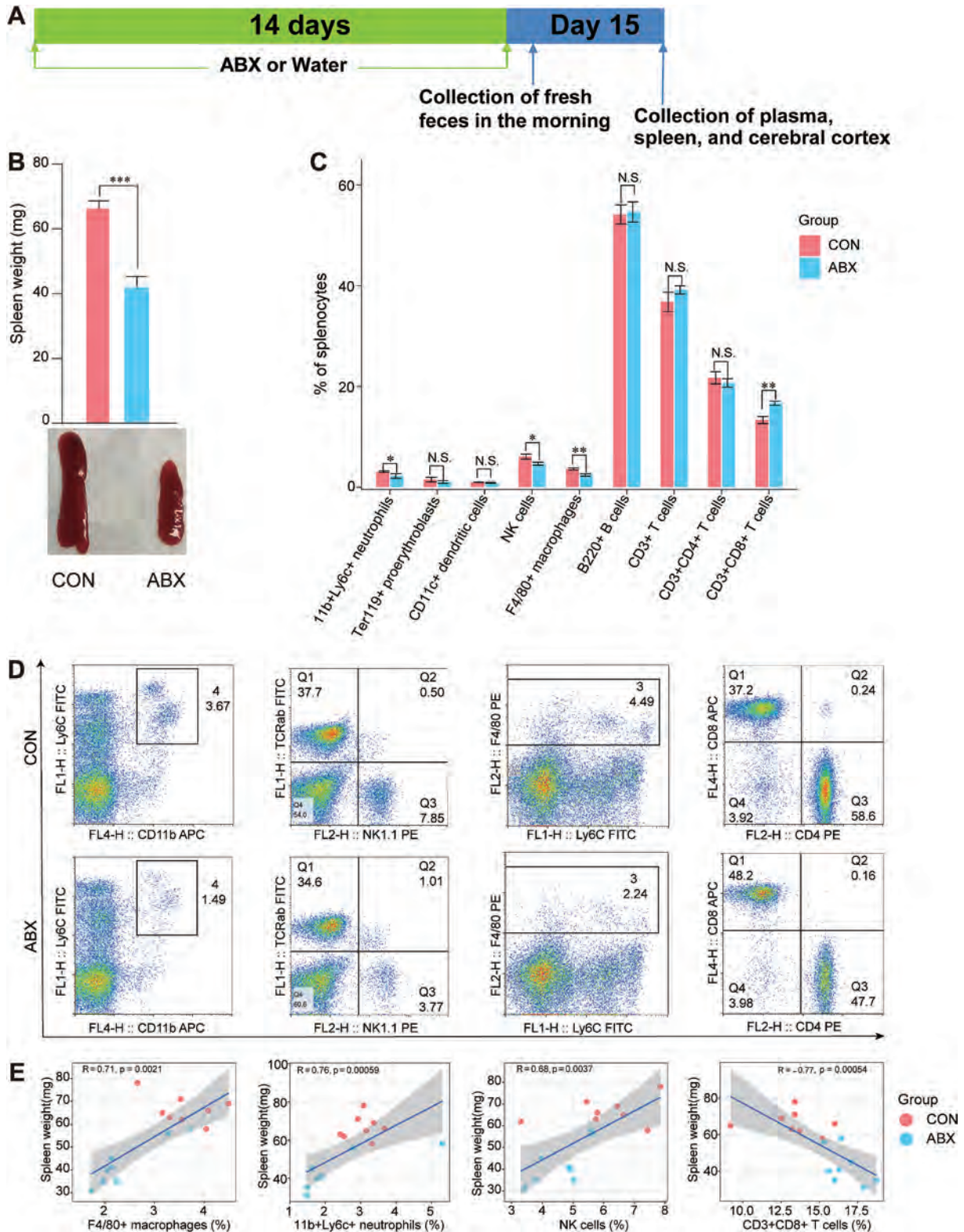
Fig. 1. Effects of ABX on spleen weight and spleen cell types

A: Schedule of the experiment. ABX or water was injected as drinking water for 14 days. Fresh feces samples were collected in the morning of day 15. Subsequently, plasma, spleen, and cerebral cortex were collected in the same day. B: ABX induced a significant reduction in spleen weight in mice (Two-tailed unpaired Student's T test, $P < 0.0001$). Representative photograph of spleen from the two groups. C: FACS analysis of spleen cell populations in all mice (Mann-Whitney test: $11b^+Ly6c^+$ neutrophils, $P = 0.0207$; $NK1.1^+$ NK cells, $P = 0.0207$; $F4/80^+$ macrophages, $P = 0.0070$; $CD3^+CD8^+$ T cells, $P = 0.002$). D: Representative FACS dot plots of neutrophils, NK cells, macrophages, and $CD8^+$ T cells. E: Spearman correlation analysis of spleen cell population and spleen weight in all mice. Values represent mean $\pm$ S.E.M. (CON: n = 8. ABX: n = 9). *$P < 0.05$, **$P < 0.01$, ***$P < 0.001$. N.S.: not significant.

discover high-dimensional biomarkers and reveal taxonomic features (Segata et al., 2011).

PICRUSt2 (Douglas et al., 2020) software was applied to predict the functional composition of the metagenome. After predicting the functions of all of the samples, the Wilcox test was used to identify different functions among the separate groups.

2.6. Untargeted metabolomics analysis

Untargeted metabolomics analysis of the plasma samples was performed following the methods described in our previous reports (Hashimoto et al., 2022; Shinno-Hashimoto et al., 2022; Wang et al., 2022b; Wan et al., 2022a; Wan et al., 2022b; Yang et al., 2022a). The spleen and cerebral cortex samples were analyzed in a manner similar to that used for the plasma samples, with slight modifications to the metabolite extraction process. Briefly, 400 μL of methanol containing internal standards (25 μM N,N-diethyl-2-phenylacetamide, and d-camphor-10-sulfonic acid) and 400 μL of ultrapure water were added to the sample, and the sample was homogenized using BioMasher Ä II with PowerMasher Ä II to extract the metabolome. The samples were then centrifuged at 14,000 g for 5 min, and 500 μL of the supernatant was passed through an ultrafiltration filter to purify it. Then, the purified supernatant was transferred to Amicon Ä Ultra-0.5 3 kDa filter columns (Merck Millipore, Tokyo, Japan) and centrifuged at $14,000 \times$ rpm for 1 h. The filtrates were transferred to glass vials for analysis. The details of the analysis are described in the supplementary material.

2.7. Statistical analysis

The data are expressed as the mean $\pm$ the standard error of the mean (S.E.M.). Student's t-test and Wilcox test (Mann-Whitney test) were employed to analyze differences between two groups based on the data distribution. Regarding the β diversity analysis, differences between groups were statistically analyzed using analysis of similarity (ANOSIM). Analyses comparing multiple time points were assessed using repeated measures analysis of variance (ANOVA). For analysis of metabolites, we used orthogonal partial least squares discriminant analysis (OPLS-DA) as a multivariate analysis model implemented in SIMCA-P (V.14.0). Then, significant peaks were determined by combination of variable importance in projection (VIP) value > 1, Wilcox rank test P value < 0.05, and false discovery rate (FDR) < 0.3 between the two groups. P-values of less than 0.05 were considered statistically significant.

3. Results

3.1. Effects of ABX treatment on spleen weight and splenocyte population

The body weight of ABX-treated mice was lower than that of control mice, and then recovered gradually, consistent with previous reports (Fig. S1A) (Pu et al., 2019; Wang et al., 2020a, 2020b). Compared with the CON group, ABX treatment resulted in a significant reduction in spleen weight and in the ratio of spleen weight to body weight (Fig. 1B and Fig. S1B). To identify the cell populations associated with the ABX-induced decrease in spleen weight, we then evaluated the frequency of neutrophils (11b⁺Ly6c⁺), proerythroblasts (Ter119⁺), dendritic cells (CD11c⁺), natural killer (NK) cells (NK1.1⁺), macrophages (F4/80⁺), B cells (B220⁺), T cells (CD3⁺), CD4⁺ T cells (CD3⁺CD4⁺), and CD8⁺ T cells (CD3⁺CD8⁺) in the spleen using flow cytometry. Of note, the percentages of 11b⁺Ly6c⁺ neutrophils, NK1.1⁺ NK cells, and F4/80⁺ macrophages were significantly lower in the ABX group compared with the CON group (Fig. 1C and D). In contrast, the percentage of CD8⁺ T cells in the ABX group was higher than that in the CON group. There were no changes in the percentage of proerythrocytes, dendritic cells, B cells, CD4⁺ T cells or CD3⁺ T cells between the two groups (Fig. 1C and D).

Positive correlations were found between the percentage of splenic macrophages, neutrophils, NK cells, and spleen weight. In contrast, a negative correlation was found between the percentage of CD8⁺ T cells and spleen weight (Fig. 1E).

3.2. ABX-treated mice exhibit altered gut microbiota composition

To examine the effect of ABX on the mouse gut microbiota, we carried out high-throughput amplicon sequencing of 16S rRNA microbial genes from mice in the CON and ABX groups. To estimate the richness, evenness, and diversity of the gut microbiota of mice in the CON and ABX groups, α-diversity was estimated using the Shannon index, Chao index, Observed species index, and Ace index. We detected a significant reduction in α-diversity in the ABX group compared to the CON group (Fig. S2A). These results suggest that the within-individual bacterial diversity of ABX-treated mice differed from that of CON mice. PCA-based β-diversity analysis revealed distinct cluster separation between the CON and ABX groups (ANOSIM analysis, P = 0.001) (Fig. S2B), indicating differences in the individual microbial communities between the two groups.

The microbial taxonomy and bacterial taxonomy of the gut microbiota were compared between the two groups at the phylum and species level (Fig. 2A). Comparing the percentages of bacteria at the phylum level, ABX eliminated or markedly reduced *Tenericutes*, *Verrucomicrobia*, *Deferribacteres*, *Bacteroidetes*, and *Firmicutes* levels compared with the CON group (Fig. 2A), while at the species level, the percentages of *Alloprevotella rava* and *Barnesiella intestinihominis* were considerably lower in the ABX group than in the CON group (Fig. 2A). Interestingly, ABX increased the percentages of the phyla *Proteobacteria* (88.7% in ABX and 1.1% in CON) and *Actinobacteria* (0.72% in ABX and 0.22% in CON) (Fig. 2A). At the species level, we observed an ABX-induced increase in the percentage of *Escherichia* (88.6% in ABX, 0.02% in CON), *Enterococcus saccharolyticus* (3.92% in ABX, 0% in CON), and *Paenibacillus relictisesami* (1.5% in ABX, 0% in CON) compared with the CON group (Fig. 2A).

Next, we investigated specific differences in the gut microbiota at different taxonomic levels in the ABX group compared with the CON group. At the phylum level, the ABX group had higher abundances of *Proteobacteria* and *Cyanobacteria* relative to the CON group; in fact, no *Cyanobacteria* were detected in the CON group (Fig. 2B, Table S1). In contrast, *Bacteroidetes* and *Firmicutes* were depleted in the ABX group in comparison with the CON group (Fig. 2B, Table S1). Three phyla were found to be completely absent in the ABX group, including *Deferribacteres*, *Tenericutes*, and *Verrucomicrobia* (Fig. 2B, Table S1). The abundance of 39 species was found to differ between the two groups (Fig. 2C, Table S2), of which 36 were significantly reduced or eliminated after ABX treatment (Fig. 2C, Table S2). Interestingly, the abundance of three species—*Cellulomonas denverensis*, *Enterococcus saccharolyticus*, and *Escherichia*—was dramatically higher in the ABX group than in the CON group (Fig. 2C, Table S2).

3.3. Microbial biomarkers and functional profiles

We employed LEfSe to determine taxonomic biomarkers that contributed to variations in the ABX-treated microbiome, with high strictness (LDA >4.8). As illustrated in the LEfSe-generated cladogram plot (Fig. 3A), the CON and ABX groups exhibited significantly different microbial community characteristics. Compared with the CON group, ABX group possessed significantly higher abundances of the class *Gammaproteobacteria*, the genus *Escherichia*, the order *Enterobacteriales*, the family *Enterobacteriacea*, the species *Escherichia*, and the phylum *Proteobacteria*. In contrast, the CON group contained higher abundances of the class *Clostridia*, the phylum *Firmicutes*, the phylum *Bacteroidetes*, the class *Bacteroidia*, the order *Bacteroidales*, the order *Clostridialesf Lachnospiraceae*, the family *Porphyromonadaceaeg Barnesiella*, and the order *Clostridialesf Lachnospiraceaeg Clostridium XlVa* (Fig. 3B).
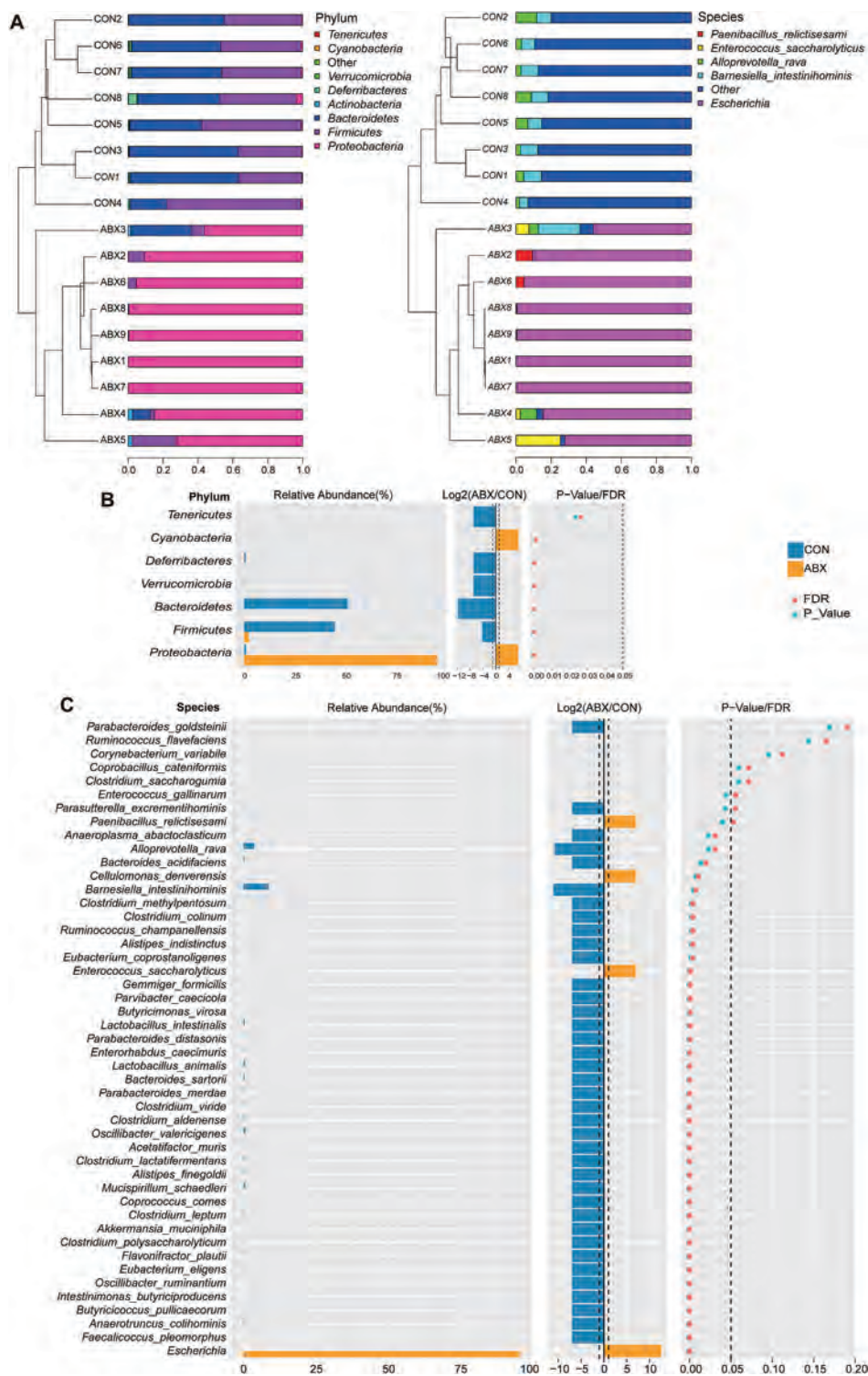
4

Fig. 2. Effects of ABX on the composition of gut microbiota

A: Bar chart of phylum-level bacterial community composition, with species level presenting the top five bacteria in abundance in all samples and the rest shown as "other". B: Differences of bacterial abundance at the phylum level in two groups (statistical results are presented in Table S1). C: Differences of bacterial abundance at the species level in two group of mice (statistical results are presented in Table S2).

Next, PICRUSt2 was used to predict the metagenomes of the gut microbes. The resulting functional profiles highlighted 34 pathways that were significantly changed in ABX mice compared with CON mice (Fig. 3C). The categories of microbial functions that changed in response to treatment with ABX included biosynthesis and degradation of fatty acids and lipids, glycan biosynthesis and degradation, aminoacyl-tRNA charging, carbohydrate biosynthesis, TCA cycle, biosynthesis and degradation of amines and polyamines, and degradation of aldehydes (Fig. 3C, Table S3). Of these, 17 metabolic pathways (e.g., TCA cycle, inorganic nutrient metabolism, amino acid degradation, amine and

polyamine biosynthesis, alcohol degradation, fatty acid and lipid degradation, aromatic compound degradation, and metabolic regulator biosynthesis, and aldehyde degradation, etc.) were significantly increased in the ABX group compared with the CON group (Fig. 3C, Table S3).

3.4. Splenic metabolomic profiles correlated with ABX-induced changes in percentage of splenic cell types, spleen weight, and the gut microbiota

To further explore ABX-induced spleen weight loss, changes in the

Fig. 3. Potential biomarkers defined by LEfSe, prediction of microbial function by PICRUSt2
A: Taxonomic cladogram generated by LEfSe analysis. B: LEfSe linear discriminant analysis (LDA) for taxa with P < 0.05 and scores >4.8. C: Significantly altered MetaCyc metabolic pathway between two groups predicted based on sequencing data of 16S rRNA gene (statistical results are presented in Table S3).

percentage of splenic cell populations, and metabolic changes, we performed untargeted metabolomic analysis of mouse spleen samples. After the initial screen, 99 metabolites from each group were selected for more detailed evaluation. We further carried out supervised data analysis using OPLS-DA to clarify metabolic variations. The OPLS-DA score plots for the CON and ABX groups were clearly separated, suggesting

that the model was able to distinguish between metabolites from the CON group and from the ABX group (Fig. S3). A volcano plot was constructed by analyzing the P-values from the Mann-Whitney test and the variable importance (VIP) scores from the OPLS-DA. Metabolites matching the requirements of P < 0.05 (FDR-corrected P < 0.05) and VIP >1 were defined as differentially represented metabolites (Fig. 4A).

6

Fig. 4. Alterations in splenic metabolites between the two groups, and Spearman correlations in splenic metabolites, spleen cell populations, and gut microbes
A: Volcano plot showing splenic metabolite profiles between the CON and ABX groups. X-axis indicates the log2 transformed fold change in splenic metabolite abundance, and y-axis indicates the -log10 transformed P-value using the Wilcox test. Horizontal lines indicate P < 0.05. Red or blue dots indicate differential metabolites between the two groups. B: Differences in abundance of splenic differential metabolites between the two groups (statistical results are presented in Table S4). C: Spearman correlation analysis of splenic differential metabolites with percentage of splenic cell population or spleen weight. D: Spearman correlation analysis of differential species (average of abundance >0.1% in all samples) with splenic differential metabolites, percentage of splenic cell populations, or spleen weight. Values represent mean ± S.E.M. (CON: n = 8. ABX: n = 9). #P (FDR-corrected) < 0.05, ##P (FDR-corrected) < 0.01, ###P (FDR-corrected) < 0.001, ####P (FDR-corrected) < 0.0001. *P < 0.05, **P < 0.01, ***P < 0.001. N.S.: not significant.

7

Eighteen metabolites, including 2-pyrrolidinone, 3-aminohexanoic acid, acetyl-DL-carnitine, cytarabine, DL-pyroglutamic acid, guanidinoethyl sulfonate, L-histidine, L-arginine, L-cysteine-glutathione disulfide, L-lysine, L-methionine, L-phenylalanine, N-alpha-(tert-butoxycarbonyl)-L-histidine, nicotinamide, phosphate, taurine, urea, and valine betaine, exhibited significantly lower abundance in the spleens of mice in the ABX group than in the CON group (Fig. 4B, Table S4). In contrast metronidazole exhibited higher abundance in the spleens of ABX mice compared with the CON mice (Fig. 4B, Table S4). Taken together, these results suggest that, instead of being due solely to the decrease in spleen weight observed in ABX-treated mice, the reduction in specific metabolites in the spleen might result from long-term exposure to ABX.

The correlations among differentially represented spleen metabolites, percentage of spleen cell types, and spleen weight were analyzed for all mice (Fig. 4C). Spleen weight was positively correlated with the abundance of the 18 metabolites that were reduced in the ABX group and negatively correlated with the abundance of metronidazole in the ABX group (Fig. 4C). The abundance of 12 metabolites, including 3-aminohexanoic acid, L-methionine, L-histidine, N-alpha-(tert-butoxycarbonyl)-L-histidine, phosphate, acetyl-DL-carnitine, DL-pyroglutamic acid, L-cysteine-glutathione disulfide, L-phenylalanine, nicotinamide, 2-pyrrolidinone, and taurine, was positively associated with the percentage of several cell types in the splenic cell population, such as NK cells, macrophages, and neutrophils, but it was negatively associated with the percentage of CD8$^+$ T cells (Fig. 4C). To determine the most unique and functionally critical taxa that differed in abundance between the ABX group and the CON group, correlation analyses were performed between the differentially represented species (>0.1% in mean abundance across all samples, henceforth referred to as differential species) and spleen weight, percentage of spleen cell populations, and spleen differential metabolites (Fig. 4D). Significant correlation was found between differential species and differential metabolites in the spleen and both the percentage of spleen cell populations and the spleen weight (Fig. 4D). Overall, the abundances of 10 species (*Barnesiella intestinihominis, Bacteroides sartorii, Clostridium lactatifermentans, Lactobacillus animalis, Lactobacillus intestinalis, Parabacteroides merdae, Oscillibacter valericigenes, Eubacterium eligens, Anaerotruncus colihominis, Mucispirillum schaedleri*) was negatively associated with the percentage of splenic CD8$^+$ T cells and the abundance of the splenic metabolite metronidazole, but it was positively associated with the percentage of splenic macrophages and spleen weight (Fig. 4D). Metronidazole was one of the antibiotics used in this study. We found that the abundance of the ABX-depleted species *Mucispirillum schaedleri, Anaerotruncus colihominis,* and *Lactobacillus intestinalis* was negatively correlated with the percentage of CD8$^+$ T cells in the ABX group, which in turn was negatively correlated with the concentration of L-cysteine-glutathione disulfide. Furthermore, L-cysteine-glutathione disulfide was positively correlated with spleen weight (Fig. S4).

3.5. Plasma metabolomic profiles correlated with ABX-induced changes in percentage of splenic cell types, spleen weight, and gut the microbiota

We further investigated whether plasma metabolomic biomarkers were associated with ABX-induced changes in the percentage of splenocyte types, spleen weight, and the gut microbiota. A total of 156 metabolite signatures were detected after preprocessing the detected signals. After 14 days of ABX treatment, the plasma metabolic profiles were significantly different between the CON and ABX groups. The OPLS-DA model shows that the metabolic profiles of the two groups were completely separated (Fig. S5). Using VIP >1 and P < 0.05 (FDR-corrected P < 0.05) as cut-offs, we identified 15 differentially represented metabolites (Fig. 5A). We identified 12 metabolites (1,2-dichloroethane, 2,4,4'-trihydroxybenzophenone, 2-alpha-mannobiose, 3',5'-cyclic inosine monophosphate, 4-O-beta-galactopyranosyl-D-mannopyranose, 6-phospho-D-gluconate, benzamide, N–1H-indol-5-yl-, D-(+)-mannose, D-gluconic acid, D-psicose, galactinol, and glutamate-

glutamine) whose abundance was significantly lower in plasma from the ABX group compared with the CON group (Fig. 5B, Table S5). In contrast, we found a significantly higher abundance of three metabolites (5-aminolevulinic acid, ethylenediaminetetraacetic acid, hydroxybutyrylglycine) in plasma from the ABX group compared with the CON group (Fig. 5B, Table S5).

Spearman correlation analysis showed a positive correlation between all 12 plasma ABX-depleted metabolites and spleen weight, but a negative correlation between all 12 plasma ABX-depleted metabolites and splenic CD8$^+$ T cell percentage (Fig. 5C). However, the two ABX-enriched plasma metabolites—5-aminolevulinic acid and hydroxybutyrylglycine—were positively correlated with splenic CD8$^+$ T cell percentage and negatively correlated with the percentage of splenic neutrophils, splenic macrophages, and spleen weight (Fig. 5C). We also detected extensive correlations between differential species, plasma metabolites, splenic cell populations, and spleen weight (Fig. 5D, Fig. S6). A total of 10 ABX-depleted species (*Barnesiella intestinihominis, Lactobacillus intestinalis, Bacteroides sartorii, Parabacteroides merdae, Oscillibacter valericigenes, Eubacterium eligens, Anaerotruncus colihominis, Mucispirillum schaedleri, Clostridium lactatifermentans,* and *Lactobacillus animalis*) were significantly positively correlated with 12 ABX-depleted plasma metabolites, percentage of splenic cell populations (NK cells, neutrophils, macrophages), and spleen weight, whereas they were negatively correlated with two ABX-enriched plasma metabolites (5-aminolevulinic acid and hydroxybutyrylglycine) and percentage of splenic CD8$^+$ T cells (Fig. 5D). These associations are shown in the correlation network diagram (Fig. S6).

3.6. Relationships between ABX-induced changes in the gut microbiota, splenic metabolites, plasma metabolites, cortical metabolites, and splenic function

We measured the expression of the microglial marker Iba1 and the astrocytic marker GFAP in the cerebral cortex samples from the ABX and CON groups by western blotting. Mice treated with ABX showed reduced levels of Iba1 expression compared with CON mice; however, GFAP expression did not differ between the two groups (Fig. 6A).

After data preprocessing, a total of 139 metabolic features were identified by untargeted metabolomics analysis of cerebral cortex samples from the ABX and CON groups. Subsequently, the OPLS-DA model was constructed to identify metabolites that contributed towards group differentiation. The metabolic profiles of the two groups as determined by the OPLS-DA model were somewhat separate (Fig. S7). Using the same procedures as that used for the spleen and plasma metabolomics analyses, six differential metabolites from the cerebral cortex were selected (P < 0.05, VIP >1, FDR-corrected P < 0.3) (Fig. 6B). Compared with the CON group, we identified four metabolites (carnosine, D-pyroglutamic acid, glutamine, and N-acetyl-L-glutamine) with elevated abundance in the ABX group and two metabolites (adenine and DL-2-aminocaprylic acid) with decreased abundance in the ABX group (Fig. 6C, Table S6).

We noticed that the level of Iba1 in the cerebral cortex was significantly and negatively correlated with the abundance of metabolites such as carnosine and D-pyroglutamic acid (Fig. 6D). Furthermore, spleen weight was negatively correlated with the four ABX-enriched metabolites in the cerebral cortex (Fig. 6D). Spearman rank correlation analysis showed extensive positive correlations between ABX-depleted species and ABX-depleted metabolites in the cerebral cortex, splenic cell populations (NK cells, neutrophils, and macrophages), and spleen weight. In contrast, significant negative correlations were found between ABX-depleted species and ABX-enriched metabolites, and splenic CD8$^+$ T cells (Fig. 6E). The Iba1 level in the cerebral cortex was positively correlated with the abundance of *Lactobacillus intestinalis* (Fig. 6E). Similar correlations were found in the correlation network plots (Fig. S8).

To investigate the relationship between spleen weight, percentage of
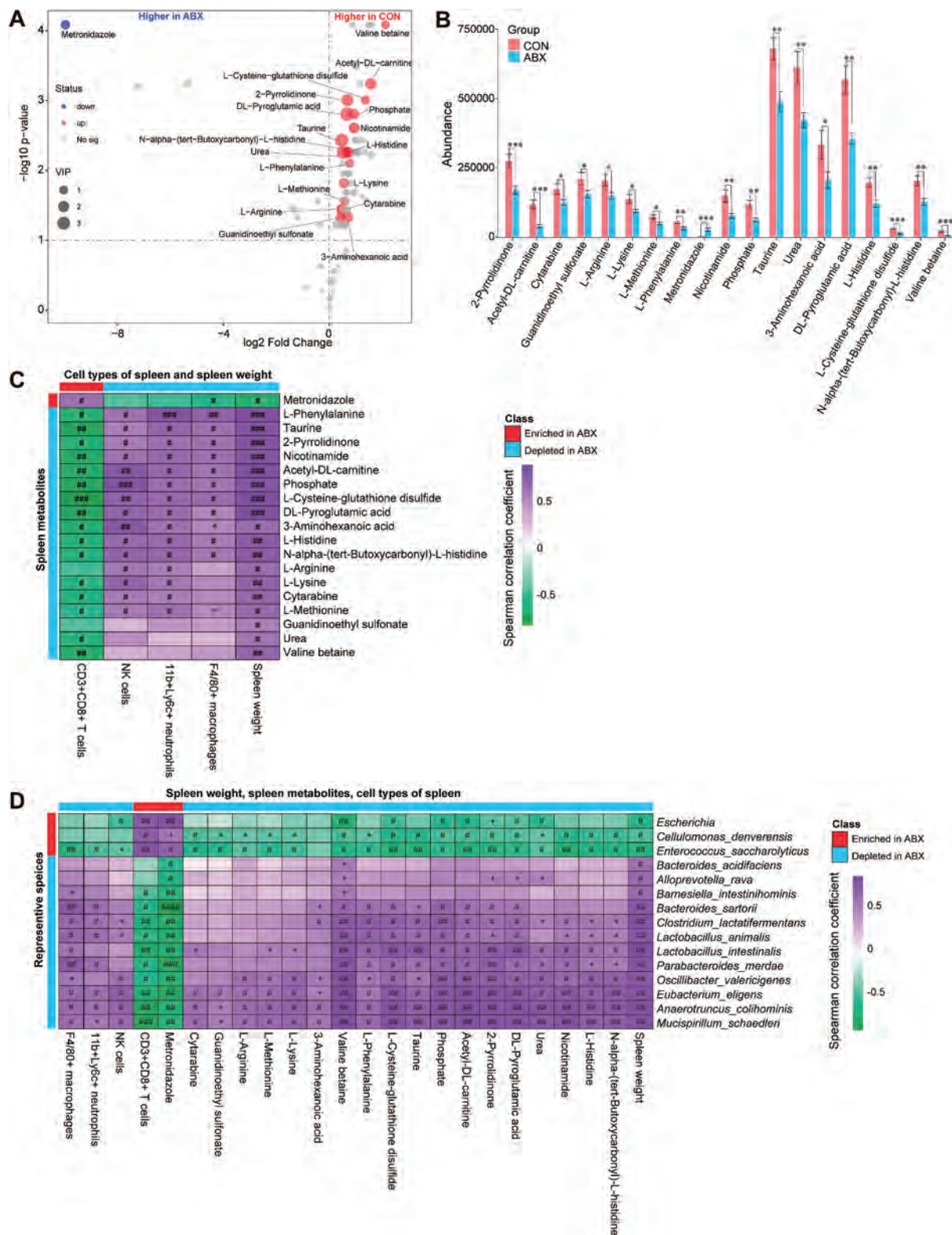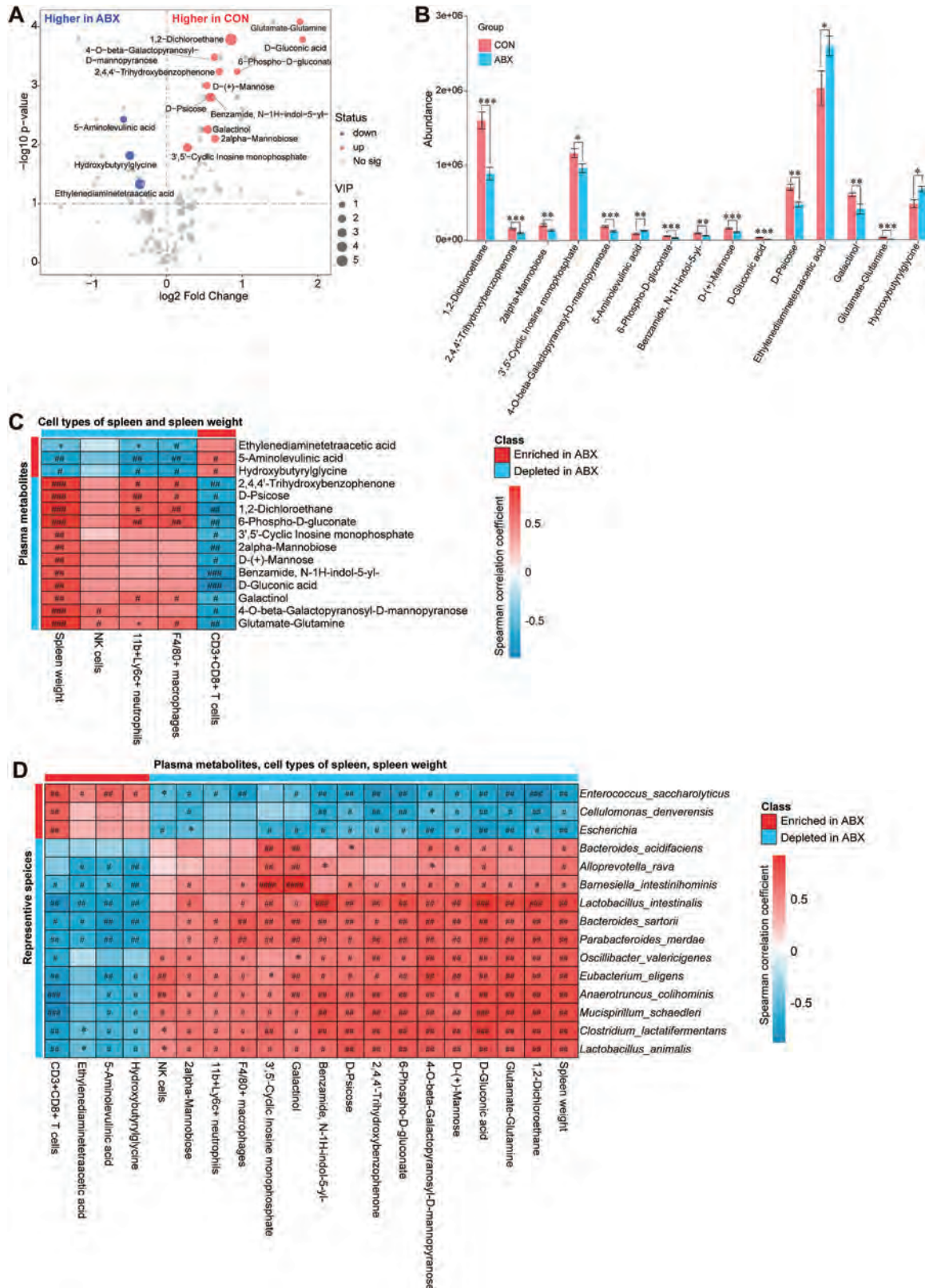
8

Fig. 5. Alterations in plasma metabolites between the two groups, and Spearman correlations in plasma metabolites, spleen cell populations, and gut microbes
A: Volcano plot showing plasma metabolite profiles between the CON and ABX groups. X-axis indicates the log2 transformed fold change in plasma metabolite abundance, and y-axis indicates the -log10 transformed P-value using the Wilcox test. Horizontal lines indicate P < 0.05. Red or blue dots indicate differential metabolites between the two groups. B: Differences in abundance of plasma differential metabolites between the two groups (statistical results are presented in Table S5). C: Spearman correlation analysis of plasma differential metabolites with percentage of splenic cell population or spleen weight. D: Spearman correlation analysis of differential species (average of abundance >0.1% in all samples) with plasma differential metabolites, percentage of splenic cell populations, or spleen weight. Values represent mean ± S.E.M. (CON: n = 8. ABX: n = 9). #P (FDR-corrected) < 0.05, ##P (FDR-corrected) < 0.01, ###P (FDR-corrected) < 0.001, ####P (FDR-corrected) < 0.0001. *P < 0.05, **P < 0.01, ***P < 0.001. N.S.: not significant.
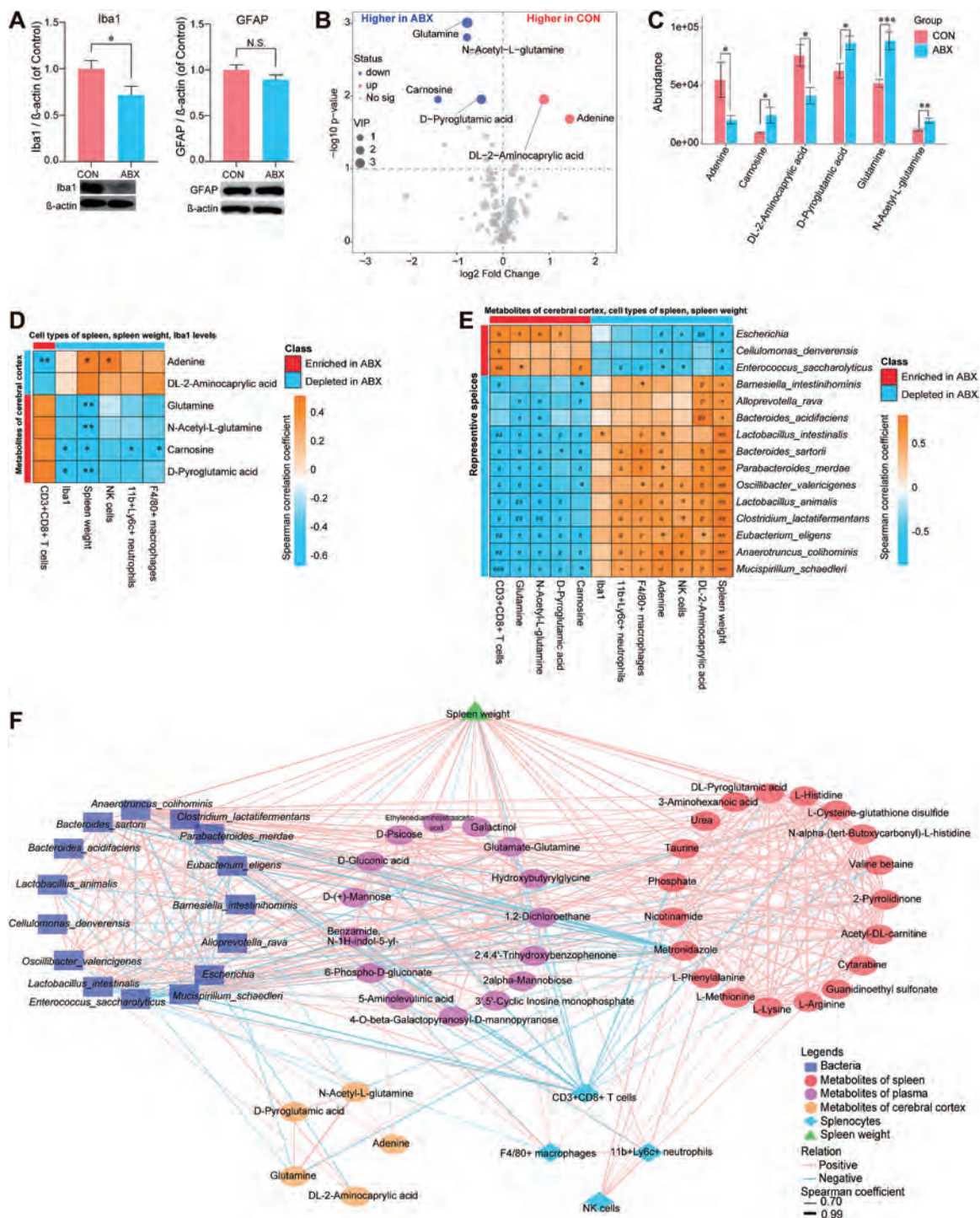
9

Fig. 6. Expression of Iba1 and GFAP in the cerebral cortex, altered metabolites in the cerebral cortex, and joint correlation analysis of microbial, multi-location metabolites, and splenic cell populations

A: Expression of Iba1 and GFAP in the cerebral cortex from two groups. B: Volcano plot showing cerebral cortical metabolite profiles between the CON and ABX groups. X-axis indicates the log2 transformed fold change in cerebral cortical metabolite abundance, and y-axis indicates the -log10 transformed P-value using the Wilcox test. Horizontal lines indicate P < 0.05. Red or blue dots indicate differential metabolites between the two groups. C: Differences in abundance of differential metabolites in the cerebral cortex between the two groups (statistical results are presented in Table S6). D: Spearman correlation analysis of differential metabolites in the cerebral cortex with percentage of splenic cell population, Iba1 expression in the cerebral cortex, or spleen weight. E: Spearman correlation analysis of differential species (average of abundance >0.1% in all samples) with differential metabolites in the cerebral cortex, Iba1 level in the cerebral cortex, percentage of splenic cell populations, or spleen weight. F: Joint correlation analysis of spleen weight, percentage of spleen cell population, representative metabolites of different tissues (spleen, plasma, cerebral cortex) and gut microbiota for all mice. Red lines denote positive correlations, blue lines denote negative correlations, and thicker lines represent larger correlation coefficients (Spearman correlation analysis, absolute value of correlation coefficient >0.7, FDR-corrected P < 0.05). Circles indicate metabolites, and different colors indicate originating from different types of tissues. Bacteria are indicated by squares, triangles indicate spleen weights, and diamonds indicate splenic cell populations. Values represent mean ± S.E.M. (CON: n = 8. ABX: n = 9). [#]P (FDR-corrected) < 0.05, [##]P (FDR-corrected) < 0.01, [###]P (FDR-corrected) < 0.001. *P < 0.05, **P < 0.01, ***P < 0.001. N.S.: not significant.

spleen cell populations, differential metabolites in the spleen, and the gut microbiota, we performed a joint analysis of the above data for all of the mice. Correlation network analysis revealed highly sophisticated patterns of interactions (463 correlations, Spearman rho ≥0.7, P < 0.05, FDR-corrected P < 0.05) between taxa (mean abundance >0.1% across all samples), splenic cell populations, spleen weight, and metabolites in the spleen, plasma, and cerebral cortex (Fig. 6F). Interestingly, the correlations were stronger between different tissues than within each tissue, suggesting strong functional associations between the brain, gut microbiota, plasma, and spleen. Of interest, the concentrations of five plasma metabolites (1,2-dichloroethane, D-gluconic acid, D-psicose, 6-phospho-D-gluconate, and 2,4,4'-trihydroxybenzophenone) were positively correlated with the abundance of *Clostridium lactatifermentans* and *Lactobacillus animalis*, which were negatively correlated with glutamine in the cerebral cortex. Plasma D-psicose was further positively correlated with the splenic metabolite L-phenylalanine, splenic neutrophil percentage, and spleen weight. Seven plasma metabolites, including D-gluconic acid, 1,2-dichloroethane, glutamate-glutamine, benzamide, N–1H-indol-5-yl-, 2,4,4'-trihydroxybenzophenone, 6-phospho-D-gluconate, and 4 -O-beta-galactopyranosyl-D-mannopyranose were positively correlated with the species *Anaerotruncus colihominis* and *Mucispirillum schaedleri*, which were further positively correlated with adenine in the cerebral cortex. Of note, the plasma D-gluconic acid level directly correlated with adenine in the cerebral cortex. The tight relationship between gut microbes, plasma metabolites, and cerebral cortical metabolites indicates that specific microbes may be involved in the metabolism of specific plasma and brain metabolites and regulate brain function. We observed correlations between plasma metabolites, splenic metabolites, and cerebral cortical metabolites. Some highly correlated features included the plasma metabolites glutamate-glutamine, 2,4,4'-trihydroxybenzophenone, and 1,2-dichloroethane, which correlated positively with the splenic metabolite valine-betaine; the latter further correlated with two metabolites (glutamine and N-acetyl-L-glutamine) in the cerebral cortex, spleen CD8^{+} T cell population, and spleen weight. We found that adenine in the cerebral cortex was positively correlated with the plasma metabolite D-gluconic acid, which was positively correlated with two splenic metabolites (phosphate and L-cysteine-glutathione disulfide); phosphate and L-cysteine-glutathione disulfide were further negatively correlated with splenic CD8^{+} T cell population and positively correlated with spleen weight.

4. Discussion

The main findings of this study are as follows. First, ABX treatment resulted in decreased spleen weight compared with the CON group. The percentage of cell types of spleen was significantly altered in the ABX group, including a decrease in the percentage of three cell types (NK cells, macrophages, and neutrophils) and, conversely, a significant increase in the percentage of CD8^{+} T cells. The percentage of these cell populations significantly correlated with spleen weight. Second, ABX treatment leads to depletion of a large proportion of the gut microbiota. The α- and β-diversity of the gut microbiota, as well as the composition of the gut microbiota, showed significant differences between the two groups. Third, LEfSe analysis determined that the class *Gammaproteobacteria,* the genus *Escherichia,* the phylum *Proteobacteria,* the order *Enterobacteriales,* and the family *Enterobacteriacea* are potential microbial markers of the ABX group. Predictive functional analysis of the gut microbiota revealed that ABX caused alterations in multiple metabolic pathways, such as those involved in biosynthesis and degradation of fatty acids and lipids, degradation of amines and polyamines, carbohydrate biosynthesis, and the TCA (tricarboxylic acid) cycle. Fourth, ABX treatment caused a reduction in the expression of the microglia marker Iba1 in the cerebral cortex. Fifth, untargeted metabolomics analysis of spleen, plasma, and cerebral cortex samples demonstrated that ABX treatment caused alterations in the levels of a number of compounds. There were strong correlations among these differential compounds, the

level of Iba1 expression in the cerebral cortex, spleen cell populations, spleen weight, and the relative abundance of microbes. Finally, joint network analysis showed strong interconnections among gut microbes and metabolites (plasma, spleen, cerebral cortex), spleen cell populations, and spleen weight. Collectively, these findings suggest that ABX-induced microbiome depletion could affect spleen and brain function through the gut–microbiota–spleen–brain axis.

In this study, we found that the percentages of neutrophils, NK cells, and macrophages were significantly reduced in the spleens of ABX-treated mice, and that these cell types were positively correlated with spleen weight. We previously reported that spleen weight positively correlates with percentages of cell types (i.e., neutrophils, pro-erythroblasts, B cells, macrophages, and dendritic cells) in imiquimod-treated mice (Shinno-Hashimoto et al., 2022). Therefore, spleen weight is likely to be affected by changes in the abundance of specific splenic cellular components. In contrast, ABX treatment caused increase in CD8^{+} T cells in the spleen, and there was a negative correlation between CD8^{+} T cell percentage and spleen weight. Antibiotic treatment can cause abnormalities in the immune cell populations in the GI tract and spleen (Kennedy et al., 2018), indicating that the immune system responds to pathogenic and commensal microbial populations. Therefore, ABX-induced microbiome depletion may alter the cellular composition of the host spleen, resulting in a reduction in spleen weight.

Escherichia was the most predominant bacterium in ABX-treated mice, with a relative abundance of 88.6%. Previous reports have demonstrated that *Escherichia coli* (*E. coli*) strains are diverse, ranging from innocuous GI residents to multiple pathotypes capable of causing intestinal or extraintestinal disease, such as infantile diarrhea, hemorrhagic colitis, and more, related to antibiotic resistance (Croxen et al., 2013; Moyenuddin et al., 1989; Subramanian et al., 2009). Given the existence of various antibiotic-resistant *E. coli* strains, the high abundance of *Escherichia* in the gut of ABX-treated mice may indicate the presence of antibiotic-resistant strains. Collectively, it seems that antibiotic use drives changes in the composition of the intestinal microbiota, leading to an imbalance in physiological homeostasis and permitting the long-term growth and colonization of antibiotic-resistant microorganisms in the gut.

The 18 ABX-reduced splenic compounds were positively correlated with the proportion of spleen cell types such as NK cells, macrophages, and neutrophils, and negatively correlated with the proportion of splenic CD8^{+} T cells. Bacterial or parasitic infections are known to possibly affect splenic responses (Lewis et al., 2019). Although the current study does not provide strong evidence for this, these compounds may be involved in splenic-mediated immune responses. The differentially represented taxa between the two groups were significantly correlated with splenic metabolites and splenic cell populations. Collectively, these findings suggest that ABX-induced microbiome depletion modulates splenic function by altering metabolite expression, although further study is needed to confirm this.

In this study, we detected *Enterococcus saccharolyticus* (Hammad et al., 2014), a bacterium that is associated with antibiotic resistance, in the intestine of ABX-treated mice. Furthermore, there was a positive correlation between plasma levels of 5-aminolevulinic acid (5-ALA) and relative abundance of *Enterococcus saccharolyticus*, suggesting that *Enterococcus saccharolyticus* in the intestine may contribute to the production of 5-ALA. Microbial production of 5-ALA by photosynthetic bacteria has been demonstrated previously (Liu et al., 2014; Sasaki et al., 2002). Increasing evidence suggests that 5-ALA-induced apoptosis can be used to treat tumors (Huang et al., 2016; Liu et al., 2019; Mamalis et al., 2016; Stummer et al., 2006). We found that plasma levels of 5-ALA were significantly elevated in the ABX-treated mice, and negatively correlated with splenic neutrophils, macrophages, and spleen weight. Given the beneficial role of 5-ALA (Jiang et al., 2022), the increase in 5-ALA levels induced by ABX treatment may have a compensatory effect on impaired splenic functions. Taken together, our findings suggest that ABX-induced microbiome depletion could affect the synthesis and

11

metabolism of a number of host metabolites that regulate splenic cell populations and spleen function via humoral circulation. Nonetheless, more detailed study is needed to elucidate the role of *Enterococcus saccharolyticus* in the production of 5-ALA, as well as the role of 5-ALA in the spleen.

Increasing evidence suggests that the gut microbiome plays a crucial role in microglial maturation and activation both in healthy individuals and in patients with CNS disease (Cook and Prinz, 2022; Erny and Prinz, 2020). Erny et al. (2015) demonstrated that GF mice have global defects in microglia and altered cell proportions, leading to an impaired innate immune response. Furthermore, microbiome-derived compounds are known to regulate microglial homeostasis in the brain (Erny et al., 2015). We previously reported that repeated administration of PLX5622 (a specific inhibitor of the colony-stimulating factor 1 receptor) affects the relative abundance of gut microbiota components, and that there are significant correlations between microglial markers in the brain and the relative abundance of gut microbiota components, suggesting microbiome-microglia crosstalk through the brain–gut axis (Yang et al., 2022b). Compared with CON mice, the ABX mice exhibited low expression of the microglia marker Iba1 in the cerebral cortex. Collectively, these findings suggest crosstalk between the gut microbiota and the microglia in the brain through the gut–microbiota–brain axis.

Carnosine, a dipeptide that is present in high concentrations in the brain, is a putative neurotransmitter (Caruso et al., 2019; Tiedje et al., 2010). A growing body of evidence shows the potentially beneficial effects of carnosine in psychiatric and neurological disorders (Schön et al., 2019). In this study, we found that carnosine was elevated in the cerebral cortex of ABX-treated mice, which is in keeping with its known neuroprotective effects in the brain. Furthermore, carnosine was negatively correlated with Iba1 expression in the cerebral cortex, consistent with the previous report that carnosine in the brain is mainly metabolized by microglia, oligodendrocytes, astrocytes, and macrophages (Caruso et al., 2019). Substantial evidence suggests that carnosine has anti-aggregatory, anti-oxidant, anti-inflammatory, and neuroprotective effects in the CNS (Caruso et al., 2019). Interestingly, we found that the level of carnosine in the cerebral cortex was negatively correlated with the proportion of splenic macrophages and neutrophils, suggesting a brain–spleen axis.

The joint analysis showed that the abundance of the probiotic bacterial strain *Lactobacillus animalis* (Sahoo et al., 2015) was correlated with plasma levels of D-psicose and negatively correlated with glutamine levels in the cerebral cortex. Glutamine is a by-product of ammonia metabolism that is capable of causing reactive oxidative stress in astrocytes and inducing the mitochondrial permeability transition, which causes neurotoxicity through the action of mitochondrial phosphate activated glutaminase (Albrecht and Norenberg, 2006). The anti-hyperlipidemic effect of D-psicose is related to its hypoglycemic, hypolipidemic, and antioxidant activities, which make it optimal for the prevention of diabetes and related health problems (Chung et al., 2012), further suggesting that plasma metabolism is regulated by intestinal microorganisms and affects the functional state of neuronal cells. Furthermore, plasma D-psicose levels were positively correlated with L-phenylalanine (an essential amino acid in the spleen) levels, which are positively correlated with the proportion of splenic neutrophils, and ultimately spleen weight. Collectively, our findings suggest that the gut–spleen–brain axis regulates the metabolic and functional state of neuronal cells via microbial-derived metabolites, and that the brain may modulate splenic cell types and splenic function.

We previously reported that ABX-induced depletion of the gut microbiome is associated with stress resilience in mice exposed to chronic social defeat stress (Wang et al., 2020b) and protects against MPTP-induced dopaminergic neurotoxicity in the brain (Pu et al., 2019) and LPS (lipopolysaccharide)-induced acute lung injury (Hashimoto et al., 2022). Furthermore, LPS-induced splenomegaly in mice was associated with higher levels of pro-inflammatory cytokines (Ma et al., 2022a, 2022b; Zhang et al., 2020b, 2021a), suggesting that an increase

in spleen weight is associated with systemic inflammation. Considering the decreased spleen weight induced by treatment with ABX, ABX treatment possibly has anti-inflammatory effects in mice. Given the anti-inflammatory role of the gut–microbiota–spleen–brain axis, it is likely that ABX-induced microbiome depletion has anti-inflammatory effects in several animal models.

This study had one limitation, in that we divided the spleen to investigate the relationship between splenic cell types and metabolites in the spleen. However, the spleen is divided by function and structure into the red pulp, white pulp, and marginal zone, suggesting that the immune cells are differentially organized in these three structures (Lewis et al., 2019). The differences in these structures may affect the functions of splenic cells and metabolites, and further detailed study is needed to address this possibility.

5. Conclusion

The findings from the present study suggest that ABX-induced microbiome depletion causes a decrease in spleen weight and abnormal expression of metabolites in the blood, spleen, and brain. In addition to microbiome depletion, ABX treatment likely affects spleen and brain function through the gut–microbiota–spleen–brain axis.

Declaration of competing interest

Dr. Hashimoto is the inventor of filed patent applications on "The use of *R*-Ketamine in the treatment of psychiatric diseases", "(*S*)-norketamine and salt thereof as pharmaceutical", "*R*-Ketamine and derivative thereof as prophylactic or therapeutic agent for neurodegeneration disease or recognition function disorder", "Preventive or therapeutic agent and pharmaceutical composition for inflammatory diseases or bone diseases", "*R*-Ketamine and its derivatives as a preventive or therapeutic agent for a neurodevelopmental disorder", and "Preventive or therapeutic agent and pharmaceutical composition for inflammatory diseases" by the Chiba University. Dr. Hashimoto also declares that he has received research support and consultant from Abbott, Boehringer Ingelheim, Daiichi-Sankyo, Meiji Seika Pharma, Seikagaku Corporation, Sumitomo-Pharma, Taisho, Otsuka, Murakami Farm and Perception Neuroscience. The other authors have no conflict of interest.

Data availability

The 16S rRNA sequencing data have been deposited to the NCBI Sequence Read Archive and are available at the accession number PRJNA887905.

Appendix A. Supplementary data

Supplementary data to this article can be found online at https://doi.org/10.1016/j.bbih.2022.100573.

12

References

Albrecht, J., Norenberg, M.D., 2006. Glutamine: a Trojan horse in ammonia neurotoxicity. Hepatology (Baltimore, Md 44 (4), 788–794. https://doi.org/10.1002/hep.21357.

Aron-Wisnewsky, J., Clément, K., 2016. The gut microbiome, diet, and links to cardiometabolic and chronic disorders. Nat. Rev. Nephrol. 12 (3), 169–181. https://doi.org/10.1038/nrneph.2015.191.

Borovikova, L.V., Ivanova, S., Zhang, M., Yang, H., Botchkina, G.I., Watkins, L.R., Wang, H., Abumrad, N., Eaton, J.W., Tracey, K.J., 2000. Vagus nerve stimulation attenuates the systemic inflammatory response to endotoxin. Nature 405 (6785), 458–462. https://doi.org/10.1038/35013070.

Breit, S., Kupferberg, A., Rogler, G., Hasler, G., 2018. Vagus nerve as modulator of the brain-gut axis in psychiatric and inflammatory disorders. Front. Psychiatr. 9, 44. https://doi.org/10.3389/fpsyt.2018.00044.

Bronte, V., Pittet, M.J., 2013. The spleen in local and systemic regulation of immunity. Immunity 39 (5), 806–818. https://doi.org/10.1016/j.immuni.2013.10.010.

Buchmann Godinho, D., da Silva Fiorin, F., Schneider Oliveira, M., Furian, A.F., Rechia Fighera, M., Freire Royes, L.F., 2021. The immunological influence of physical exercise on TBI-induced pathophysiology: crosstalk between the spleen, gut, and brain. Neurosci. Biobehav. Rev. 130, 15–30. https://doi.org/10.1016/j.neubiorev.2021.08.006.

Caporaso, J.G., Kuczynski, J., Stombaugh, J., Bittinger, K., Bushman, F.D., Costello, E.K., Fierer, N., Peña, A.G., Goodrich, J.K., Gordon, J.I., Huttley, G.A., Kelley, S.T., Knights, D., Koenig, J.E., Ley, R.E., Lozupone, C.A., McDonald, D., Muegge, B.D., Pirrung, M., Reeder, J., Sevinsky, J.R., Turnbaugh, P.J., Walters, W.A., Widmann, J., Yatsunenko, T., Zaneveld, J., Knight, R., 2010. QIIME allows analysis of high-throughput community sequencing data. Nat. Methods 7 (5), 335–336. https://doi.org/10.1038/nmeth.f.303.

Caruso, G., Caraci, F., Jolivet, R.B., 2019. Pivotal role of carnosine in the modulation of brain cells activity: multimodal mechanism of action and therapeutic potential in neurodegenerative disorders. Prog. Neurobiol. 175, 35–53. https://doi.org/10.1016/j.pneurobio.2018.12.004.

Chang, L., Wei, Y., Hashimoto, K., 2022. Brain-gut-microbiota axis in depression: a historical overview and future directions. Brain Res. Bull. 182, 44–56. https://doi.org/10.1016/j.brainresbull.2022.02.004.

Chung, M.Y., Oh, D.K., Lee, K.W., 2012. Hypoglycemic health benefits of D-psicose. J. Agric. Food Chem. 60 (4), 863–869. https://doi.org/10.1021/jf204050w.

Cook, J., Prinz, M., 2022. Regulation of microglial physiology by the microbiota. Gut Microb. 14 (1), 2125739 https://doi.org/10.1080/19490976.2022.2125739.

Croxen, M.A., Law, R.J., Scholz, R., Keeney, K.M., Wlodarska, M., Finlay, B.B., 2013. Recent advances in understanding enteric pathogenic *Escherichia coli*. Clin. Microbiol. Rev. 26 (4), 822–880. https://doi.org/10.1128/CMR.00022-13.

Cryan, J.F., O'Riordan, K.J., Sandhu, K., Peterson, V., Dinan, T.G., 2020. The gut microbiome in neurological disorders. Lancet Neurol. 19 (2), 179–194. https://doi.org/10.1016/S1474-4422(19)30356-4.

Cryan, J.F., O'Riordan, K.J., Cowan, C.S.M., Sandhu, K.V., Bastiaanssen, T.F.S., Boehme, M., Codagnone, M.G., Cussotto, S., Fulling, C., Golubeva, A.V., Guzzetta, K. E., Jaggar, M., Long-Smith, C.M., Lyte, J.M., Martin, J.A., Molinero-Perez, A., Moloney, G., Morelli, E., Morillas, E., O'Connor, R., Cruz-Pereira, J.S., Peterson, V.L., Rea, K., Ritz, N.L., Sherwin, E., Spichak, S., Teichman, E.M., van de Wouw, M., Ventura-Silva, A.P., Wallace-Fitzsimons, S.E., Hyland, N., Clarke, G., Dinan, T.G., 2019. The microbiota-gut-brain axis. Physiol. Rev. 99 (4), 1877–2013. https://doi.org/10.1152/physrev.00018.2018.

Douglas, G.M., Maffei, V.J., Zaneveld, J.R., Yurgel, S.N., Brown, J.R., Taylor, C.M., Huttenhower, C., Langille, M.G.I., 2020. PICRUSt2 for prediction of metagenome functions. Nat. Biotechnol. 38 (6), 685–688. https://doi.org/10.1038/s41587-020-0548-6.

Erny, D., Hrabĕ de Angelis, A.L., Jaitin, D., Wieghofer, P., Staszewski, O., David, E., Keren-Shaul, H., Mahlakoiv, T., Jakobshagen, K., Buch, T., Schwierzeck, V., Utermöhlen, O., Chun, E., Garrett, W.S., McCoy, K.D., Diefenbach, A., Staeheli, P., Stecher, B., Amit, I., Prinz, M., 2015. Host microbiota constantly control maturation and function of microglia in the CNS. Nat. Neurosci. 18 (7), 965–977. https://doi.org/10.1038/nn.4030.

Erny, D., Prinz, M., 2020. How microbiota shape microglial phenotypes and epigenetics. Glia 68 (8), 1655–1672. https://doi.org/10.1002/glia.23822.

Fan, Y., Pedersen, O., 2021. Gut microbiota in human metabolic health and disease. Nat. Rev. Microbiol. 19 (1), 55–71. https://doi.org/10.1038/s41579-020-0433-9.

Hammad, A.M., Shimamoto, T., Shimamoto, T., 2014. Genetic characterization of antibiotic resistance and virulence factors in *Enterococcus spp.* from Japanese retail ready-to-eat raw fish. Food Microbiol. 38, 62–66. https://doi.org/10.1016/j.fm.2013.08.010.

Hashimoto, K., 2020. Molecular mechanisms of the rapid-acting and long-lasting antidepressant actions of (*R*)-ketamine. Biochem. Pharmacol. 177, 113935 https://doi.org/10.1016/j.bcp.2020.113935.

Hashimoto, Y., Eguchi, A., Wei, Y., Shinno-Hashimoto, H., Fujita, Y., Ishima, T., Chang, L., Mori, C., Suzuki, T., Hashimoto, K., 2022. Antibiotic-induced microbiome depletion improves LPS-induced acute lung injury via gut-lung axis. Life Sci. 307, 120885 https://doi.org/10.1016/j.lfs.2022.120885.

Huang, Q., Ou, Y.S., Tao, Y., Yin, H., Tu, P.H., 2016. Apoptosis and autophagy induced by pyropheophorbide-α methyl ester-mediated photodynamic therapy in human osteosarcoma MG-63 cells. Apoptosis 21 (6), 749–760. https://doi.org/10.1007/s10495-016-1243-4.

Huston, J.M., Ochani, M., Rosas-Ballina, M., Liao, H., Ochani, K., Pavlov, V.A., Gallowitsch-Puerta, M., Ashok, M., Czura, C.J., Foxwell, B., Tracey, K.J., Ulloa, L., 2006. Splenectomy inactivates the cholinergic antiinflammatory pathway during lethal endotoxemia and polymicrobial sepsis. J. Exp. Med. 203 (7), 1623–1628. https://doi.org/10.1084/jem.20052362.

Jiang, M., Hong, K., Mao, Y., Ma, H., Chen, T., Wang, Z., 2022. Natural 5-aminolevulinic acid: sources, biosynthesis, detection and applications. Front. Bioeng. Biotechnol. 10, 841443 https://doi.org/10.3389/fbioe.2022.841443.

Kennedy, E.A., King, K.Y., Baldridge, M.T., 2018. Mouse microbiota models: comparing germ-free mice and antibiotics treatment as tools for modifying gut bacteria. Front. Physiol. 9, 1534. https://doi.org/10.3389/fphys.2018.01534.

Lewis, S.M., Williams, A., Eisenbarth, S.C., 2019. Structure and function of the immune system in the spleen. Sci. Immunol. 4 (33), eaau6085 https://doi.org/10.1126/sciimmunol.aau6085.

Liu, S., Zhang, G., Li, X., Zhang, J., 2014. Microbial production and application of 5-aminolevulic acid. Appl. Microbiol. Biotechnol. 98, 7349–7357. https://doi.org/10.1007/s00253-014-5925-y.

Liu, T., Ma, X., Ouyang, T., Chen, H., Xiao, Y., Huang, Y., Liu, J., Xu, M., 2019. Efficacy of 5-aminolevulinic acid-based photodynamic therapy against keloid compromised by downregulation of SIRT1-SIRT3-SOD2-mROS dependent autophagy pathway. Redox Biol. 20, 195–203. https://doi.org/10.1016/j.redox.2018.10.011.

Ma, L., Zhang, J., Fujita, Y., Qu, Y., Shan, J., Wan, X., Wang, X., Ishima, T., Kobayashi, K., Wang, L., Hashimoto, K., 2022a. Nuclear factor of activated T cells 4 in the prefrontal cortex is required for prophylactic actions of (*R*)-ketamine. Transl. Psychiatry 12 (1), 27. https://doi.org/10.1038/s41398-022-01803-6.

Ma, L., Zhang, J., Fujita, Y., Shinno-Hashimoto, H., Shan, J., Wan, X., Qu, Y., Chang, L., Wang, X., Hashimoto, K., 2022b. Effects of spleen nerve denervation on depression-like phenotype, systemic inflammation, and abnormal composition of gut microbiota in mice after administration of lipopolysaccharide: a role of brain-spleen axis. J. Affect. Disord. 317, 156–165. https://doi.org/10.1016/j.jad.2022.08.087.

Mamalis, A., Koo, E., Sckisel, G.D., Siegel, D.M., Jagdeo, J., 2016. Temperature-dependent impact of thermal aminolaevulinic acid photodynamic therapy on apoptosis and reactive oxygen species generation in human dermal fibroblasts. Br. J. Dermatol. 175 (3), 512–519. https://doi.org/10.1111/bjd.14509.

Mebius, R.E., Kraal, G., 2005. Structure and function of the spleen. Nat. Rev. Immunol. 5 (8), 606–616. https://doi.org/10.1038/nri1669.

Miyauchi, E., Shimokawa, C., Steimle, A., Desai, M.S., Ohno, H., 2022. The impact of the gut microbiome on extra-intestinal autoimmune diseases. Nat. Rev. Immunol. https://doi.org/10.1038/s41577-022-00727-y online ahead of print.

Mok, S.W., Wong, V.K., Lo, H.H., de Seabra Rodrigues Dias, I.R., Leung, E.L., Law, B.Y., Liu, L., 2020. Natural products-based polypharmacological modulation of the peripheral immune system for the treatment of neuropsychiatric disorders. Pharmacol. Ther. 208, 107480 https://doi.org/10.1016/j.pharmthera.2020.107480.

Moyenuddin, M., Wachsmuth, I.K., Moseley, S.L., Bopp, C.A., Blake, P.A., 1989. Serotype, antimicrobial resistance, and adherence properties of *Escherichia coli* strains associated with outbreaks of diarrheal illness in children in the United States. J. Clin. Microbiol. 27 (10), 2234–2239. https://doi.org/10.1128/jcm.27.10.2234-2239.1989.

Noble, B.T., Brennan, F.H., Popovich, P.G., 2018. The spleen as a neuroimmune interface after spinal cord injury. J. Neuroimmunol. 321, 1–11. https://doi.org/10.1016/j.jneuroim.2018.05.007.

Pu, Y., Chang, L., Qu, Y., Wang, S., Zhang, K., Hashimoto, K., 2019. Antibiotic-induced microbiome depletion protects against MPTP-induced dopaminergic neurotoxicity in the brain. Aging (Albany NY) 11 (17), 6915–6929. https://doi.org/10.18632/aging.102221.

Pu, Y., Tan, Y., Qu, Y., Chang, L., Wang, S., Wei, Y., Wang, X., Hashimoto, K., 2021. A role of the subdiaphragmatic vagus nerve in depression-like phenotypes in mice after fecal microbiota transplantation from *Chrna7* knock-out mice with depression-like phenotypes. Brain Behav. Immun. 94, 318–326. https://doi.org/10.1016/j.bbi.2020.12.032.

Rhee, S.H., Pothoulakis, C., Mayer, E.A., 2009. Principles and clinical implications of the brain-gut-enteric microbiota axis. Nat. Rev. Gastroenterol. Hepatol. 6 (5), 306–314. https://doi.org/10.1038/nrgastro.2009.35.

Rosas-Ballina, M., Ochani, M., Parrish, W.R., Ochani, K., Harris, Y.T., Huston, J.M., Chavan, S., Tracey, K.J., 2008. Splenic nerve is required for cholinergic antiinflammatory pathway control of TNF in endotoxemia. Proc. Natl. Acad. Sci. U.S. A. 105 (31), 11008–11013. https://doi.org/10.1073/pnas.0803237105.

Sahoo, T.K., Jena, P.K., Nagar, N., Patel, A.K., Seshadri, S., 2015. *In vitro* evaluation of probiotic properties of lactic acid bacteria from the gut of *Labeo rohita* and *Catla catla*. Probiotics Antimicrob. Proteins 7 (2), 126–136. https://doi.org/10.1007/s12602-015-9184-8.

Sasaki, K., Watanabe, M., Tanaka, T., Tanaka, T., 2002. Biosynthesis, biotechnological production and applications of 5-aminolevulinic acid. Appl. Microbiol. Biotechnol. 58, 23–29. https://doi.org/10.1007/s00253-001-0858-7.

Schön, M., Mousa, A., Berk, M., Chia, W.L., Ukropec, J., Majid, A., Ukropcová, B., de Courten, B., 2019. The potential of carnosine in brain-related disorders: a comprehensive review of current evidence. Nutrients 11 (6), 1196. https://doi.org/10.3390/nu11061196.

Segata, N., Izard, J., Waldron, L., Gevers, D., Miropolsky, L., Garrett, W.S., Huttenhower, C., 2011. Metagenomic biomarker discovery and explanation. Genome Biol. 12 (6), R60. https://doi.org/10.1186/gb-2011-12-6-r60.

Sharon, G., Sampson, T.R., Geschwind, D.H., Mazmanian, S.K., 2016. The central nervous system and the gut microbiome. Cell 167 (4), 915–932. https://doi.org/10.1016/j.cell.2016.10.027.

Shinno-Hashimoto, H., Eguchi, A., Sakamoto, A., Wan, X., Hashimoto, Y., Fujita, Y., Mori, C., Hatano, M., Matsue, H., Hashimoto, K., 2022. Effects of splenectomy on skin inflammation and psoriasis-like phenotype of imiquimod-treated mice. Sci. Rep. 12 (1), 14738 https://doi.org/10.1038/s41598-022-18900-7.

13

Stummer, W., Pichlmeier, U., Meinel, T., Wiestler, O.D., Zanella, F., Reulen, H.J., ALA-Glioma Study Group, 2006. Fluorescence-guided surgery with 5-aminolevulinic acid for resection of malignant glioma: a randomised controlled multicentre phase III trial. Lancet Oncol. 7 (5), 392–401. https://doi.org/10.1016/S1470-2045(06)70665-9.

Subramanian, K., Selvakkumar, C., Vinaykumar, K.S., Goswami, N., Meenakshisundaram, S., Balakrishnan, A., Lakshmi, B.S., 2009. Tackling multiple antibiotic resistance in enteropathogenic *Escherichia coli (EPEC)* clinical isolates: a diarylheptanoid from *Alpinia officinarum* shows promising antibacterial and immunomodulatory activity against EPEC and its lipopolysaccharide-induced inflammation. Int. J. Antimicrob. Agents 33 (3), 244–250. https://doi.org/10.1016/j.ijantimicag.2008.08.032.

Tiedje, K.E., Stevens, K., Barnes, S., Weaver, D.F., 2010. Beta-alanine as a small molecule neurotransmitter. Neurochem. Int. 57 (3), 177–188. https://doi.org/10.1016/j.neuint.2010.06.001.

Wan, X., Eguchi, A., Fujita, Y., Ma, L., Wang, X., Yang, Y., Qu, Y., Chang, L., Zhang, J., Mori, C., Hashimoto, K., 2022a. Effects of (*R*)-ketamine on reduced bone mineral density in ovariectomized mice: a role of gut microbiota. Neuropharmacology 213, 109139. https://doi.org/10.1016/j.neuropharm.2022.109139.

Wan, X., Eguchi, A., Qu, Y., Yang, Y., Chang, L., Shan, J., Mori, C., Hashimoto, K., 2022b. Gut-microbiota-brain axis in the vulnerability to psychosis in adulthood after repeated cannabis exposure during adolescence. Eur. Arch. Psychiatr. Clin. Neurosci. 272 (7), 1297–1309. https://doi.org/10.1007/s00406-022-01437-1.

Wang, S., Ishima, T., Qu, Y., Shan, J., Chang, L., Wei, Y., Zhang, J., Pu, Y., Fujita, Y., Tan, Y., Wang, X., Ma, L., Wan, X., Hammock, B.D., Hashimoto, K., 2021. Ingestion of *Faecalibaculum rodentium* causes depression-like phenotypes in resilient *Ephx2* knock-out mice: a role of brain-gut-microbiota axis via the subdiaphragmatic vagus nerve. J. Affect. Disord. 292, 565–573. https://doi.org/10.1016/j.jad.2021.06.006.

Wang, S., Ishima, T., Zhang, J., Qu, Y., Chang, L., Pu, Y., Fujita, Y., Tan, Y., Wang, X., Hashimoto, K., 2020a. Ingestion of *Lactobacillus intestinalis* and *Lactobacillus reuteri* causes depression- and anhedonia-like phenotypes in antibiotic-treated mice via the vagus nerve. J. Neuroinflammation 17 (1), 241. https://doi.org/10.1186/s12974-020-01916-z.

Wang, S., Qu, Y., Chang, L., Pu, Y., Zhang, K., Hashimoto, K., 2020b. Antibiotic-induced microbiome depletion is associated with resilience in mice after chronic social defeat stress. J. Affect. Disord. 260, 448–457. https://doi.org/10.1016/j.jad.2019.09.064.

Wei, Y., Chang, L., Ishima, T., Wan, X., Ma, L., Wuyun, G., Pu, Y., Hashimoto, K., 2021. Abnormalities of the composition of the gut microbiota and short-chain fatty acids in mice after splenectomy. Brain Behav. Immun. Health 11, 100198. https://doi.org/10.1016/j.bbih.2021.100198.

Wang, X., Chang, L., Wan, X., Tan, Y., Qu, Y., Shan, J., Yang, Y., Ma, L., Hashimoto, K., 2022a. (*R*)-ketamine ameliorates demyelination and facilitates remyelination in cuprizone-treated mice: a role of gut-microbiota-brain axis. Neurobiol. Dis. 165, 105635 https://doi.org/10.1016/j.nbd.2022.105635.

Wang, X., Eguchi, A., yang, Y., Chang, L., Wan, X., Shan, J., Qu, Y., Ma, L., Mori, C., Yang, J., Hashimoto, K., 2022b. Key role of the gut–microbiota–brain axis via the subdiaphragmatic vagus nerve in demyelination of the cuprizone-treated mouse brain. Neurobiol. Dis. 176, 105951 https://doi.org/10.1016/j.nbd.2022.105951.

Wei, Y., Chang, L., Hashimoto, K., 2022a. Molecular mechanisms underlying the antidepressant actions of arketamine: beyond the NMDA receptor. Mol. Psychiatr. 27 (1), 559–573. https://doi.org/10.1038/s41380-021-01121-1.

Wei, Y., Wang, T., Liao, L., Fan, X., Chang, L., Hashimoto, K., 2022b. Brain-spleen axis in health and diseases: a review and future perspective. Brain Res. Bull. 182, 130–140. https://doi.org/10.1016/j.brainresbull.2022.02.008.

Yang, B., Ren, Q., Zhang, J.C., Chen, Q.X., Hashimoto, K., 2017. Altered expression of BDNF, BDNF pro-peptide and their precursor proBDNF in brain and liver tissues from psychiatric disorders: rethinking the brain-liver axis. Transl. Psychiatry 7 (5), e1128. https://doi.org/10.1038/tp.2017.95.

Yang, Y., Eguchi, A., Wan, X., Chang, L., Wang, X., Qu, Y., Mori, C., Hashimoto, K., 2022a. A role of gut-microbiota-brain axis via subdiaphragmatic vagus nerve in depression-like phenotypes in *Chrna7* knock-out mice. Prog. Neuro-Psychopharmacol. Biol. Psychiatry 120, 110652. https://doi.org/10.1016/j.pnpbp.2022.110652.

Yang, Y., Ishima, T., Wan, X., Wei, Y., Chang, L., Zhang, J., Qu, Y., Hashimoto, K., 2022b. Microglial depletion and abnormalities in gut microbiota composition and short-chain fatty acids in mice after repeated administration of colony stimulating factor 1 receptor inhibitor PLX5622. Eur. Arch. Psychiatr. Clin. Neurosci. 272 (3), 483–495. https://doi.org/10.1007/s00406-021-01325-0.

Zhang, J., Chang, L., Pu, Y., Hashimoto, K., 2020a. Abnormal expression of colony stimulating factor 1 receptor (CSF1R) and transcription factor PU.1 (SPI1) in the spleen from patients with major psychiatric disorders: a role of brain-spleen axis. J. Affect. Disord. 272, 110–115. https://doi.org/10.1016/j.jad.2020.03.128.

Zhang, J., Ma, L., Chang, L., Pu, Y., Qu, Y., Hashimoto, K., 2020b. A key role of the subdiaphragmatic vagus nerve in the depression-like phenotype and abnormal composition of gut microbiota in mice after lipopolysaccharide administration. Transl. Psychiatry 10 (1), 186. https://doi.org/10.1038/s41398-020-00878-3.

Zhang, J., Ma, L., Wan, X., Shan, J., Qu, Y., Hashimoto, K., 2021a. (*R*)-Ketamine attenuates LPS-induced endotoxin-derived delirium through inhibition of neuroinflammation. Psychopharmacology (Berl) 238 (10), 2743–2753. https://doi.org/10.1007/s00213-021-05889-6.

Zhang, K., Sakamoto, A., Chang, L., Qu, Y., Wang, S., Pu, Y., Tan, Y., Wang, X., Fujita, Y., Ishima, T., Hatano, M., Hashimoto, K., 2021b. Splenic NKG2D confers resilience versus susceptibility in mice after chronic social defeat stress: beneficial effects of (*R*)-ketamine. Eur. Arch. Psychiatr. Clin. Neurosci. 271 (3), 447–456. https://doi.org/10.1007/s00406-019-01092-z.

Supported by
日本
財団
THE NIPPON
FOUNDATION

第 44 期　　研究者番号：G4404　　　　　　　　作成日　：2023 年 3 月 10 日

氏　名	蒋 夢恬	JIANG MENGTIAN	性別	F	生年月日　1996/03/15

所属機関（役職）	東京医科歯科大学大学院医歯学総合研究科（大学院生）
研究先（指導教官）	東京医科歯科大学大学院医歯学総合研究科 口腔機能再構築学講座生体補綴歯科学分野（若林 則幸　教授）
研究テーマ	暗条件下での血清及び唾液中の二酸化チタンの殺菌効果に及ぼす３種類のイオン性抗菌剤の影響に関する研究 Development of antibacterial dental materials using cation-doped TiO2 nanosheet in dark condition
専攻種別	□論文博士　　　　　　　☑課程博士

研究者評価（指導教官記入欄）

成績状況	優 学業成績係数=	取得単位数 18／30
学生本人が行った 研究の概要	研究課題では，優れた抗菌活性を有する新規歯科補綴装置用材料の創製のため，光析出法にて金属ナノ粒子を担持させたチタニアナノシートを開発することを目的としている．本年度は，基材となるチタニアナノシートを水熱合成法により作製した後に，光析出法による 3 種類の金属ナノ粒子のチタニアナノシート上での析出を試みた．作製した試料は X 線回折法にて解析し，すべての試料がアナターゼ型チタニアであることが明らかとなった．また，透過型電子顕微鏡にて観察し，金属ナノ粒子の析出を確認した．次に，エネルギー分散型 X 線分光法により組成分析を行い，出発原料に含まれる各種金属がチタニアナノシートに固溶していることが明らかとなった．以上より，本年度は 3 種類の金属ナノ粒子を担持したアナターゼ型チタニアナノシートの開発に成功した．次年度より，抗菌活性の評価を行う予定である．	
総合評価	【良かった点】 　本年度は，実験計画の立案から，水熱化学合成によるチタニアナノシートの合成法と光析出法による金属ナノ粒子の合成法の習得までを行い，十分な研究活動を行ったと評価できる．特に，実験計画の立案をする際には，過去の報告を基に十分なエビデンスを構築したうえで討論することができた．実験においては，水熱化学合成法と光析出法を用いた実験の手技の習熟に努め，独立して実験を遂行することが可能となった．また，研究室のチームとも協調性をもって活動することができた． 【改善すべき点】 　今後，自立した研究者として活躍するためには，過去の報告を検討する上で良質な論文を探すことが重要である．また，そのデータを吟味し参考にすることが必要であるが，論文の読み込みが不十分であることが見受けられた．改善の傾向が見受けられるが，今後一層の研鑽が必要である． 【今後の展望】 　作製した金属ナノ粒子は数 nm サイズのため，学内機器では詳細な解析を行うことができない．そこで次年度は，東京都立産業技術センターにてキャラクタリゼーションを行う予定である．また，歯科材料への応用のため，光触媒活性と抗菌活性の評価を行う予定である．	
学位取得見込	研究は順調に進捗しており，本学が定める学位取得の単位も到達している．次年度は論文の執筆にとりかかり，学術雑誌への投稿を予定しており，十分に学位取得の要件を満たすと考える．	

評価者　若林　則幸

第44期	研究者番号： G4404		作成日：2023年3月 5 日	
氏名	蒋 梦恬	JIANG MENGTIAN	性別	F	生年月日 1996/03/15

所属機関(役職)	東京医科歯科大学大学院医歯学総合研究科（大学院生）	
研究先(指導教官)	東京医科歯科大学大学院医歯学総合研究科 口腔機能再構築学講座生体補綴歯科学分野（若林 則幸 教授）	
研究テーマ	暗条件下での血清及び唾液中の二酸化チタンの殺菌効果に及ぼす3種類のイオン性抗菌剤の影響に関する研究 Development of antibacterial dental materials using cation-doped TiO₂ nanosheet in dark condition	
専攻種別	論文博士 □	課程博士 ☑

1．研究概要(1)
1）目的(Goal)
Bacterial contamination is a serious problem that can affect numerous applications. As a semiconductor with photocatalysis function, Nano-titanium dioxide (TiO2) not only has the advantages of high activity, fast antibacterial speed, good thermal stability, long-term effectiveness, low price and no harm to human body, but also can decompose endotoxin, with the functions of purification, self-cleaning, deodorization, etc. However, there are still some problems in the use of Nano-TiO2 as inorganic antibacterial agent. In this study, the antibacterial effect of metal doped TiO2 nanosheets (TiO2 NS) made by photodeposition in serum and saliva under dark condition will be evaluated comprehensively, so as to obtain the best bactericide for specific bacteria in specific environment and provide reference for exploring the bactericidal effect of Ag^+, Cu^{2+}, Ce^{3+} and TiO2 nanosheets.

2）戦略(Approach)
The photodeposition method is based on the photocatalytic property of semiconductor materials afforded by their band gap. Several conditions are needed to enable the photodeposition method. First, the photon energy of the exposure light should be larger than the energy band gap of the semiconductor. When light that has the proper energy level for the band gap of the semi-conductor is absorbed, electrons from the valence band can be excited. Second, the reduction potential of the metal ion should be more positive than the conduction band energy level of the semi- conductor. Third, the efficient separation and migration of photo- generated electron-hole pairs is necessary. Finally, the semiconductor should act as a template for active sites of metal deposition and have a large surface area. If these four conditions are met, the synthesis of metal/semiconductor nanocomposite by photodeposition method is possible, since nanoscale semiconductor materials have many active sites that have large surface energy due to their morphology. Also, this is a simple and green method since it does not require the addition of chemical reagents or any conditions other than light exposure[1].

3）材料と方法(Materials and methods)
1. Synthesis of TiO2 nanosheets
Dissolve 1 g Ammonium hexafluorotitanate into 5 ml of hydrochloric acid (5 M). Add a controlled amount titanium (IV) butoxide to the above solution to make that the total F/Ti molar ratio is 1.0 under strong stirring and white gels formed. The gels are placed into a 50 ml Teflon tube for a 6-hour hydrothermal reaction at 180° C. The products of the hydrothermal reaction are washed with ultrapure water three times and by methanol once, all with subsequent centrifugal separation. The obtained TiO2 nanosheets are then freeze dried[2,3].
2. Characterization of the TiO2 nanosheets
Use X-ray diffractometer, scanning electron microscope, transmittance electron microscope and energy-dispersive X-ray spectrometer to show the crystal structure, morphology and chemical composition of the precipitates. The length and thickness are measured from TEM images.
3. Preparation of metal doped TiO2 nanosheets by photodeposition
For preparation of metal-modified TiO2 nanosheets, silver nitrate, copper sulfate pentahydrate and cerium nitrate hexahydrate are used as metal precursors. The codes of metal-modified TiO2 nanosheets samples are defined as Ag/TiO2 nanosheets, Cu/TiO2 nanosheets and Ce/TiO2 nanosheets,respectively. The amount of each metal doped on 1500mg TiO2 nanosheets is $1.2*10^{-4}$ mol , which means that the quantity of silver nitrate,
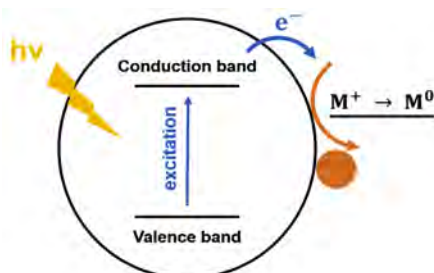
Schematic diagram of photodeposition method. When light is absorbed in the band gap, electrons from valence band are excited and migrate to reduce metal ions to metal. hv, light energy; e^-, photoexcited electron; M^+, metal ion; M^0, metal.

1．研究概要（2）

Copper sulfate and cerium nitrate is 20.40mg, 30.00mg and 52.08mg respectively(which means that the weight ratio is 0.8562wt%, 0.5058wt% and 1.1082% respectively). The weighted TiO_2 nanosheets powder is put into a Pyrex glass tube equipped with a magnetic stirrer, to which 75ml of methanol(99.5%) aqueous solution(50vol%, distilled water) is added. Then, the aqueous solution of metal salt is slowly dropped while being stirred(75ml distilled water). The suspension is gas-sparged (N_2) for 15 min. The tube is photoirradiated for 3 hours for silver doped TiO_2, copper doped TiO_2 and cerium doped TiO_2 with magnetic stirring (500rpm) by a 121-W high-pressure mercury lamp under thermostatic control at 298K. The thus-obtained photocatalysts is centrifuged (15,000rpm for 30 min), washed three times with methanol and three times with distilled water, and freeze-dried, and then the product is collected for further study[4].

4. Characterization of three composite materials

The deposition of various metals on TiO_2 nanosheets is determined by Inductively Coupled Plasma Atomic Emission Spectrometry (ICP-AES)[5]. X-ray diffractometer, scanning electron microscope, transmittance electron microscope, energy-dispersive X-ray spectrometer and TEM image analysis are also used for characterization.
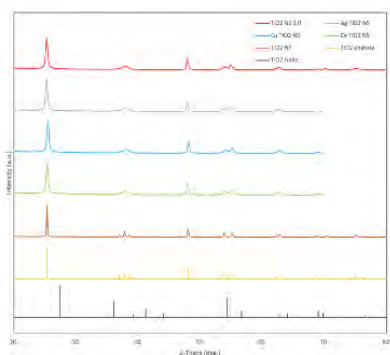
4）実験結果（Results）

Fig. 1 XRD spectra of TiO_2 NS, Ag doped TiO_2 NS, Cu doped TiO_2 NS and Ce doped TiO_2 NS and TiO_2 nanoparticle.

Table 1 EDS data of TiO_2 NS, Ag doped TiO_2 NS, Cu doped TiO_2 NS and Ce doped TiO_2 NS

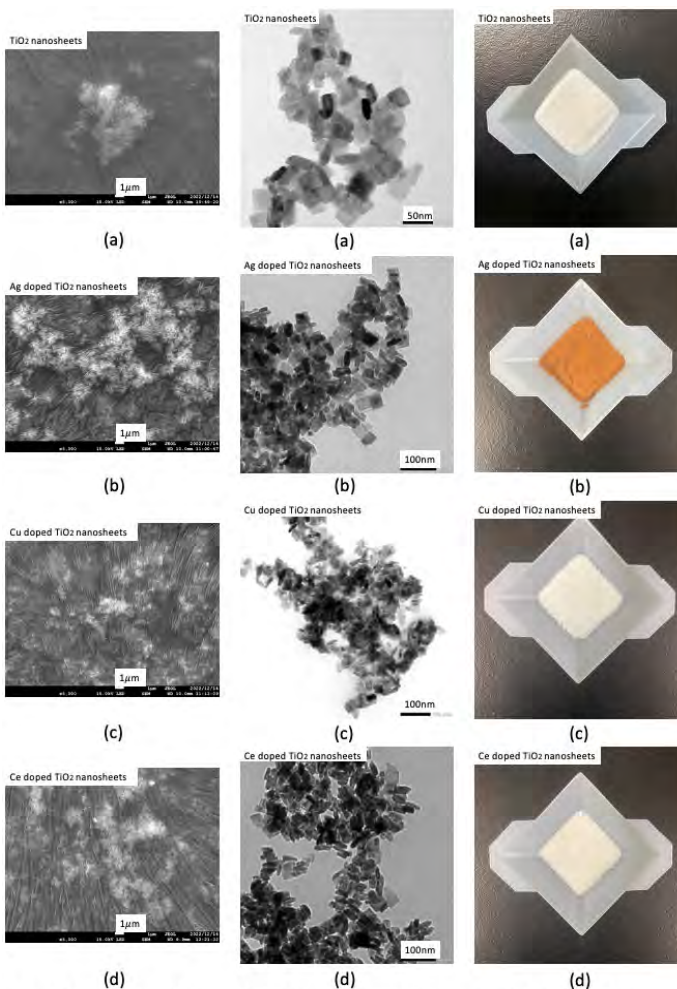|	TiO_2 NS	Ag doped TiO_2 NS	Cu doped TiO_2 NS	Ce doped TiO_2 NS
O Mass%, Sigma	64.98, 0.47	86.86, 0.83	84.05, 0.64	72.23, 0.52
Ti Mass%, Sigma	35.02, 0.28	12.53, 0.38	14.82, 0.31	27.17, 0.29
Ag Mass%, Sigma	/	0.61, 0.18	/	/
Cu Mass%, Sigma	/	/	1.12, 0.23	/
Ce Mass%, Sigma	/	/	/	0.60, 0.11

Fig. 2 SEM images of TiO_2 NS(a), Ag doped TiO_2 NS(b), Cu doped TiO_2 NS(c) and Ce doped TiO_2 NS(d)

Fig. 3 TEM images of TiO_2 NS(a), Ag doped TiO_2 NS(b), Cu doped TiO_2 NS(c) and Ce doped TiO_2 NS(d)

Fig. 4 Images of TiO_2 NS(a), Ag doped TiO_2 NS(b), Cu doped TiO_2 NS(c) and Ce doped TiO_2 NS(d)

5）考察（Discussion）

Metals including silver, copper and cerium could be doped on titanium dioxide by photodeposition.

6）参考文献（References）

[1].Lee, Y. et al. Photodeposited metal-semiconductor nanocomposites and their applications. J. Materiomics 4, 83-94 (2018).
[2].Hayashi, K. et al. Enhanced Antibacterial Property of Facet-Engineered TiO2 Nanosheet in Presence and Absence of Ultraviolet Irradiation. Materials 13, 78 (2019).   [3].Tan, Z. et al. Particle size for photocatalytic activity of anatase TiO2 nanosheets with highly exposed {001} facets. RSC Adv. 3, 19268 (2013).
[4].Wei, Z. et al. Noble metal-modified octahedral anatase titania particles with enhanced activity for decomposition of chemical and microbiological pollutants. Chem. Eng. J. 318, 121-134 (2017).
[5].Effects of catalyst preparation method and reaction parameters on the ultrasound assisted Photocatalytic oxidation of reactive yellow 84 dye.

2．執筆論文　Publication of thesis　※記載した論文を添付してください。Attach all of the papers listed below.

論文名 1 Title							
掲載誌名 Published journal							
	年	月	巻（号）	頁　〜	頁	言語 Language	
第1著者名 First author			第2著者名 Second author		第3著者名 Third author		
その他著者名 Other authors							
論文名 2 Title							
掲載誌名 Published journal							
	年	月	巻（号）	頁　〜	頁	言語 Language	
第1著者名 First author			第2著者名 Second author		第3著者名 Third author		
その他著者名 Other authors							
論文名 3 Title							
掲載誌名 Published journal							
	年	月	巻（号）	頁　〜	頁	言語 Language	
第1著者名 First author			第2著者名 Second author		第3著者名 Third author		
その他著者名 Other authors							
論文名 4 Title							
掲載誌名 Published journal							
	年	月	巻（号）	頁　〜	頁	言語 Language	
第1著者名 First author			第2著者名 Second author		第3著者名 Third author		
その他著者名 Other authors							
論文名 5 Title							
掲載誌名 Published journal							
	年	月	巻（号）	頁　〜	頁	言語 Language	
第1著者名 First author			第2著者名 Second author		第3著者名 Third author		
その他著者名 Other authors							

3．学会発表　Conference presentation　※筆頭演者として総会・国際学会を含む主な学会で発表したものを記載してくだ

※Describe your presentation as the principal presenter in major academic meetings including general meetings or international me

学会名 Conference	
演　題 Topic	
開催日 date	年　　　　　月　　　　　日	開催地 venue	
形式　method	□　　口頭発表 Oral　　□　　ポスター発表 Poster| 言語 Language| □　　日本語　□　　英語　　□　　中国語
共同演者名 Co-presenter	

学会名 Conference	
演　題 Topic	
開催日 date	年　　　　　月　　　　　日	開催地 venue	
形式　method	□　　口頭発表 Oral　　□　　ポスター発表 Poster| 言語 Language| □　　日本語　□　　英語　　□　　中国語
共同演者名 Co-presenter	

学会名 Conference	
演　題 Topic	
開催日 date	年　　　　　月　　　　　日	開催地 venue	
形式　method	□　　口頭発表 Oral　　□　　ポスター発表 Poster| 言語 Language| □　　日本語　□　　英語　　□　　中国語
共同演者名 Co-presenter	

学会名 Conference	
演　題 Topic	
開催日 date	年　　　　　月　　　　　日	開催地 venue	
形式　method	□　　口頭発表 Oral　　□　　ポスター発表 Poster| 言語 Language| □　　日本語　□　　英語　　□　　中国語
共同演者名 Co-presenter	

4．受賞（研究業績）Award（Research achievement）

名　称 Award name					
	国名 Country		受賞年 Year of	年　　　　月
名　称 Award name					
	国名 Country		受賞年 Year of	年　　　　月

5．本研究テーマに関わる他の研究助成金受給 Other research grants concerned with your resarch theme

受給実績 Receipt record	■ 有　　　□ 無						
助成機関名称 Funding agency	国立研究開発法人科学技術振興機構次世代研究者挑戦的研究プログラム						
助成金名称 Grant name	東京医科歯科大学卓越大学院生制度(Ⅱ)						
受給期間 Supported period	2022　　年　　4　　月　～　　2025　　年　　3　　月						
受給額 Amount received	50万/年 円						
受給実績 Receipt record	□ 有　　　□ 無						
助成機関名称 Funding agency							
助成金名称 Grant name							
受給期間 Supported period	年　　　　月　～　　　　　年　　　　月						
受給額 Amount received	円						

6．他の奨学金受給 Another awarded scholarship

受給実績 Receipt record	■ 有　　　□ 無
助成機関名称 Funding agency	国立研究開発法人科学技術振興機構次世代研究者挑戦的研究プログラム
奨学金名称 Scholarship name	東京医科歯科大学卓越大学院生制度(Ⅱ)
受給期間 Supported period	2022　　年　　4　　月　～　　2025　　年　　3　　月
受給額 Amount received	16万/月 円

7．研究活動に関する報道発表 Press release concerned with your research activities

※記載した記事を添付してください。Attach a copy of the article described below

報道発表 Press release	□ 有　　　■ 無	発表年月日 Date of release	
発表機関 Released medium			
発表形式 Release method	・新聞　・雑誌　・Web site　・記者発表　・その他（　　　　　　　　　　）		
発表タイトル Released title			

8．本研究テーマに関する特許出願予定 Patent application concerned with your research theme

出願予定 Scheduled	□ 有　　　■ 無	出願国 Application	
出願内容（概要） Application contents			

9．その他 Others

指導責任者（記名）　　　若林　則幸

第 44 期	研究者番号：G4405		作成日 ： 2023 年 3 月　日		

氏　名	陳 曹傑	CHEN CAOJIE	性別	M	生年月日　1984/01/23
所属機関（役職）	慶應義塾大学医学部（大学院生）				
研究先（指導教官）	慶應義塾大学医学部形成外科学教室（貴志 和生　教授）				
研究テーマ	創傷治癒とオートファジーの関係 The relationship between autophagy and wound healing				
専攻種別	□論文博士			☑課程博士	

研究者評価（指導教官記入欄）

成績状況	（優）良　可　不可 学業成績係数=	取得単位数 取得単位数／取得すべき単位総数
学生本人が行った 研究の概要	公開されているデータベースを基にオートファジー創傷治癒、瘢痕形成の研究を行った。	
総合評価	【良かった点】 データ解析の能力が素晴らしく、根気よく研究を行っているところ。 【改善すべき点】 質疑応答での適切な受け答え。 【今後の展望】 臨床、研究双方で頑張っていただきたい。	
学位取得見込	半年遅れで取得できるものと思われス。	

評価者（指導教官名）　貴志 和生